UNCLASSIFIED

AD NUMBER
ADB014045
LIMITATION CHANGES
TO: **Approved for public release; distribution is unlimited.**
FROM: **Distribution authorized to U.S. Gov't. agencies only; Proprietary Information; SEP 1976. Other requests shall be referred to Air Force Avionics Laboratory, AFAL/RWA, Wright-Patterson AFB, OH 45433.**
AUTHORITY
afwal ltr, 8 oct 1981

THIS PAGE IS UNCLASSIFIED

UNCLASSIFIED

AD B014045

AUTHORITY: AFWAL

ltr, 8 OCT 81

DEPARTMENT OF DEFENSE

UNITED STATES OF AMERICA

UNCLASSIFIED

AFAL-TR-76-130

2

Q-FLEX ACCELEROMETER THERMAL PERFORMANCE STUDY

Sundstrand Data Control, Inc.
Overlake Industrial Park
Redmond, Wa. 98052

September 1976

Final Report For Period 13 June 1975 - 7 May 1976

Prepared for

AIR FORCE AVIONICS LABORATORY
Air Force Wright Aeronautical Laboratories
Air Force Systems Command
Wright-Patterson Air Force Base, Ohio 45433

S/C
390539

NOTICE

When Government drawings, specifications, or other data are used for any purpose other than in connection with a definitely related Government procurement operation, the United States Government thereby incurs no responsibility nor any obligation whatsoever; and the fact that the government may have formulated, furnished, or in any way supplied the said drawings, specifications, or other data, is not to be regarded by implication or otherwise as in any manner licensing the holder or any other person or corporation, or conveying any rights or permission to manufacture, use, or sell any patented invention that may in any way be related thereto.

This technical report has been reviewed and is approved for publication.

ROBERT W. MCADORY, Project Engineer
Reference Systems Technology Group
Reference Systems Branch, Reconnaissance and Weapon Delivery Division

EDWIN V. HARRINGTON, Jr. Capt. USAF
Technical Manager, Reference Systems Technology Group, Reference Systems Branch, Reconnaissance and Weapon Delivery Division

FOR THE COMMANDER

MERLE G. CARR
Asst Chief, Reconnaissance and Weapon Delivery Division

Copies of this report should not be returned unless return is required by security considerations, contractual obligations, or notice on a specific document.

SECURITY CLASSIFICATION OF THIS PAGE (When Data Entered)

19 REPORT DOCUMENTATION PAGE

READ INSTRUCTIONS BEFORE COMPLETING FORM

1. REPORT NUMBER 18 AFAL-TR-76-130 / 19	2. GOVT ACCESSION NO. 9 Final Rept. 13 Jun 75 - 7 May 76 / 3. RECIPIENT'S CATALOG NUMBER
4. TITLE (and Subtitle) 6 Q-Flex Accelerometer Thermal Performance Study	5. TYPE OF REPORT & PERIOD COVERED Final Report 6/13/75 - 5/7/76
	6. PERFORMING ORG. REPORT NUMBER 14 070-0955-001
7. AUTHOR(s) 10 Norm J. Klein, David B. Grindeland, Bruce D. Strachan	8. CONTRACT OR GRANT NUMBER(s) 15 In part under: F33615-75-C-1281
9. PERFORMING ORGANIZATION NAME AND ADDRESS Sundstrand Data Control, Inc. Overlake Industrial Park Redmond, Wa 98052	10. PROGRAM ELEMENT, PROJECT, TASK AREA & WORK UNIT NUMBERS P.E. 62204F Proj. 60950602
11. CONTROLLING OFFICE NAME AND ADDRESS Air Force Avionics Laboratory (RWA), Air Force Wright Aeronautical Lab. Air Force System Command, Wright-Patterson AFB, OH 45433	12. REPORT DATE 11 Sep[redacted]976 / 13. NUMBER OF PAGES 210
14. MONITORING AGENCY NAME & ADDRESS (if different from Controlling Office) 16 AF-6095 12 212p.	15. SECURITY CLASS. (of this report) Unclassified / 15a. DECLASSIFICATION/DOWNGRADING SCHEDULE

16. DISTRIBUTION STATEMENT (of this Report)

Distribution limited to U.S.Government agencies only; contains proprietary information: 21 May 1976. Other requests for this document must be referred to the Air Force Avionics Laboratory (AFAL/RWA) Wright-Patterson AFB, OH 45433

17. DISTRIBUTION STATEMENT (of the abstract entered in Block 20, if different from Report)

17 609506

18. SUPPLEMENTARY NOTES

19. KEY WORDS (Continue on reverse side if necessary and identify by block number)

Accelerometers; low cost; low thermal sensitivity; strapped down systems

20. ABSTRACT (Continue on reverse side if necessary and identify by block number)

The significance of this investigative effort to the Air Force is in thepursuit of low cost accelerometer with low thermal sensitivity and suitable for strapped down system application. The results of this Air Force research and development program indicate that the Q-Flex sensor can be modified to exhibit satisfactory performance characteristics under a "rapid-reaction" wide range static temperature environment. The results obtained demonstrate the ability to thermal model the characteristics of both bias and scale factor and suggest modifications to the structural design. With these modifications the Air Force may expect an →

1B

DD FORM 1 JAN 73 1473 EDITION OF 1 NOV 65 IS OBSOLETE

390539

SECURITY CLASSIFICATION OF THIS PAGE (When Data Entered)

20. ABSTRACT (Continued)

increase in both quantity and quality of accelerometers meeting the strapdown system thermal design goals through the Sundstrand sorting and selection process for inertial grade units.

FOREWORD

This publication is a final report of work performed under Wright Patterson Air Force Base Contract No. F33615-75-C1281 dated June 13, 1975. This report covers work conducted from June 1975 through April 1976. In addition, supplemental data has been provided within this report that was accomplished under Sundstrand internal research and development funding extending from the period June 1973 through April 1976.

The work was conducted by the Sundstrand Data Control Division of Sundstrand Corporation, Overlake Industrial Park, Redmond, Washington under the direction of N. J. Klein, Engineering Section Manager. The principal investigator was B. D. Strachan. A major contributor to the program was D. B. Grindeland. Extensive test and data support were provided by H. Meyer-Christians and J. K. Murphy.

TABLE OF CONTENTS

LIST OF FIGURES

LIST OF FIGURES (CONTINUED)

LIST OF FIGURES (CONTINUED)

LIST OF FIGURES (CONTINUED)

LIST OF FIGURES (CONTINUED)

LIST OF FIGURES (CONTINUED)

LIST OF FIGURES (CONTINUED)

LIST OF FIGURES (CONCLUDED)

LIST OF TABLES

LIST OF TABLES (CONTINUED)

LIST OF TABLES (CONTINUED)

LIST OF TABLES (CONCLUDED)

SECTION I

INTRODUCTION

The Sundstrand Q-Flex accelerometer is being used or proposed for use in many DOD strapdown inertial systems. The inherent problem with strapdown, body mounted measurement systems and one that delayed their development and limited some applications is the more rugged environment for both shock and vibration under which the sensors must operate. The Q-Flex design has demonstrated the ability to perform within the current performance requirements under most of these severe dynamic environments. Its ability to satisfy these goals has resulted in its use on production systems such as Harpoon, ACMR, Standard Missile, F111, B1 HARS and various missile systems.

Its flexure suspension system with no wear-out mechanism has allowed it to meet or exceed the the system reliability goals and the unique production philosophy of the Sundstrand Q-Flex has resulted in a high quality inertial accelerometer at two-thirds the cost of the next lowest cost unit within the present accelerometer market. For these reasons, it is being used or considered on development systems such as ATIGS and RCG.

With the aforementioned systems, where the Ring Laser Gyro provides "instant-on" performance, as well as the systems where the application of temperature control is undesirable and costly, the accelerometer should perform without thermal control over a wide static temperature range. Therefore, to satisfy these new objectives and to be cost effective, the Q-Flex accelerometer design must provide adequate accuracy by improving the thermal sensitivities and their related effects on performance. This program was thus aimed at studying the Q-Flex thermal characteristics and recommending corrective action to the design as required to satisfy the long term objectives of "instant-on" readiness for the current and the next generation of missiles and autonavigators in the weapon system arsenal.

The program goal for Phase I of the study contract was to perform a theoretical and experimental investigation of the Q-Flex thermal sensitivities and to develop design approaches for a thermal model that has eliminated, improved, or circumvented these sensitivities. The thrust of the effort was to characterize the existing design, correlate and analyze the interdependence of these sensitivities with their repeatability and stability parameters and then to recommend design modifications. This would lead to a preliminary accelerometer design which would allow the accelerometer to be used under wide temperature excursions without active thermal control.

Note that system performance is dependent upon the mission profile which includes accuracy of the output characteristics over specified temperature ranges. Since the Q-Flex may be integrated into systems where stringent inertial grade performance is required or into tactical missile applications where lesser performance is required, the goal for this program was to develop one design approach that would satisfy all the basic requirements. The fundamental approach was thus to develop a stable, predictable, modelable thermal profile of the bias and scale factor characteristics. The secondary goal was to develop preliminary design modifications that would significantly reduce these sensitivities. Both design approaches were subjected to close scrutiny to insure that satisfactory consideration was given towards reliability, maintainability and production cost of the accelerometer and its eventual integration into system hardware.

This report is intended to present the findings that relate specific Q-Flex parameters to the design goals. The study covers empirical test results from two classes of thermal, environmental exposure. The predominant effort concentrated on test results at various ambients after thermal exposure to narrow and wide static temperature ranges. Bias and scale factor characteristics after being subjected to this "rapid reaction" static temperature exposure is presented in Section III.

To characterize the structural design of the Q-Flex in a rapidly changing thermal environment and to isolate and to optimize the sensing point within the structure for thermal modeling of the instrument output, a "rapid warm-up" test program was performed. Test results of this activity are presented in Section IV.

SECTION II

SENSOR CONSTRUCTION

An objective of the program was to examine the phenomena which affect Q-Flex sensor scale factor and bias characteristics and their relationship to their thermal sensitivities. In order to satisfy this objective an overview of the construction and operation of the existing design is presented.

The heart of the Q-Flex accelerometer is the seismic system of fused quartz with integral pendulum, dual flexure suspension and outer support rim as shown in Figure 1. The choice of this material was based on its nearly perfect elasticity, which eliminates the hysteretic behavior characteristic of multimaterial or metal flexures.

The integral quartz pendulum, suspension and support structure are shaped from a ground and polished flat disc by a process of chemical milling. The parallel quartz flexures are batch processed from the original blank to a final thickness which is, in the last step, an individually controlled vernier etch to reduce the spring constant to within a family tolerance of ± 10%.

The sensor is shown in exploded view, Figure 2. The proof mass assembly consists of the monolithic, specially processed fused silica element to which two aluminum-bobbin, series-wound torquer coils are attached. Conducting leads for the differential pick-offs and the torquer coil drive current are provided by vacuum depositing a chrome-gold thin layer on the quartz structure and carrying these metallic films across both sides of the quartz flexures. The torque coils are bonded symmetrically to the sides of the central disc and the copper wire terminations to the conducting torquer traces. The gold traces across the flexures are terminated on the support rim

Figure 1

FUSED QUARTZ PROOF MASS ELEMENT WITHOUT GOLD DEPOSIT

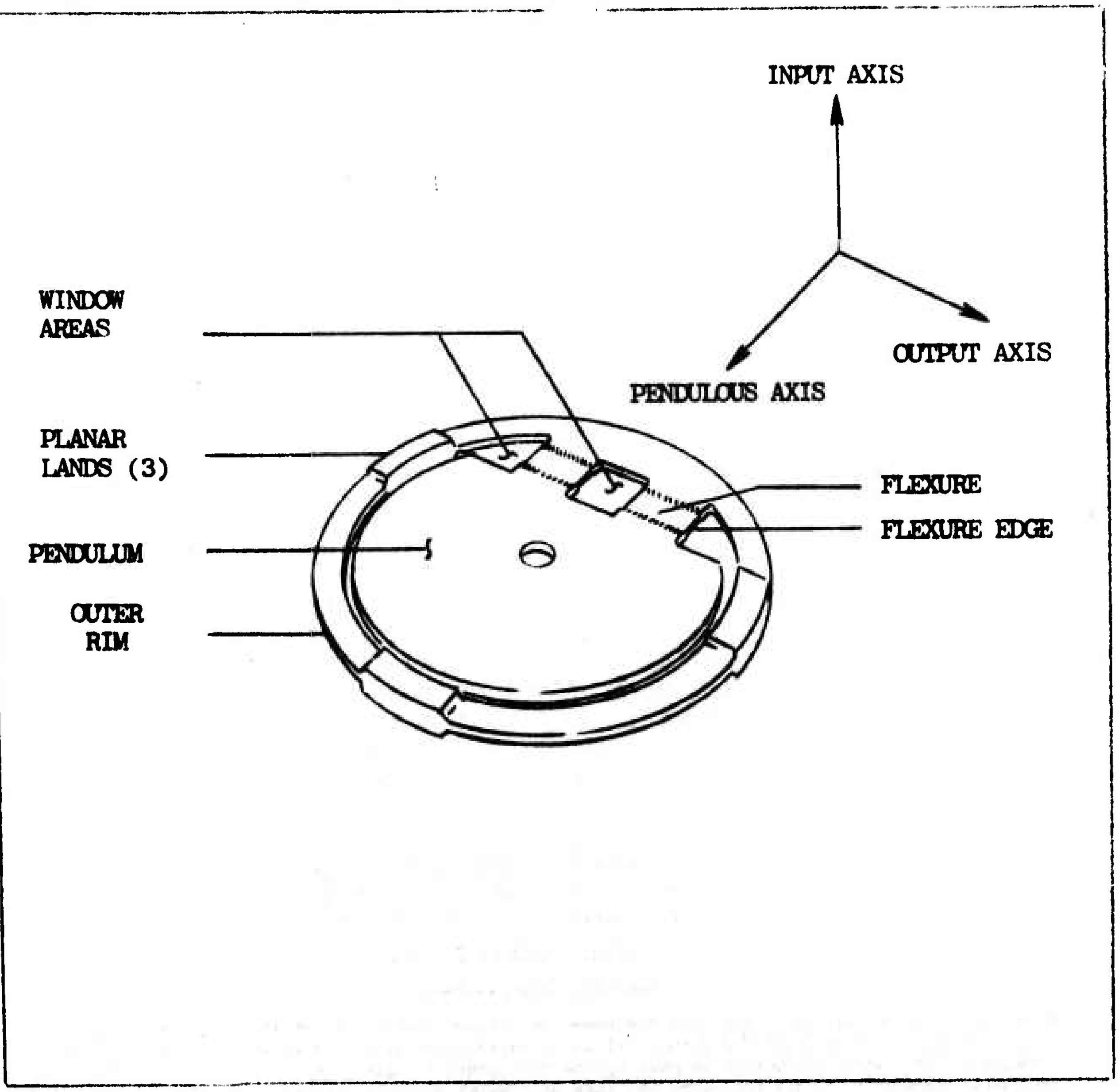

Figure 2

EXPLODED VIEW OF THE Q-FLEX SENSOR

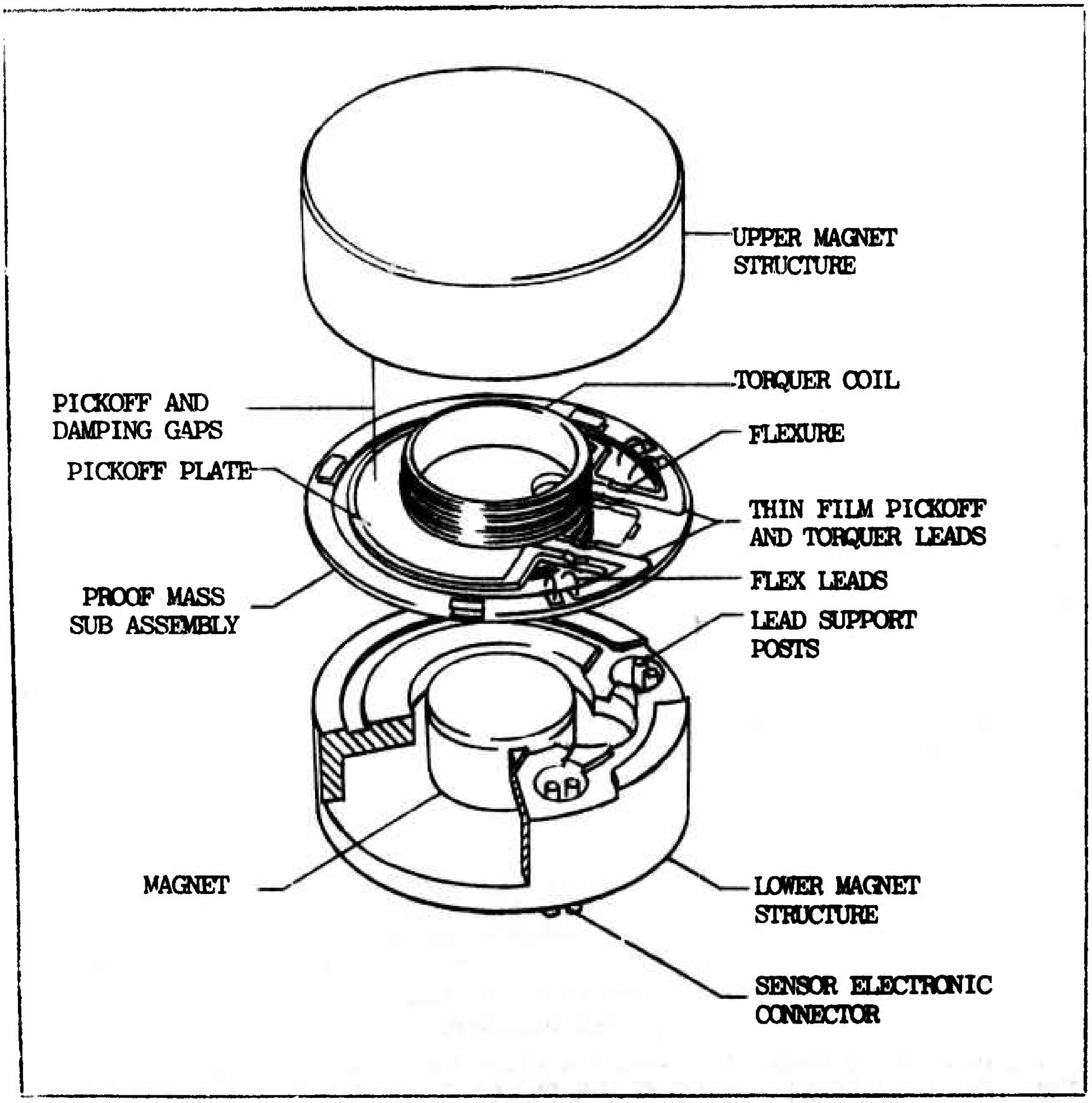

[redacted]

where four thermocompression bonded one mil wires are used to couple the signal junctions from the seismic element to the signal posts in the lower magnet structure.

The sensor, which constitutes the basic measuring element of the Q-Flex accelerometer, is comprised of the quartz seismic assembly and two cylindrical, low coefficient Invar permanent magnetic structures with lapped planar faces which clamp the quartz support ring of the seismic assembly on three planar lands which are elevated above the planar surface of the pendulum on each side by 750 micro-inches (3/4 mil). (See Figure 1.) This planar separation defines the limits of pendulum motion in the acceleration-sensing (Input-Axis) direction between mechanical stops; and it establishes the spacing between vacuum-deposited gold electrodes on the faces of the pendulum and corresponding planar lapped faces of the Invar magnetic structures which form two capacitors which electrically define the position of the pendulum.

The three-part sensor is assembled on tooling rails such that the two torquer coils carried by the pendulum are centered in corresponding annular permanent magnetic gaps. The normal loading of the three-part sandwich, which maintains alignment of the parts, is made permanent by a median band of Invar with a width which bridges on the outside diameter between the two Invar magnetic structures, and which is fixed in place by epoxy bonding.

For the standard Q-Flex product line, the sensor is mounted from the inside diameter of a standard one-inch O.D. stainless steel cover with integral mounting flange having a planar mounting face which is perpendicular to the cylindrical axis of the cover.

The sensor is installed inside the cover such that the input axis of the sensor is orthogonal to the mounting surface of the flange within acceptable tolerance for axis misalignment. The

sensor is fixed to the I.D. of the cover by a continuous band of epoxy, which preserves electrical insulation between signal ground potential of the sensor and the outer case ground.

The sensor/cover assembly of the Sundstrand Q-Flex (quartz flexure) accelerometer is made as a standard product for all applications. All standard Q-Flex sensor screening tests are performed at this level since, after the sensor is mated permanently with its outer cover, quantitative performance characteristics may be permanently identified with each serialized unit.

Standard sensor/cover screening tests grade the Q-Flex sensors for performance over a wide range of temperature, and for survivability to 250 g levels of shock in any axis. Additional special tests are applied to qualify candidate sensor/cover assemblies for the requirements of special programs. All sensors fulfilling the most basic requirements of the standard screening tests qualify for use in salable Q-Flex Instrumentation Grade accelerometers. Higher performance sensors are used first to satisfy more demanding program requirements. Economy of all Q-Flex products is achieved by commonality of all sensor parts, fabrication and assembly processes, and basic sensor screening tests at the sensor/cover level.

STARTING DATA

Prior to this program and through the 1975 time frame several thousand Q-Flex sensors have been tested. Quarterly data summaries from these tests are presented in Figures 3 and 4. This data represents normal production performance from instruments screened and sorted during sensor testing. Since the introduction, in July 1973, of thermocompression bonds on the seismic element for flex lead attachment, the performance data have been extremely well behaved and consistent. The uncompensated sensor bias and bias temperature coefficient as depicted in Figure 3 are relatively constant. The absolute and algebraic values for bias are approximately 1 milli-g and 100 micro-g's respectively. The absolute and algebraic values for bias thermal sensitivity are approximately 9 micro-g per °F and 1.5 micro-g per °F respectively. The significance of the algebraic mean approaching zero value is that it connotes design symmetry within the sensor for these two parametric functions.

The characteristic of bias, bias thermal hysteresis, defined as the difference between ambient bias measured after a cold soak at -65°F and bias measured after a hot exposure at 225°F is also displayed. The data depict an absolute bias thermal hysteresis of approximately 240 μg in early 1974 decreasing to less than 180 μg in January 1976. The algebraic mean which had always closely followed the absolute value has recently become much smaller, and approaches 60 μg's. These improvements are attributed to better process control and modified assembly techniques to improve processing symmetry. The reduction in the algebraic hysteresis function during the last six months is informative. The significance of this characteristic will be discussed in the Section III.

Scale factor characteristics have also been tabulated for the 1974 to 1976 time frame and are presented in Figure 4. The average value of scale factor is controlled by magnet strength and geometry design. Small variations in vendor material and variations in coil bobbin weight contribute primarily to scale factor variations. The scale factor thermal hysteresis has decreased during the two and one-half year time frame from 320 ppm to 170 ppm. Ana-

Figure 3

Q-FLEX PRODUCTION BIAS DATA
Six Month Averages For 1974-1976
Absolute (■) And Algebraic (●)

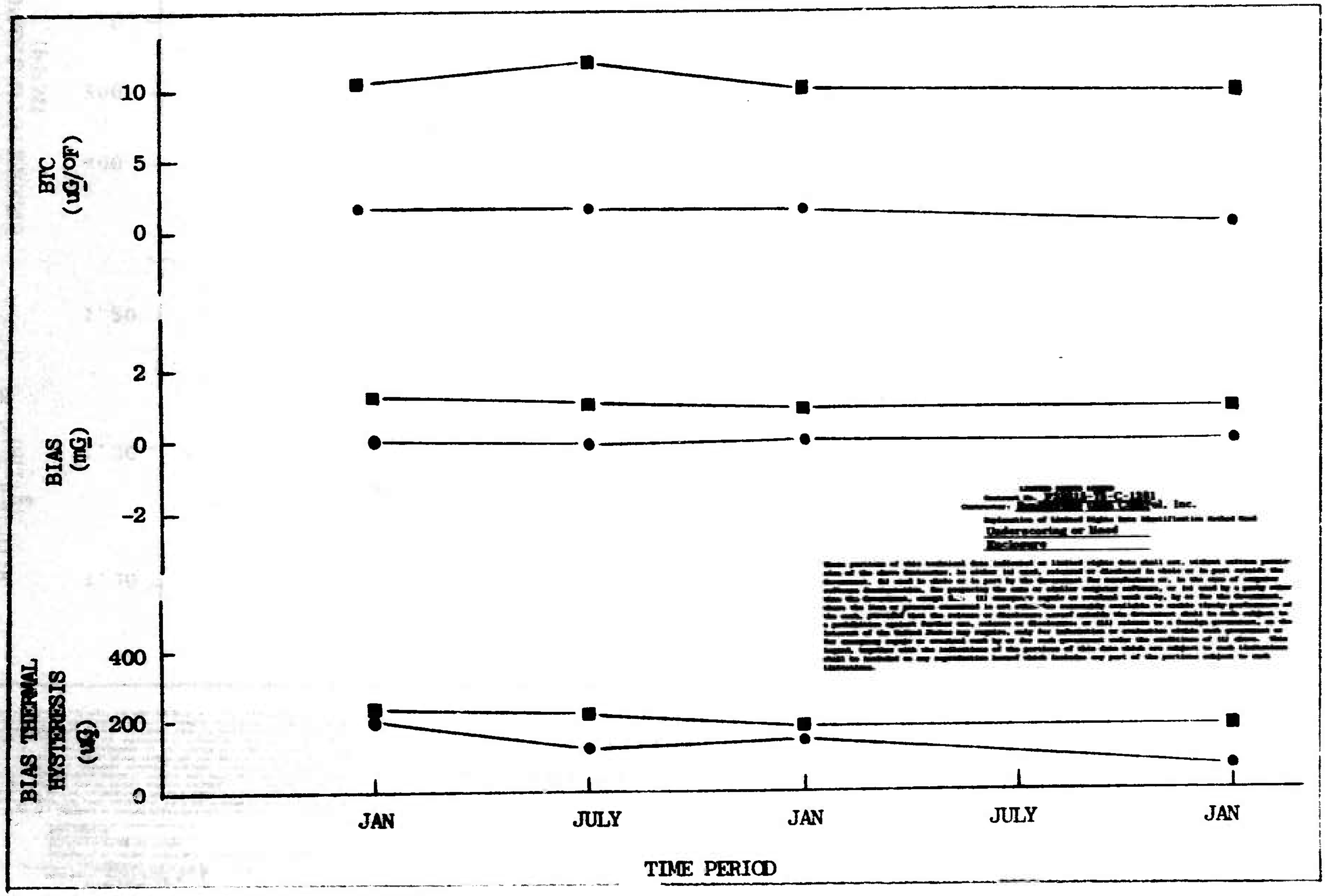

Figure 4

Q - FLEX PRODUCTION SCALE FACTOR DATA

SIX MONTH AVERAGES FOR
1974 - 1976

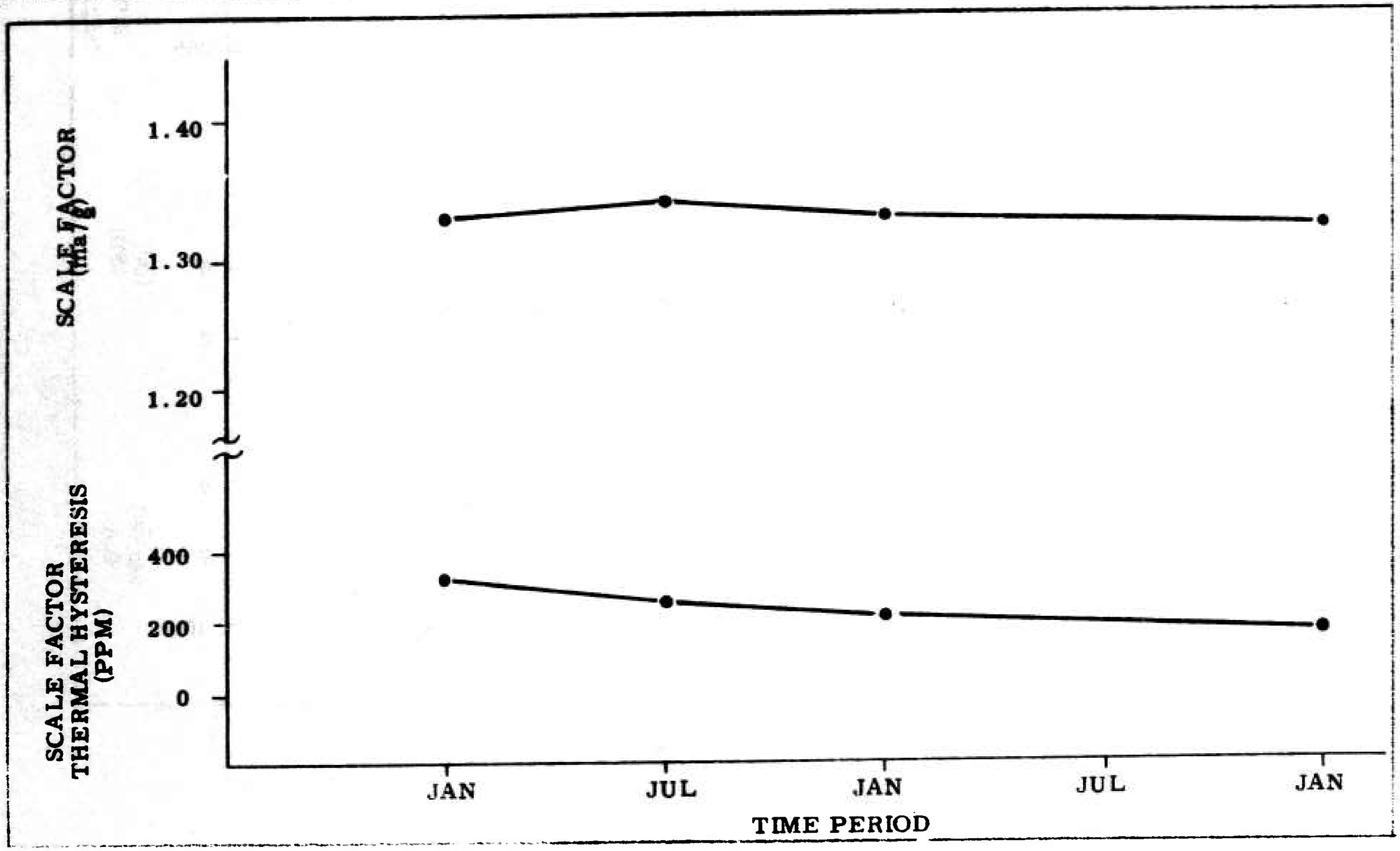

lysis of this characteristic is discussed in Section III.

Since it appeared at the outset that the hysteretic behavior of bias and scale factor would prove difficult to model, the characterization of the thermal hysteresis parameters and an understanding of their driving functions was one goal of the study.

In addition to thermal parameters, data could be provided to demonstrate the performance characteristics due to other environmental exposures such as vibration and shock. This data is important in evaluating the overall performance capability of any device, especially the intertial strapdown unit which is subjected to a much harsher environment than in the gimballed system. To satisfy the total system objectives, but not compromise the major thrust of the thermal study, limited data is provided demonstrating existing performance characteristics to strapdown environments.

Figures 5 through 9 display Engineering Design Integrity Test data for the Harpoon program accelerometer, Sundstrand Part Number 979-0050-005. These tests were performed during the July-August 1975 time period. Figures 5 and 6 depict bias and scale factor stability through severe vibration and shock environments over the one month test period. The large jumps in scale factor are due to scale factor thermal hysteresis effects, i.e. scale factor once measured after hot soak and the next time after cold soak. Figures 7 through 9 present vibration rectification coefficient data from S/N 155 which is typical of these instruments. It demonstrates the small sensitivity to vibration with the unique Q-Flex pendulum construction.

Additional data on bias and scale factor shock repeatability are provided in Table 1 from 9 ATIGS units delivered to Honeywell around January 1975. These units were tested for repeatability characteristics to support potential use on the "fly-shock-fly" system for Cruise Missile evaluation.

Pyrotechnic shock data was provided for a Harpoon evaluation program and data are presented in Table 2 and Figure 10. The above data provide the technical baseline for performance characteristics of the existing Q-Flex design.

Figure 5

SHEET NO. A2-1

TEST DATA

TEST: BIAS REPEATIBLITY (SUMMARY) **SPECIMENS:** HARPOON ACCELEROMETER

CONDUCTED PER: 979-0050-101 Para. 4.4 **PART NO.** 979-0050-005

DATE STARTED: 7-9-75 **ENDED:** 8-6-75 **SERIAL NO.** 155,156,&157

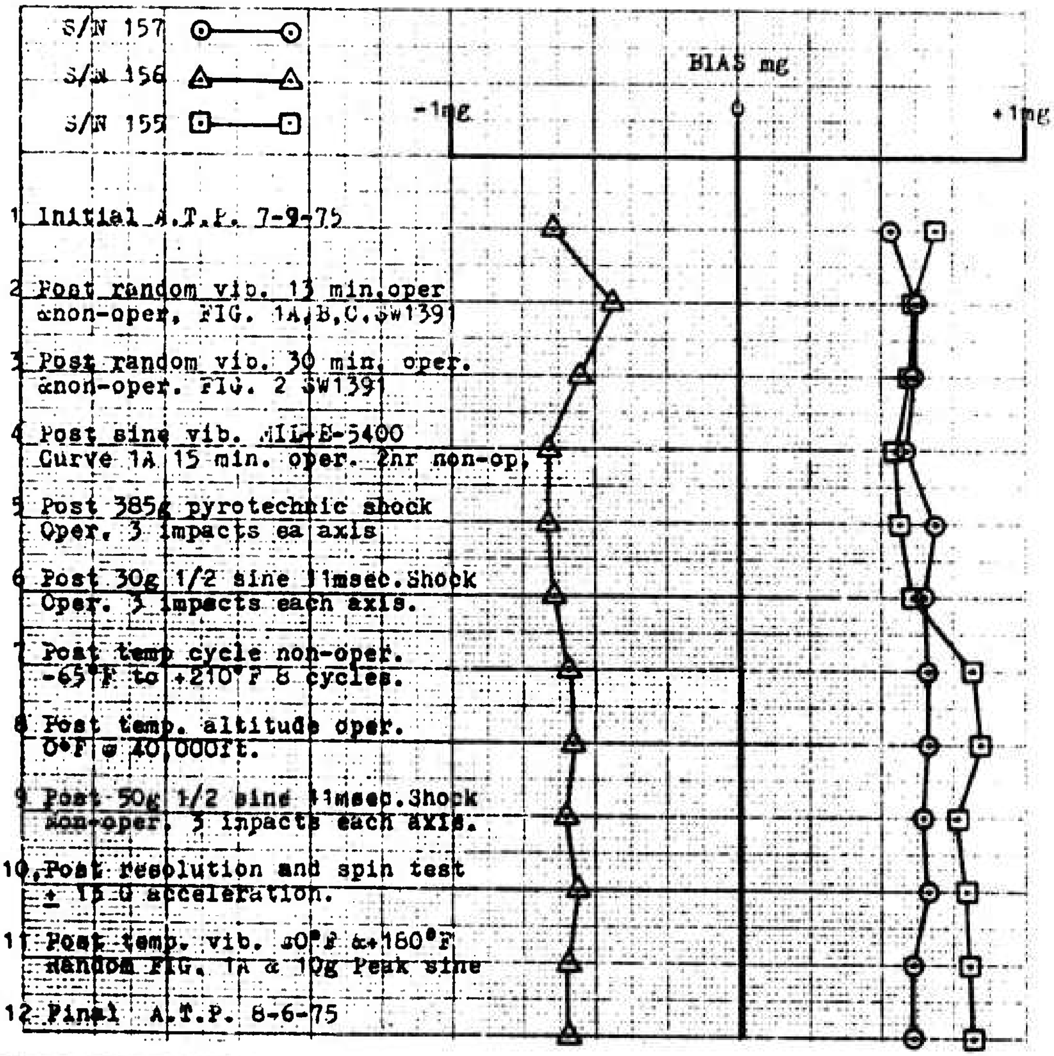

CONDUCTED BY	CODE IDENT	SIZE	PAGE NUMBER	UNIVERSAL REPORT NUMBER
M.C. [illegible]			A2-1	
APPROVED BY	NO. 97896	A	REVISION	ORIGINATORS REPORT DOC NO.
F.W. [illegible]				979-0050-405

[illegible]

Figure 6

SHEET NO. A2-2

TEST DATA

TEST: SCALE FACTOR STABILITY (SUMMARY) **SPECIMENS:** HARPOON ACCELEROMETER

CONDUCTED PER: 979-0050-101 Para. 4.4 **PART NO.** 979-0050-005

DATE STARTED: 7-9-75 **ENDED:** 8-6-75 **SERIAL NO.** 155,156,&157

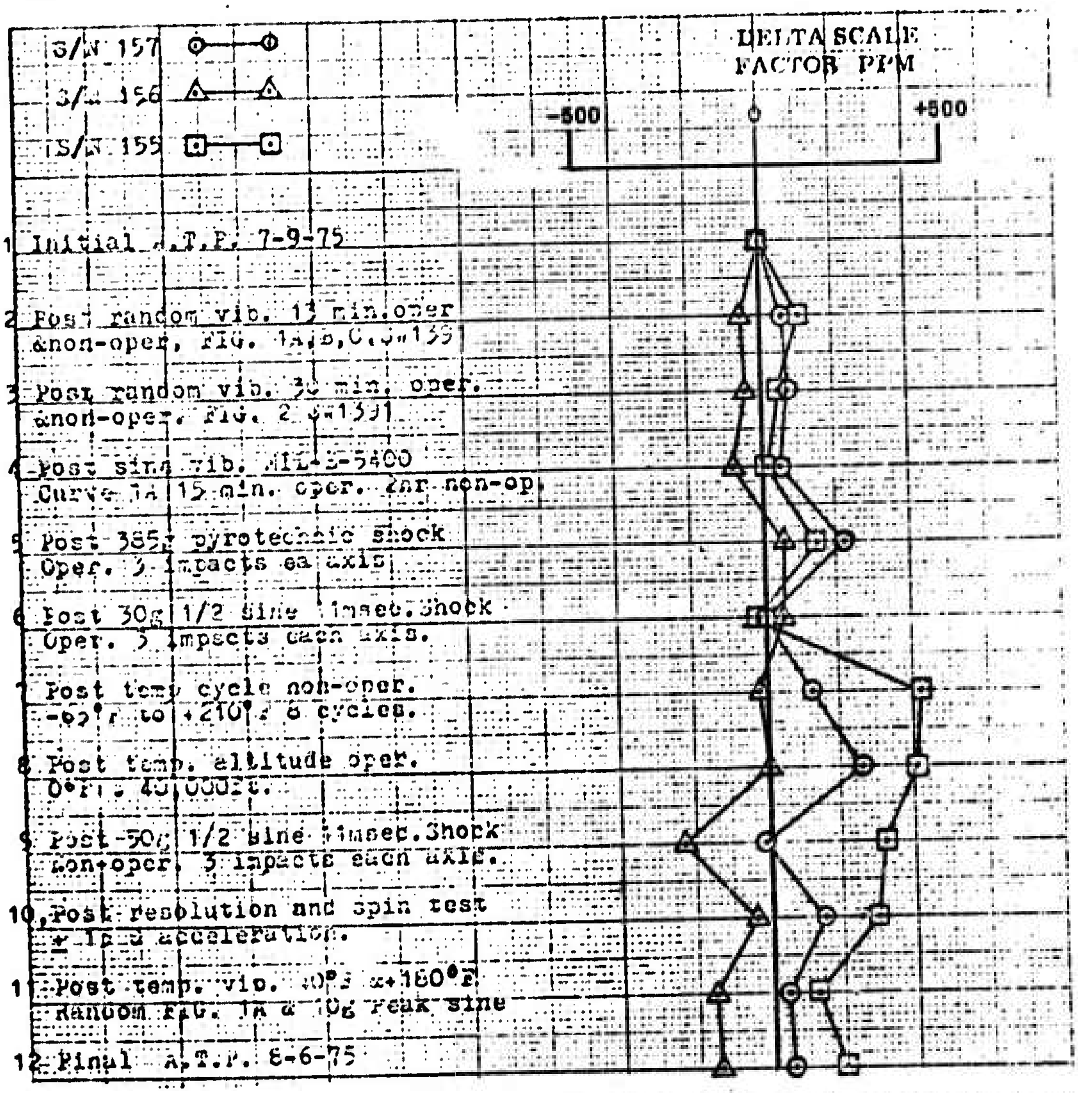

CONDUCTED BY	CODE IDENT	SIZE	PAGE NUMBER	UNIVERSAL REPORT NUMBER
M.C. Thompson			A2-2	
APPROVED BY	NO. 97396	A	REVISION	ORIGINATORS REPORT DOC NO. 979-0050-405
F. Hahn				

[illegible]

Figure 7

SHEET NO.

TEST DATA

TEST: VIBRATION RECTIFICATION RANDOM SUMMARY **SPECIMENS:** HARPOON ACCELEROMETER

CONDUCTED PER: L.S.I. SW 1391 FIGURE'S 1 A, B, &C. **PART NO.** 979-0050-005

DATE STARTED: 7-11-75 **ENDED:** 7-15-75 **SERIAL NO.** 155

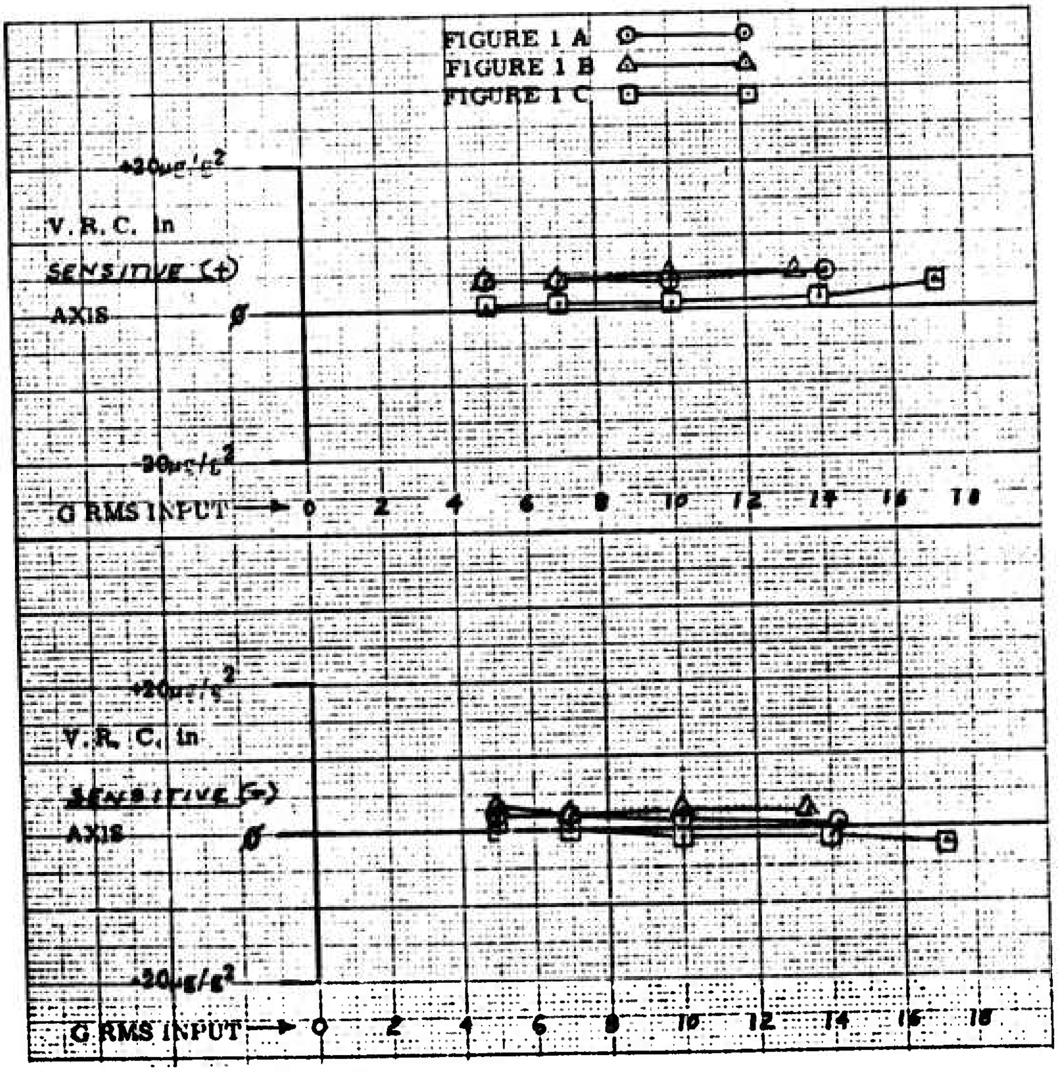

CONDUCTED BY	CODE IDENT	SIZE	PAGE NUMBER	UNIVERSAL REPORT NUMBER
M.C. [signature]			A2-3	
APPROVED BY F.U. [signature]	NO. 97896	A	REVISION	ORIGINATORS REPORT DOC NO. 979-0050-405

Figure 8

SHEET NO. A2-4

TEST DATA

TEST: VIBRATION RECTIFICATION RANDOM SUMMARY

SPECIMENS: HARPOON ACCELEROMETER

CONDUCTED PER: L.S.I. SW 1391 FIGURE'S 1 A, B, &C.

PART NO. 979-0050-005

DATE STARTED: 7-11-75 ENDED: 7-15-75 SERIAL NO. 155

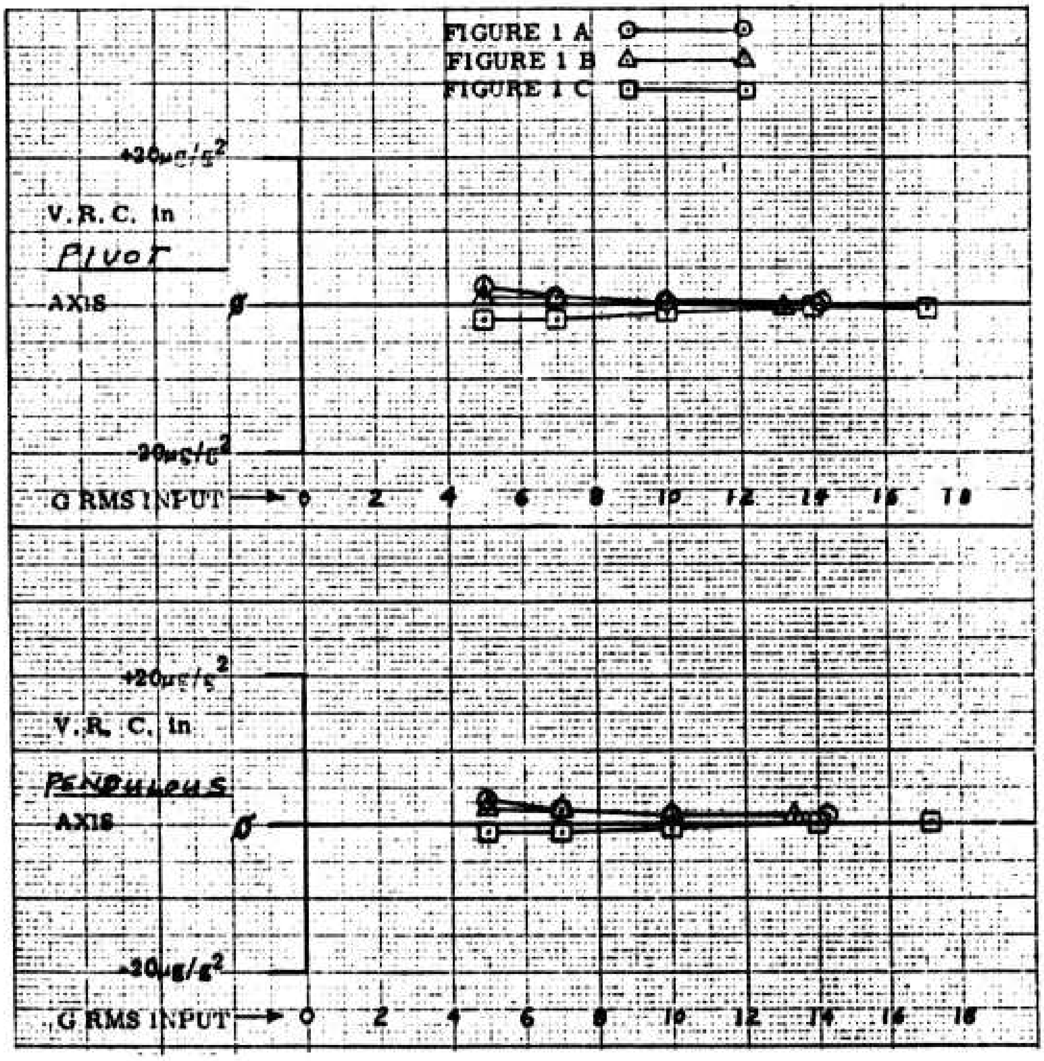

CONDUCTED BY	CODE IDENT	SIZE	PAGE NUMBER	UNIVERSAL REPORT NUMBER
H.C. [illegible]			A2-4	
APPROVED BY F.U. Holden	NO. 97096	A	REVISION	ORIGINATORS REPORT DOC NO. 979-0050-405

Contract No. [illegible]-C-1381
Contractor: [redacted]el. Inc.

[illegible]

15

Figure 9

TEST DATA

SHEET NO. [illegible]

TEST: TEMPERATURE VIBRATION RANDOM V.R.C. (SUMMARY) **SPECIMENS:** HARPOON ACCELEROMETER

CONDUCTED PER: TEMP. VIBRATION PER SW1391 FIGURE 1 A **PART NO.** 979-0050-005

DATE STARTED: 8-1-75 **ENDED:** 8-4-75 **SERIAL NO.** 155

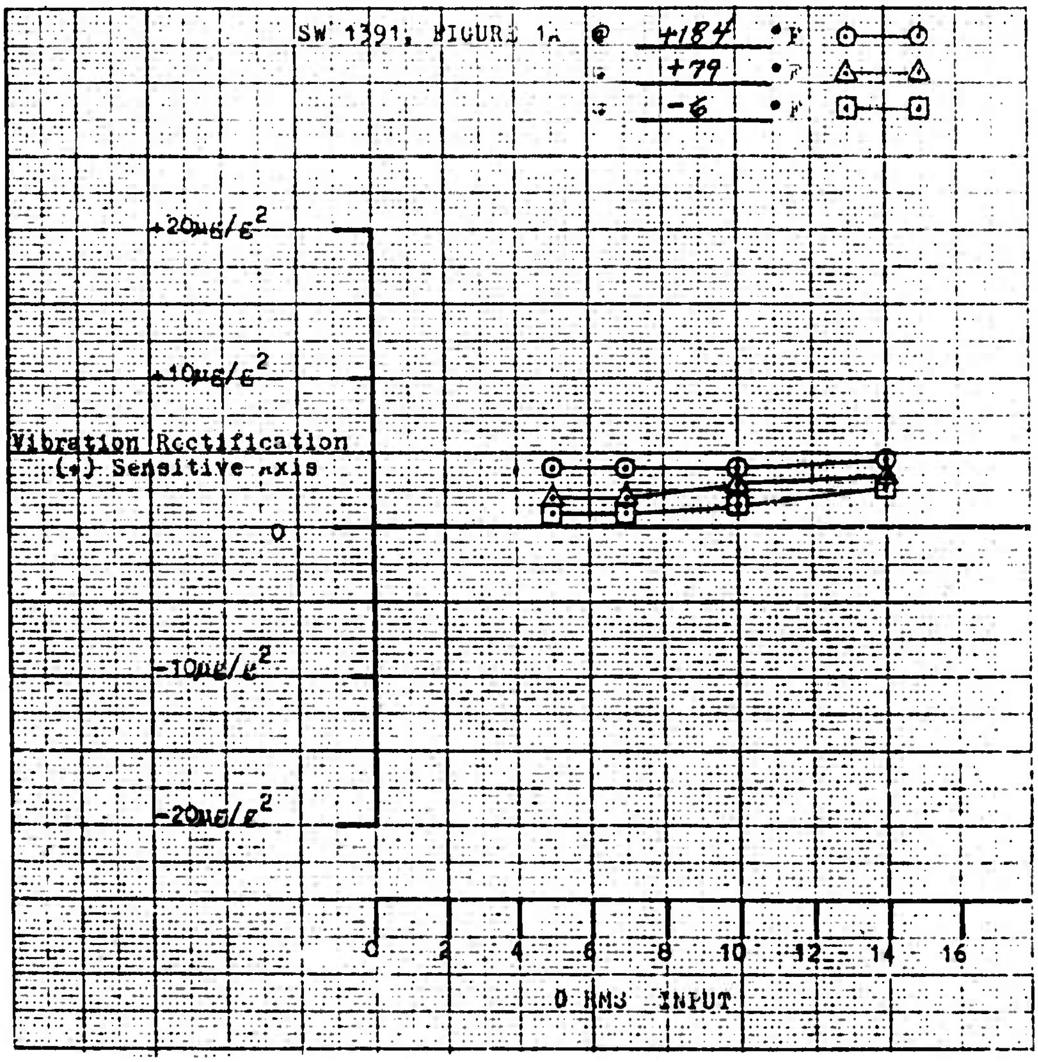

CONDUCTED BY	CODE IDENT	SIZE	PAGE NUMBER	UNIVERSAL REPORT NUMBER
APPROVED BY	NO. 97896	A	A2-11	
			REVISION	ORIGINATORS REPORT DOC NO. 979-0050-405

Figure 9

SHEET NO.

TEST DATA

TEST: TEMPERATURE VIBRATION RANDOM V.R.C. (SUMMARY) **SPECIMENS:** HARPOON ACCELEROMETER

CONDUCTED PER: TEMP. VIBRATION PER SW1391 FIGURE 1 A **PART NO.** 979-0050-005

DATE STARTED: 8-1-75 **ENDED:** 8-4-75 **SERIAL NO.** 155

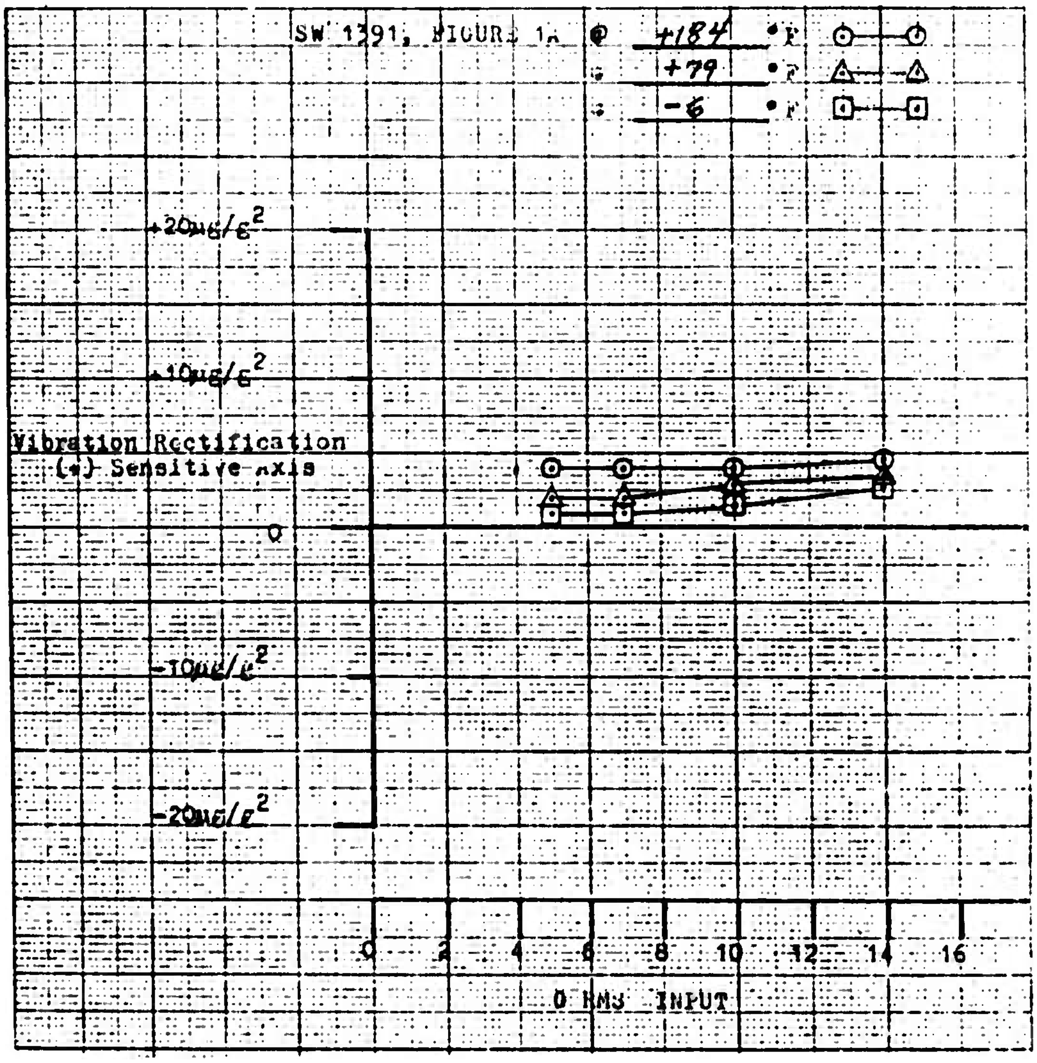

CONDUCTED BY	CODE IDENT	SIZE	PAGE NUMBER	UNIVERSAL REPORT NUMBER
APPROVED BY	NO. 97896	A	A2-11	
			REVISION	ORIGINATORS REPORT DOC NO. 979-0050-405

Table 1

GROOVE AND SLOT BIAS REPEATABILITY THRU SHOCK

Sample - 9 ATIGS UNITS

Shock Pulse - 6 msec - 1/2 sine

Direction - 250 G 3 times, Preconditioning Exposure / 50, 100, 150, 200 G 10 times — along each of 6 axes

Shock Level (g's Peak)	50	100	150	200
ABS AVE Bias Change (ug)	33	31	32	35
SIGMA (ug)	44	27	20	19
ABS AVE Scale Factor Change ppm	63	93	60	96
SIGMA (ppm)	64	91	39	93

NOTE: 9 units each exposed to 258 mechanical shocks.
bias also includes mounting sensitivity.

Table 2

GROOVE AND SLOT BIAS REPEATABILITY
THRU PYROTECHNIC SHOCK

SAMPLE - 7 S/C Assy's

SHOCK PULSE - 1 msec, 1/2 sine

DIRECTION - C ce along each of 6 axes

Shock Level (g's peak)	250	320	385
ABS Avg Bias Change (ug)	23	31	29
Sigma (ug)	40	27	37

NOTE: Bias measured after each shock without removal from shock fixture, therefore Bias does not include mounting sensitivity.

Each unit exposed to 18 mechanical shocks.

Figure 10

BIAS STABILITY THRU SHOCK

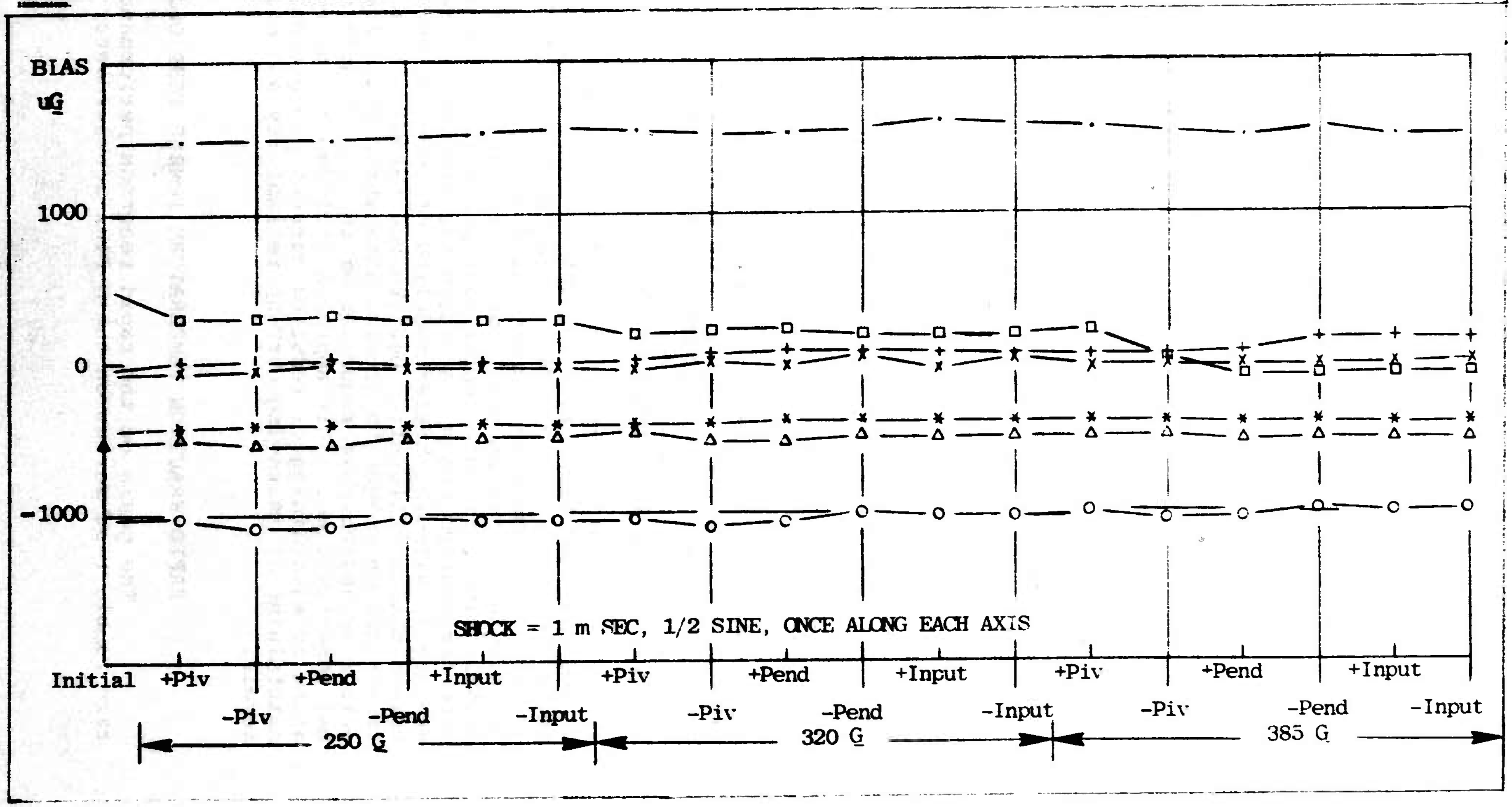

SECTION III

DESCRIPTION OF "RAPID REACTION"

Widespread use of strapdown systems has become a reality because they offer more configuration flexibility and lower cost potential than their predecessor gimballed systems. One major system cost factor common to both types of inertial guidance systems is inertial sensor thermal sensitivity. Active thermal control has historically been a system design approach to reduce thermal performance effects by tightly controlling the system temperature at a level higher than any ambient that may be encountered. This approach becomes detrimental in day-to-day operations such as aircraft applications where in effect, the system is thermally cycled each time the system is turned on and shut down.

High thermal gradients are induced across the inertial sensors during 'fast' warm-up to the control temperature. These gradients induce mass shifts which degrade sensor accuracy and necessitate frequent recalibration. Besides the variable warm up time from different initial system ambient temperatures, additional time must be allowed for system stabilization prior to system alignment. Stable element warpage due to strip heater location and its effect on inertial sensor input axes relative to each other are serious design factors limiting the earliest time that system alignment procedures can begin. Complex and expensive multistage Kalman filters have been utilized to model the combined inertial sensor, stable element, and system thermal environment response to warm up heater input. Additional system cost factors include separate heater power supplies and heater cut-off and control temperature BITE circuit monitors.

Recently, experimental data indicate adequate accuracy can be obtained from dry, 'instant-on' instruments without active thermal control over a wide temperature range. This 'rapid reaction' environment is characterized as being a static or slowly changing system ambient temperature over the range -70° to +200°F. The inertial sensors must perform accurately over this wide temperature range. Although the temperature rates of change are small, allowing better modeling of inertial sensor temperature versus static calibration performance parameters, the following investigation sought to provide data which could lead to the elimination or appreciable reduction of the Q-Flex accelerometer thermal sensitivities. This approach included giving equal consideration to maintaining or reducing current production cost and maintaining or improving current reliability and maintainability levels.

RAPID REACTION TEMPERATURE TUMBLE TEST OBJECTIVES

The goals of the rapid reaction performance temperature tumble test series on the Q-Flex accelerometer were:

1) Measure and model the magnitudes and thermal sensitivities of scale factor and bias.

2) Determine the degree of model fit to actual scale factor and bias measured values (individual test RMS residuals).

3) Measure and model scale factor and bias at least three times over the -65°F to +225°F temperature range under rigorously controlled conditions to determine the time stability of the Q-Flex scale factor and bias characteristics referenced to the initial model.

4) From the wide temperature range measurements, determine the degree of scale factor and bias thermal hysteresis by modeling ascending temperature and descending temperature output data independently and analyzing the differences in the models obtained.

5) Design and perform a series of limited temperature range tests to measure and model scale factor and bias thermal hysteresis as a function of temperature cycle center temperature and extent.

6) Analyze the above minor loop data to determine whether the thermal hysteresis values for the limited range temperature cycles are a subset within the thermal hysteresis values measured over the full -65°F to +225°F temperature cycle range.

7) Investigate all test result anomalies and construct additional special tests to further isolate and identify the characteristics and possible source of each anomaly. (Note: Scale factor 'relaxation' following hot soak and its time dependent affect on measured values of scale factor thermal hysteresis were investigated as a result of this goal.

8) Review the test results and the possible Q-Flex design sources for thermal sensitivities in order to identify specific

design features warranting modification to eliminate, reduce, or circumvent Q-Flex accelerometer thermal performance characteristics.

THERMAL STUDY PROGRAM

The performance history of the Q-Flex accelerometer was reviewed with the objective of identifying sources of thermal sensitivity. The thermal sensitivity characteristics of scale factor and bias were subjected to intense scrutiny for common factors suggesting interdependence. No common factors in either temperature sensitivity or thermal hysteresis characteristics were observed. Thus, the results of this thermal study program and the effects on instrument design factors are presented in separate bias characteristic and scale factor characteristic sections.

Sundstrand Data Control, Inc. funded development experiments on configuration modifications have paralleled the investigation of the current Q-Flex production design. The results of development activities prior to and during this study program are presented in the discussion of present design test results. The insight gained from conducting these rigorously controlled thermal environment tests is significant.

The data bank of actual Q-Flex accelerometer performance results over widely varying time and thermal conditions, by itself, is a valuable tool for system error budget analysis.

The model chosen to represent the Q-Flex accelerometer output current as a function of ambient temperature, T, and input acceleration, G, is: $I(T) = K_1(T)(G + K_o(T) \times 10^{-3})$ where:

$I(T)$ = output current, mA
G = input acceleration, g
$K_1(T)$ = scale factor, mA per g
$K_o(T)$ = bias, milli-g

The factors $K_1(T)$ and $K_o(T)$ have been further defined as polynomial models normalized to 0°F and having coefficients to the first, second, and third power of ambient temperature, T. Separate calculations of the scale factor, K_1, and bias, K_o, models for temperature increasing from -65°F to +225°F and for temperature decreasing from +225°F to -65°F permit examination of thermal hysteresis characteristics.

DESCRIPTION OF TESTING PROGRAM AND ANALYSIS

Hysteresis Test Program

The rapid reaction performance temperature tumble tests consisted of a series of experiments where four Q-Flex accelerometers were tumble tested at ± 1 g for various environmental temperature sequences. The hysteresis series consisted of six

minor temperature cycles in the range of -65°F to 225°F and are designated A through F. Accelerometers were temperature cycled twice between a low temperature, T_L, and a high temperature, T_H, and ± 1 g tumble test data taken at T_L, T_H, and the mean cycle temperature, T_M. The accelerometers were hot soaked at 240 ± 10°F no more than 16 hours prior to each minor temperature cycle and a tumble test at 70 ± 1°F was performed immediately prior to each temperature cycle.

The values of T_L, T_M, and T_H, as well as the cycle extent, ΔT, for the six minor temperature cycles are listed in Table 3. Each minor cycle required one day to perform. The series A through F was performed three times during 42 days of testing.

Extended Temperature Tumble Tests, ET3, were performed before each series. The resulting models of scale factor and bias temperature coefficient were used to reduce the minor temperature cycle data.

Table 3

RAPID REACTION TEMPERATURE TUMBLE TESTS

LOOP	T_L (°F)	T_M (°F)	T_H (°F)	ΔT (°F)
A	-65	80	225	±145
B	-30	80	190	±110
C	0	80	160	± 80
D	30	80	130	± 50
E	-65	15	95	± 80
F	+65	145	225	± 80

Thermal hysteresis data as a function of ΔT at constant T_M and as a function of T_M at constant ΔT was derived from the minor temperature cycles. Cycles A, B, C, and D provide thermal hysteresis data for ΔT ranging between ±50°F and ±145°F and T_M = 80°F. Cycles C, E, and F provide thermal hysteresis data for T_M ranging between 15°F and 145°F and ΔT = ± 80°F. Stability data at -65°F, 15°F, 70°F, 145°F and 225°F were obtained from appropriate minor cycles in the series.

The order of temperatures in a minor cycle was 70°F, T_L, T_M, T_H, T_M, T_L, T_M, T_H, T_M and the accelerometers were tumble tested twice at each temperature. Data measured at each temperature was:

1) T_A Lab ambient temperature, °F
2) T_B Bracket or accelerometer flange temperature, °F
3) $V_T(+1\underline{g})$ Torque coil voltage in +1$\underline{g}$ position, VDC
4) $V_O(+1\underline{g})$ +1$\underline{g}$ output voltage, VDC
5) $V_O(-1\underline{g})$ -1$\underline{g}$ output voltage, VDC

Scale factor, bias, and torque coil resistance were calculated from this data to monitor the experiment.

Minor temperature cycle data was reduced and tabulated with the computer program RAPRED. The program calculated raw torque coil temperature, scale factor and bias and these values were compensated for ambient temperature variations. Since the temperatures T_L, T_M, and T_H were set only to an accuracy of $\pm$5°F, the current polynomial models for scale factor and bias temperature coefficient were used to correct the measured scale factor and bias to the assigned minor cycle temperatures.

Thermal hysteresis values were calculated at T_M for each half of the minor temperature cycle. Also the shift of average scale factor and bias at T_M was calculated to determine systematic trend in the thermal hysteresis center. The reduced results of minor cycles were tabulated giving the cycle temperatures, center and extent, reduced scale factor and bias, and thermal hysteresis data.

Extended Tumble Test (ET3) Program

Each ET3 consisted of an increasing temperature leg from -65°F to 225°F on the first day of testing followed by an overnight dwell at 225°F and a decreasing temperature leg from 225°F to -65°F on the second day. Two to three days prior to each ET3, the accelerometers were nonoperatively hot soaked at 240 $\pm$ 10°F for 1.0 hour and stored at ambient prior to testing. Scale factor and bias data were measured in $\pm$1$\underline{g}$ tumble tests at eight temperatures on both the increasing and decreasing temperature legs. Two $\pm$1$\underline{g}$ output voltage readings were made at the following temperatures: -65°F, -24°F, 18°F, 59°F, 101°F, 142°F, 184°F, 225°F. Temperatures were set to $\pm$10°F and measured to a differential accuracy of $\pm$ .1°F by calculating the torque coil resistance. Prior to the increasing temperature leg of the ET3, a tumble test at 70°F was performed to monitor scale factor and bias stability.

Extended temperature tumble tests were conducted three times on each of four Q-Flex accelerometers over a period of 29 days. These ET3's are contained within the interval of 42 days of rapid reaction performance testing. Data reduction for the ET3 was performed with the ET3FIT computer program. The raw ET3 data was used to calculate raw scale factors, biases, temperatures, and load resistances at 16 points on the increasing and decreasing temperature legs. Polynomial models for scale factor, bias, and thermal hysteresis were determined using orthogonal polynomial least squares and coefficient transformation routines. Values for scale factor, bias, and residuals were calculated and printed in tabular form. Polynomial coefficients were printed in a second table.

Analysis - Thermal Hysteresis Versus Temperature Cycle Center and Extent

Scale factor and bias thermal hysteresis data collected from temperature tumble tests was modeled versus temperature cycle extent and center, ΔT and T_M. The minor cycles have temperature extents of $\pm$ 80°F and temperature center at 15°F, 80°F, and 145°F. The ET3 hysteresis models have an extent of $\pm$ 145°F and are centered at 80°F.

Straight lines were fitted to each data set using least squares calculations. Thermal hysteresis at the middle of temperature cycle was modeled because thermal hysteresis normally has a maximum value near midcycle.

For thermal hysteresis versus ΔT at constant T_M the general model equation was:

$$TH(\Delta T) = C_1 \times \Delta T + C_2$$

where

$TH(\Delta T)$ = Thermal hysteresis in PPM or μg at ΔT

C_1 = Slope in PPM per °F or μg per °F

ΔT = temperature cycle extent in °F

C_2 = thermal hysteresis at $\Delta T=0$ calculated by least squares fit.

The temperature cycle extent ΔT was defined as

$$\Delta T = \pm (T_H - T_L)/2$$

and values of $\pm$ 50°F, $\pm$ 80°F, $\pm$ 110°F and $\pm$ 145°F were available for modeling. The center of these minor cycles was 80°F. Two or three values of thermal hysteresis were available for modeling at each value of ΔT, giving a total of 8 to 12 points for modeling. In the plots which follow, thermal hysteresis points at each value of ΔT are averaged to clarify the plots but individual points were used for modeling.

The modeling equation for thermal hysteresis versus T_M at constant Δ T was

$$TH(T_M) = C_3 \times T_M + C_4$$

where

$TH\ T_M)$ = thermal hysteresis at T_M in PPM or μg.

C_3 = slope in PPM/°F or μg/°F

T_M = center temperature of the minor cycle in °F.

C_4 = thermal hysteresis at T_M = 0°F.

The temperature cycle center temperatures available were 15°F, 80°F and 145°F and the temperature cycle extent was ±80°F.

Major Loop Thermal Hysteresis Polynomial Models

Polynomial models for both scale factor and bias were determined for temperature increasing from -65°F to 225°F and for temperature decreasing from 225°F to -65°F. These profiles are called the increasing and decreasing models respectively. The difference between increasing and decreasing models was defined as the thermal hysteresis function for scale factor and bias. The scale factor thermal hysteresis function, SFTH(T), in PPM was defined as follows:

$$SFTH(T) = \frac{SFI(T) - SFD(T)}{SFD1} \times 10^6$$

where

SFI(T) = increasing temperature scale factor polynomial

SFD(T) = decreasing temperature scale factor polynomial

SFD1 = decreasing temperature scale factor at 0°F

The coefficients of SFTH(T) are calculated as follows:

$$SFTH(T) = SFTH1 + SFTH2 \times T + SFTH3 \times T^2 + SFTH4 \times T^3$$

where

$$SFTH1 = \frac{SFI1 - SFD1}{SFD1} \times 10^6 = PPM$$

$$SFTH2 = \frac{SFI2 \times SFI1 - SFD2 \times SFD1}{SFD1} = PPM/°F$$

$$SFTH3 = \frac{SFI3 \times SFI1 - SFD3 \times SFD1}{SFD1} = PPM/°F^2$$

$$SFTH4 = \frac{SFI4 \times SFI1 - SFD4 \times SFD1}{SFD1} = PPM/°F^3$$

The bias thermal hysteresis function, BTH(T), in μ*g* was defined as follows:

$$BTH(T) = (BI(T) - BD(T)) \times 10^3$$

where

$BI(T)$ = increasing temperature bias polynomial, milli-*g*

$BD(T)$ = decreasing temperature bias polynomial, milli-*g*

The coefficients of BTH(T) are calculated as follows:

$$BTH(T) = BTH1 + BTH2 \times T + BTH3 \times T^2 + BTH4 \times T^3$$

where

$$BTH1 = (BI1 - BD1) \times 10^3 = \mu g$$

$$BTH2 = BI2 - BD2 = \mu g/°F$$

$$BTH3 = BI3 - BD3 = \mu g/°F^2$$

$$BTH4 = BI4 - BD4 = \mu g/°F^3$$

The thermal hysteresis functions are models of the detailed shape of thermal hysteresis on a temperature cycle over -65°F to 225°F under ± 1*g* acceleration, and these functions can be viewed as worst case peak to peak error functions about the average scale factor and bias polynomial models.

RAPID REACTION BIAS DATA

The bias, $K_o(T)$, can be expressed as the polynomial:

$$K_o(T) = C1 + C2 \times T + C3 \times T^2 + C4 \times T^3$$

where bias units are milli-g and temperature is in °F, the units of the coefficients C1 through C4 are:

C1, milli-g

C2, milli-g per °F

C3, milli-g per $(°F)^2$

C4, milli-g per $(°F)^3$

Bias temperature coefficient, BTC, is typically expressed in units of μg per °F. Thus the above equation becomes:

$$K_o(T) = B1 + 10^{-3}(B2 \times T + B3 \times T^2 + B4 \times T^3)$$

Where: B1 = Q-Flex bias, milli-g, at 0°F

$$BTC(T) = \frac{d}{dT}(B2 \times T + B3 \times T^2 + B4 \times T^3)$$

$$BTC(T) = B2 + (2)(B3)(T) + (3)(B4)(T^2)$$

and: B2, μg per °F

B3, μg per $(°F)^2$

B4, μg per $(°F)^3$

Three of the four Q-Flex sensors chosen for these tests were of current production configuration (Sundstrand P/N 617-2736). They had been assembled in September, 1975 and had received only standard practice artificial aging and performance screen testing. Recently implemented development improvements included a 'groove and slot' modification to eliminate electrostatic charge buildup during cyclical self-test and coil attachment with a resilient adhesive, DC 3144. Two of the three units (S/N's 20204 and 20210) were utilized for rapid warm-up tests prior to entering this test cycle. The fourth Q-Flex sensor was chosen to represent an exaggerated example of an older configuration sensor (Sundstrand P/N 617-2230). Besides having non-grooved metal pick-off surfaces and rigid coil attachment adhesive, LCA4/LV, this unit (S/N 10450) had a deliberate excessive application of conductive epoxy at the torquer coil center tap interface. As a group, this "shorted bobbin" lot of sensors exhibited large bias temperature coefficients and large bias thermal hysteresis. Sensor assembly had occurred in May, 1974, so natural aging stabilitzation should have occurred during room ambient temperature storage.

Thermal Study Bias and BTC Test Reduction

Q-Flex accelerometer bias and BTC for the initial decreasing temperature test are shown in Figures 11 and 12 respectively. The calculated BTC coefficients for the four accelerometers are given in Table 4. As expected, S/N 10450 had the largest bias temperature coefficient.

Figure 11

INITIAL DECREASING TEMPERATURE BIAS POLYNOMIAL MODEL FOR FOUR Q-FLEX ACCELEROMETERS

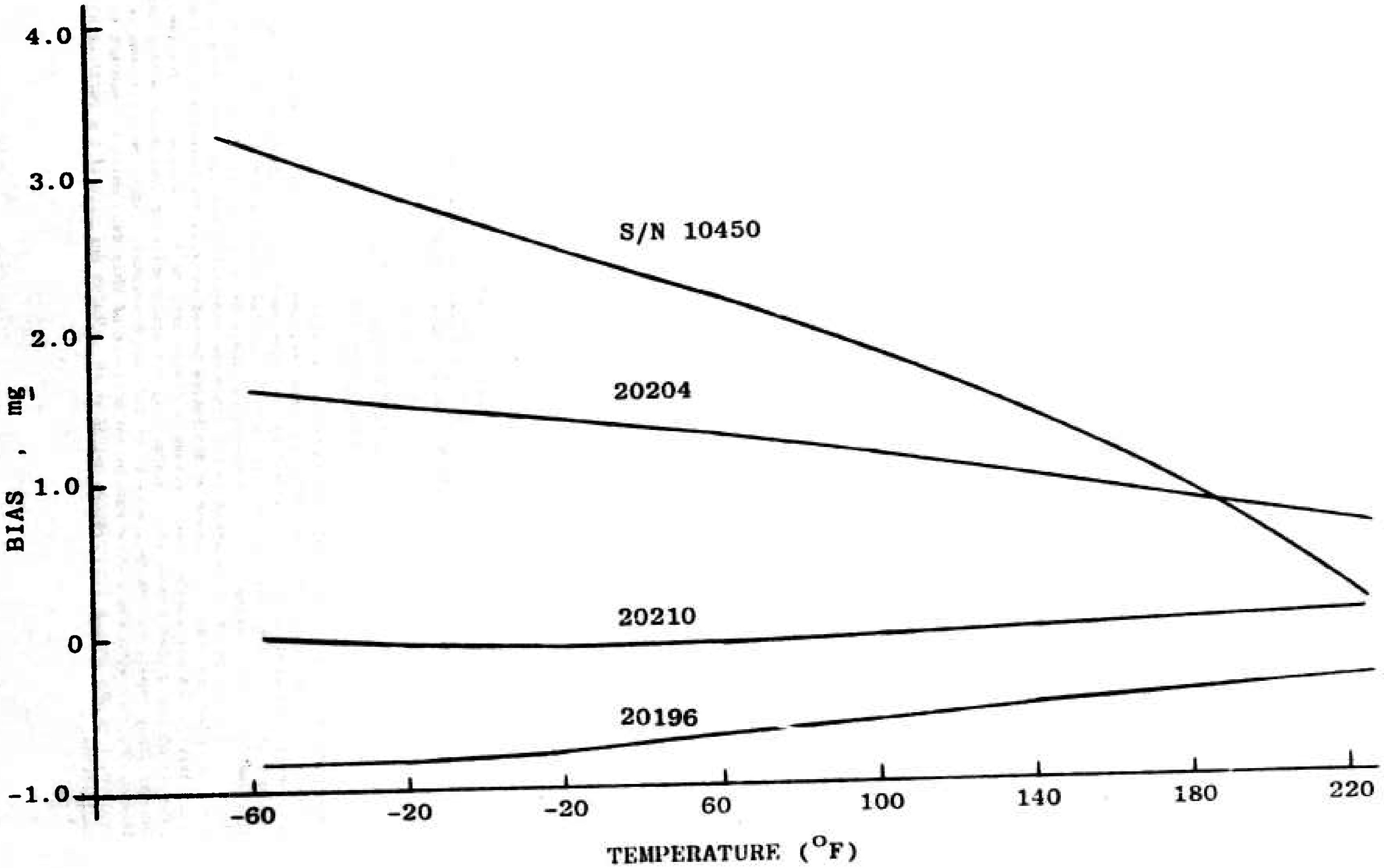

Figure 12

INITIAL DECREASING TEMPERATURE BIAS TC MODELS FOR FOUR Q-FLEX ACCELEROMETERS

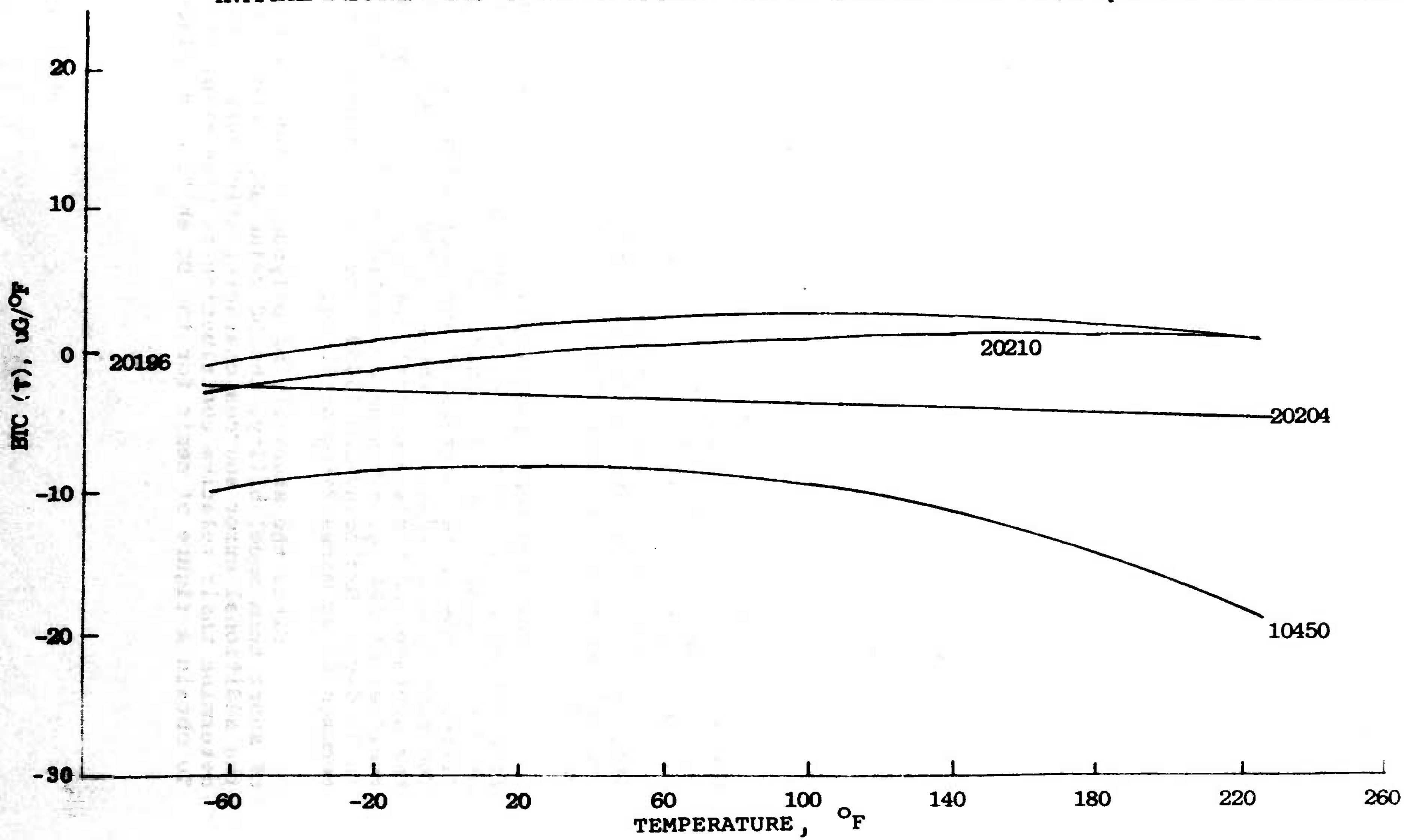

Table 4

Q-FLEX BIAS TEMPERATURE COEFFICIENTS FOR INITIAL DECREASING TEMPERATURE LEG, +225°F to -65°F, NORMALIZED TO 0°F

S/N	B2 μg/°F	2 x B3 μg/(°F)^2	3 x B4 μg/(°F)^3
10450	-8.1	0.0104	-0.00261
20196	1.2	0.0220	-0.000111
20204	-3.0	-0.0078	-0.000006
20210	-0.7	-0.0240	-0.000075

The following data will demonstrate bias performance over approximately a one month test period. During this exposure the units were subjected to rigorous temperature cycling from -65°F to 225°F and to hot soaks at 240°F. Approximately 40 thermal cycles and 40 hot soaks were accrued during this test period.

Bias Model Stability

Extended temperature tumble tests, ET3, were performed three times over an interval of 29 days. The bias polynomial models were computed for each increasing temperature segment and for each decreasing temperature segment on each of the three ET3's. Table 5 shows the RMS residuals after curve fitting each of the individual segments. The overall RMS residual, indicating short term bias uncertainty, was 24 μg.

The long term stability of the bias model of the four Q-Flex accelerometers can be expressed as the increase of RMS residuals when each subsequent segment of raw data is fitted to the inital increasing and decreasing bias models. The resulting residuals are shown in Table 6. Subtracting the average individual residual, 14 ug, from the overall residual of 104 μg, gives an indication of 80 μg bias shift in 29 days. Excluding S/N 10450, the 29 day bias stability becomes 85 μg minus 24 μg or 61 μg.

Since the stability of polynomial model is a function of short term modelability, the DC value and shape of the curve, the additional error sources characteristics were explored to determine their relative contribution to bias stability. To obtain a figure of merit for the DC shift or displacement

Table 5

INDIVIDUAL BIAS POLYNOMIAL RESIDUALS

INCREASING TEMPERATURE BIAS POLYNOMIAL RESIDUALS ug				
S/N	11/24	12/9	12/22	RMS
10450	27	17	16	21
20196	44	28	32	35
20204	23	38	32	32
20210	9	6	8	8
RMS	29	26	24	26
DECREASING TEMPERATURE				
S/N	11/25	12/10	12/23	RMS
10450	21	26	18	22
20196	37	30	27	32
20204	12	10	15	13
20210	3	10	9	8
RMS	22	22	18	21

OVERALL RMS RESIDUAL = 24 ug

Table 6

EXTENDED TEMPERATURE TUMBLE TEST BIAS RESIDUALS
REF. TO INITIAL (11/24) POLYNOMIALS

UPPER BIAS POLYNOMIAL RESIDUALS
ug

S/N	12/9	12/22
10450	44	96
20196	104	124
20204	45	59
20210	18	42
RMS	—	86
RMS less 10450	—	83

LOWER BIAS POLYNOMIAL RESIDUALS
ug

S/N	12/10	12/23
10450	65	184
20196	55	118
20204	65	59
20210	59	76
RMS	—	120
RMS less 10450	—	87

RMS-all sensors after 29 days = 104 ug
RMS-all sensors after 29 days less 10450 = 85ug

of the entire curve as a time dependent phenomena, an evaluation of the algebraic average residuals from the initial and decreasing temperature segment models was computed. Table 7 lists the results of this analysis. The weighted average residual for the 29 day data is 76 ug's. The residual excluding data for S/N 10450 is 62 ug's. If the 24 ug short term model uncertainty is subtracted, the displacement or drift of the entire curve is estimated at 52 ug's or 38 ug's dependent upon whether S/N 10450 is included.

To determine how well the three major elements contribute to overall bias stability of the model, the root sum square of these elements was computed and compared to the 29 day stability model. Table 8 lists this data. It can be seen that the RMS values computed by evaluating modelability, DC stability and shape stability are within the measured RMS stability data.

The second element to the polynomial model stability is the change in shape of the curve. Shape can be determined by examining the change in bias temperature coefficient BTC residuals with respect to the initial BTC model. Table 9 shows that the 29 day test overall residual is only 0.74 ug/°F. Integrating this BTC residual shift over the entire ± 145°F temperature range results in an estimated worst case RMS error of 60 ug.

Table 7

AVERAGE BIAS RESIDUALS WITH RESPECT TO INITIAL BIAS MODEL

UPPER BIAS RESIDUALS ug		
S/N	12/9	12/22
10450	23	64
20196	-95	-109
20204	-16	-38
20210	-13	0
RMS	-	53
RMS LESS 10450	-	49

LOWER BIAS RESIDUALS ug		
S/N	12/10	12/23
10450	-46	-172
20196	-19	-111
20204	-62	46
20210	-34	-66
RMS	-	99
RMS LESS 10450	-	74

ABS AVER.
OVERALL = 76 ug

ABS AVER.
OVERALL LESS 10450 = 62 ug

Table 8

RMS RESIDUAL ERRORS

TYPICAL DATA

	Increasing Temperature Bias Polynomial Residuals (ug)					
S/N	29 Day Stability 11/24 - 12/22	Modelability (Avg.3 Rdgs)	Shape Stability ug/^{o}F	Shape Stability Ⓐ Computed (ug)	DC Stability (0^{o}F)	RSS Computed
10450	96	21	.936	76	64	102
20196	124	35	1.018	82	-109	141
20204	59	32	.614	49	-38	70
20210	42	8	.643	52	0	53
RMS	86	26	.822	66	66	97

Ⓐ - Based upon $\pm$ 145^{o}F ΔT

Table 9

BIAS TEMPERATURE COEFFICIENT RESIDUALS WITH RESPECT TO THE INITIAL POLYNOMIAL MODEL

Decreasing Temp BTC Polynominal Residuals, ug/^{O}F			
S/N	12/9/75	12/22/75	RMS
10450	.615	.936	.792
20196	.662	1.0[illegible]5	.859
20204	.682	.614	.649
20210	*	.643	.643
RMS	——	.822	.754

Increasing Temp BTC Polynomial Residuals ug/^{O}F			
S/N	12/10/75	12/23/75	RMS
10450	.680	.649	.665
20196	1.071	.659	.889
20204	.425	.700	.579
20210	*	.586	.586
RMS	——	.650	.705

RMS - all sensors 29 days = .741 ug/^{O}F

* Limited data set for modeling

Thus, it can be seen that the size of the bias residuals, mainly attributed to shifts in bias null during the testing period, can be significantly affected by small changes in the bias model shape. The data analysis of the DC value and shape indicate that both segments of the stability model appear to have been affected during this testing period.

Another technique used to analyze stability and shape of the bias model was to review minor loop data and correlate the two elements of the bias profile through thermal exposure.

Bias Stability - Minor Loop Analysis

Bias stability through thermal environment for four Q-Flex accelerometers is plotted at -65°F, 15°F, 70°F, 145°F and 225°F in Figures 13 through 17. The data covers 42 days of rapid reaction performance testing. In addition, stability at 70°F over 100 days for two of the accelerometers is plotted in Figure 18 and 19. For each data set a straight line was fitted to the data using least squares curve fitting in order to determine bias trending apart from scatter about the average bias value. The model used was

$$\Delta B = M_B \times t + \Delta B_O$$

Where

ΔB = bias deviation from the initial bias in ug

M_B = the bias stability slope in ug per day

t = time since the inital bias reading in days

ΔB_O = calculated initial bias deviation for a least squares fit in ug

Note that ΔB is defined as

$$\Delta B = (B(t) - B(O)) \times 10^3$$

Where

B(O) = initial bias in mg

B(t) = bias at day t in mg

The bias stability slopes for all the data sets are summarized in Table 10. The last column of Table 10 gives the absolute average stability slope between -65°F and 225°F for each accelerometer. This quantity ranges between 0.5 and 2.6 ug per day and is a measure of the accelerometer bias trend

Figure 13
Q - FLEX BIAS STABILITY AT -65°F

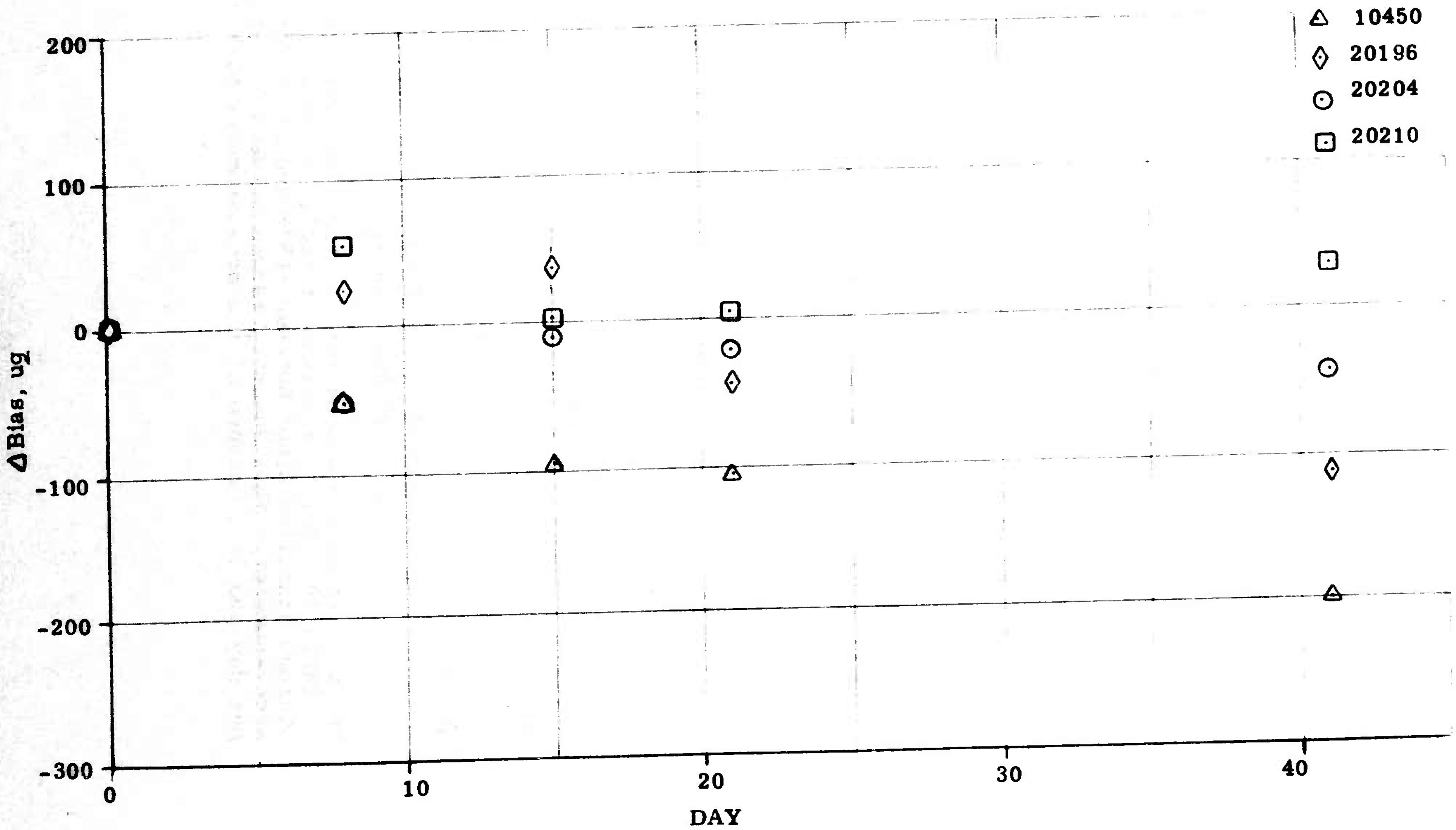

Figure 14
Q - FLEX BIAS STABILITY AT +15°F

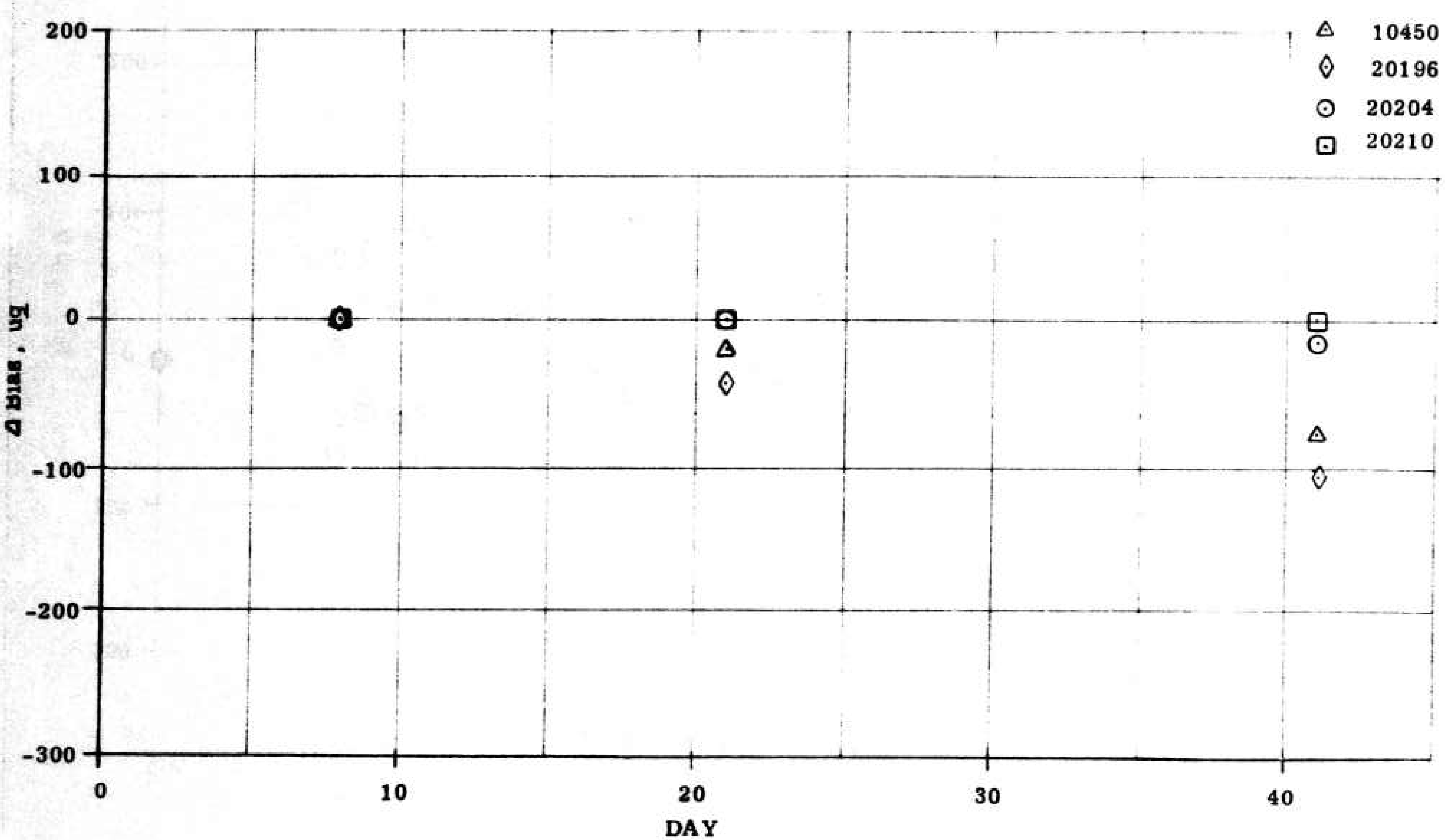

Figure 15

Q-FLEX BIAS STABILITY AT +70°F

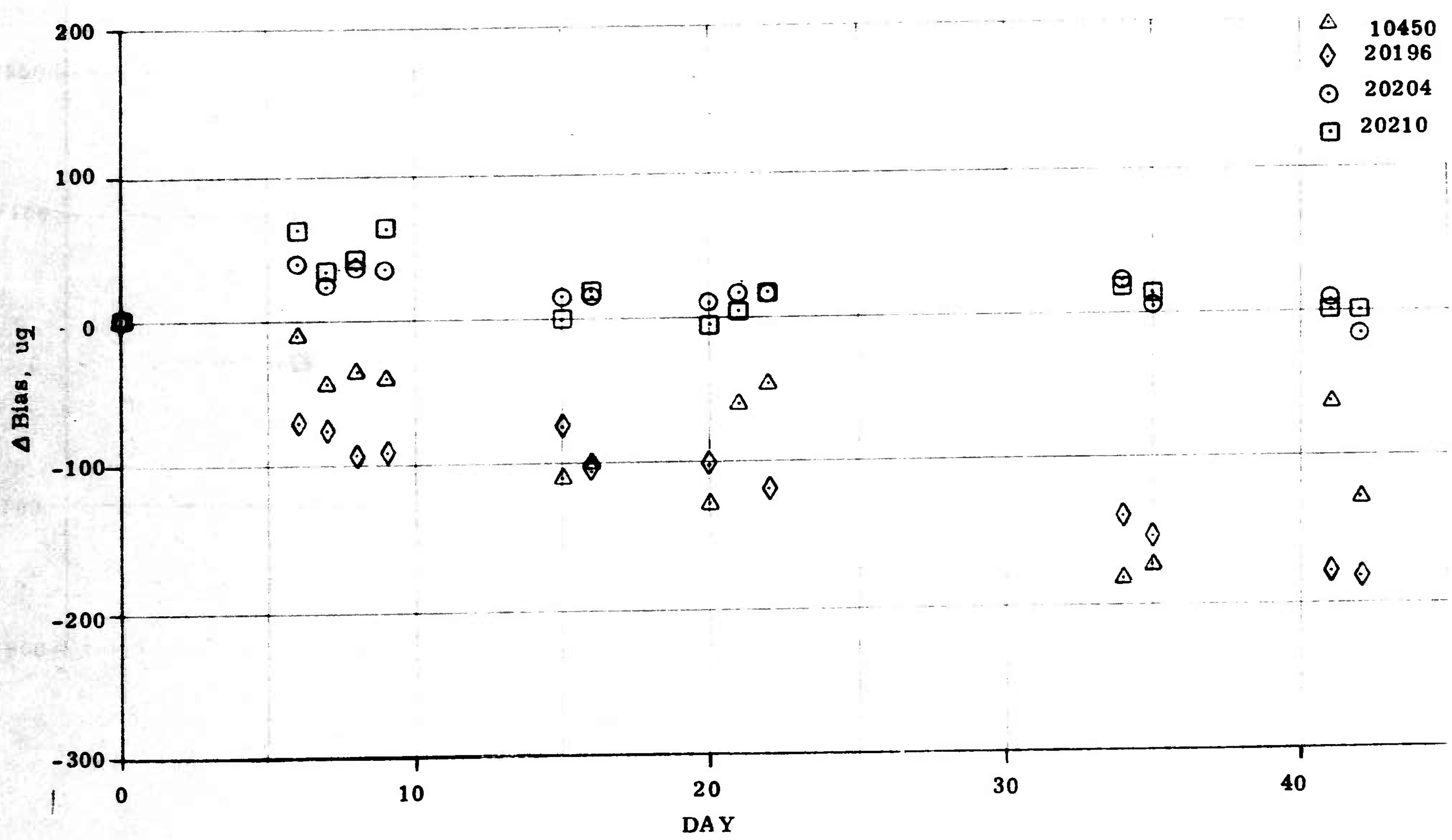

Figure 16

Q - FLEX BIAS STABILITY AT +145°F

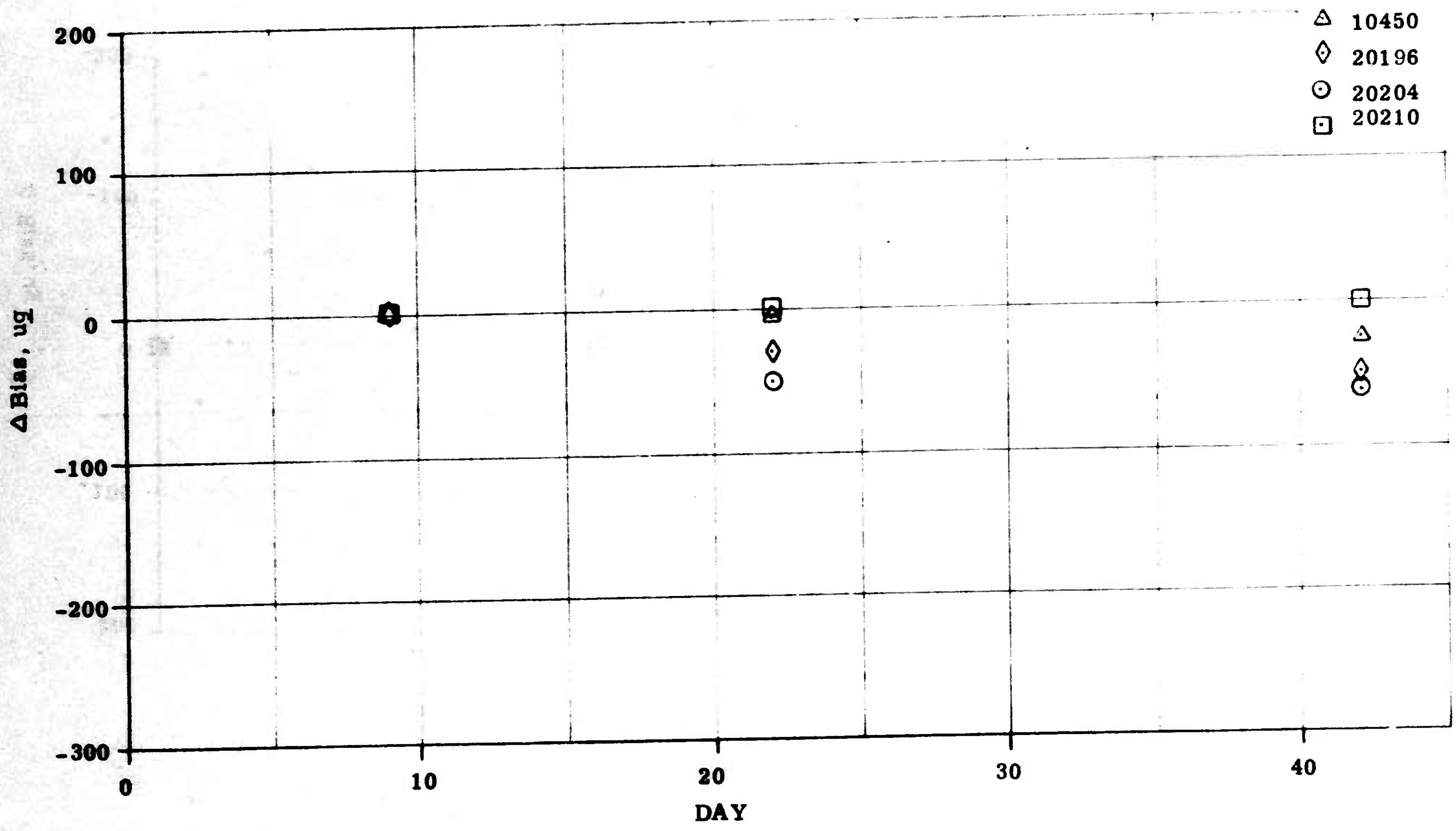

Figure 17

Q - FLEX BIAS STABILITY AT +225°F

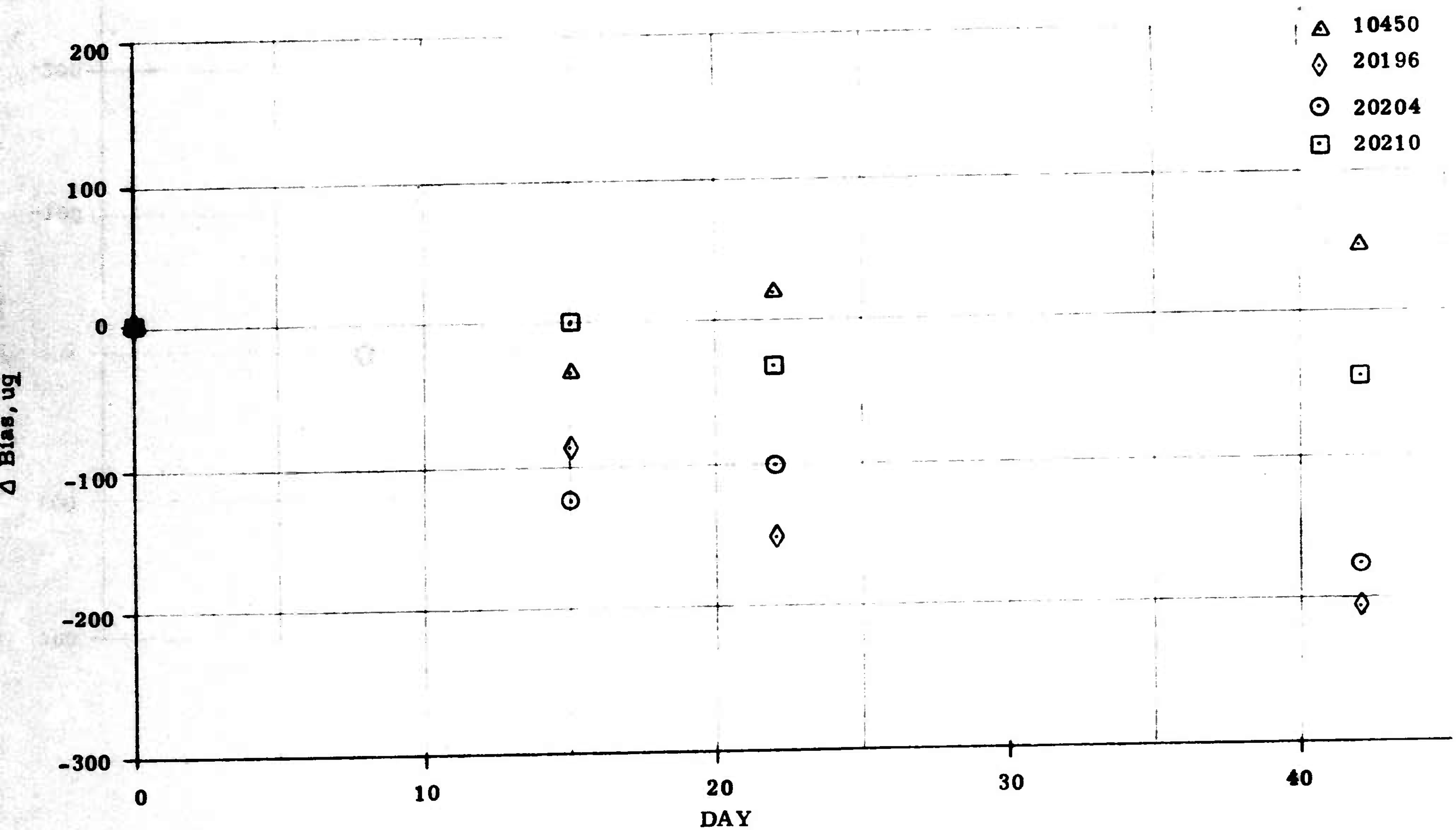

Figure 18

Q-FLEX BIAS STABILITY FOR 100 DAYS

SN20210

TEMPERATURE = 70°F

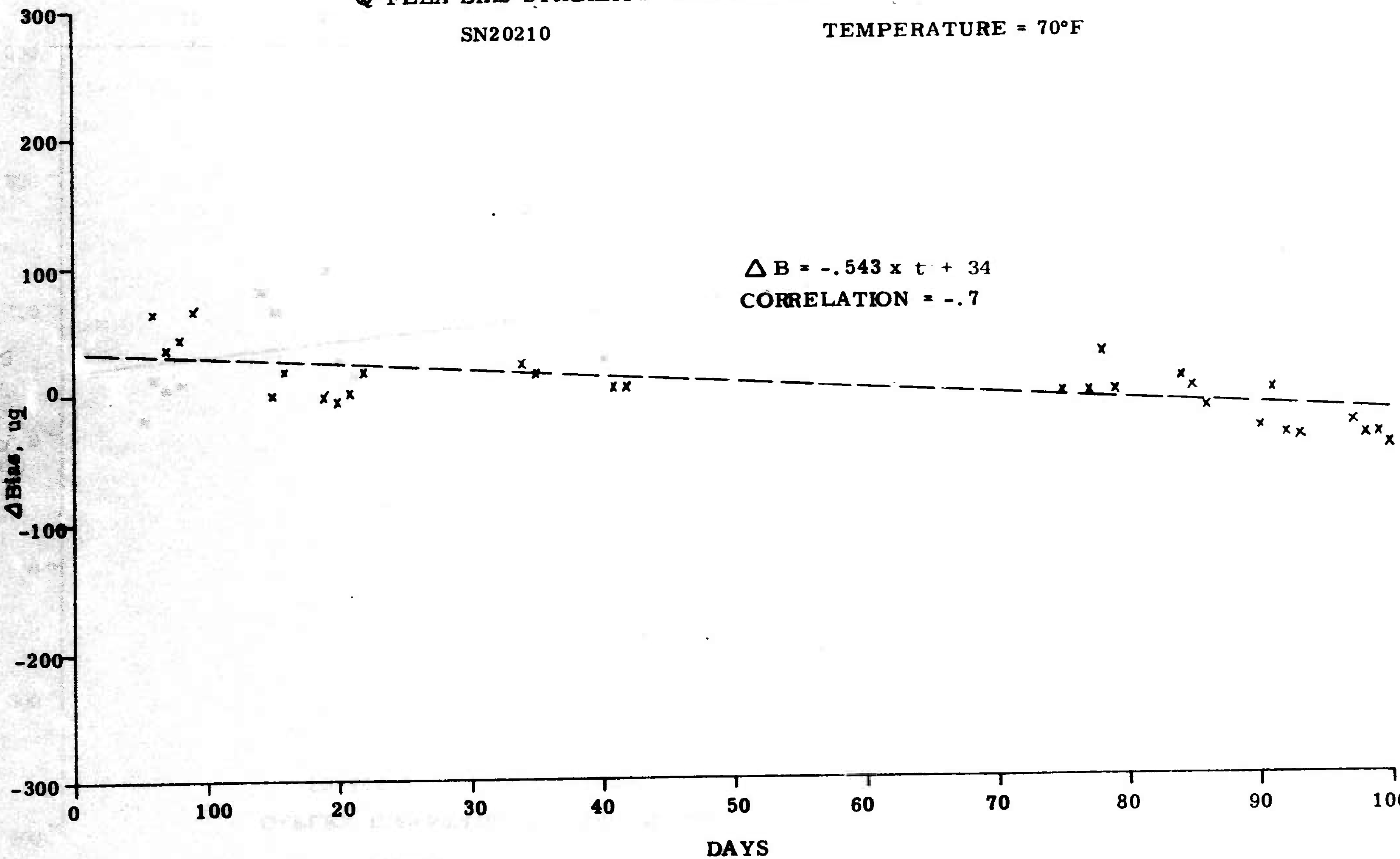

FIGURE 19

Q-FLEX BIAS STABILITY FOR 100 DAYS

SN 10450 TEMPERATURE = 70° F

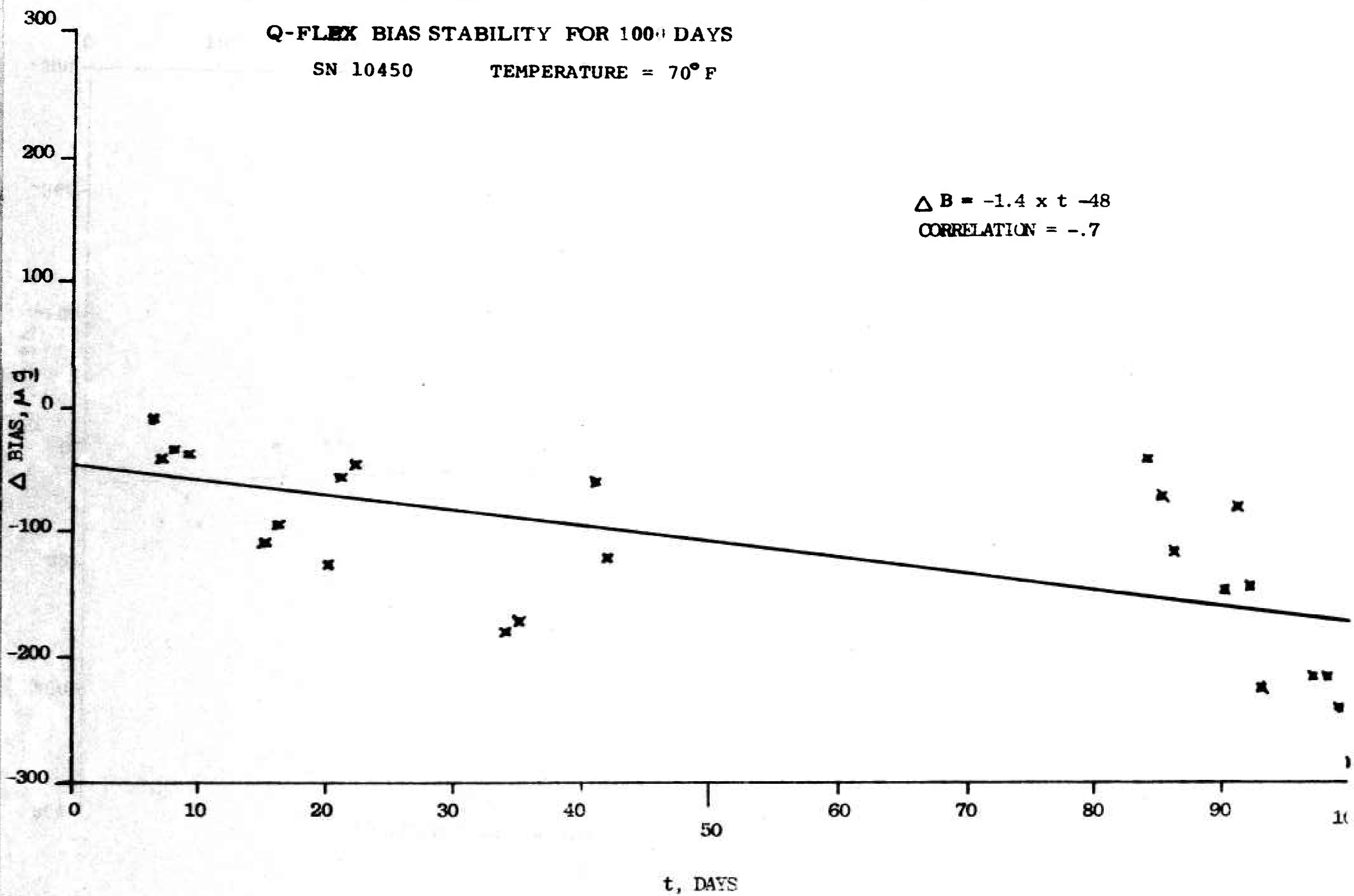

Table 10

BIAS STABILITY SLOPES (ug/day)

42 DAY DATA

S/N	-65°F	15°F	70°	145°F	225°F	ABS AV Temp Over Range
10450	-4.6	-2.5	-2.8	-0.9	+1.6	2.5
20196	-3.8	-3.3	-.01	-1.2	-4.6	2.6
20204	-0.6	-0.5	-0.6	-1.6	-3.6	1.4
20210	+0.2	+.06	-0.9	-.01	-1.1	0.5
ABS AV For all Sensors	2.3	1.6	1.1	0.9	2.8	1.7

<u>100+ DAY DATA</u>

SN 20210 @ 70°F: -0.5 ug/day

SN 10450 @ 70°F: -1.4 ug/day

ABS Average Correlation Coefficient = .7

over the entire temperature range. The last row of Table 10 gives the absolute average bias stability for the accelerometers at each temperature. This quantity ranges between 0.9 and 2.8 ug per day and indicates that this sample of Q-Flex accelerometers trends most at the extremes of the operating temperature range. The absolute average bias stability slope for all accelerometers at all temperatures is 1.7 ug per day for the 42 day period. For the 100 day data at 70°F the absolute average bias stability slope is 1.0 μg per day which is comparable to the 42 day result of 1.1 μg per day.

The RMS scatter of Δ B for each accelerometer and each temperature about the average Δ B was calculated to determine the band of bias stability apart from trend in the bias. The RMS values are listed in Table 11 and these values are larger than the RMS residuals of the least squares fit. The average RMS error between -65°F and 225°F for each sensor is listed in the last column of Table 11 and ranges between 15 and 52 μg. In the last row the average RMS error for the test sample ranges between 19 and 51 μg. The average RMS errors for all four sensors at all temperatures is 34 μg or a 3 sigma average RMS error of 102 μg over 42 days of thermal cycling.

The information to be denoted and stressed is the characteristic difference between S/N 10450 and the family of the three other units. S/N 10450 exhibits both a larger drift at ambient temperature and a significant shape change of the bias profile. The shape change is characterized by a large negative bias change at -65°F gradually decreasing to a positive or increasing bias at 225°F. The significance of these characteristics and their relationship to the other units are discussed under Q-Flex Bias Design Factors.

Bias Thermal Hysteresis Versus Δ T and T_M

The models of BTH versus Δ T and T_M for four Q-Flex accelerometers are plotted in Figures 20 and 21. The coefficients of the models are summarized in Table 12 along with absolute averages of the coefficients to characterize the sample.

Figure 20 shows that absolute BTH is an increasing function of Δ T. Three accelerometers in the test sample for example, exhibit BTH less than 50 μg for Δ T = ± 40°F. This limit is valid for T_M between 15°F and 120°F because BTH is essentially independent of T_M as can be seen in Figure 21. It is assumed that BTH converges to zero for Δ T < ± 40°F. The linear models cannot be justifiably extended beyond ±50°F and ± 145°F because actual data is not available.

Table 11

BIAS STABILITY RMS ERRORS (ug)
42 DAY DATA

SN	-65°F	15°F	70°F	145°F	225°F	AV OVER ALL TEMP
10450	70	36	56	13	31	41
20196	58	48	47	24	81	52
20204	21	8	16	30	70	29
20210	22	1	23	7	22	15
AV of all Sensors	43	23	36	19	51	34

<u>100+ DAY DATA</u>

SN 20210 @ 70°F: 28 μg

SN 10450 @ 70°F: 73 μg

Figure 20

BIAS THERMAL HYSTERESIS VERSUS $\Delta T @ T_m = 80°F$

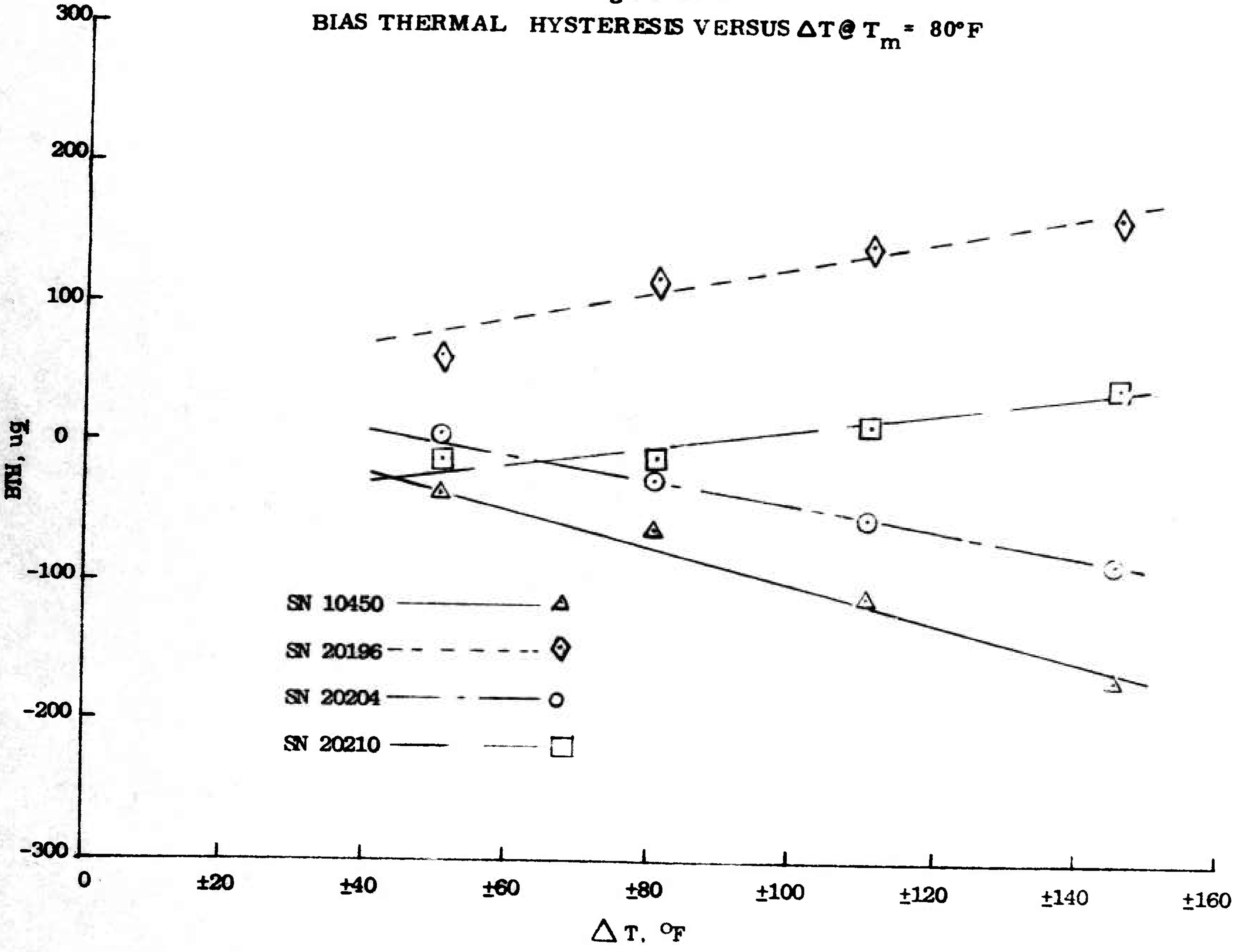

Figure 21

BIAS THERMAL HYSTERESIS VERSUS T_m @ $\Delta T = \pm 80$ °F

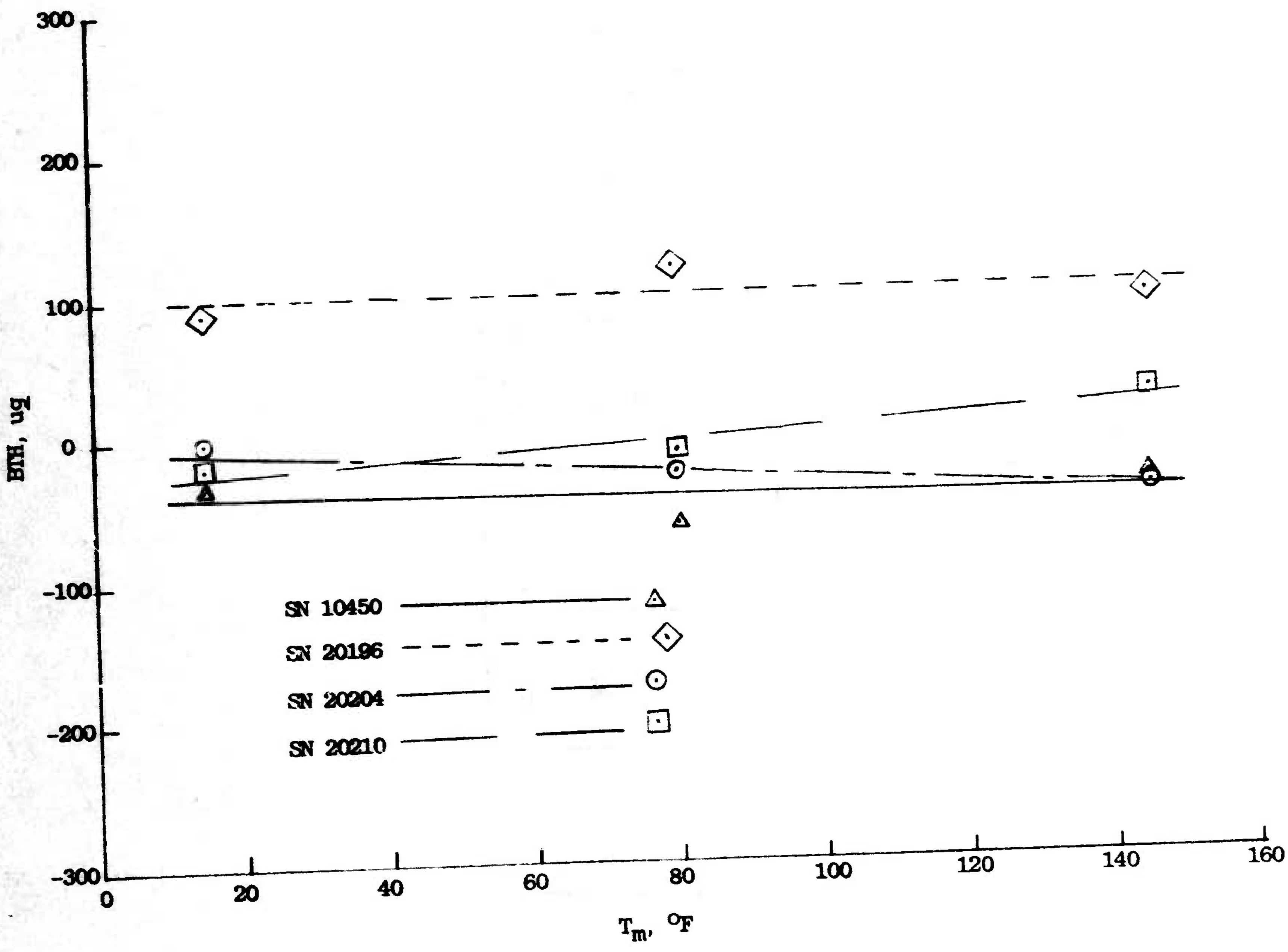

Table 12

BTH MODEL VS ΔT AND T_M

Coef-ficient	10450	20196	20204	20210	Abso-lute Average	Ave
C_1	-1.32	.946	-.870	.642	.940	-.151
C_2	30	32	42	-55	40	12

$$BTH(\Delta T) = C_1 \times \Delta T + C_2, \text{ ug}$$

BTH VS T_M @ $\Delta T = \pm 80^{\circ}F$

Coeff	10450	20196	20204	20210	Abs Average	Ave
C_3	.677	-.006	-.234	.339	.319	.194
C_4	-84	101	-8	-32	56	-6

$$BTH(T_M) = C_3 \times T_M + C_4, \text{ ug}$$

The absolute average values of the BTH model coefficients C_1, C_2, C_3, and C_4 have been used to plot BTH bands versus T and T_M in Figure 22. This figure characterizes the bias thermal hysteresis behavior of the test sample.

Bias Thermal Hysteresis Models and Relative Minor Cycle Thermal Hysteresis

Figures 23 through 26 show the bias thermal hysteresis models and relative minor temperature cycles. The bias temperature cycles are less well behaved than the SFTH cycles but fall within the RMS error bands of most of the BTH models. The non-zero values of BTH at the model end points are within the RMS errors of the increasing and decreasing polynomial models. Also the BTH models do not show a characteristic shape as SFTH shows. BTH can vary from relatively constant as with SN 20204 to highly curved and bivalent as with SN 10450. The significance of the data again should be noted. That is, the hysteresis function is directly dependent upon the temperature range and thus, a small Δ T will produce a small bias hysteresis.

Figure 22

ABSOLUTE BIAS THERMAL HYSTERESIS BANDS VS ΔT AND T_M

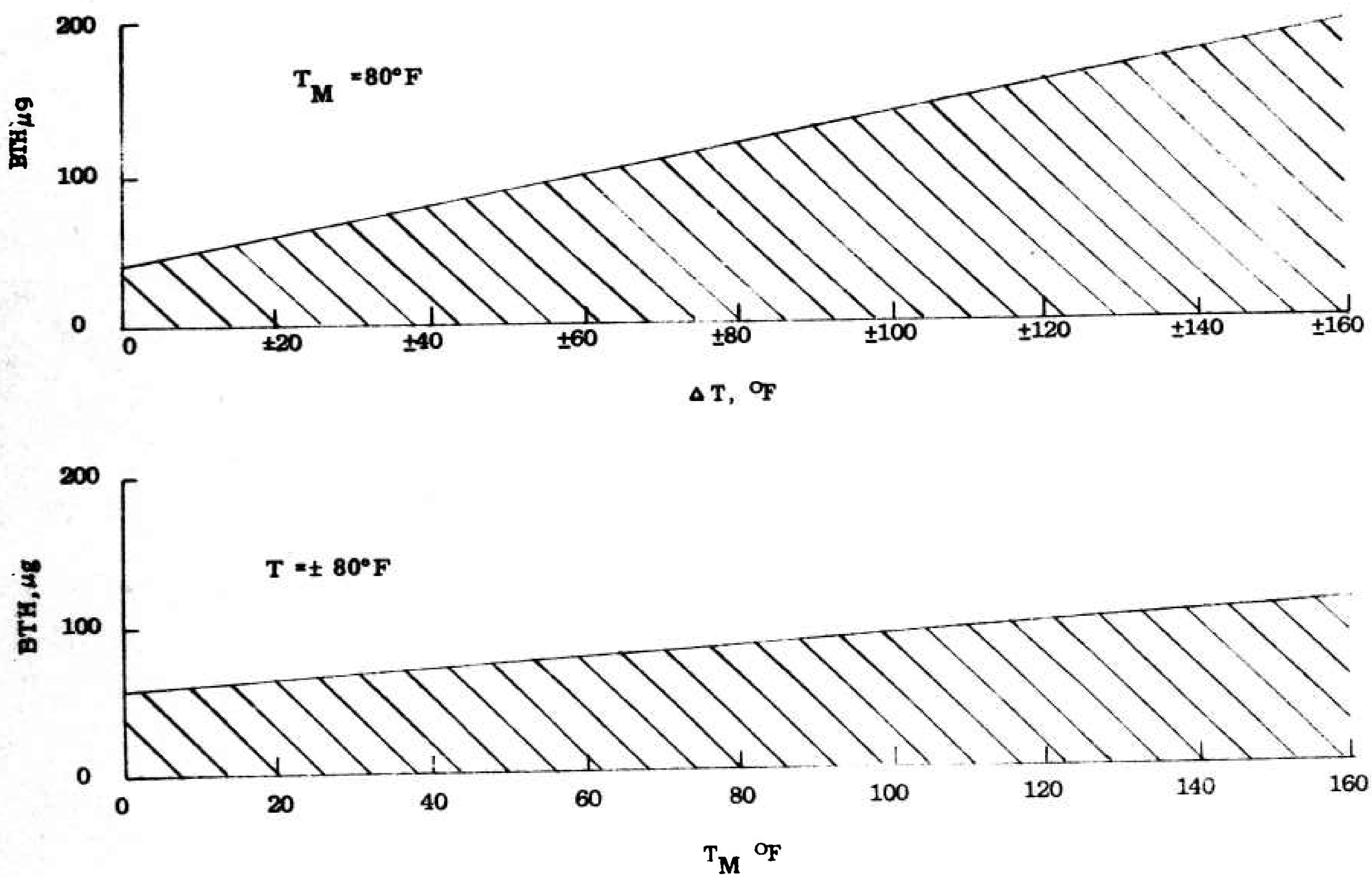

Figure 23

RELATIVE MINOR LOOP BIAS THERMAL HYSTERESIS

SN 10450 DATES: 11/22/75–12/5/75

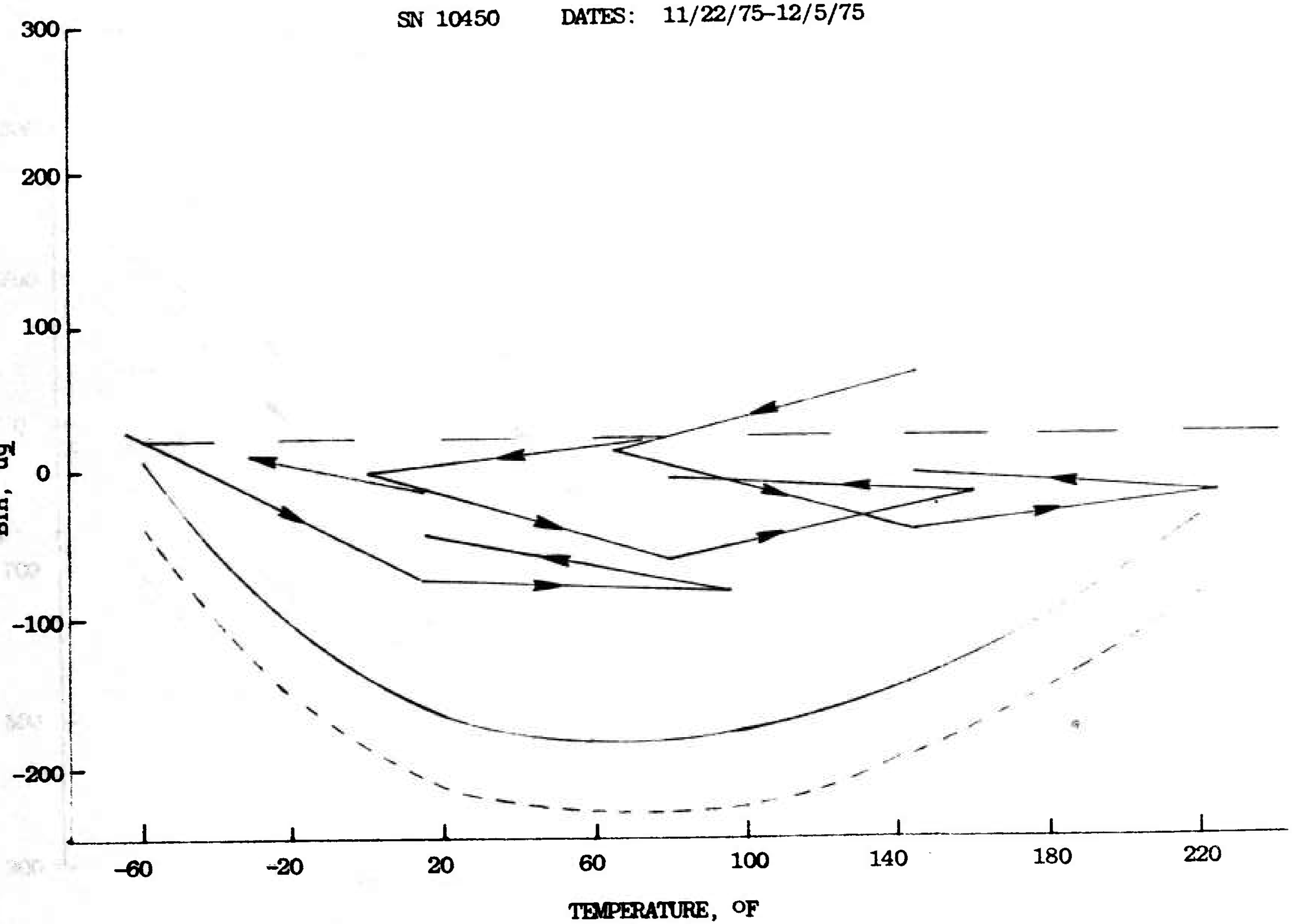

Figure 24

RELATIVE MINOR LOOP BIAS THERMAL HYSTERESIS

SN 20196 DATES: 1/22/75 - 12/5/75

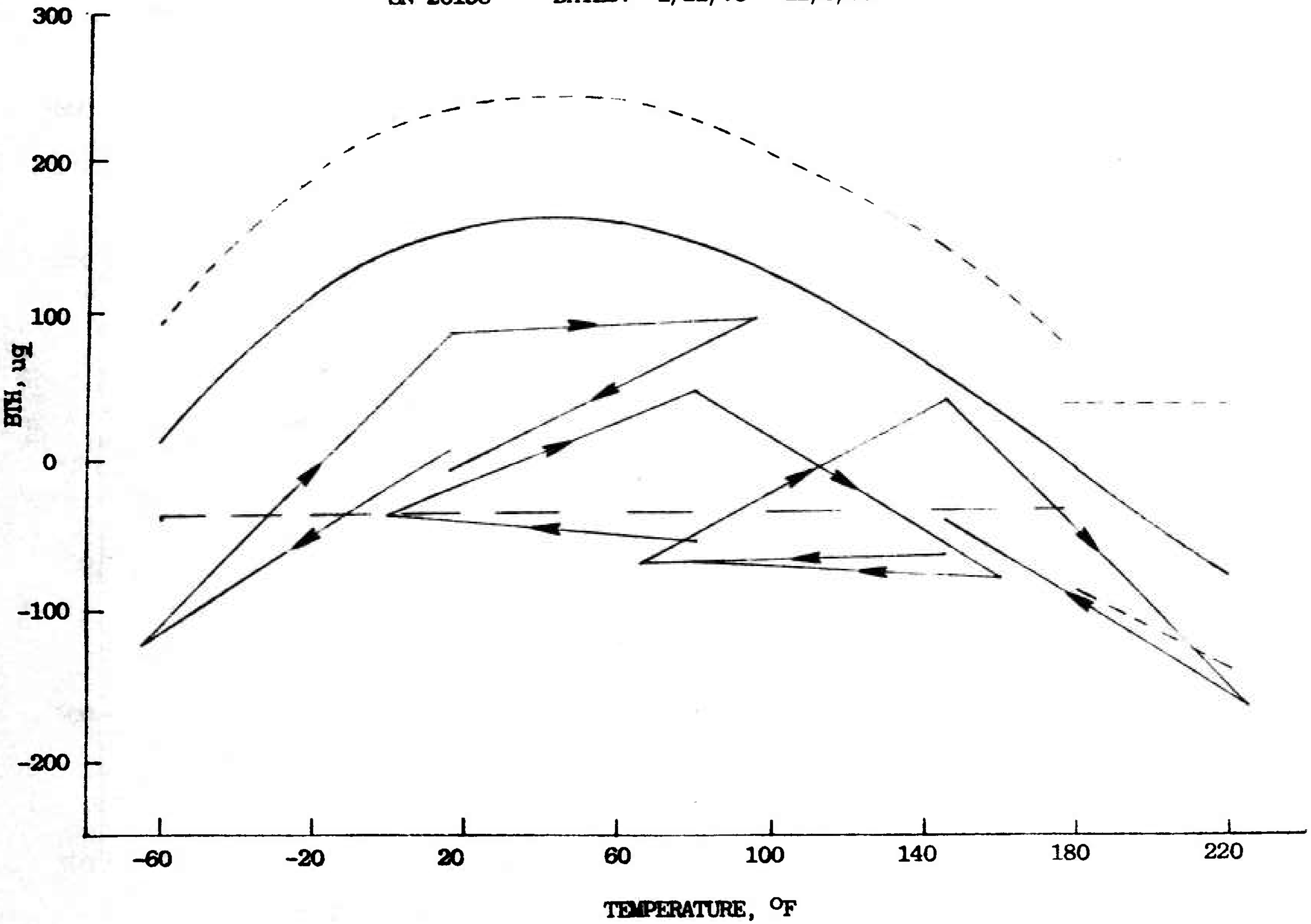

Figure 25

RELATIVE MINOR LOOP BIAS THERMAL HYSTERESIS

SN 20204 DATES: 11/22/75-12/5/75

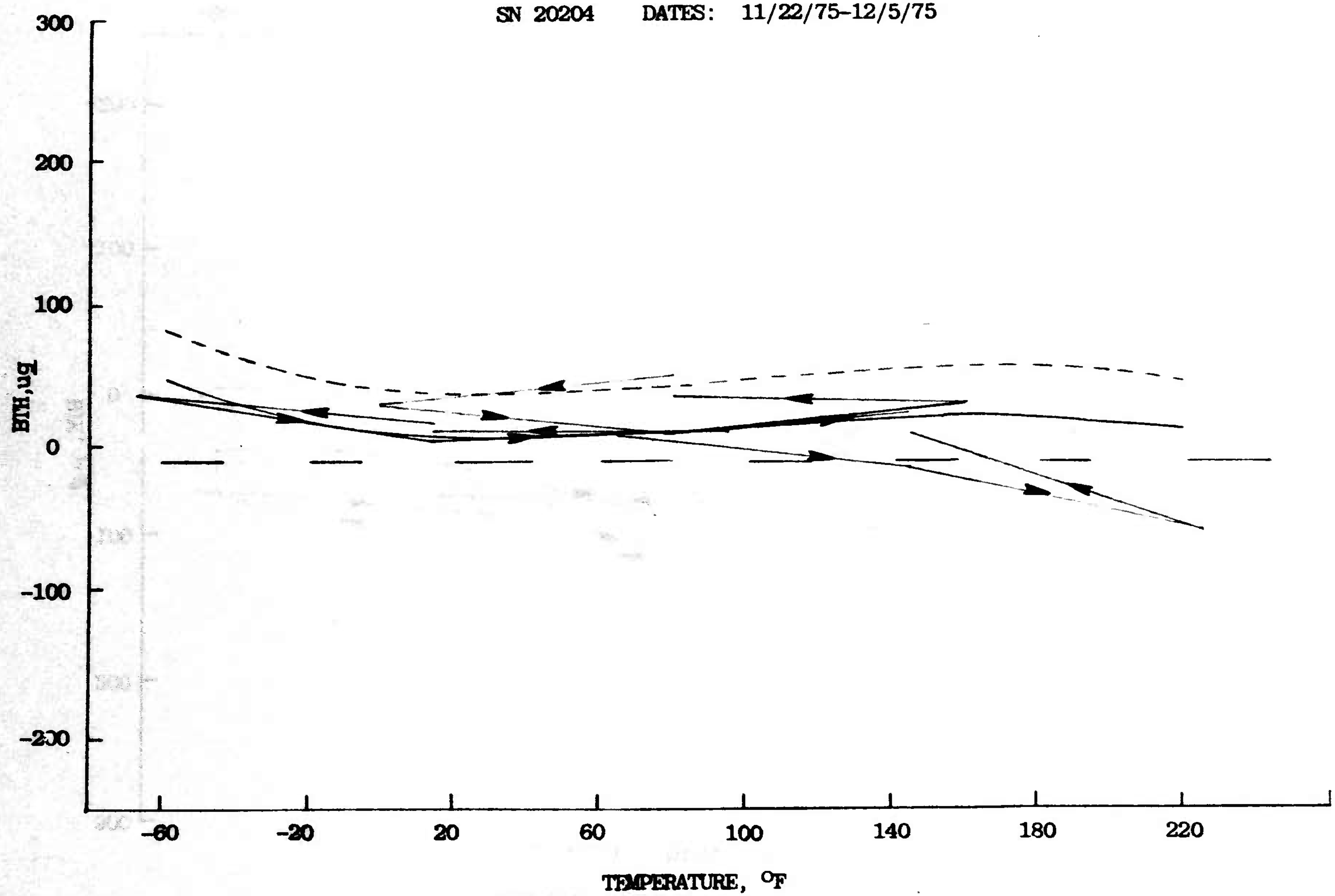

Figure 26

RELATIVE MINOR LOOP BIAS THERMAL HYSTERESIS

SN 20210 DATES: 12/23/75-1/7/76

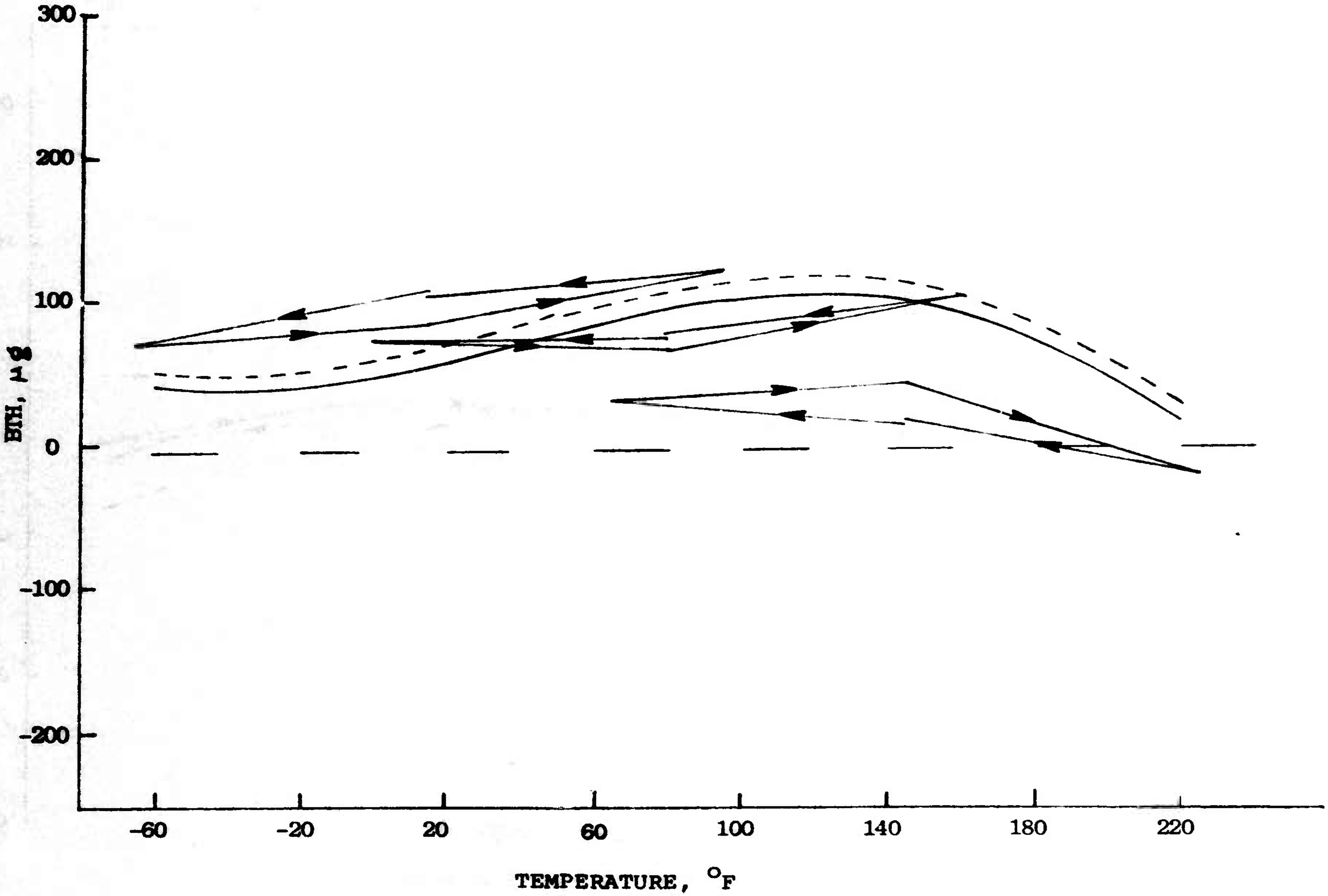

Long Term Bias Stability

Data in previous sections spanned a 42-day test period. To gain perspective over a longer time frame a final test was performed early in April. The long term bias stability was evaluated over a 4.5 month period by comparing the ET3 decreasing temperature bias model coefficients. In addition, the increasing temperature bias model was utilized to obtain the stability of bias thermal hysteresis at 70°F. Results are shown in Table 13.

Bias Data Summary

A review of the entire rapid reaction bias performance test leads to the following conclusions:

1) In terms of residuals to fitted curves for individual ET3 tests, all four Q-Flex accelerometers look alike. No indication of long term performance stability is apparent from the degree to which the raw data from any single test can be least squares fit to the bias polynomial model.

2) Two Q-Flex accelerometers, 10450 and 20196, were clearly less stable than the remaining test units, 20204 and 20210. An approximate factor of 2 times less stable, evident at the end of 29 days of extensive temperature cycling, increased to a factor of 4 to 5 times less stable when results of 119 to 135 day test intervals are compared. The least stable accelerometer, as anticipated, is the old configuration, 10450, having rigid LCA4 epoxy coil attachment and deliberately excessive torquer coil center-tap conductive epoxy. Although two of the three current production Q-Flex accelerometers showed good bias stability throughout, the third, 20196, evidenced significant bias and bias temperature coefficient (BTC) shifts during the 29 day test period. This variation between accelerometers of the current production design indicates that driving functions for bias parameter shifts are still present on the proof mass though clearly much reduced over those of the old configuration. For wide temperature operation, small BTC shifts are a significant error source and therefore warrant design modification improvement.

3) Bias thermal hysteresis (BTH) is significantly larger on both of the less stable accelerometers than on

Table 13

LONG TERM BIAS STABILITY

Parameter	Units	10450	20196	20204	20210
Test Period	Calendar	11/25/75-4/ 7/76	11/25/75-12/23/75	11/25/75-4/ 7/76	12/10/75-4/ 7/76
	Days	135	29	135	119
Initial Bias	ug	2663	-783	1452	205
Bias	ug	-608	-109	- 85	-109
Bias Stability	ug/day	- 4.5	- 3.8	- 0.6	- 0.9
Initial BTC	ug/$^{\circ}$F	- 8.1	1.2	- 3.0	1.0
BTC	ug/$^{\circ}$F	3.4	0.5	0.1	0.5
BTC Stability	ug/$^{\circ}$F/day	.025	.017	.001	.004
Initial BTH	ug	-184	153	9	- 21
BTH	ug	209	17	-98	74
BTH Stability	ug/day	1.5	0.6	- 0.7	0.6

- Based on ET3 Bias Model for Decreasing Temperature
- Time Period Variation Due to Servo Electronics Changes
- Referenced to 0°F, Except BTH at 70°F.

the stable bias units. Sensor level performance testing could possibly sort out low BTH sensors for best long term performance, but a better, long-run approach to improved bias stability is to eliminate the proof mass strain contributors.

4) The maximum bias thermal hysteresis (BTH) error occurs near the temperature range midpoint. For temperature excursions less than full range, the resulting minor loop BTH error stays within the extended range BTH error envelope.

In summary, the data demonstrate that two units, S/N 20204 and 20210 with the present design construction performed extremely well over the 42-day test period. The RMS bias residuals from the initial calibration curve was approximately 60 μg's and the thermal hysteresis was less than 30 μg's when tested over a 220°F temperature span (±110°F about midpoint). In addition data accrued on S/N 20204 over a five month test period where the unit was subjected to extensive thermal testing demonstrate excellent long term stability characteristics.

The third present construction unit exhibited both larger hysteresis and bias trend during the test period.

The fourth unit under test, S/N 10450, exhibited extremely poor performance when compared to the present design family. Bias trend and shape change of the model polynomial was dramatic. In order to properly interpret the data accrued during the rigorous thermal testing program an analysis of the error torques that constitute the sources for bias must be examined. In fact, the significance of S/N 10450 unit's performance and its relationship to the total conceptual understanding of the design and therein, design modifications for improved performance shall be shown in the following section.

Q-Flex Bias Design Factors

Bias is expressed as the summation of all torques acting upon the Q-Flex proof mass and requires a torque generated rebalance current to servo these error torques to electrical null. The sources of bias stress can be equated to strain related bending moments about the proof mass flexure suspension axis.

In a perfect structure there would be no transverse stress applied to the proof mass assembly and the only contribution to bias and bias thermal coefficient would result from the inherent stresses within the quartz element itself and the thermal effects which arise within the body of the pendulum. Within the current understanding of the mechanics which influence Q-Flex performance, the following factors represent potential sources of bias and bias error.

Mechanical structure strain contributors <u>external</u> to the proof mass and transmitted through the proof mass assembly rim are listed below.

1) Change in preload at the sensor belly band due to relaxation in epoxy material causing axial force changes on proof mass rim.

2) Dimensional changes of the rim clamping metal structures (excitation rings) due to small thermal mismatch in the invar-quartz interface producing radial forces on the proof mass rim.

3) Quartz rim pad geometry asymmetry due to processing variations.

4) Thermal expansion coefficient strain across the annular epoxy ring joining the sensor assembly to its housing cover.

5) Warpage of the sensor mounting flange when clamped due to non-planar mounting pads transmits strain into the sensor assembly.

6) Servo electronics pick-off null stability.

Internal proof mass strain contributors are as follows.

1) Conductive epoxy-quartz interface.

2) Conductive epoxy bridging opposing torquer coils.

3) Coil-epoxy-quartz interface.

4) Vapor deposited metal-quartz interface.

5) Changing quartz internal strain.

6) Magnetic particle contamination.

7) Electrostatic charge build up on unplated quartz area.

External Strain Contributor Discussion

During the entire development and production history of Q-Flex at Sundstrand Data Control, Inc., mechanical structure strain contributors have been explored. Early development efforts centered on dimensional changes of the then two-piece Armco-Invar excitation rings and proof mass rim strain from flex lead attachment. Single piece Invar excitation rings and the development of a thermo-compression flex lead attachment process resulted. Dramatic reduction in bias and bias temperature coefficients were demonstrated. See Table 14. Surface preparation techniques were developed for improved epoxy bonding adhesion in this time frame.

Axial Preload Stress- Elaborate techniques to provide constant clamp preload utilizing spring-loaded, welded sleeves were devised. Additional quartz disk spacers were interposed between the proof mass rim pads and the excitation ring interface surfaces to decouple the proof mass rim from external forces. These additional parts added to cost and made assembly operations much more difficult with no significant bias performance improvement. Therefore, these changes were not incorporated into the Q-Flex standard design.

Radial Stress- During the 1975-1976 time frame, development activity was directed toward evaluating variations in proof mass rim clamp geometry. Twelve sensors were built with a rim clamp pad behind the flexures and highly compliant rim sections to two additional spacer pads. Six more sensors were built with continuous clamping over a portion of the rim and gradually changing limit stop gaps over the remainder of the rim. Several units were fabricated with relieved rim sections for increased radial compliance. No significant reduction in bias, BTC, BTC linearity (BTCL), or bias thermal hysteresis (BTH) were observed.

Table 14

SENSOR DESIGN - TYPICAL COMPARATIVE DATA

	Configuration	PRIOR TO Oct 1973 Std	OCT. 1973-OCT 1974 TC Bonded Flex leads
	Sample Size	328	1700
BIAS (MG)	Mean (ALG)	-2.44	+0.25
	Mean (ABS)	3.67	1.04
BTC (ug/^{o}F)	Mean (ALG)	+23.5	+1.4
	Mean (ABS)	23.5	10.1

Quartz Rim Pad Geometry- If the three planar lands which ultimately interface with the invar magnet structures are eroded or improperly formed, the outer rim of the fused quartz element will be deformed when the sensor is assembled. This will cause stress to be transmitted to the pendulous element and again give rise to bias. This will be especially significant with respect to the thermal coefficient of bias since the compressive force on the lands will be temperature dependent.

Extensive development and improvement in processing techniques have occurred during the last several years to reduce effects from the phenomena. Geometry control and 100% inspection of each processed part after chemical milling has enabled this characteristic to be well controlled as evidenced from the production bias and bias temperature coefficient plots in Figure 3.

Sensor/Cover Stress- Results of $\pm 1g$ tumble tests performed on sensor assemblies before and after being assembled into sensor/cover housings have shown no significant bias parameter shifts. Thus, the location and annular symmetry of the epoxy bridge between the sensor assembly and its stainless steel cover have been retained.

Mounting Flange Stress- The Q-Flex mounting flange is flat when machined to drawing requirements. When the flange mounting pads are mechanically lapped to adjust input axis alignment, improper lapping technique may round off one or more pads unevenly. Then, when the accelerometer is mounted with its hold down screws, flange warpage strain is transmitted asymmetrically through the annular epoxy ring. Bias changes with respect to torquing sequence and torque magnitude resulted. Sundstrand developed and implemented an 'active' axis alignment technique as an integral step prior to epoxy application in the sensor canning operation. This precludes the need to mechanically lap the mounting flange pads.

Electronics Stability- Servo electronics contributions to bias and BTC performance errors are an order of magnitude below the sensor's contributions. The thermal study tests were conducted with 'Harpoon type' transformer pickoff servo hybrid electronics. A new 'monochip' servo hybrid was developed and released for production late in 1975. All new program accelerometer designs incorporate this better performing and more reliable servo hybrid.

The results of the thermal study confirmed the repeatability of bias parameters through several accelerometer remove and remount operations. In order to mount thermocouples in sensors designated for rapid warm-up experiments, sequential temperature tumble tests were performed on 'canned' sensors, then on the same sensors after machining off their housings and recanning in modified housings. No significant bias parameter shifts were observed.

In conclusion, the influence of external forces on proof mass bias have been rigorously examined. Corrective action has been implemented where warranted. The remaining bias strain contributors appear low level and consistent. It is recommended that the mechanical structure configuration be held fixed while major proof mass internal strain contributors are eliminated.

If the stresses transmitted from without the proof mass assembly are small and contribute low level changes to performance that cannot be analyzed until the larger error torques are eliminated, then the source for these large strains must lie within or on the seismic element.

The following analysis shall show that performance should be dramatically improved if two of the stress sources on the proof mass system are eliminated or significantly attenuated.

Conductive Epoxy/Quartz Interface- As denoted previously, a significant bias performance improvement resulting from the substitution of thermocompression bonding for the four asymmetrical conductive epoxy attachments on the proof mass rim dramatically highlights the degree to which this rigid, high thermal expansion coefficient adhesive can produce strain in the low thermal expansion quartz. Now being developed at Sundstrand Data Control, Inc., is a feasible technique to replace the last remaining conductive epoxy bonds for the three torquer coil connections. Two of the bonds connect the torquer start turn wires to the vapor-deposited gold traces on the quartz and the third bond is a lap joint at the torquer coil center-tap. See Figure 27.

One of the Q-Flex accelerometers utilized in this thermal study program, S/N 10450, was one of eight units fabricated with a deliberately excessive quantity of conductive epoxy at the center tap location. The effect was a bridging of the quartz proof mass and overlap connection to both coil forms. Comparison of bias thermal hysteresis for this lot to companion lot units is presented in Table 15.

The present design thermal study test results show correlation between large bias thermal hysteresis (BTH) and inferior bias stability. In addition, production sensor/cover 100% performance screen test data now shows an interdependence between BTH and BTC linearity (BTCL). This relationship was just recently discovered. BTH data as displayed in Figure 3 shows that absolute and algebraic BTH were equal in value until the January 1976 reporting period when the algebraic mean approached zero. Analysis performed on the data showed the strong relationship between these two characteristics.

Figure 27

PROFF MASS ASSEMBLY EPOXY INTERFACE

THREE SIGNAL ATTACHMENTS STILL REMAIN ON SEISMIC ELEMENT.
TWO FORCER COIL SIGNAL LEADS TO DEPOSITED GOLD TRACES.
ONE LAP JOINT FOR CENTER TAP CONNECTION.

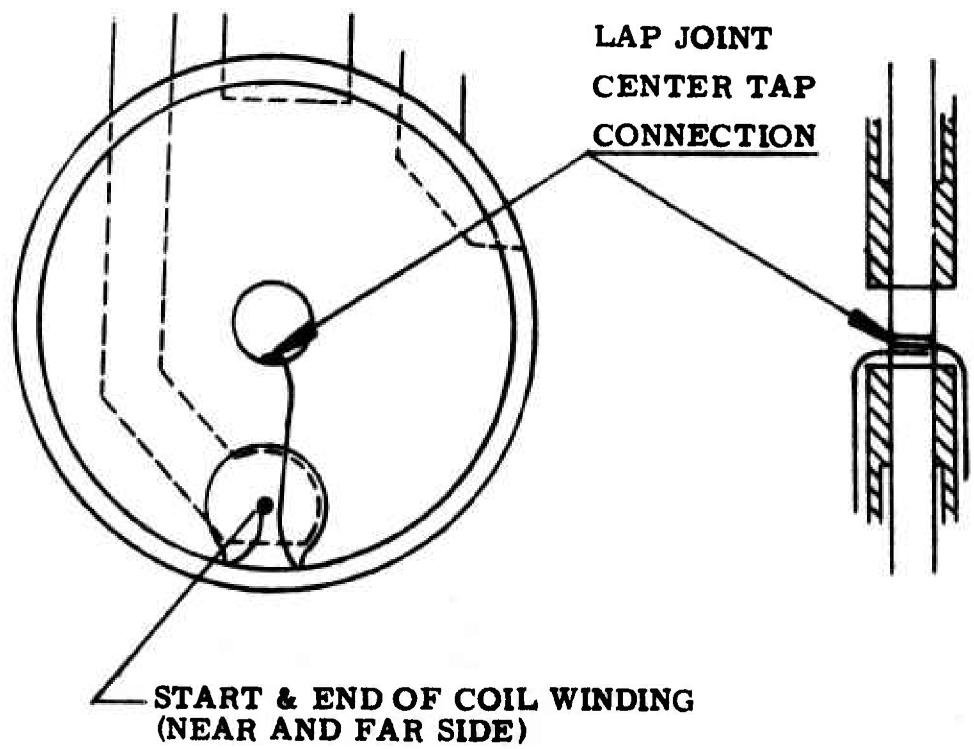

Table 15

SHORTENED BOBBIN EXPERIMENT

	SHORTED BOBBINS	MAY, 74 BUILD
NO. UNITS	11	116
$\overline{\text{BTH}}$	432 ug	108 ug
$\lvert \overline{\text{BTH}} \rvert$	446 ug	212 ug

Figure 28 shows that units with large positive BTH have large negative BTCL and negative BTH accompanies positive BTCL. Minor process changes in assembly techniques, providing a more consistant but random assembly application is the probable cause for this performance change. A prime design objective for reducing BTH and BTCL errors while improving long term bias stability is the elimination of all conductive epoxy from the proof mass assembly, thus eliminaating a major stress contributor on the seismic element.

To accomplish this goal research was initiated in late 1975 to investigate alternate attachment techniques. Preliminary results of these company funded experiments have demonstrated the feasibility of bonding the copper wire to a gold ribbon utilizing resistance welding techniques. Samples of this gold ribbon tab have then been parallel gap welded to the vapor-deposited gold traces using a new thin film bonder. Before experimental hardware can be fabricated new tooling masks to replace the conductive epoxy center-tap lap joint with a vapor-deposited wrap-around gold trace and further refinement in the resistance parallel gap weld schedules are required.

Coil-Quartz Interface - The second major source of strain on the proof mass assembly occurs from coil-quartz interface stresses. See Figure 29. Torquer coil to quartz proof mass attachment was formerly accomplished with rigid LCA4 adhesive. Dimensional stability and strength to tolerate harsh shock and vibration environments are firm design constraints. Coupling the aluminum coil form through rigid epoxy to the low thermal expansion quartz results in strain at all temperatures except the epoxy cure temperature. This can be observed in Figure 30.

Figure 28

INTERDEPENDANCE OF BTCL AND BTH

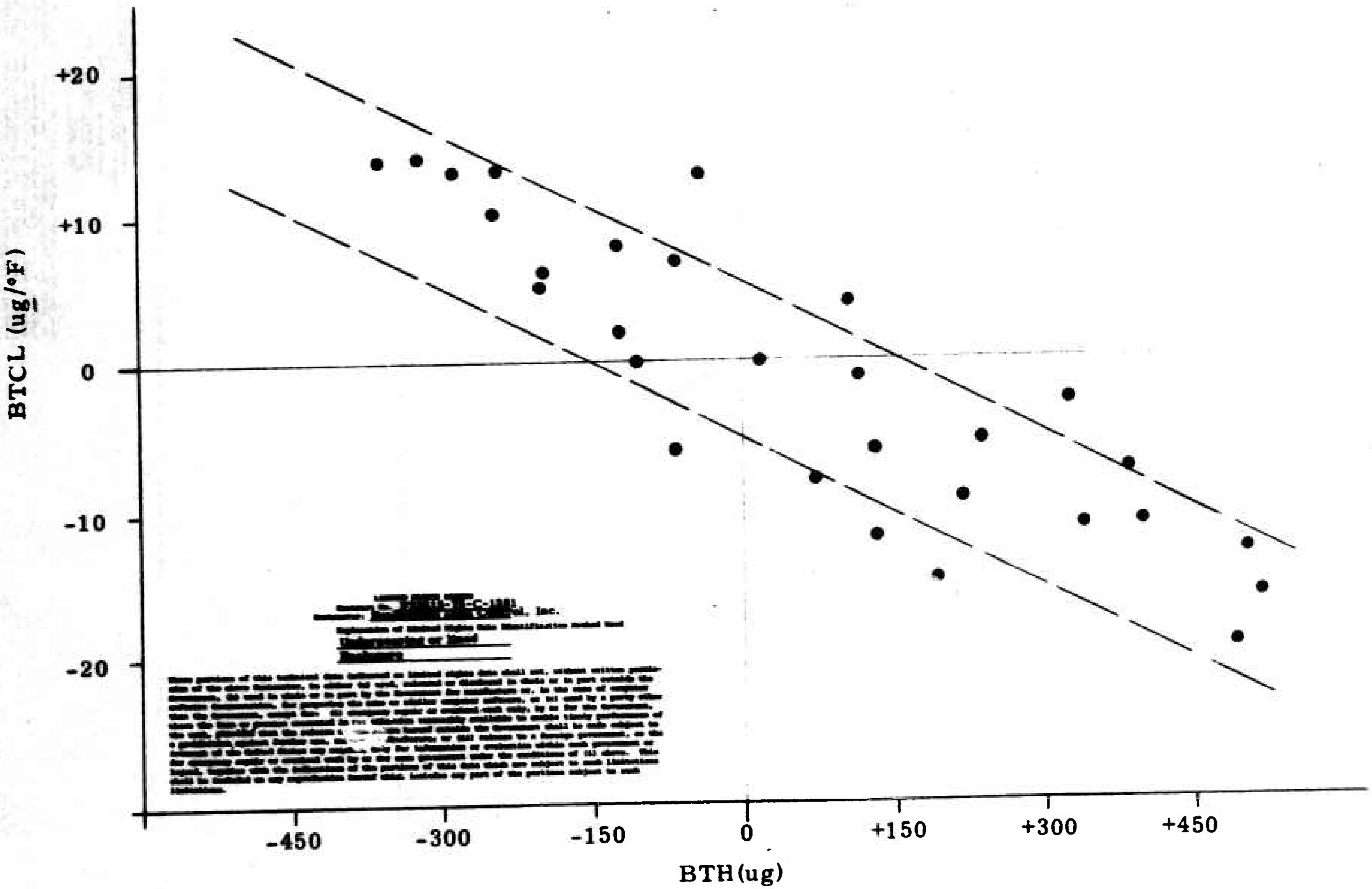

Figure 29

COIL MOUNTING TO QUARTZ

INITIAL CONFIGURATION: LCA4 EPOXY BOND BETWEEN QUARTZ AND ALUMINUM BOBBIN.

PRESENT DESIGN: ELASTOMER BOND BETWEEN QUARTZ AND BOBBIN.

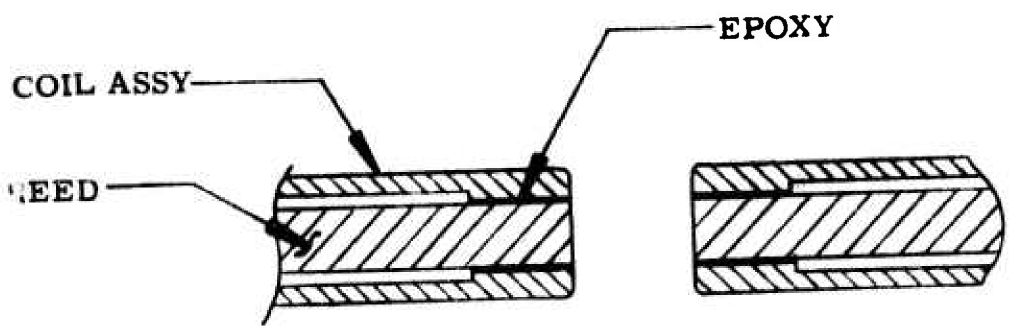

COIL - QUARTZ INTERFACE STRAIN DUE TO THERMAL MISMATCH.

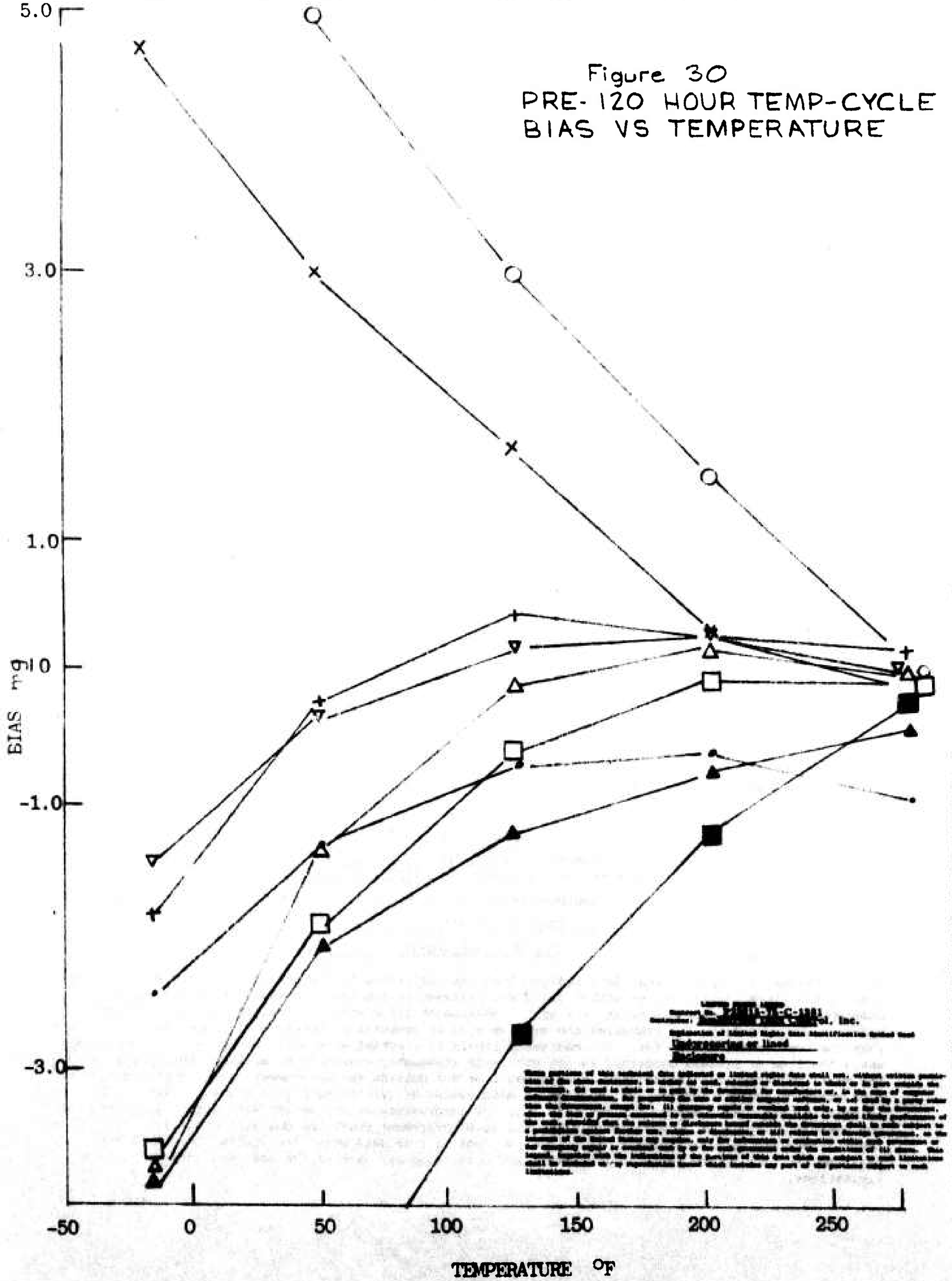

Figure 30
PRE-120 HOUR TEMP-CYCLE
BIAS VS TEMPERATURE

As test temperature approaches 170°F, the plotted sensor biases approach zero. Figure 31 shows how some, but not all, of the units relax with 120 hours of -75 to +250°F temperature cycling such that BTC becomes smaller and more linear. This is additionally demonstrated in Figures 32 and 33 where bias changes radically at -65°F and gradually diminishes as the temperature approaches the epoxy cure temperature.

Figure 34 shows the sensitivity to controlled quantity and location of the LCA4 versus results from a trained, but less experienced assembler.

Table 16 compares attachment with a resilient silastic adhesive, DC3144, to the then standard LCA4 adhesive. Note the dramatic performance improvement for the LCA4 units indicating rapid changes in BTCL, BTH and bias itself. Smaller changes and a more linear BTC characterize the flexible coil adhesive. A flexible silicone elastomer adhesive, DC96-083, is the current standard adhesive, chosen to provide resiliency, yet be heat catalyst curable for ease of assembly operations.

Parallel to the thermal study testing, a development effort has evaluated a sample group of rare earth magnets. Bias stability for 150 days is plotted in Figure 35 for room ambient shelf storage conditions. Several of the units were removed from this test on the 82nd day to support an evaluation of scale factor thermal hysteresis relaxation. Bias temperature coefficient for the same units is shown in Figure 36. It is apparent that the units with the most linear BTC's have the best long term bias stability, even though they do not have the lowest magnitude BTC's. Bias thermal hysteresis on the less stable units is approximately 100 to 200 μg larger than for the best stability units.

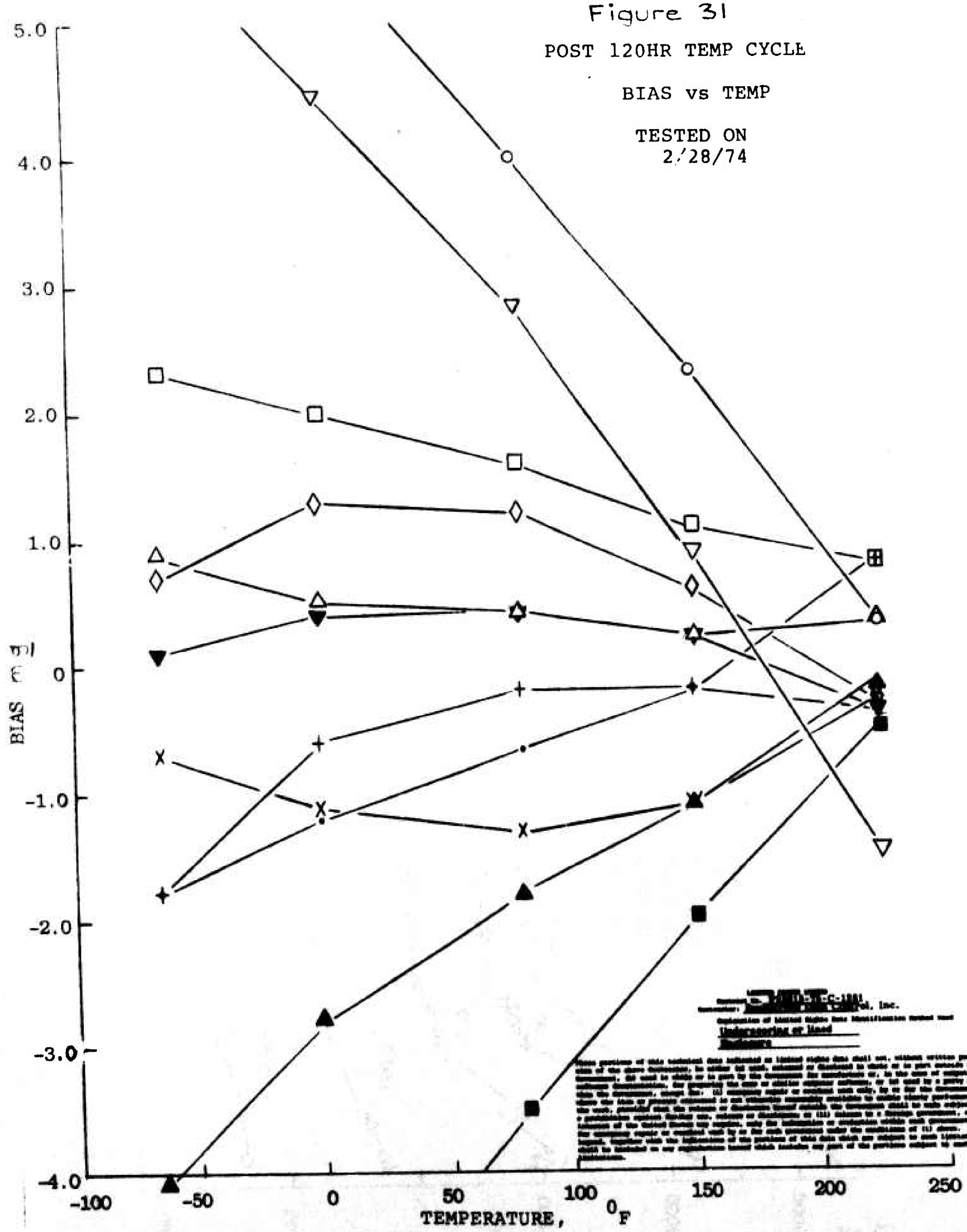

Figure 31
POST 120HR TEMP CYCLE
BIAS vs TEMP
TESTED ON
2/28/74

Figure 32

TEMPERATURE TUMBLE-LIFE TEST UNIT #1
BIAS STABILITY

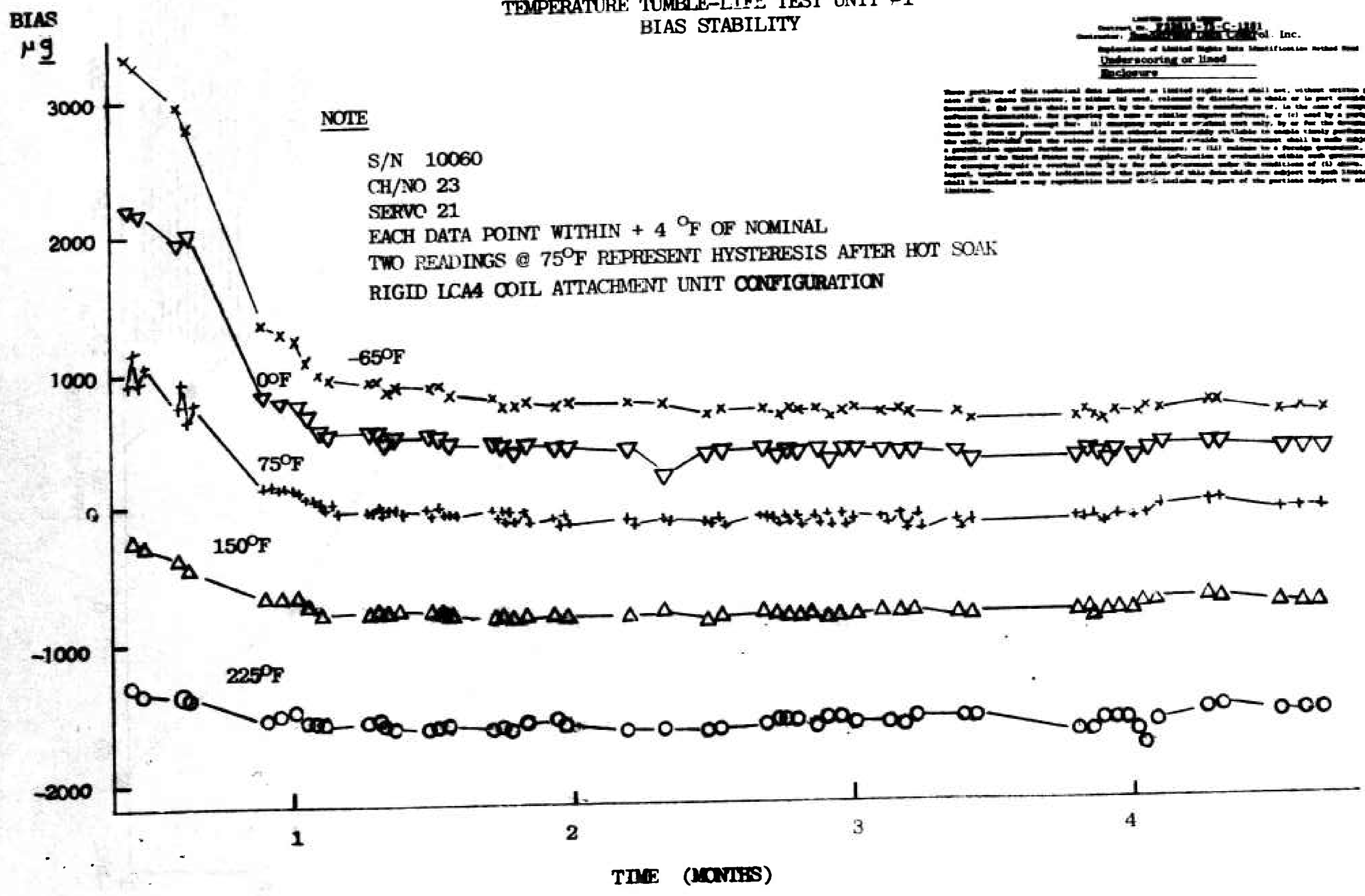

Figure 33

BIAS STABILITY VS TIME-TEMPERATURE

DATA NORMALIZED TO MARCH 27 READING
AND STANDARD TEST TEMPERATURES

SYMBOL	BIAS μg @	Δ T FROM COIL CURE
×	-65°F	-235 °F
▽	0°F	-175 °F
+	75°F	- 95 °F
△	150°F	- 20 °F
o	225°F	+ 55 °F

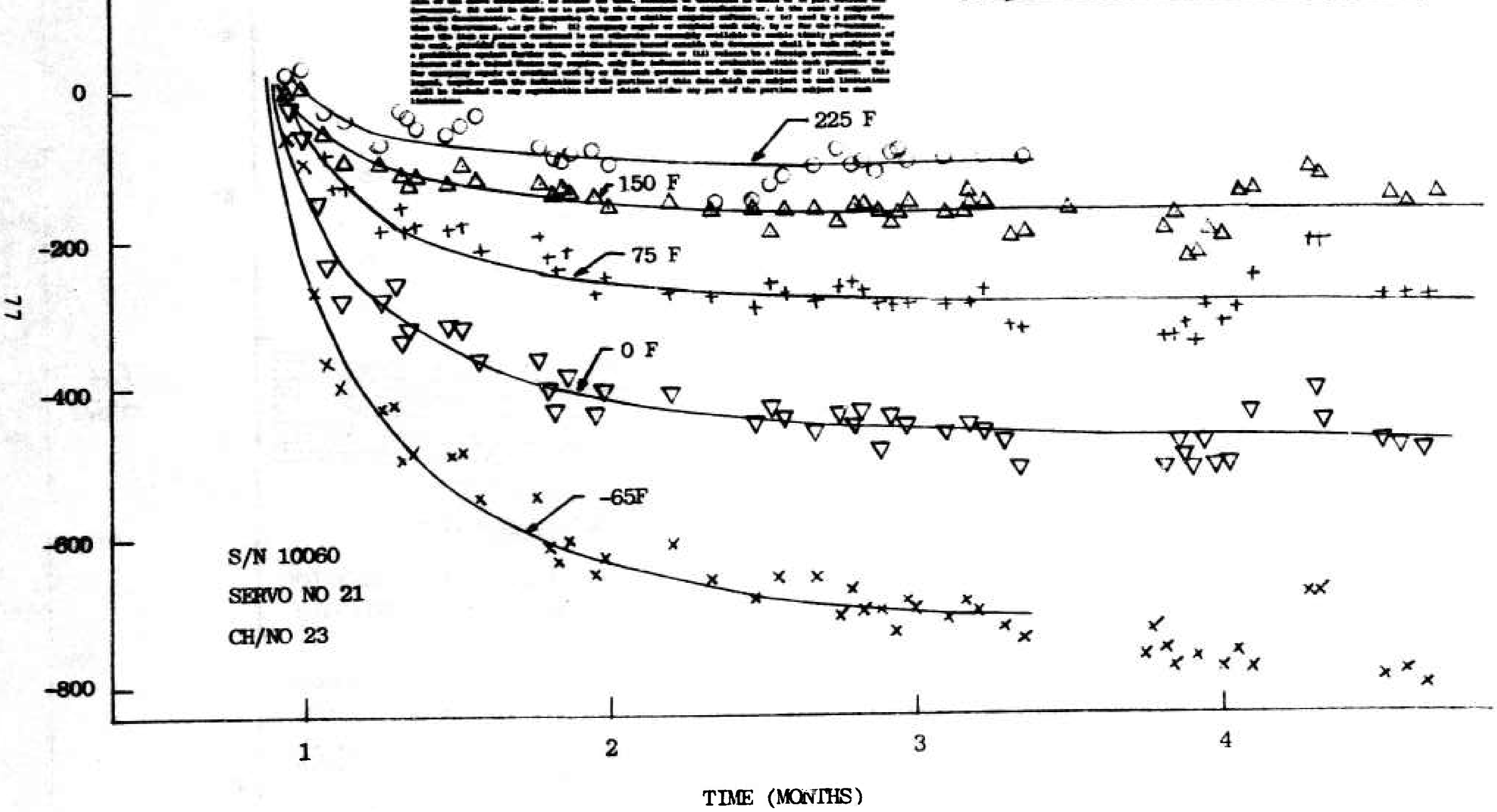

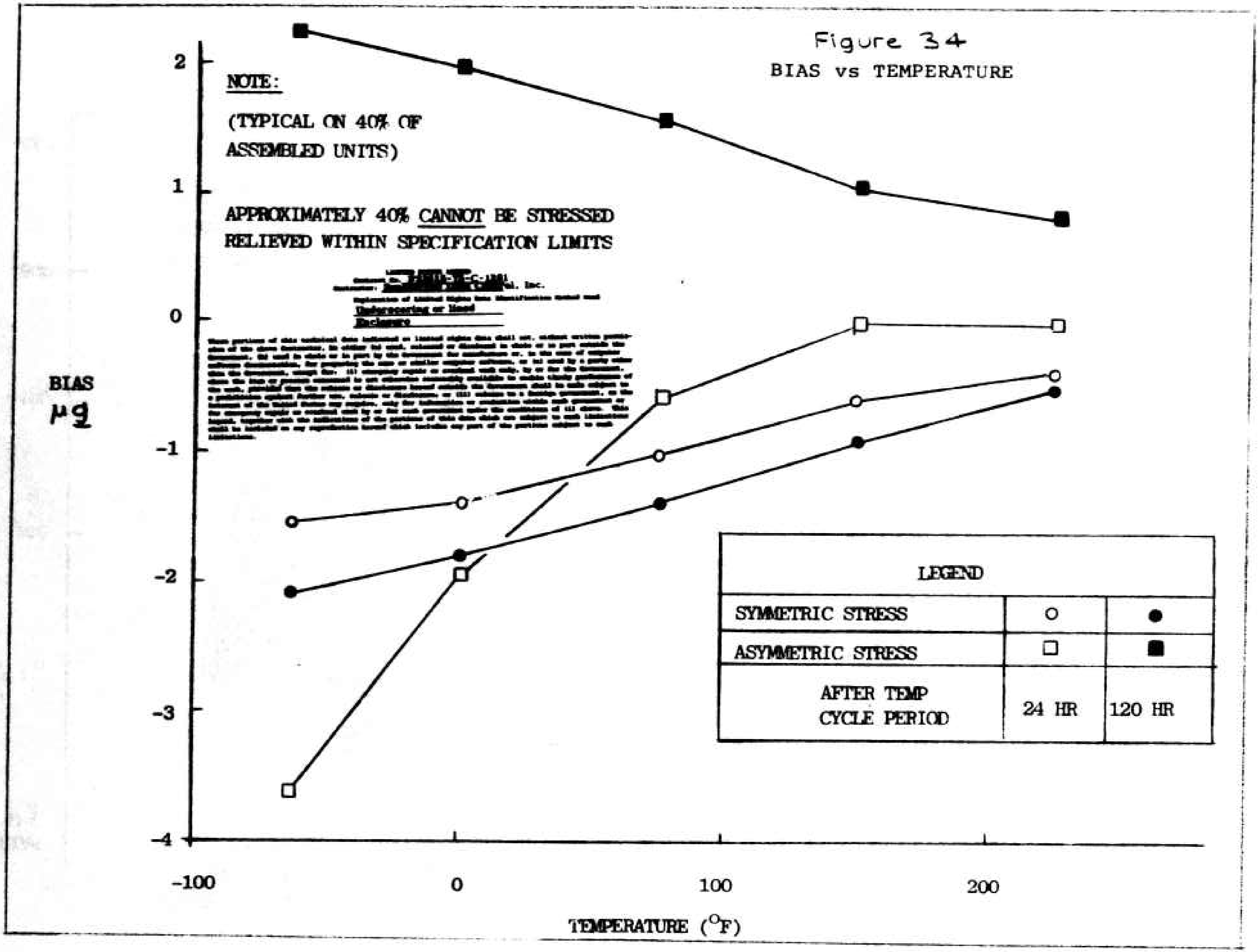

Figure 34
BIAS vs TEMPERATURE

Table 16

COIL - QUARTZ STRESS - TEMPERATURE TUMBLE TEST

	BEFORE 120 HR TEMP CYCLE				AFTER 120 HR TEMP CYCLE			
	FLEXIBLE COIL ADHESIVE		STANDARD CONTROL GROUP		FLEXIBLE COIL ADHESIVE		STANDARD CONTROL GROUP	
NO. UNITS	6		6		5		6	
	$\overline{X}$	$\lvert \overline{X} \rvert$	$\overline{X}$	$\lvert \overline{X} \rvert$	$\overline{X}$	$\lvert \overline{X} \rvert$	$\overline{X}$	$\lvert \overline{X} \rvert$
BIAS, mg	-.70	.88	-1.16	1.91	-.82	.92	-.76	1.40
BTC, $\mu g/^{o}F$	12	12	2	15	9	9	.8	14
BTH, μg	207	207	382	531	153	175	143	161
BTCL, $\mu g/^{o}F$	--	5.5	--	10.8	--	5.8	--	7.2

AFTER TEMP CYCLE

- CONTROL GROUP - PERFORMANCE IMPROVED
  - BTC LINEARITY
  - BIAS TEMPERATURE HYSTERESIS
  - BIAS
- FLEXIBLE ADHESIVE GROUP - NO DRAMATIC IMPROVEMENT
  - SMALL CHANGES THRU TEMP CYCLE
  - MORE LINEAR BTC

Figure 35
150-DAY BIAS STABILITY

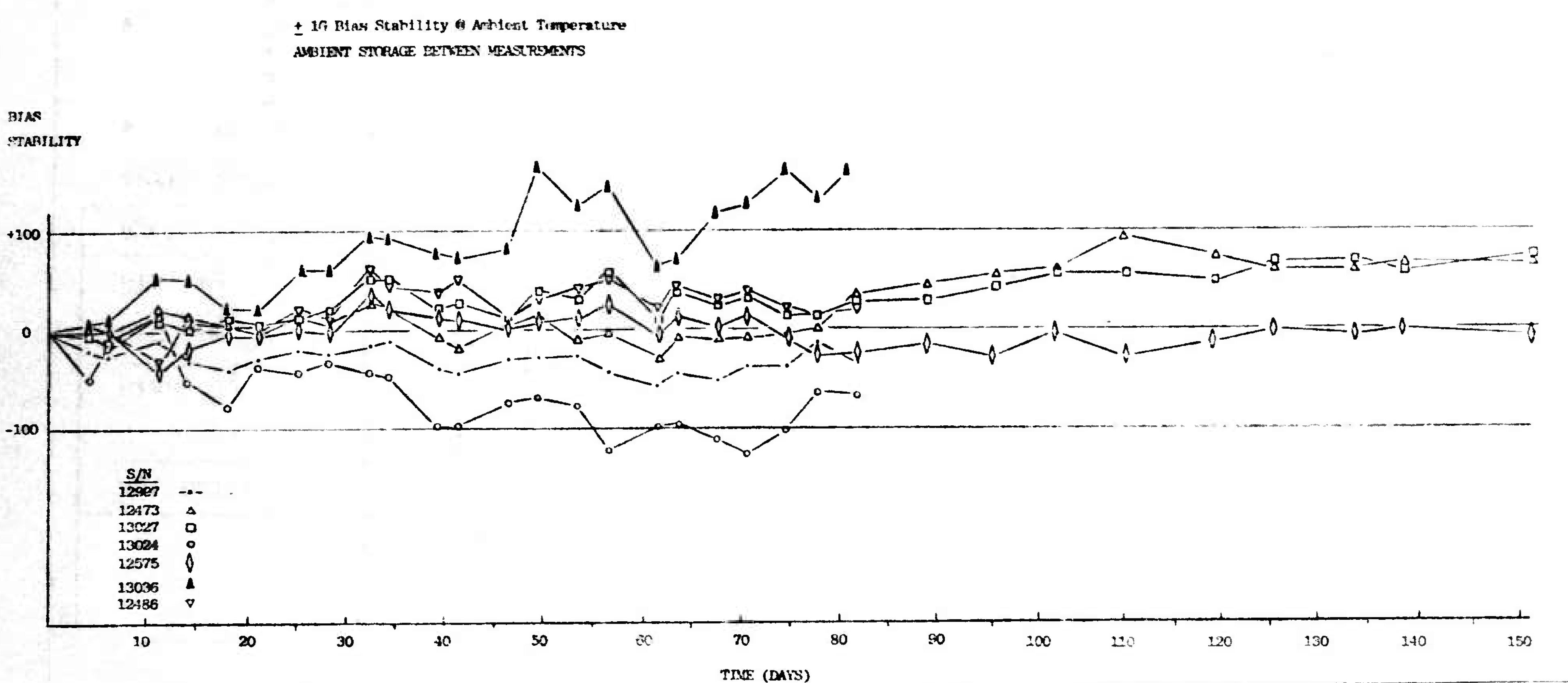

Figure 36
BIAS TEMPERATURE COEFFICENT
RARE EARTH DATA

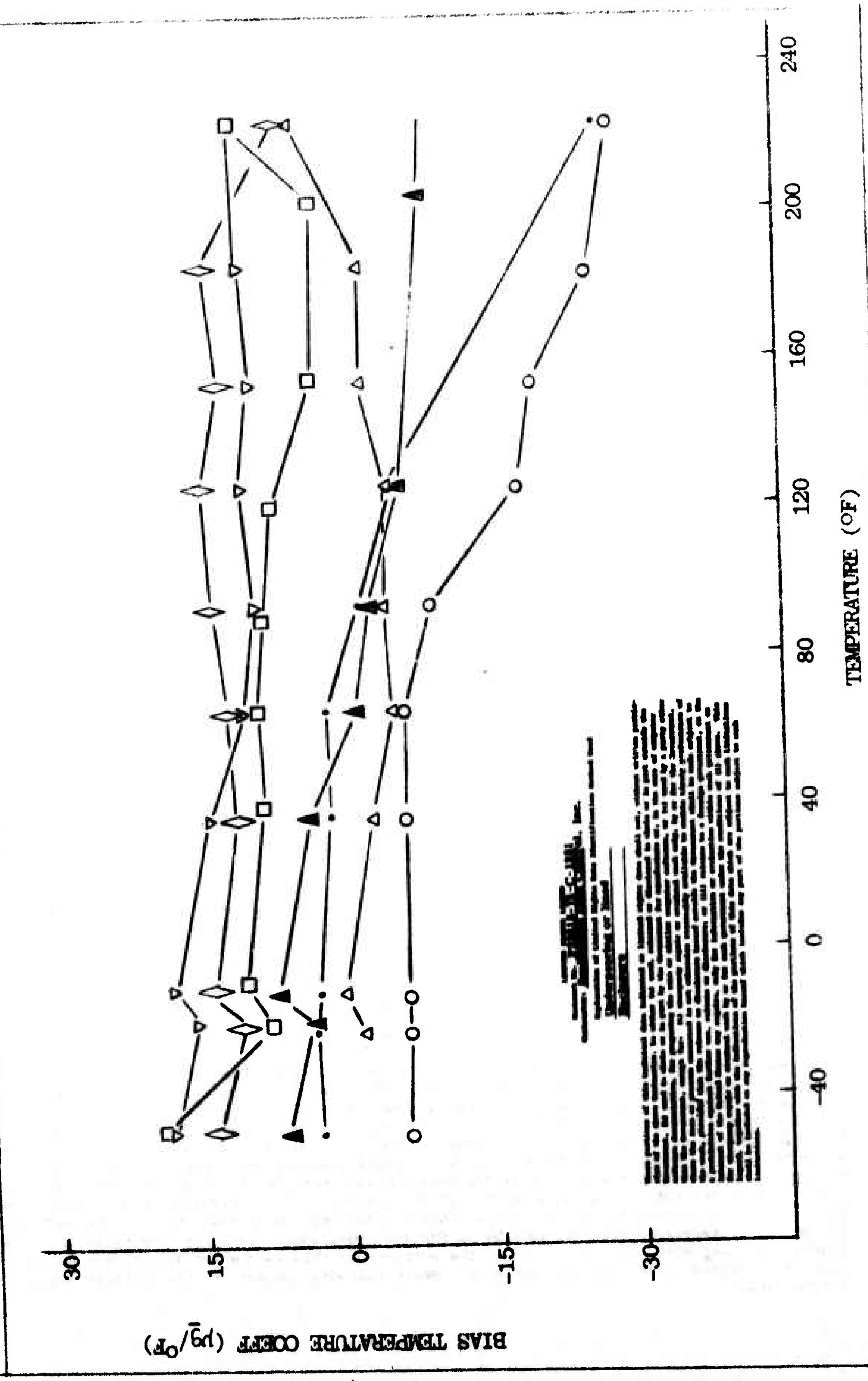

This thermal study has shown that, for many temperature cycles, the shape change in the bias polynoial model is small (< 1μg/°F in 29 days). However, when the wide temperature range desired for rapid reaction is considered, such an error is a significant contributor to bias uncertainty. Thus substitution of a low thermal expansion quartz or ceramic material for the present aluminum coil bobbin material will reduce the thermal expansion coefficient difference stress at the attachment interface.

The present proof mass design attempts to balance these coil attachment stresses in that the two torquer coils have identical 'footprints', are centrally located, and are mounted opposite each other. To determine the most producible, least coercive adhesive-coil form material system for the next configuration of Q-Flex sensor, single coil-proof mass assemblies will be fabricated. This technique will dramatically exaggerate the thermal strains at the quartz-coil interface by allowing direct measurement of the effects of the different adhesives or coil bobbin materials.

Vapor Deposited Metal-Quartz Interface- Another source of bias in the Q-Flex accelerometer is the residual stress in the vapor deposited thin-film metals put on the proof mass and across the flexures for torquer coil leads and capacitor plates. Extreme care is taken to match the side-to-side areas by mask dimensional control, to align the circuits rotationally for symmetry, and to average the side-to-side thickness by depositing at slow rates while rotating the reed. Both the magnitude of the stress level and the degree of matching affect the resultant bias. It is hypothesized that these same mismatched stresses acting as a force couple across the flexure thickness are a source of bias thermal sensitivity.

A company-funded research method, utilizing an autocollimator, rotatable front surface mirror, reed holder,

and single-side deposited etched reed sample, has demonstrated reduced stress levels for aluminum and aluminum/gold depositions as compared to the standard chrome/gold deposition. However, the degree of mismatch is presently thought to be less than 1%. Based on three times normal deposition, single-sided deposition measurements, and 1% mismatch, the bias contribution is estimated at only 60 to 70 μg. In addition, changes to the proven chrome/gold metalization raise questions as to the thermo-compression bondability and possible long term diffusion of aluminum through the thin film of gold. Softer metals than chrome may exhibit lower initial residual stress, but may suffer from metalization creep phenomena (bias trend) or poor adhesion (catestrophic failure). Due to the possibility of lower reliability and the small degree of improvement anticipated, it is recommended that no substitute metal depositions be considered until major strain contributors have been eliminated or appreciably reduced. Additional research at a later date may then be in order to achieve further bias improvement.

Quartz Internal Strain- Internal strain inherent in the fused silica raw material or induced by cutting, grinding, lapping, or polishing processes during reed blank fabrication is a possible source of bias. However, the optical quality fused silica specified by drawing requirement is certified to have a striae rating of grade 'A' and reed blank processes are carefully planned to meet and maintain rigid flatness criteria. The classic stress relief method for this material is total immersion in hydrofluoric acid. As a reed blank, the part is totally etched to aid inspection for scratches and the final flexure trim etch operation involves total immersion. No additional effort is recommended at this time.

Magnetic Particle Contamination- A source of fixed bias can be the attraction of a ferrous metal particle contaminant on the proof mass to the fixed permanent magnet flux field. The fused silica material purity is evident. Other materials chosen

for the proof mass assembly have been closely examined for magnetic properties. The coil bobbins, electropolished for deburring purposes prior to anodizing, are thereby assured free of contamination. Epoxy mixing and coil winding operations are performed in laminar flow clean benches.

Finally, sample proof mass assemblies have been tested for attraction to magnetic fields with negative results. No changes are recommended at this time, except to verify that any process or material change planned by reviewed for possible magnetic properties.

Electrostatic Charge Build Up on Proof Mass- The unplated quartz planar surfaces of the proof mass have been shown to build up a persistent electrostatic charge under certain conditions. Mirror image, opposite sign charges are attracted to the planar capacitor pickoff surfaces of the metal subassemblies. The resulting electrostatic attractive force on the proof mass is a source of bias.

The metal part 'groove and slot' modification prevents the formation of electrostatic charge by forcing contact between the proof mass and the metal parts to occur at the chrome/gold capacitor area. In addition, the sensitivity to electrostatic charge build-up from any source has been decreased by a factor of 200 to 400 by reason of the groove depth and the reduction in the effect as the square of the distance.

No changes are recommended at this time. However, as the major sources of bias are eliminated or appreciably reduced, further refinement activity may be warranted to research the method of achieving an underlying high impedance ground plane that totally covers the proof mass planar surfaces.

In conclusion, the improvement in bias characteristics anticipated from the modifications to eliminate conductive epoxy, change bobbin material, and optimize coil attachment are shown in Table 17. The recommended changes appear feasible, are of comparable cost and ease of assembly and maintain or improve the Q-Flex accelerometer reliability.

Table 17

Q-FLEX BIAS PARAMATER COMPARASION

	Time Frame	ABSOLUTE AVERAGE			LONG TERM TREND		
		Bias (mg)	BTC (ug/^{o}F)	BTH (ug)	Bias (ug/day)	BTC (ug/^{o}F/day)	BTH (ug/day)
Old Design	1971-1974	4	24	300	3	.03	1.5
Present Design	1975-1976	1	10	200	0.7	.01	0.7
New Design	1977-	0.5	5	50	0.2	.003	0.1

Q-Flex Scale Factor

The scale factor model used in this thermal study was:

$$K_1(T) = k_1 + k_2T + k_3T^2 + k_4T^3$$

Where:

$k_1(T)$ = Scale factor model, mA/g

K_2 = mA/g/°F

K_3= mA/g/°F^2

K_4 = mA/g/°F^3

The coefficents, k, can be normalized to the scale factor at 0°F and the thermal model given terms of mA/g and PPM/°F as follows:

$$K_1(T) = SF1(1 + 10^{-6}(SF2 \times T + SF3 \times T^2 + SF4 \times F^3)), \text{ mA/g}$$

Where

$$SFTC(T) = SF2 + (2)(SF3)(T) + (3)(SF4)(T^2), \text{ppm/°F}$$

and

$SF1 = k_1$, mA/g

$SF_2 = k_2 \times 10^6/k_1$, PPM/°F

$SF_3 = k_3 \times 10^6/k_1$, PPM/°$F^2$

$SF_4 = k_4 \times 10^6/k_1$, PPM/°$F^3$

The initial decreasing temperature scale factor polynomial models for four Q-Flex accelerometers are plotted in Figure 37. The scale factor temperature coefficient is similar for all Q-Flex accelerometers and provides a characteristic property with which to discuss Q-Flex performance. The scale factor temperature coefficient models for the four Q-Flex accelerometers are plotted in Figure 38. The coefficients for the polynomial models are listed in Table 18.

Figure 37

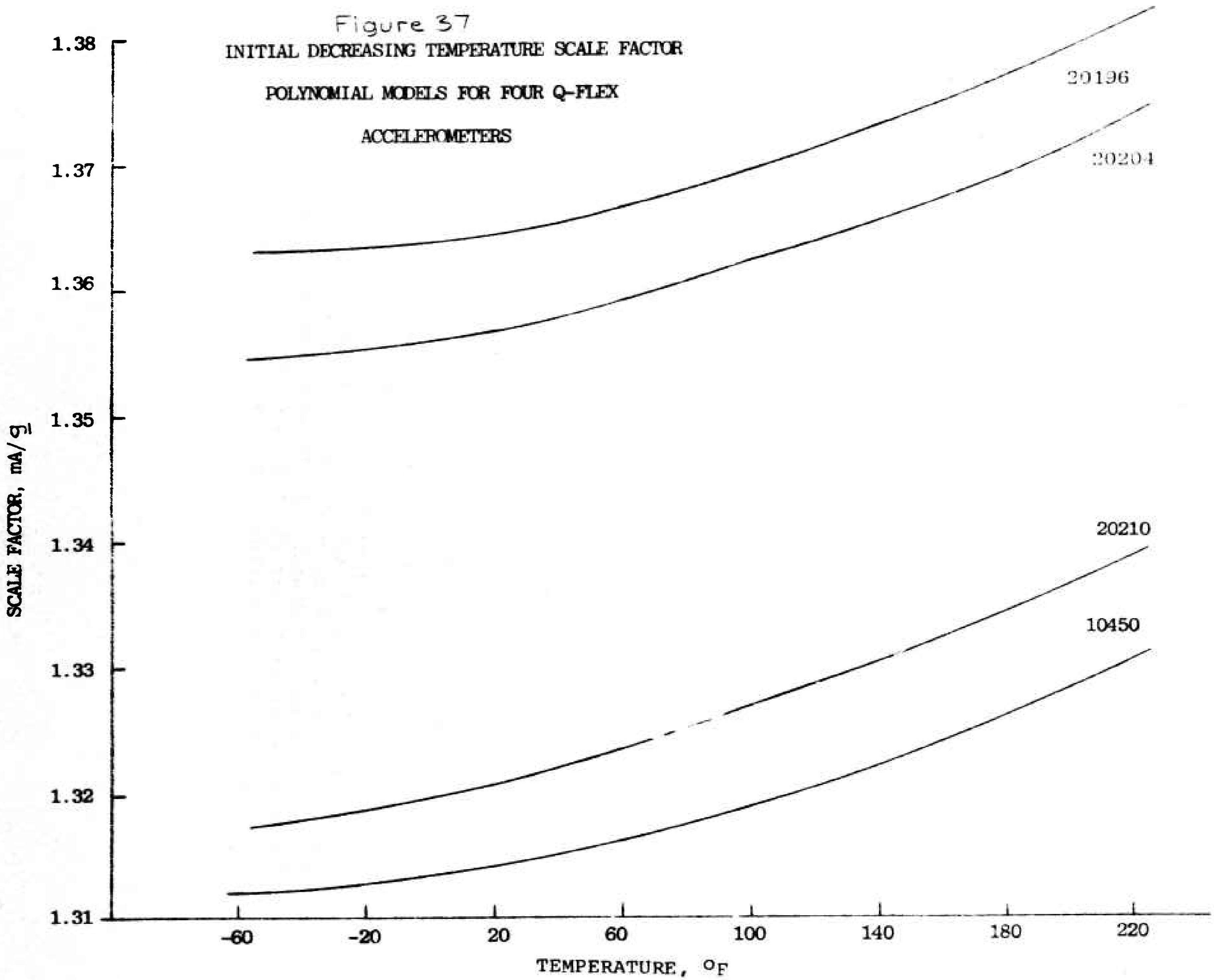
INITIAL DECREASING TEMPERATURE SCALE FACTOR
POLYNOMIAL MODELS FOR FOUR Q-FLEX
ACCELEROMETERS
1.38
1.37
1.36
1.35
1.34
1.33
1.32
1.31
SCALE FACTOR, mA/g
-60
-20
20
60
100
140
180
220
TEMPERATURE, °F
20196
20204
20210
10450

Figure 38

INITIAL DECREASING TEMPERATURE SCALE FACTOR TC MODELS

FOR FOUR Q-FLEX ACCELEROMETERS

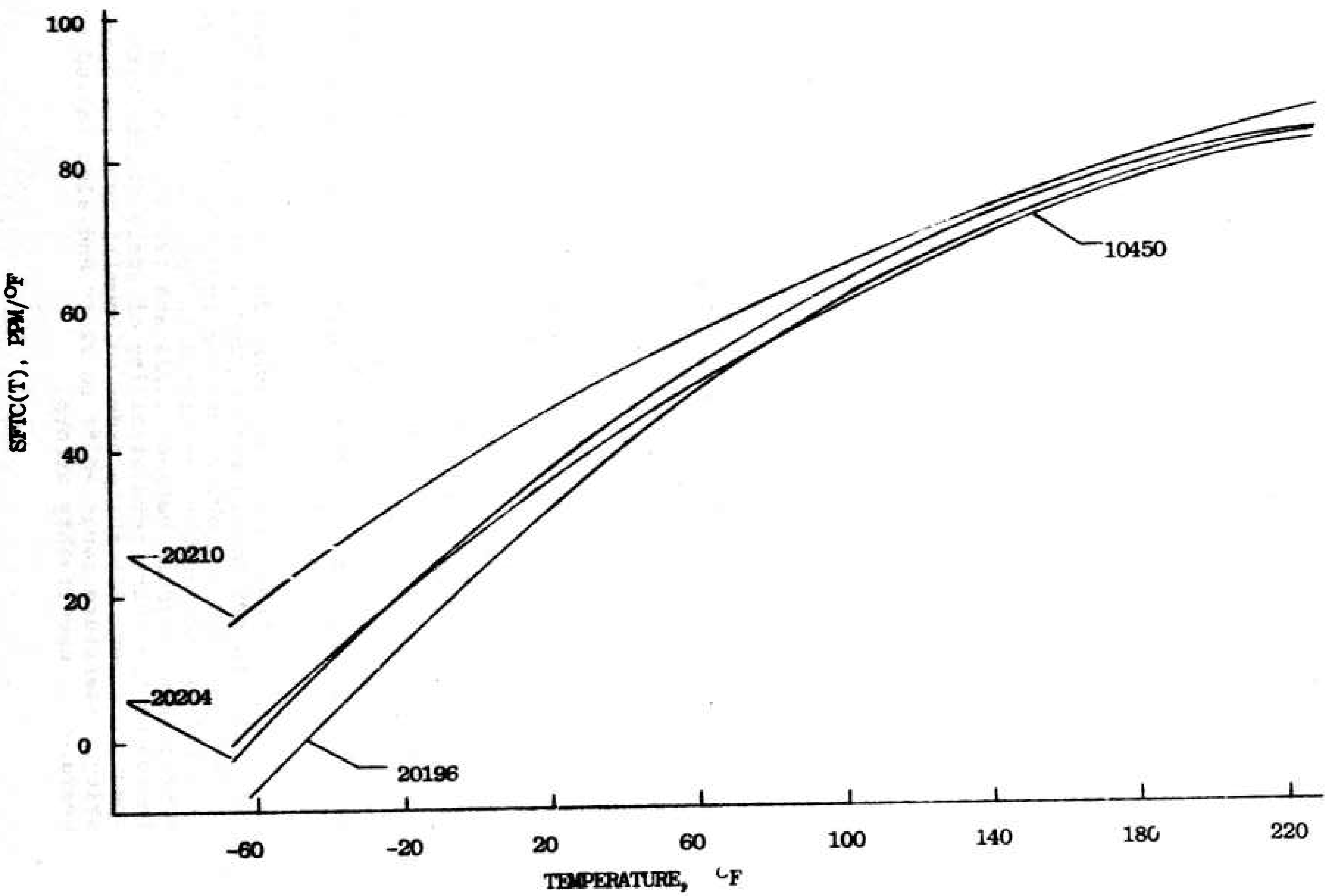

Table 18

Scale Factor Temperature Coefficent Polynomial

For Four Q-Flex Accelerometers

S/N	SF2 PPM/°F	2 x SF3 PPM/°F^2	3 x SF4 PPM/°F^3
10450	28.3	0.38	-.00063
20196	23.0	0.26	-.00084
20204	29.3	0.42	-.00078
20210	39.4	0.30	-.00042

Scale Factor Model Stability

The stability of the scale factor models is determined by examining the RMS residuals of individual polynomial modelings and RMS residual with respect to the initial models computed from tests on 11/24/75 and 11/25/75. Also the temperature coefficient RMS residual with respect to the initial model is examined.

Models for four accelerometers between 11/24 and 12/23 are available. This data set was taken in conjunction with minor loop rapid reaction performance tests with the load resistor hard wired into the test fixture. A supplemental set of data is available on 4/6/76 and 4/7/76. This data was taken with an alternate resistor which was measured to within 23 PPM of the original resistor. The April data does not include modeling for S/N 20196 which had an incomplete data set due to saturated electronics. The most reliable data covers the 29 day period for four accelerometers and will be discussed first.

The individual increasing and decreasing temperature scale factor models were fitted using 16 points each (except as noted in tables) and the individual RMS residuals for all the models are listed in Table 19. The average RMS residual between 11/24 and 12/23 is 36 PPM. This indicates the short term stability of scale factor with respect to a best fit third order polynomial over the operating temperature range -65°F to 225°F and also includes measurement uncertainty errors.

Table 19

INDIVIDUAL SCALE FACTOR POLYNOMIAL RESIDUALS

Increasing Temperature Scale Factor Polynomial Residuals (PPM)

S/N	11/24	12/9	12/22	4/6/76
10450	44	30	30	48
20196	39	32	31	-
20204	43	35	35	47
20210	40	6	35	38

Decreasing Temperature Scale Factor Polynomial Residuals (PPM)

S/N	11/25	12/10	12/23	4/6/76
10450	28	29	28	72
20196	33	50	30	-
20204	41	56	29	47
20210	39	38	30	30

Average RMS Residual for Fits to 12/22 = 36 PPM

Overall RMS Residual for All Fits = 37 PPM

The stability of scale factor over 29 days with respect to the initial models on 11/24 and 11/25 is given by the RMS residuals listed in Table 20. The weighted average residual for this period is 50 PPM, larger than the RMS residuals obtained for individual models to a given data set. The quantities affecting this total RMS residual for later data are residuals due to short term modelability, shift in the scale factor and change in the scale factor shape. To differentiate the significant contributors to the total RMS errors over the test periods, the total RMS value of RMS residuals of scale factor attributed to modelability, temperature coefficient and average scale factor were examined.

The average scale factor with respect to the initial scale factor models are listed in Table 21 and have an average value of -10 PPM for the models on 12/22 and 12/23. This value is well within the 36 PPM for individual modelability. In Table 22 the scale factor temperature coefficient RMS residuals with respect to the initial models are listed and the weighted average value for the 29 day period ending 12/23 was computed at 0.522 PPM/°F. This variation in SFTC when integrated over the temperature range gives an RMS error in scale factor of 44 PPM. This is reasonable since it is comparable to the spread of scale factor about an individual model.

Table 23 depicts the 29 day stability RMS residual using upper polynomial shift residual, the shape residual due to temperature coefficient, and the modelability residual. The total RMS residual, upper and lower, is shown to be $((-10)^2 + 44^2 + 36^2)^{1/2}$ or 58 PPM. This value is comparable to the total residual originally obtained in Table 19. In the 29 day data it is clear that the shape contributes the most variation of the scale factor polynomial model with the short term modelability the next most significant contributor. Shift in the scale factor model is essentially negligible. Data analyzed 135 days after the initial model indicates that the residual due to change in the temperature coefficient does not grow significantly larger. (See Table 22).

The models determined on 4/6/76 and 4/7/76 are well suited for comparison of scale factor temperature coefficient because SFTC is a differential quantity independent of the load resistance. The data is not reliable for determining average change in the scale factor model since a different load resistor was used to test the accelerometers. The original resistor was built into a test console following the first set of test and was not available for testing. The average shift in scale factor models can only be considered to be an upper limit on stability over 135 days.

Table 20

EXTENDED TEMPERATURE TUMBLE TEST SCALE FACTOR RESIDUALS

Referred to Initial Models on 11/24 and 11/25

Increasing Temperature Scale Factor Polynomial Residuals(PPM)

S/N	11/24	12/9	12/22	4/6/76
10450	44	46	65	121
20196	39	36	43	--
20204	43	55	54	100
20210	40	39	42	72

Decreasing Temperature Scale Factor Polynomial Residuals(PPM)

S/N	11/25	12/10	12/23	4/7/76
10450	46	66	55	141
20196	33	59	35	--
20204	42	108	55	124
20210	39	65	44	97

4 Units, 29 days Average RMS Residual;between 11/24 & 12/23= 50 PPM

3 Units, 135 days Average RMS Residual between 11/24 & 4/7 = 105 PPM

Table 21

AVERAGE SCALE FACTOR RESIDUALS WITH RESPECT TO

INITIAL SF MODEL

Increasing Temp. Scale Factor Residuals (PPM)

S/N	12/9	12/22	4/6/76
10450	-21	-34	-72
20196	-9	-21	-
20204	-45	-18	-37
20210	-4	12	-48

Decreasing Temp Scale Factor Residuals (PPM)

S/N	12/10	12/23	4/7/76
10450	-23	-21	-87
20196	-29	-10	--
20204	-49	4	-97
20210	-40	12	-86

28 Days Average Residual Change between 11/24 & 12/23, Hardwired Resistor = -10 PPM

135 Days Average Residual Change between 11/24 & 4/7, New Resistor = -68 PPM

Table 22

SCALE FACTOR TEMPERATURE COEFFICIENT RESIDUALS
WITH RESPECT TO THE INITIAL POLYNOMIAL MODEL

UPPER SFTC POLYNOMIAL RESIDUALS, (PPM/^{O}F)

S/N	12/9/75	12/22/75	4/6
10450	.320	.747	.474
20196	.318	.571	--
20204	.474	.684	.857
20210	*	.612	.457

LOWER SFTC POLYNOMIAL RESIDUALS (PPM/^{O}F)

S/N	12/10/75	12/23/75	4/7
10450	.336	.164	1.41
20196	.574	.183	--
20204	.514	.513	.768
20210	*	.358	.780

4 Accelerometers
29 days Average RMS Residual between 11/24 & 12/23 =.522PPM/^{O}F

3 Accelerometers
135 Days Average RMS Residual between 11/24 & 4/7 =(.688 PPM/^{O}F)

* Limited data set for modeling.

Table 23

RMS RESIDUAL ERRORS

TYPICAL DATA

INCREASING TEMPERATURE SCALE FACTOR POLYNOMIAL RESIDUALS (PPM)						
	29 DAY STABILITY	MODELABILITY	SHAPE STABILITY		DC STABILITY	RSS
S/N	11/24 - 12/22	(AVG. 3 READ.)	PPM/^{o}F	COMPUTED (PPM) Ⓐ	(0^{o}F)	COMPUTED
10450	65	30	.747	61	-34	76
20196	43	31	.571	46	-21	59
20204	54	35	.684	55	-18	68
20210	42	35	.612	49	12	61
RMS	52	33	.660	53	23	67

Ⓐ - BASED UPON $\pm$ 145^{o}F ΔT

The individual model residuals for the April data are included on Table 19 and the overall residual for all models (excluding S/N 10450 on 4/7/76) was computed to be 37 PPM. The model for S/N 10450 on 4/7/76 was a RMS residual of 72 caused by 3 points more than ±120 PPM away from the scale factor model. Since such a large deviation of scale factor data was not observed for any other model throughout the study, this model is excluded from discussion of the results over 135 days.

The RMS residual of the 5 April models relative to the original model are listed in Table 20 and the average residual is 105 PPM over 135 days. This value is 55 PPM larger than the 29 day data mainly due to shift in the scale factor. The average shift given in Table 21 is -68 PPM and the RMS residual due to a .688 PPM/°F RMS residual in SFTC (see Table 22) is 58 PPM. The residual due to SFTC change increased only 14 PPM between the 29th and 135th day. Thus the shape of the scale factor model is more stable than would be indicated by the 29 day data.

Total RMS residual over 135 days was calculated to be 105 PPM. By evaluation of the individual residuals, the total is estimated to be $((-68)^2 + 37^2)^{1/2}$ or 97 PPM over the four and one half month test period.

Scale Factor stability - Minor Loop Data

Scale factor stability data through thermal environments for Q-Flex accelerometers over 42 days and 100 days at -65°F, 15°F, 70°F, 145°F, and 225°F are plotted in Figures 39 through 43. As with bias, a straight line was fitted by least squares to each data set to determine scale factor trending. The model used was:

$$\Delta SF(t) = M_{SF} \times t + \Delta SF_o$$

Where

$\Delta SF(t)$ = deviation of scale factor at time t, in PPM

M_{SF} = scale factor stability slope, in PPM per day

t = time since initial test, in days

ΔSF_o = initial scale factor deviation determined by least square fit, in PPM

$\Delta SF(t)$ is defined as follows:

$$\Delta SF(t) = \frac{(SF(t) - SF_o)}{SF_o} \times 10^6$$

Figure 39
Q-FLEX SCALE FACTOR STABILITY AT -65°F.

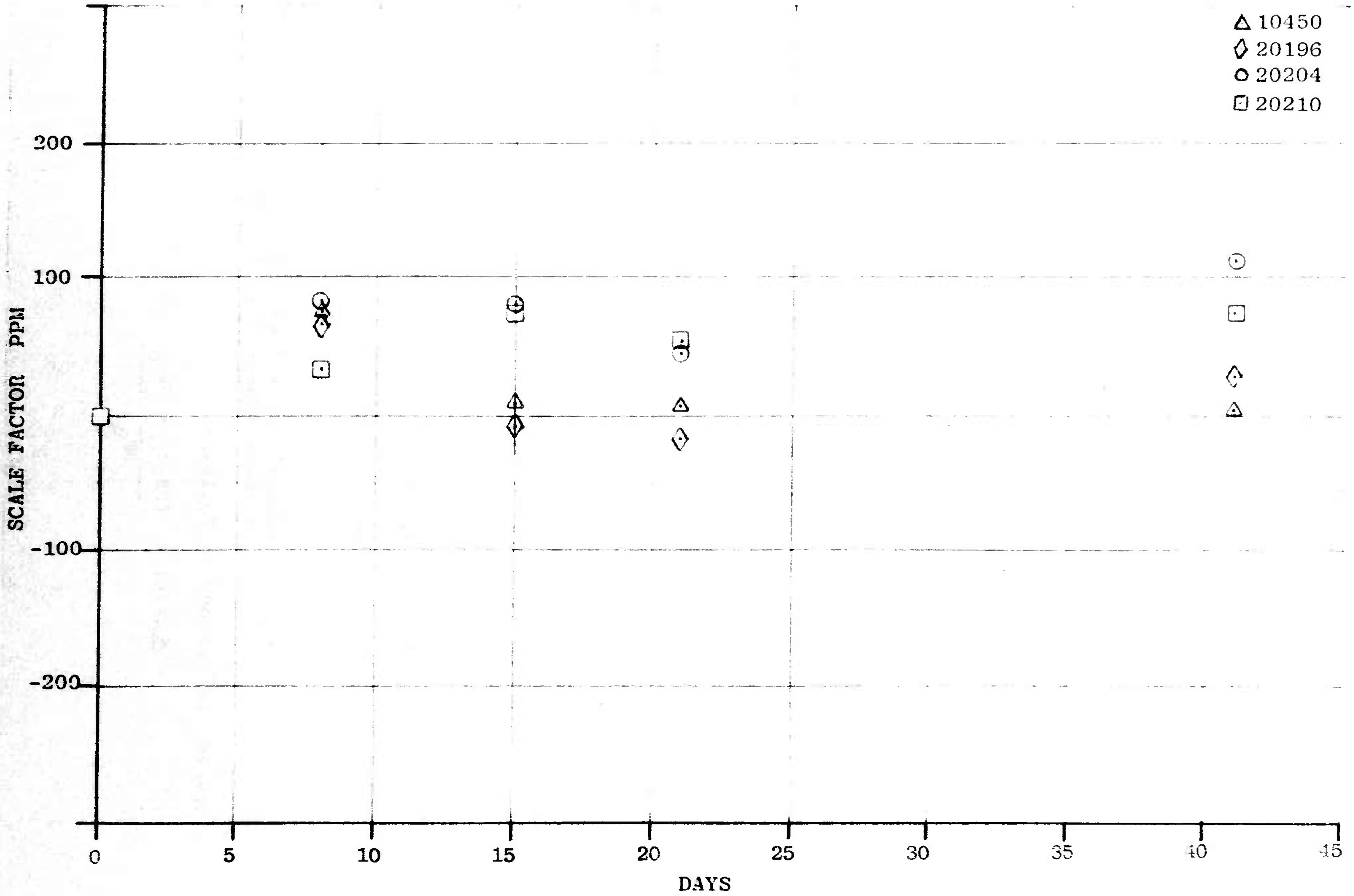

Figure 40
Q-FLEX SCALE FACTOR STABILITY AT +15°F

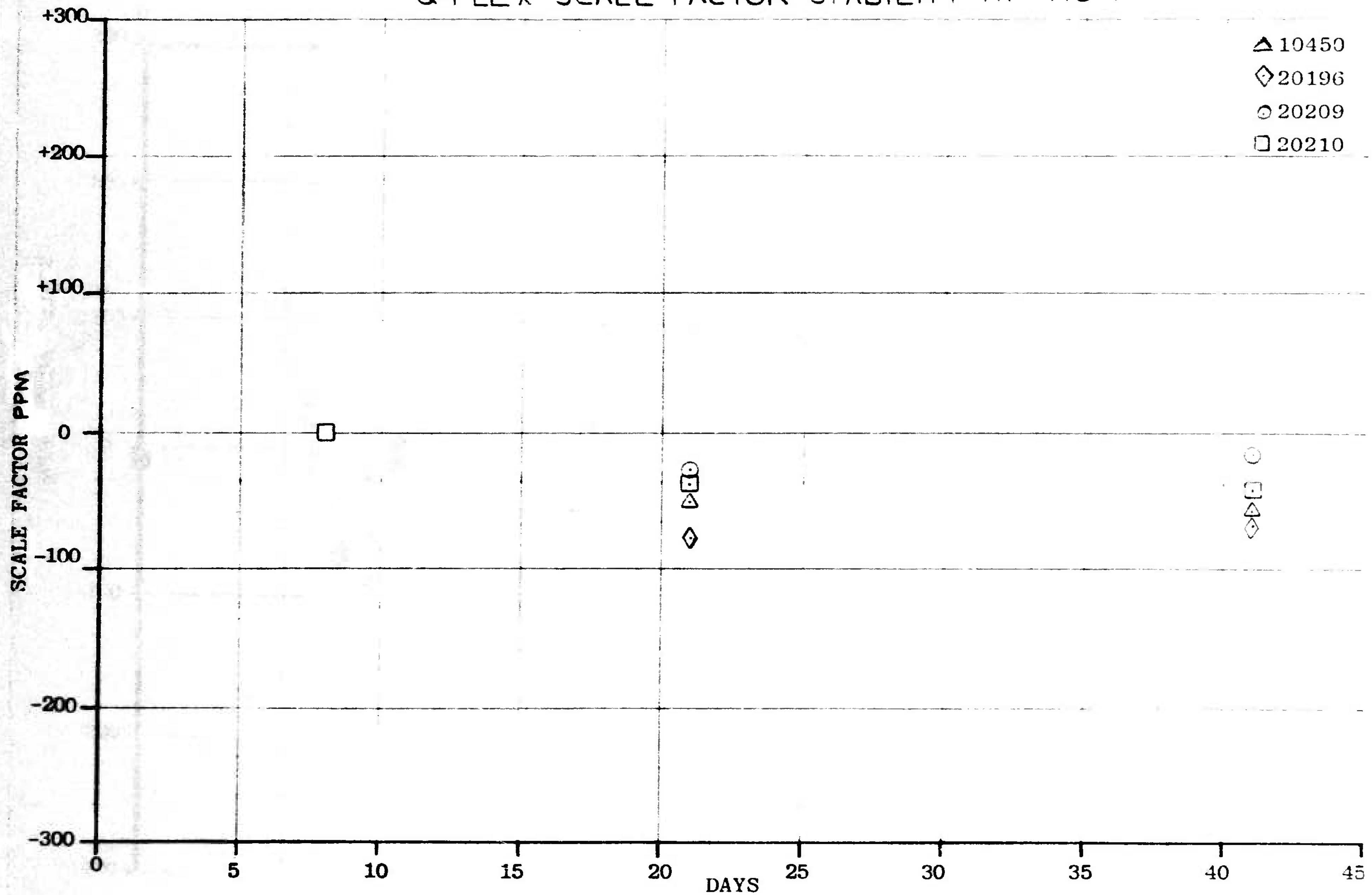

Figure 41

Q-FLEX SCALE FACTOR STABILITY AT +70°F.

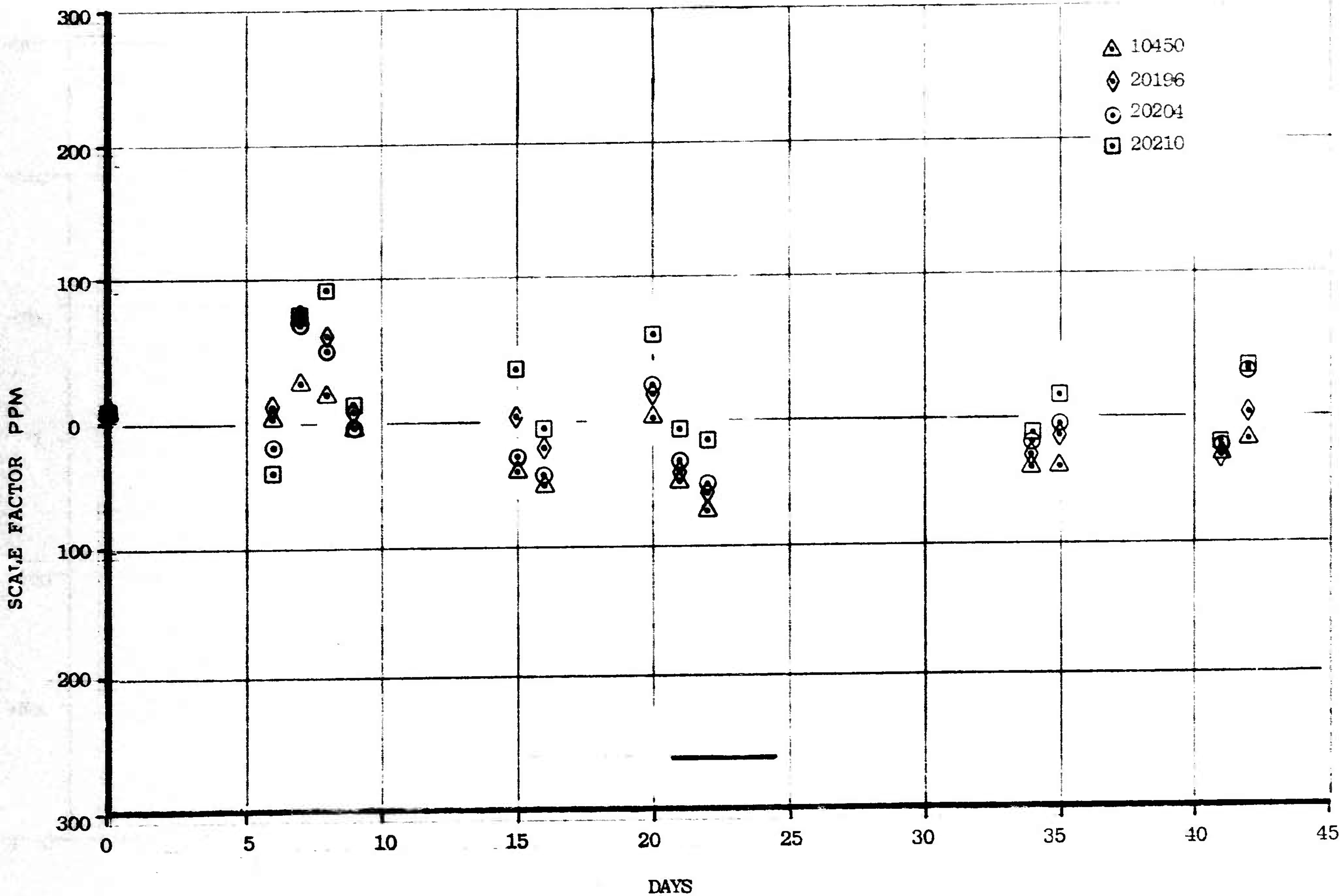

Figure 42

Q-FLEX SCALE FACTOR STABILITY AT +145

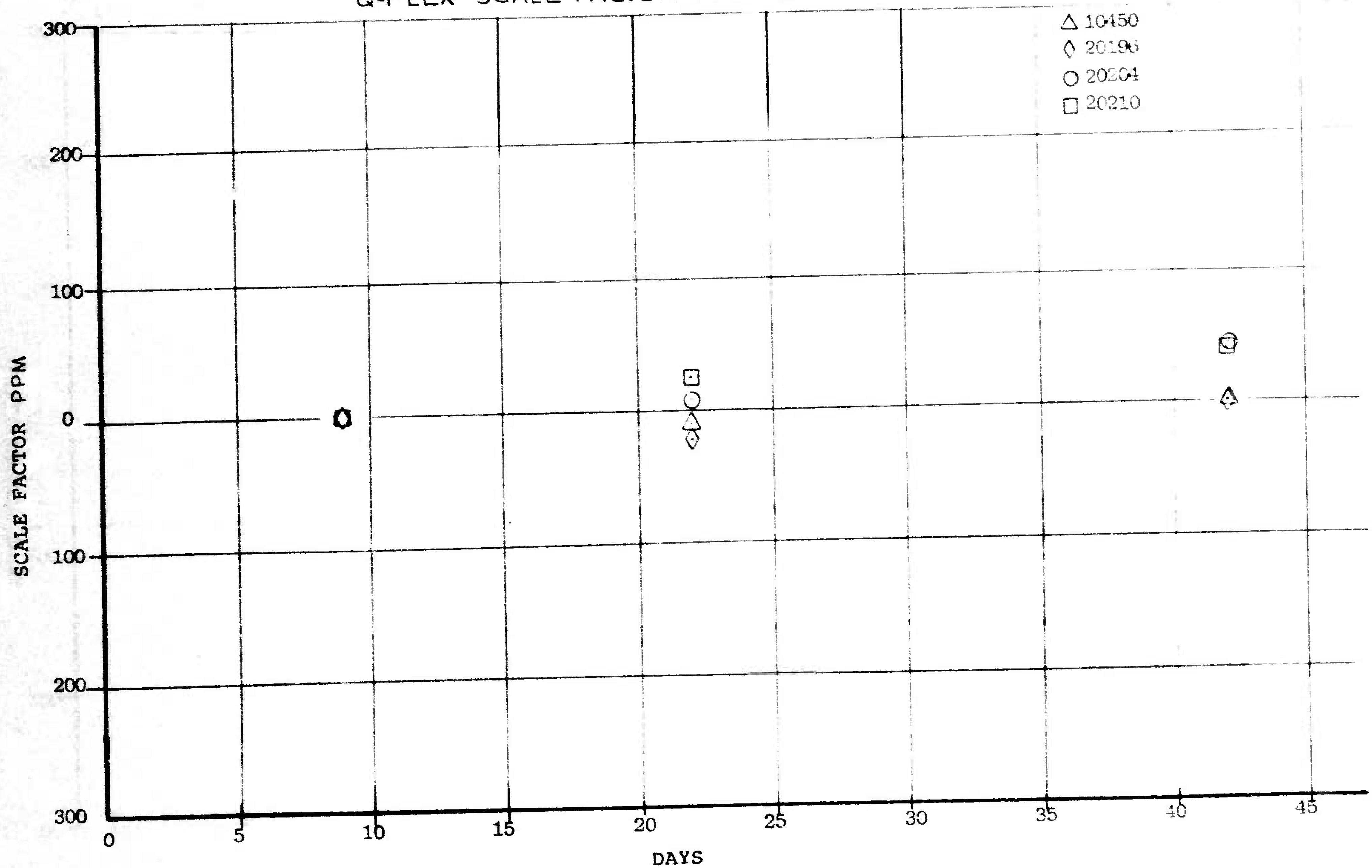

Figure 43

Q-FLEX SCALE FACTOR STABILITY AT +225 °F

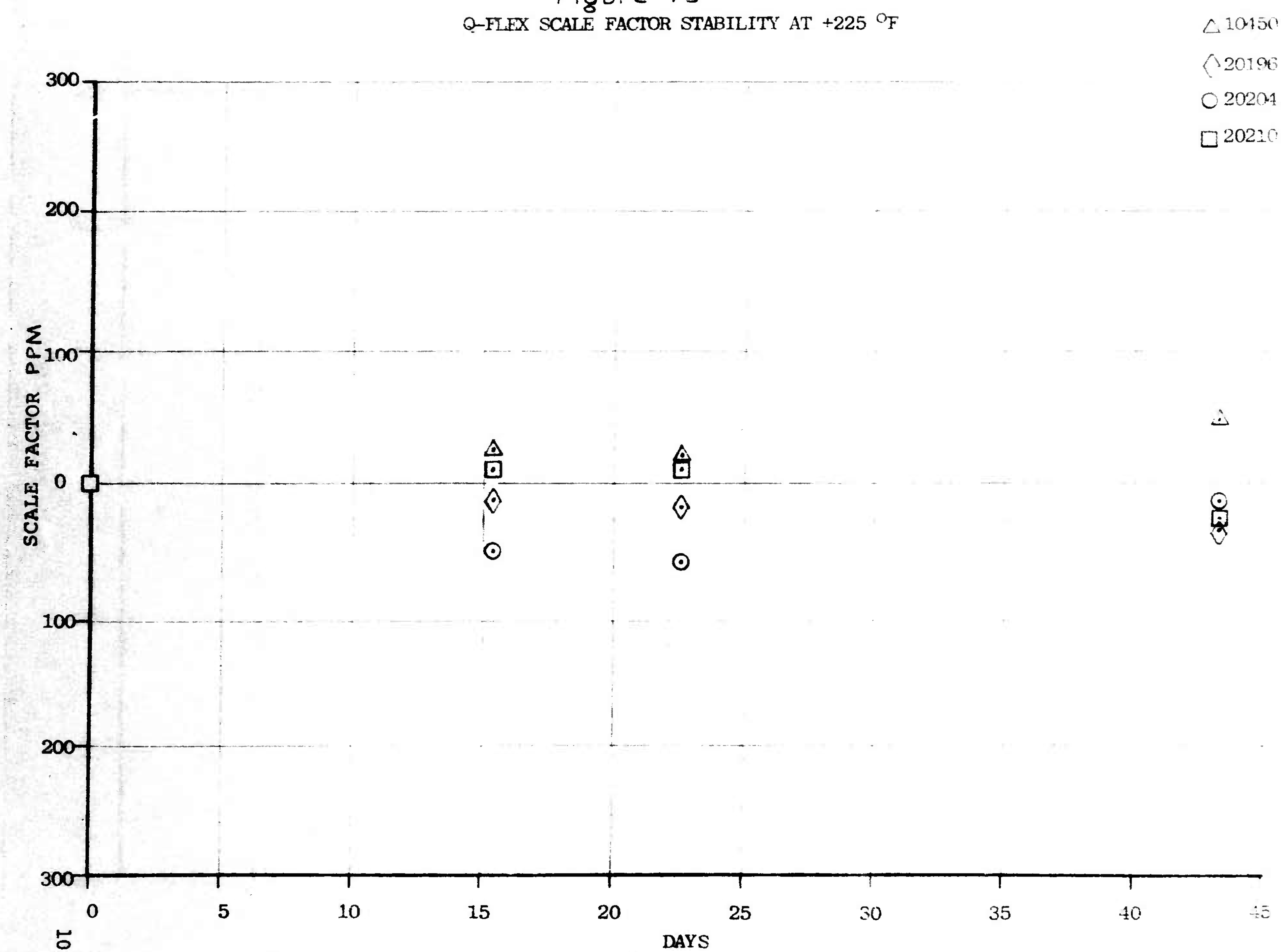

Where

$SF(t)$ = scale factor at time t, in mA per g

SF_o = initial scale factor at t = 0, mA per g

The RMS errors about the average scale factors for the same 42 day and 100 day stability data are listed in Table 24. These RMS errors are not the RMS errors to the individual polynomial fits but rather define the error band of stability for each accelerometer at each temperature. The average RMS error is 35 PPM over 42 days and for S/N 20210 over 100 days at 70°F, the RMS error is 36 PPM.

Table 24

RMS ERRORS ABOUT THE AVERAGE SCALE FACTOR BETWEEN -65°F and 225°F

S/N	-65°F	15°F	70°F	145°F	225°F
10450	30	28	28	6	20
20196	32	38	36	12	12
20204	40	11	36	23	27
20210	30	21	39	18	15

Average RMS ERROR for all Accelerometers over 42 days at all temperatures = 35 PPM

RMS ERROR for S/N 20210 at 70°F over 100 days = 36PPM

The stability slopes at each temperature are shown in Table 25.

The stability slope of 0.9 PPM per day determined for the 42 day data is deemed not significant because the error due to such a slope would be 38 PPM in 42 days but the RMS value from all error sources for the same period based upon the model was 43 PPM (See Table 20). In addition, accelerometer S/N 20210 displays an absolute average slope of over 42 days of 0.9 PPM per day, making it typical of the four units measured for 42 days, but over a 100 day time frame S/N 20210 shows no scale factor trend and has an RMS error for that period of 36 PPM. See Figure 45. The data thus gives no convincing evidence of trend over 42 days.

ET3 data for scale factor stability has been previously discussed in terms of model RMS errors over the entire operating temperature range. Table 26 lists the stability of scale factor parameters at 0°F for four Q-Flex accelerometers over various time periods. The pointwise stability of the ET3 data can thus be seen to be comparable to the minor temperature loop data.

The RMS errors observed in this data are comparable to the short term modelability observed for all ET3 data discused previously. Finally the 42 day data does not show any systematic change in shape among the four accelerometers.

Scale Factor Stability Conclusions

The following conclusions are obtained from the ET3 data and minor loop data.

1) Short term modelability of the Q-Flex scale factor is better than 40 PPM.

2) The scale factor temperature coefficient is stable to better than .7 PPM/°F over 135 days.

3) The temperature coefficient stability is influenced significantly by the inherent modelability of scale factor and does not appear to have major impact upon rapid reaction performance.

4) Scale factor stability was bounded below 0.5 PPM per day over 135 days by the study data.

Table 25

SCALE FACTOR STABILITY SLOPES BETWEEN

$-65^{O}F$ and $225^{O}F$

OVER 42 DAYS

S/N	$-65^{O}F$	$15^{O}F$	$70^{O}F$	$145^{O}F$	$225^{O}F$
10450	-.10	-1.4	-1.1	.04	1.1
20196	-.1	-1.5	-1.2	.02	-.8
20204	+1.7	-0.2	-0.5	1.4	.3
20210	+1.4	-1.1	-0.8	1.0	-.4

Absolute average slope for all sensors over all temperatures is 0.9 PPM per day.

Slope for S/N 20210 at 70F over 100 days is -.03 PPM per day.

Figure 44
Q-FLEX SCALE FACTOR STABILITY FOR 100 DAYS
S/N 10450 TEMP = 70°F

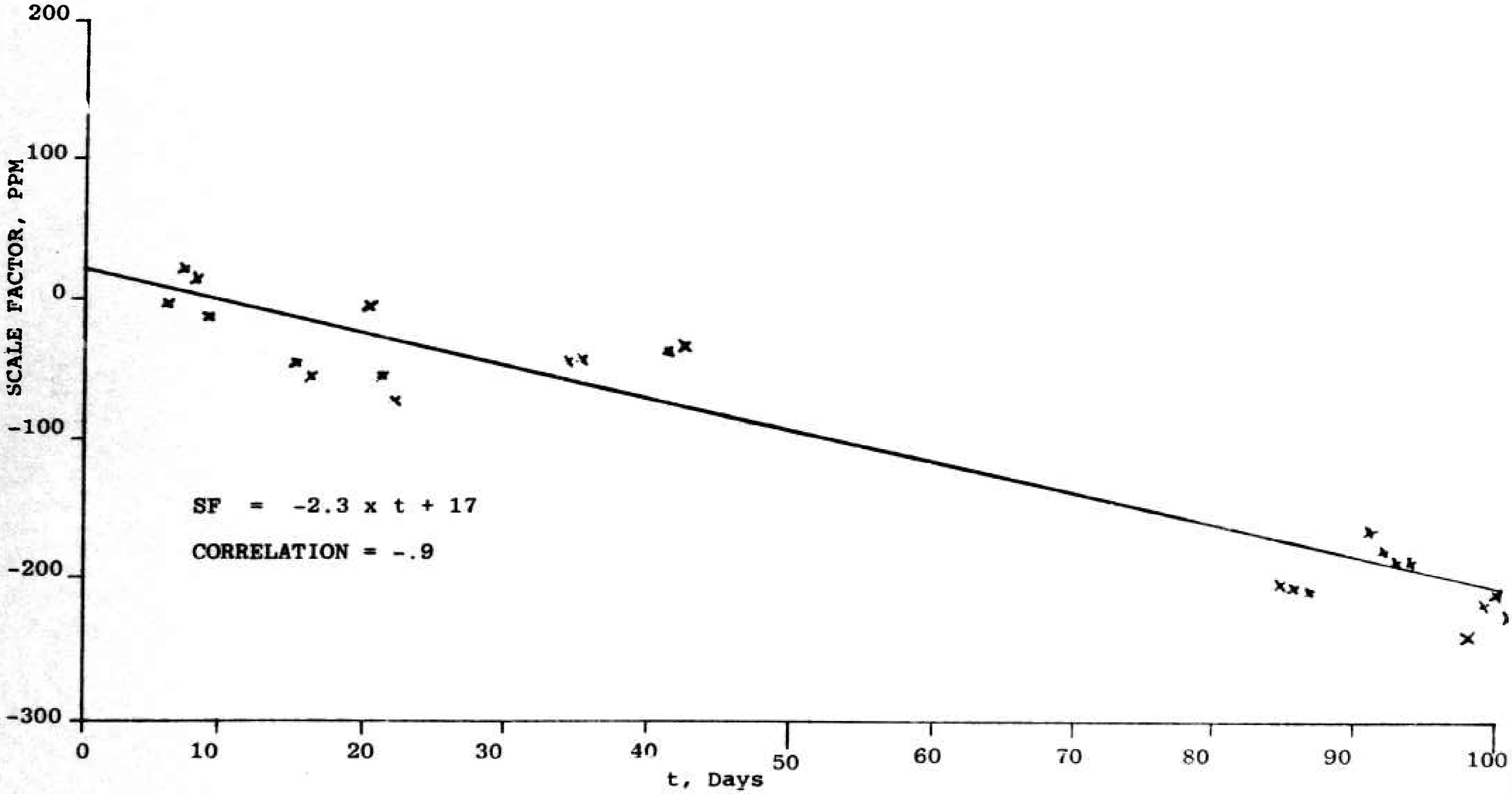

Figure 45

SCALE FACTOR STABILITY FOR 100 DAYS

SN 20210 TEMP = 70 $\pm .1^{O}F$

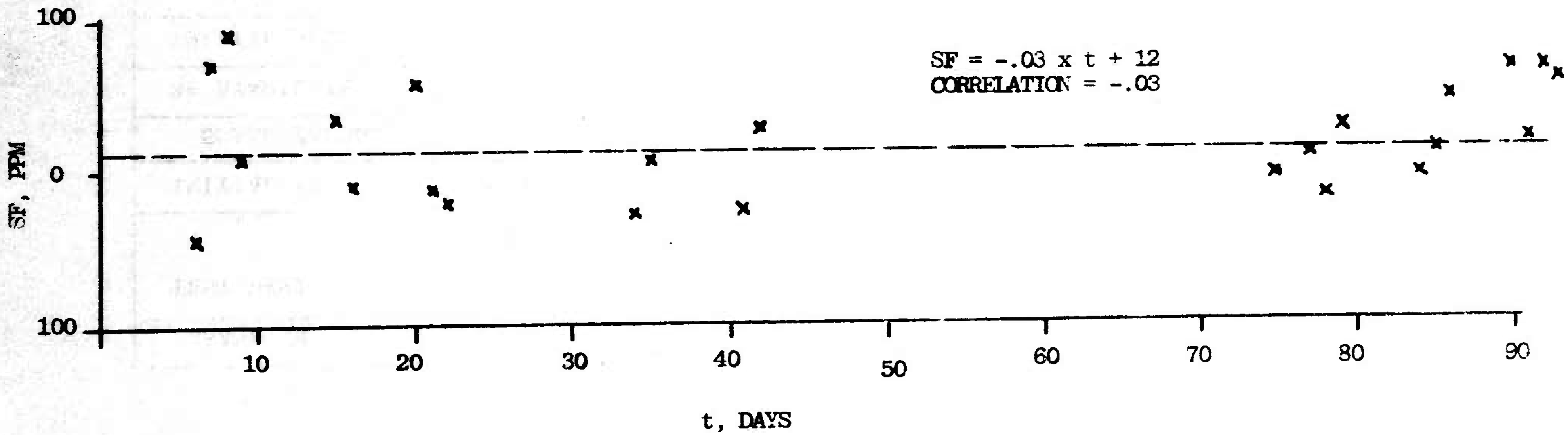

Table 26

LONG TERM SCALE FACTOR STABILITY

PARAMETER	UNITS	10450	20196	20204	20210
TEST PERIOD	CALENDAR	11/25/75-4/7/76	11/25/75-12/23/75	11/25/75-4/7/76	11/25/75-4/7/76
	DAYS	135	29	135	135
INITIAL SF	ma/g	1.313051	1.363946	1.255876	1.319856
SCALE FACTOR	PPM	-129	4	-38	-103
SF STABILITY	PPM/DAY	-1.0	0.1	-0.3	-0.9*
INITIAL SFTC	PPM/°F	28.3	23.0	29.3	39.2
SFTC	PPM/°F	-1.0	-0.1	-0.3	-0.7
SFTC STABILITY	PPM/°F/DAY	.002	-.003	-.007	-.005

- o Based on ET3 Scale Factor model for decreasing temperature
- o Time period variation due to servo electronics changes
- * 100 day data based upon approximately 20 data points depicts no trend.

5) It should be noted that the ability to model is very much dependent upon the ability to accurately measure the steady state temperature for each data point. Since the average scale factor temperature coefficient is approximately 50 PPM/°F, a 0.5°F measurement error would result in a 25 ppm deviation from the true reading. To overcome this sensitivity the torquer coil was monitored and data corrected to ± 0.1°F of the measured reading. An error analysis of this measurement indicates that temperature is, however, only accurate to 0.5°F RMS. Thus, as noted above, data can be counted as a probably worst case error.

Q-Flex Scale Factor Thermal Hysteresis

<u>Background</u>- All Q-Flex accelerometers exhibit positive scale factor thermal hysteresis. That is, the scale factor following a hot soak is smaller in magnitude than that before hot soak at all temperatures within the operating range. Prior to this study scale factor thermal hysteresis was only measured at room temperature for thermal cycles between 225°F and -65°F. For individual accelerometers the value of scale factor thermal hysteresis under these conditions has been demonstrated to be very repeatable.

This study has significantly modified the knowledge of SFTH phenomena. During this study program SFTH was measured over numerous ambients and temperature cycles within the operating temperature range. The shape of SFTH over the temperature range of -65°F to 225°F was modeled with a third order polynomial. SFTH was modeled as a function of temperature cycle extent and cycle center and the minor loops were demonstrated to fall within the major loop thermal hysteresis envelope.

Scale Factor Thermal Hysteresis Models and Relative Minor Cycle Thermal Hysteresis- Figures 46 through 49 show the SFTH models and three minor temperature cycles of four Q-Flex accelerometers. The dashed lines are one sigma error bands about the models. The dome shaped SFTH curve is coincident with the decreasing temperature scale factor model. The SFTH models include effects of scale factor relaxation to be dicussed in the following section. It is noted that the end points of the thermal hysteresis models at -65°F and 225°F do not converge on zero as would be expected for a closed hysteretic cycle. The SFTH models thus form a peak to peak error band into which all thermal cycles fall. It was found that this non-convergence of loop ends was due to scale factor decreasing due to hot soaks and indeed, as a test design requirement, all accelerometers dwelled at 225°F for up to 12 hours between increasing and decreasing modeling runs.

Scale Factor Thermal Hysteresis versus T_M and ΔT- Figures 50 and 51 show the scale factor thermal hysteresis of Q-Flex accelerometers versus ΔT and T_M. Table 27 gives the models' coefficients and Figure 52 shows the average scale factor thermal hysteresis bands versus ΔT and T_M.

The SFTH models versus ΔT and T_M fall into a family of curves and show less variation among accelerometers than the BTH models. This indicates that there is a well behaved driving force behind SFTH which is probably related to structure and materials rather than assembly methods. SFTH is a strong function of ΔT and a weaker function of T_M.

Figure 46

RELATIVE MINOR LOOP SCALE FACTOR THERMAL HYSTERESIS

SN 10450 DATES: 11/22/75 - 12/5/75

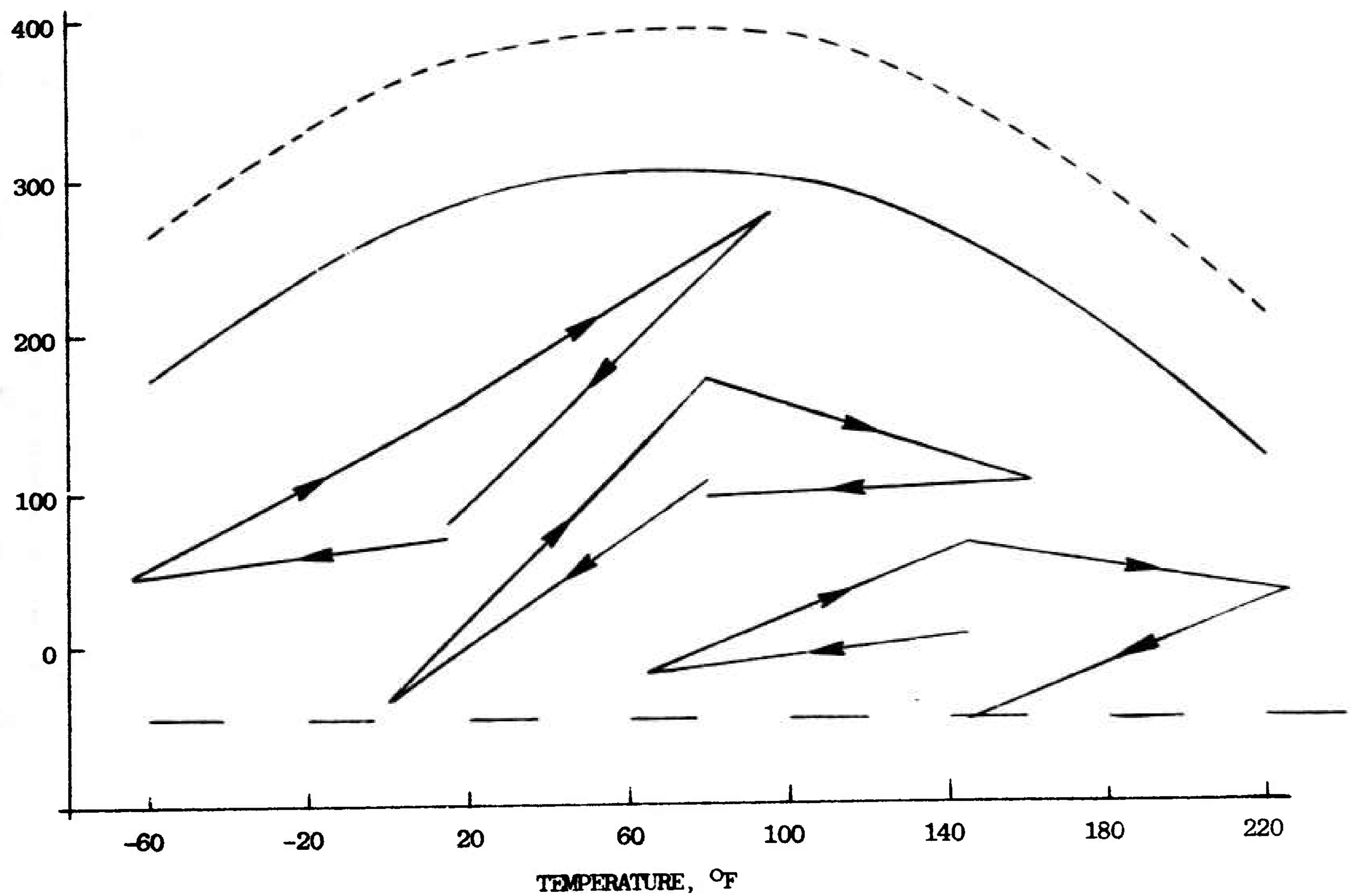

Figure 47

RELATIVE MINOR LOOP SCALE FACTOR THERMAL HYSTERESIS

SN 20196   DATES: 11/22/75 - 12/5/75

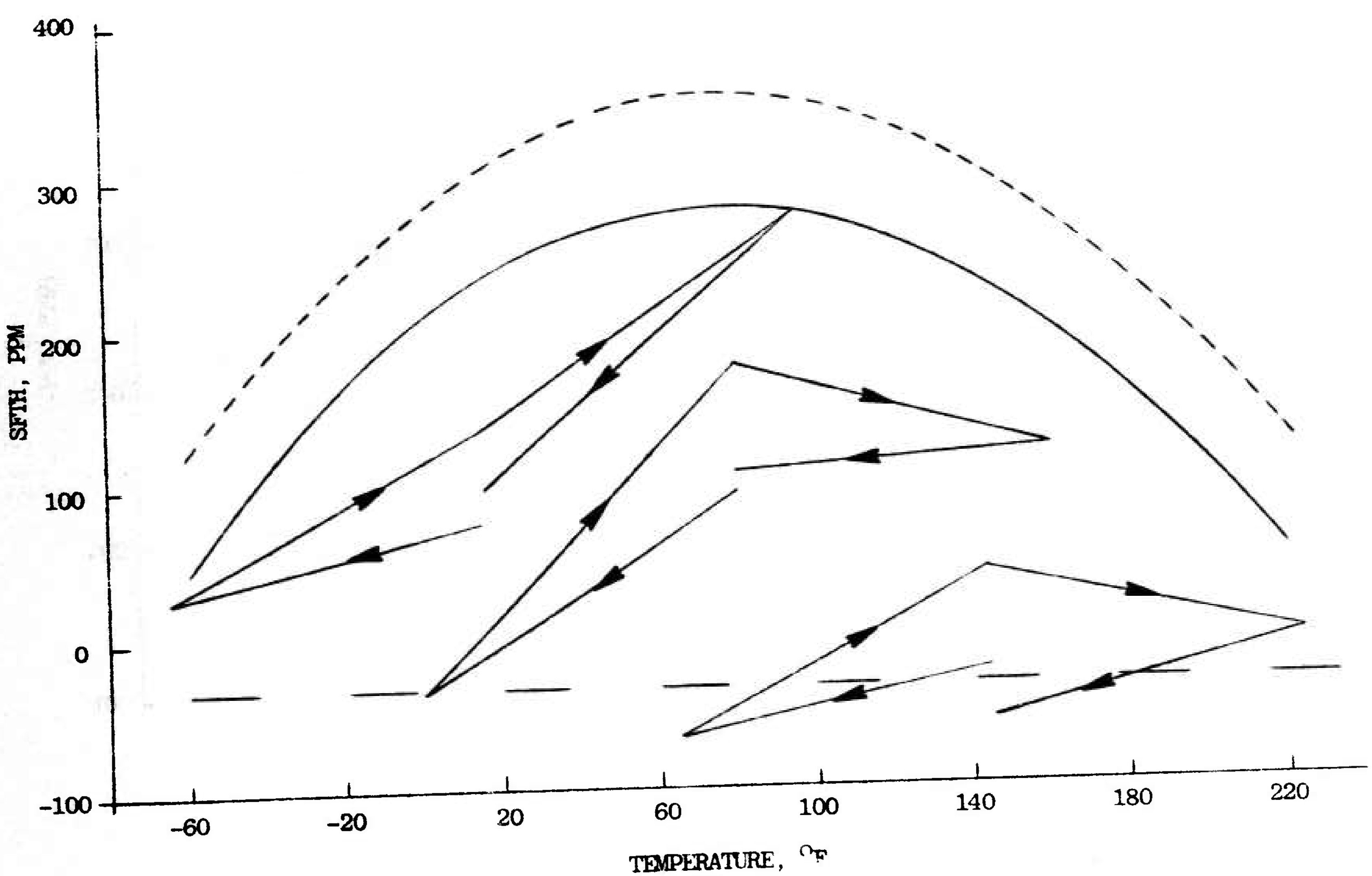

Figure 48

RELATIVE MINOR LOOP SCALE FACTOR THERMAL HYSTERESIS

SN 20204 DATES: 11/22/75 - 12/5/75

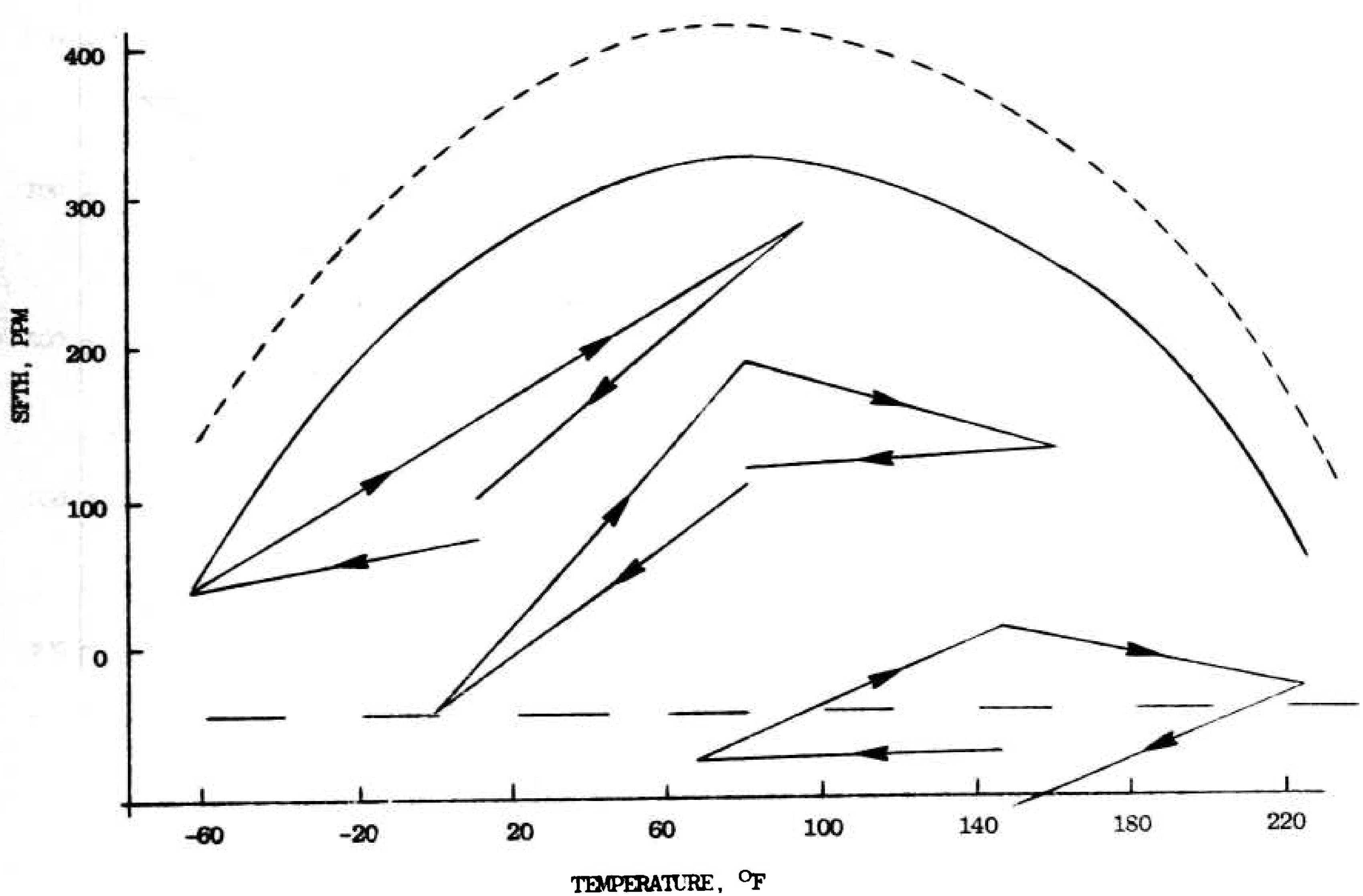

Figure 49

RELATIVE MINOR LOOP SCALE FACTOR THERMAL HYSTERESIS

SN 20210 DATES: 12/23/75 - 1/7/76

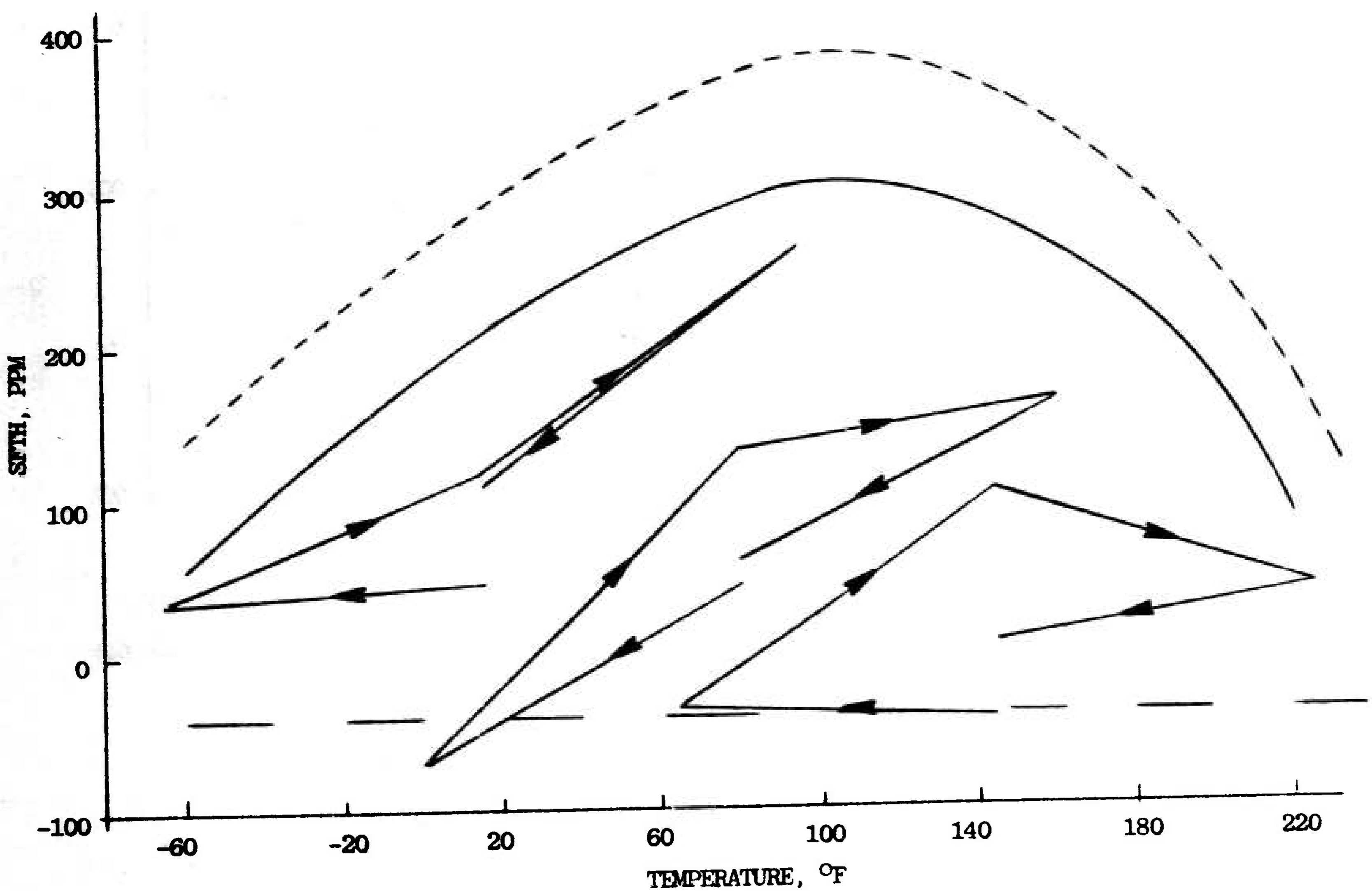

Figure 50

SCALE FACTOR THERMAL HYSTERESIS VERSUS ΔT AT $T_M = 80°F$

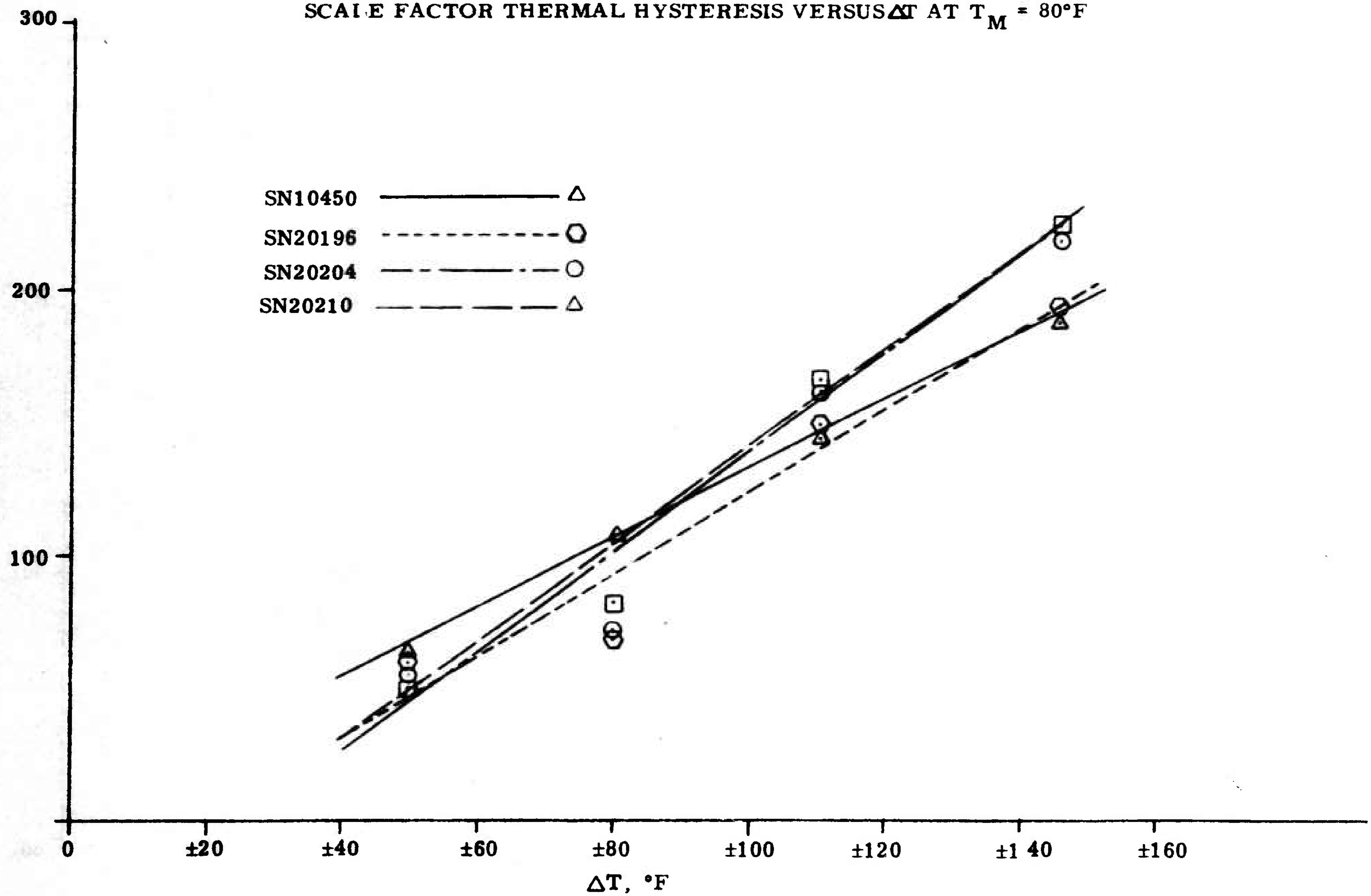

Figure 51
SCALE THERMAL HYSTERESIS VERSUS T_M° $\Delta T = \pm 80°F$

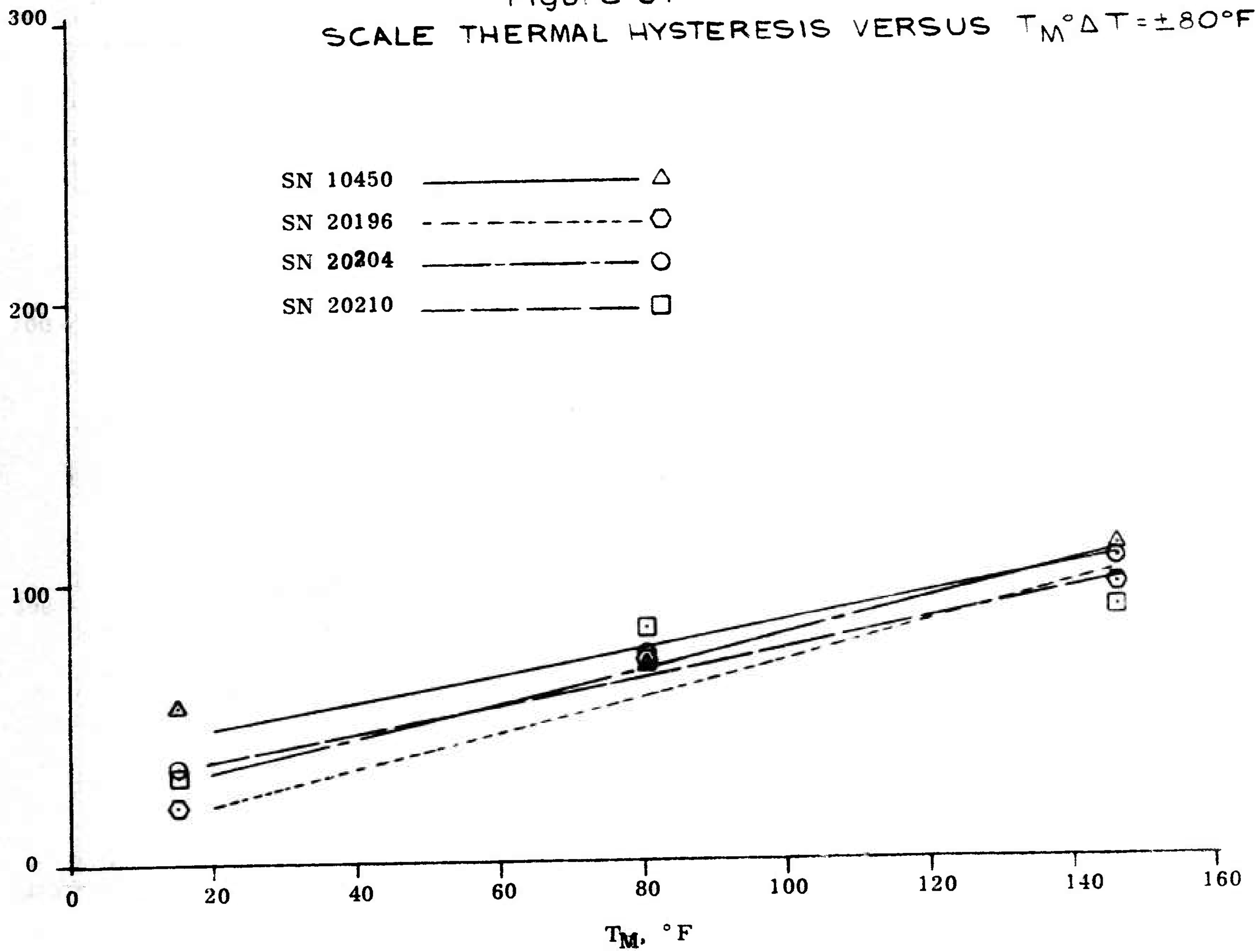

Table 27

SFTH vs ΔT & T_M Modeling

SFTH VS ΔT at T_M = $80^{o}F$

Coeff	10450	20196	20204	20210	ABS Ave	Ave
C_1	1.29	1.53	1.88	1.83	1.63	1.63
C_2	4	-3^{0}	-48	-42	31	-29

SFTH VS T_M at ΔT = $\pm 80^{o}F$

Coeff	10450	20196	20204	20210	ABS Ave	Ave
C_3	.482	.649	.606	.497	.559	.559
C_4	38	6	20	26	23	23

Figure 52
AVERAGE SF THERMAL HYSTERESIS BANDS
VS ΔT AND T_M

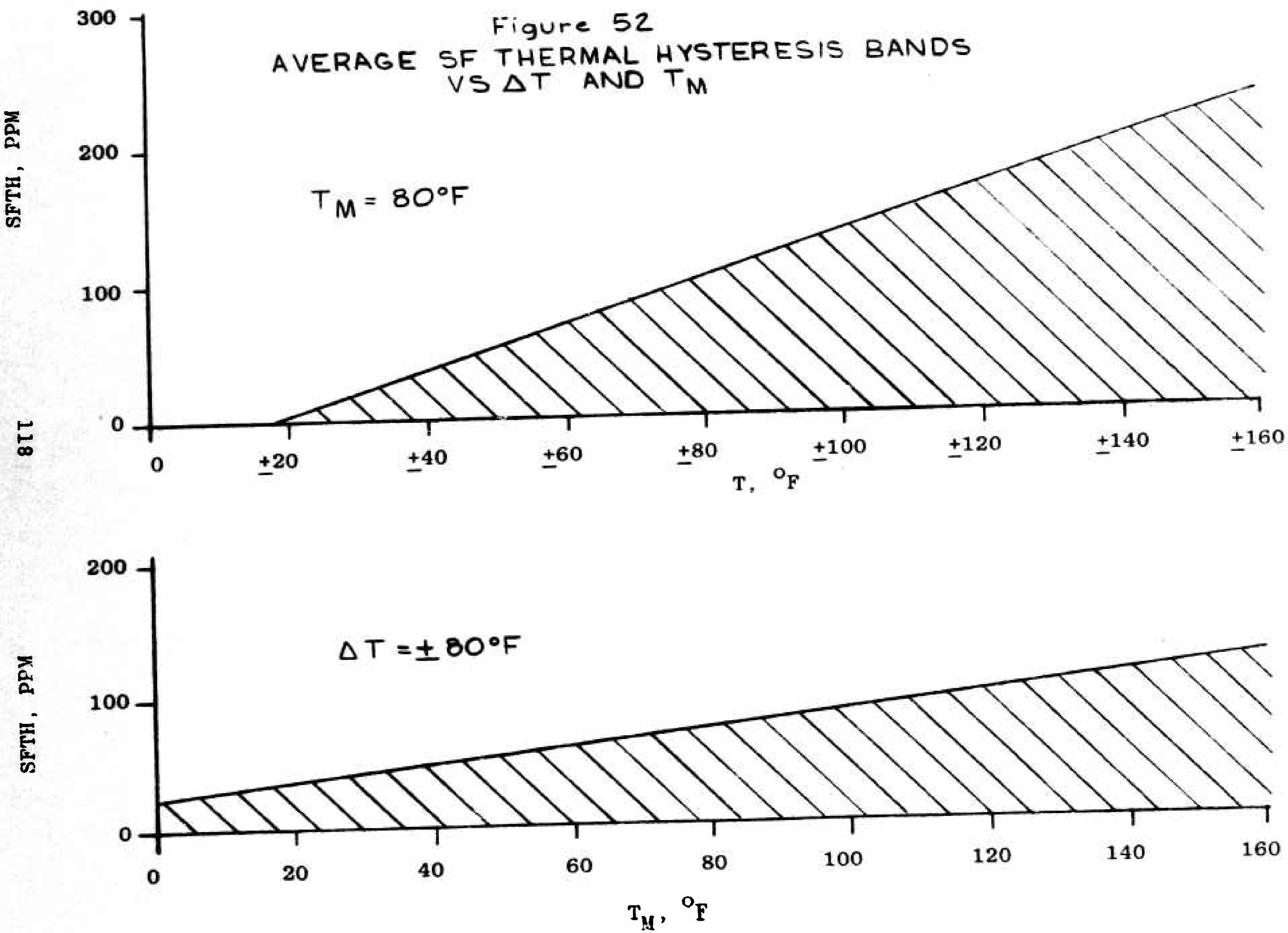

The average SFTH versus ΔT shows that SFTH is zero for $\Delta T = \pm 20°F$. If scale factor relaxation accounts for 50% of SFTH then the average SFTH is less than 100 PPM for $\Delta T = \pm 140°F$ at T_M = 80°F.

Scale Factor Relaxation

Analysis of stability data obtained from rapid reaction performance tests disclosed a correlation between time since hot soak and scale factor deviation from a reference level. This phenomena had not been detected in any previous testing because scale factor stability tests were always performed at regular time intervals before and after hot soak. Usually, stability following hot soak is measured as soon as the accelerometer is stable or about 1 hour following hot soak.

To evaluate this new discovery about thermal hysteresis, specific tests were conducted to confirm that scale factor relaxes over a finite period following exposure to hot and cold temperature extremes. Bias was also measured in these tests to verify its stability following temperature extreme exposures. The tests confirmed the following:

1) Scale factor relaxes up to 300 PPM during the 100 hours following hot soak at 240°F ± 10°F. The time constant for the relaxation phenomena is less than 40 hours.

2) Scale factor does not relax following cold soak at -70° ± 10 °F for soaks up to 2 hours.

3) Bias is stable following both hot or cold soak.

4) Scale factor relaxation contributes up to 63% of the observed scale factor thermal hysteresis.

An explanation of scale factor relaxation data and analysis follows.

Figure 53 shows the initial data showing scale factor relaxation and bias during the same experiments. The accelerometer, S/N 20210, was hot soaked at 240 ± 10°F for 1 hour and then both unit and chamber temperature were returned to ambient and stabilized at 70 ± 1° F. The scale factor and bias were measured during the following 90 hours after the initial stabilization at 70°F. The hot soak and measuring process were repeated several times to obtain additional data. The same scale factor and bias reference levels were used for all runs.

The scale factor deviation, ΔSF, versus time was modeled to an exponential:

$$\Delta SF = (\Delta SF_o)(\exp(-t/\tau))$$

A semi-logorithmic plot of this function is a straight line:

$$Ln(\Delta SF) = Ln(\Delta SF_o) - t/\tau$$

Figure 54 shows the semi-log plot of the first relaxation data. The values of ΔSF_o and τ as determined by least squares curve fitting were:

$$\Delta SF_o = -240 \text{ PPM}$$

$$\tau = 32.8 \text{ hours}$$

The correlation coefficient of the least squares fit was -0.9. (A coefficient value of +1 indicates a one to one correlation between the dependent and independent variables of the data set.) This data quantitatively confirmed that scale factor relaxation occurred in the accelerometer.

Figure 53

SCALE FACTOR RELAXATION FOLLOWING HOT SOAK

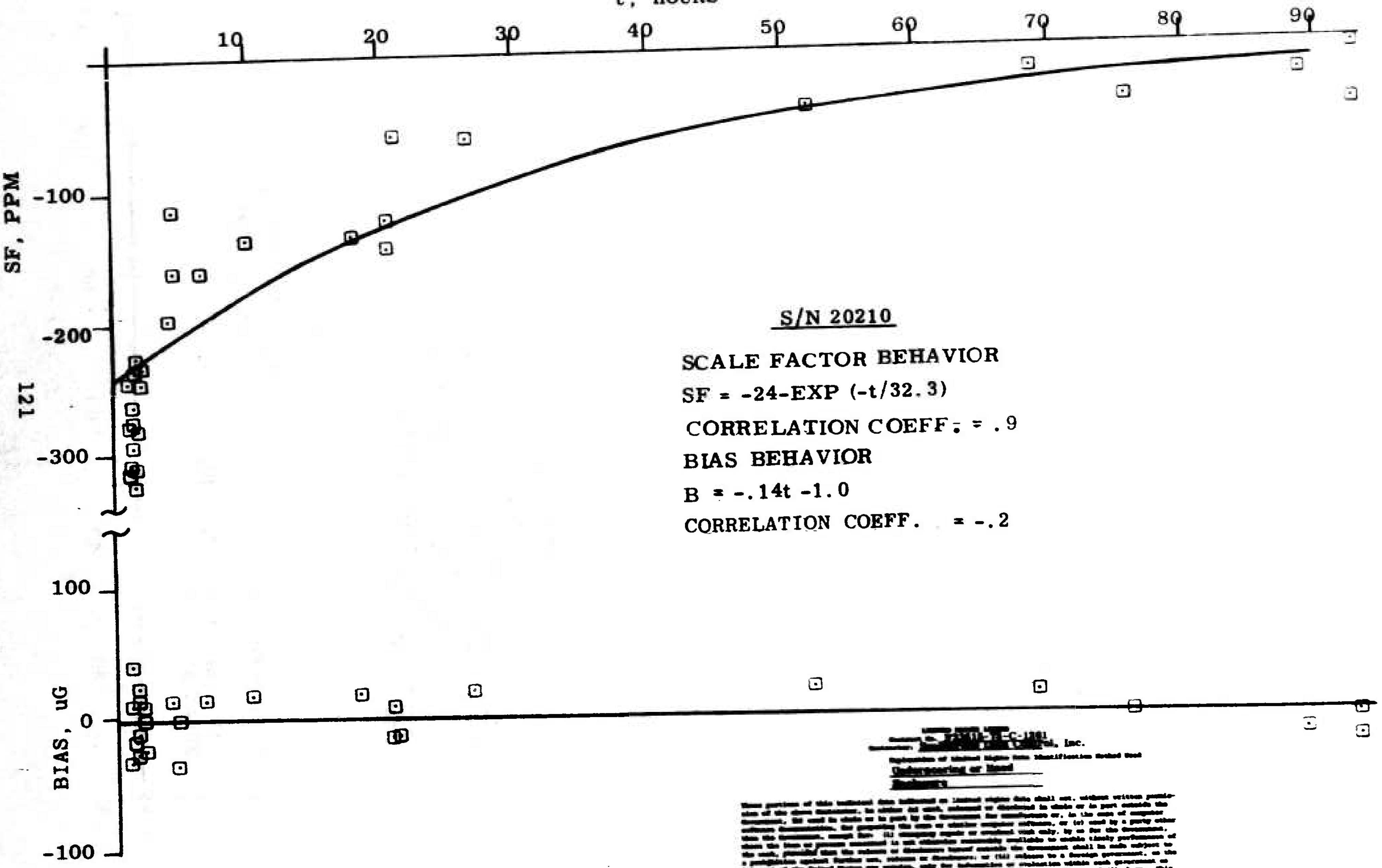

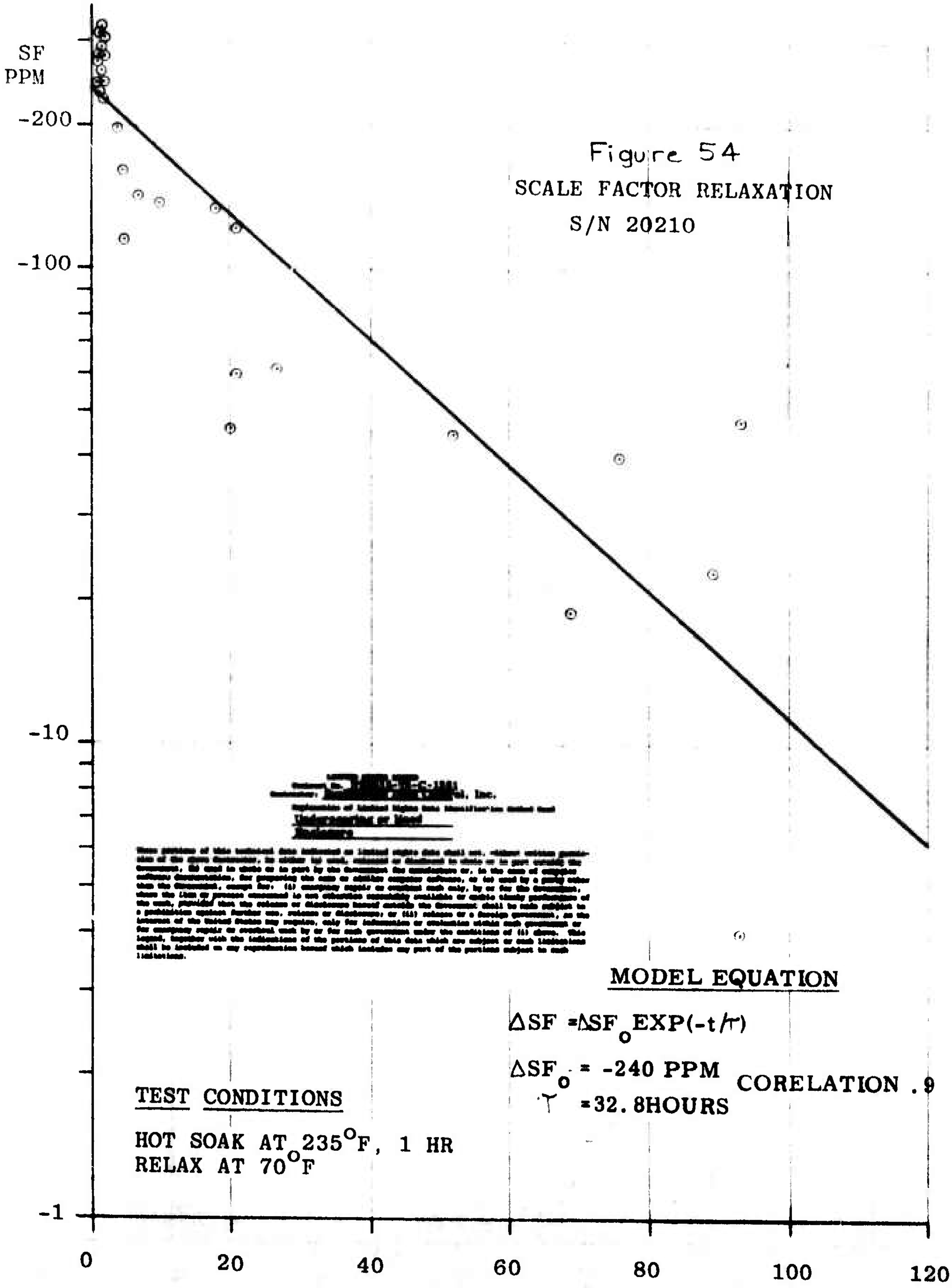
SF
PPM
-200
-100
-10
-1
0
20
40
60
80
100
120
Figure 54
SCALE FACTOR RELAXATION
S/N 20210
MODEL EQUATION
ΔSF = ΔSF$_o$ EXP(-t/τ)
ΔSF$_o$ = -240 PPM
τ = 32.8HOURS
CORELATION .9
TEST CONDITIONS
HOT SOAK AT 235°F, 1 HR
RELAX AT 70°F

The scale factor thermal hysteresis by definition is positive for all Q-Flex accelerometers and thus the scale factor is smaller at a given temperature following hot soak than before hot soak. If scale factor is stable after hot and cold soak, the scale factor thermal hysteresis would be independent of the time since either soak as shown in Figure 55. If the scale factor following hot and cold soak is unstable, then the thermal hysteresis would vary with the time as shown in Figure 56. It is therefore obvious that scale factor relaxation contributes dramatically to thermal hysteresis and makes it a function of time following exposure to temperature extremes.

Additional relaxation tests similar to the initial test were conducted on three additional Q-Flex accelerometers. They were soaked at 70° $\pm$ 10°F as well as 235° $\pm$ 10°F for 2 hours instead of 1 hour. Scale factor deviation about a reference level during 100 hours following the soaks were modeled for relaxation to show the time dependent scale factor thermal hysteresis. Bias was also measured and modeled to show thermal hysteresis.

Figure 55
SCALE FACTOR FOLLOWING
HOT AND COLD SOAK

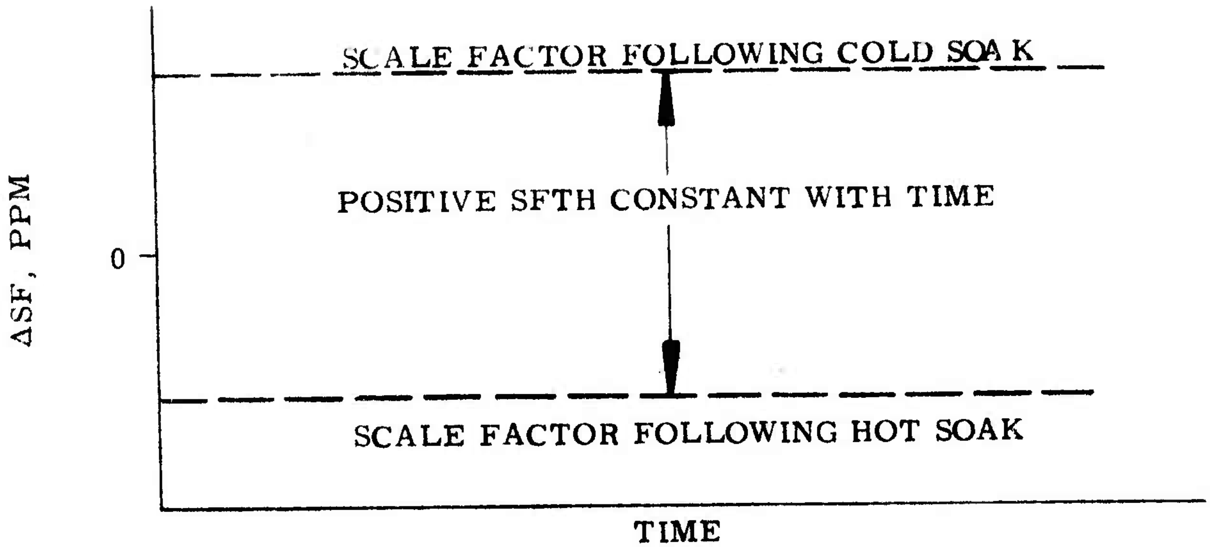

Figure 56
TIME DEPENDENT SCALE FACTOR
THERMAL HYSTERESIS

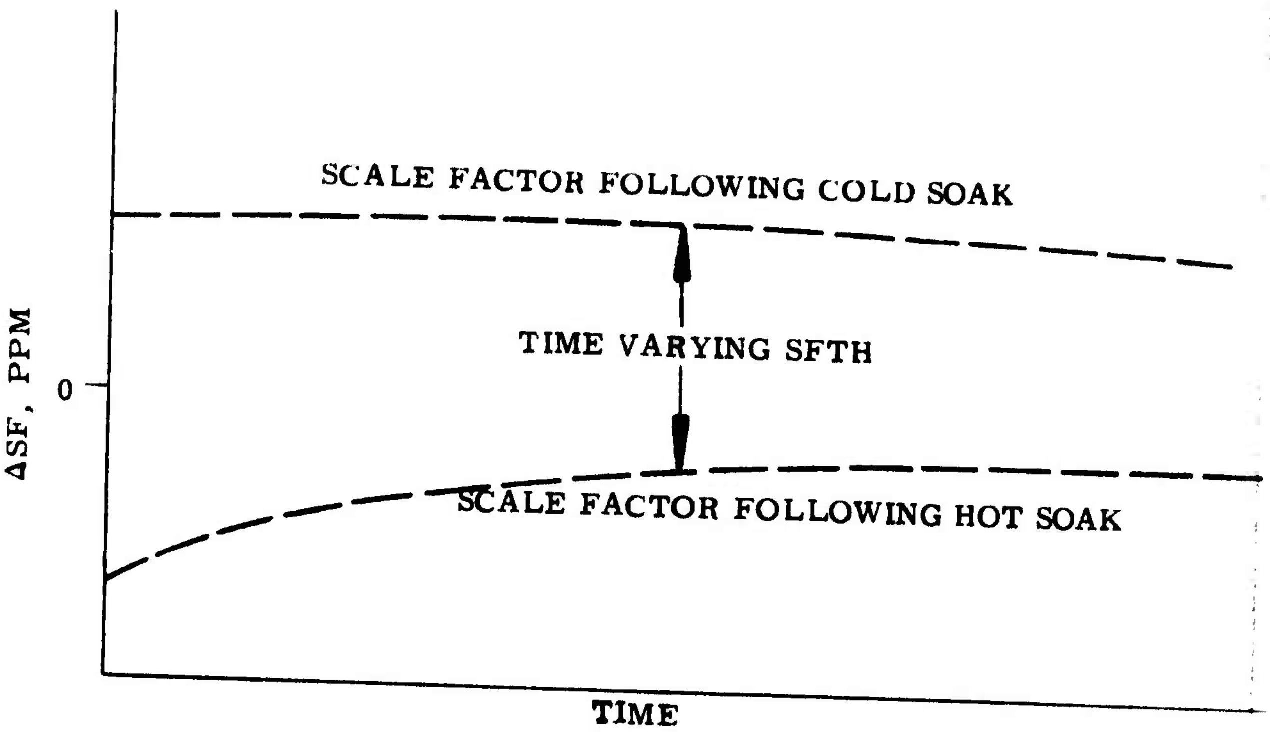

Figures 57 through 59 show the scale factor results. No relaxation of appreciable amplitude was observed following cold soak. The scale factor data following cold soak suggests a relaxation process but the data did not fit an exponential relaxation model with sufficient statistical significance to justify predicting relaxation following cold soak. The correlation coefficients for the cold soak data were less than 0.5.

Following hot soak the relaxation amplitude ranges between -178 and -240 PPM and the time constants range between 13.5 and 15.6 hours. It is apparent from the plots that the scale factor thermal hysteresis is largest at time 0.0 and decreases to a constant, finite value after three time constants. The relaxation process contributes up to 63% of the time zero thermal hysteresis for these three Q-Flex accelerometers.

The bias following hot and cold soak are shown in Figures 60 through 62. The bias thermal hysteresis for the three accelerometers ranges between -180 μg and +263 μg. Note, although hysteresis is large, no bias relaxation is observed from these units.

In an attempt to understand the phenomena that contribute to the relaxation, hysteresis and stability effects on the scale factor coefficient and also the contributing error sources for the scale factor thermal coefficient, an analysis of scale factor is presented.

Figure 57

SCALE FACTOR RELAXATION FOLLOWING HOT AND COLD SOAK

SN 10450 RELAXATION TEMPERATURE = 70 + 1°F

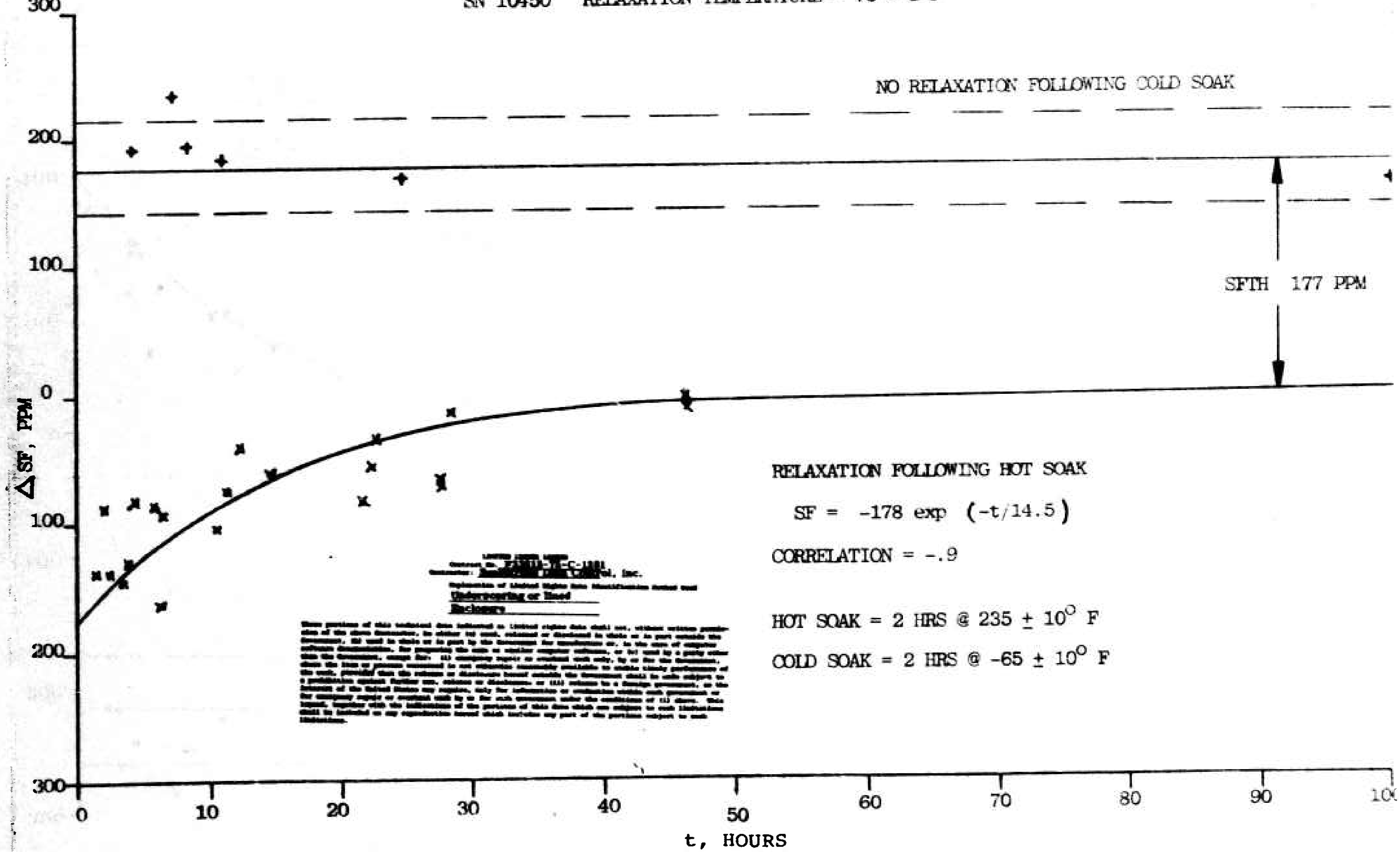

Figure 58

SCALE FACTOR RELAXATION FOLLOWING HOT AND COLD SOAK

SN 20114

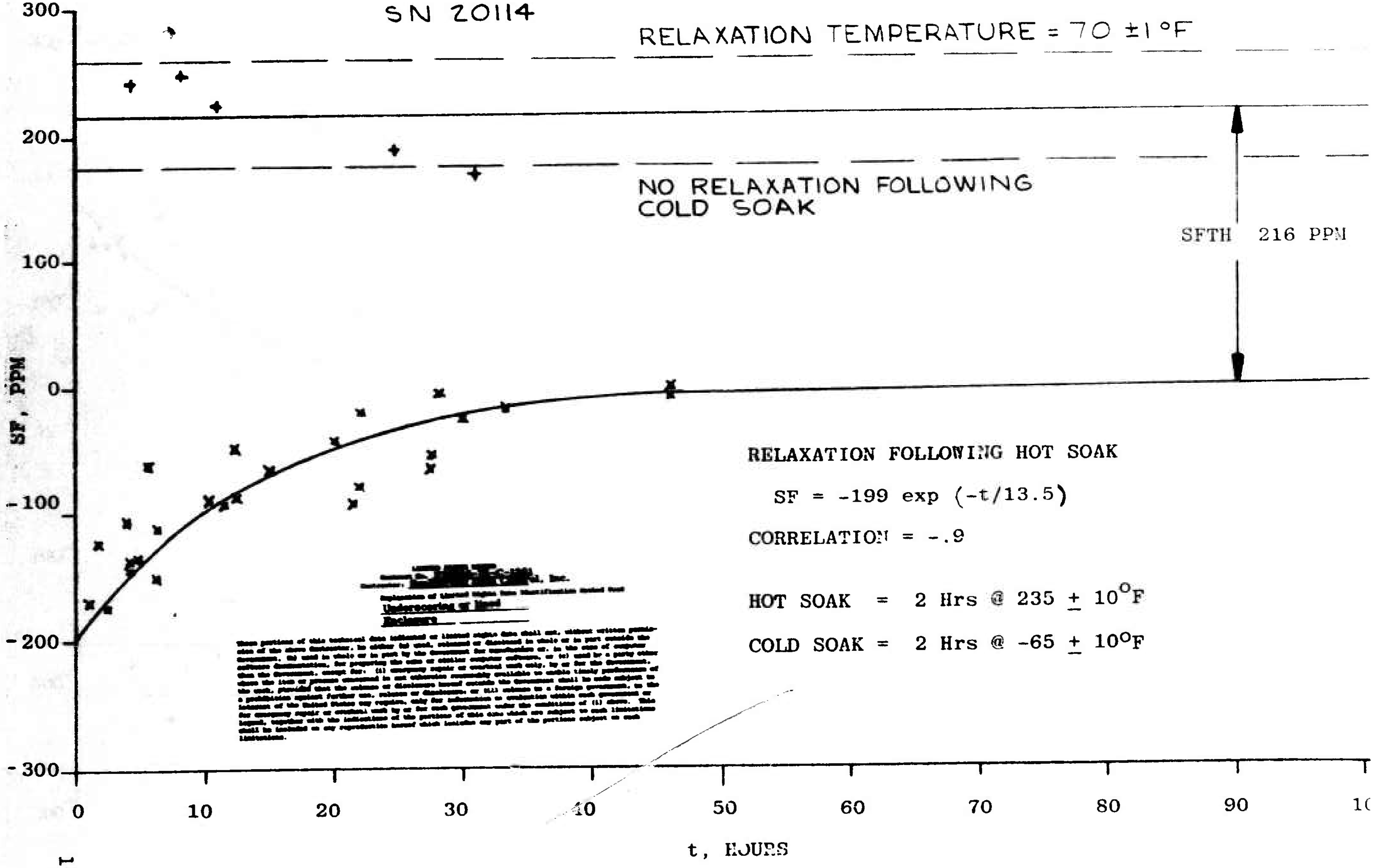

Figure 59

SCALE FACTOR RELAXATION FOLLOWING HOT AND COLD SOAK

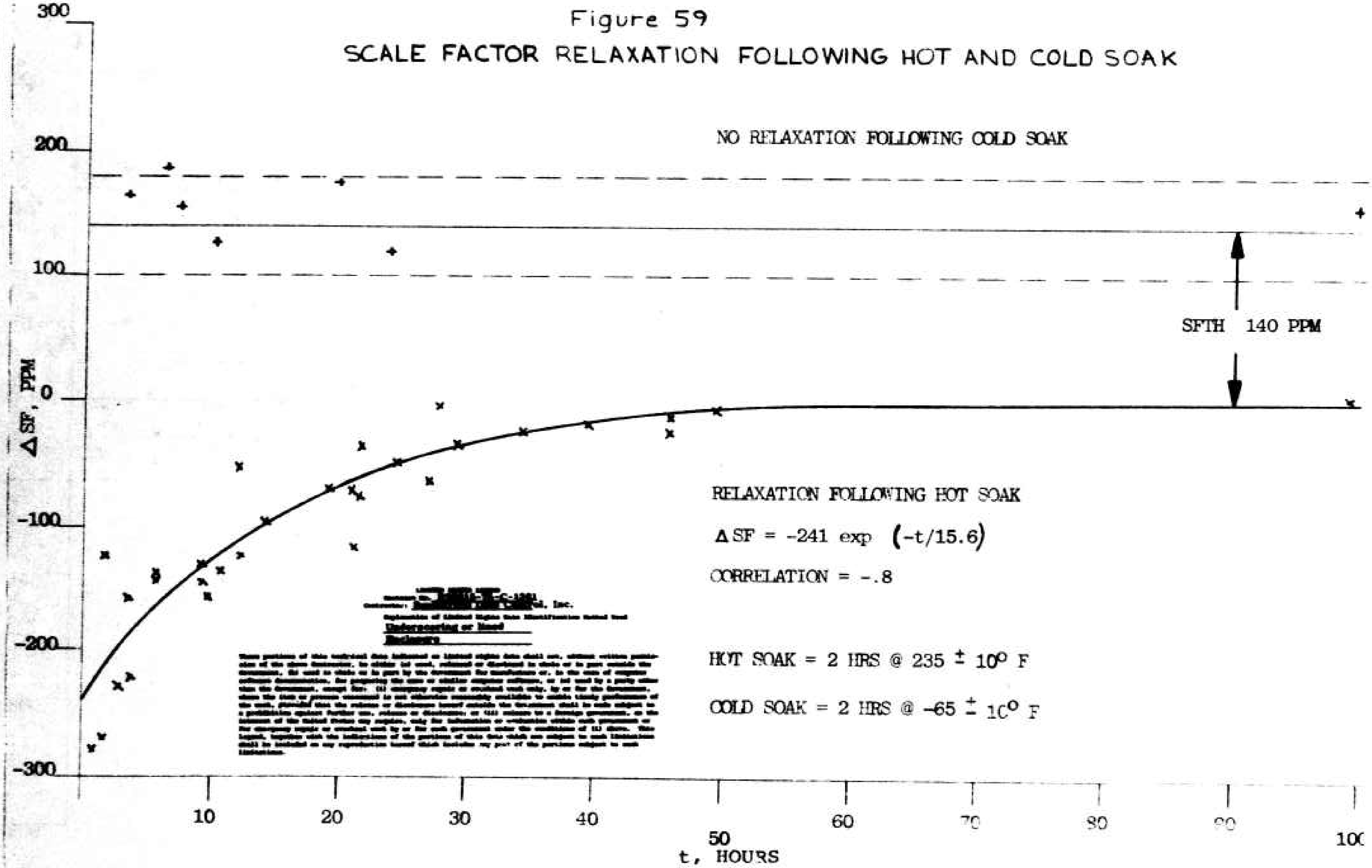

Figure 60

BIAS DURING SCALE FACTOR RELAXATION FOLLOWING HOT AND COLD SOAK

SN 10450 TEMPERATURE = 70± 1° F.

AVERAGE BIAS AFTER 2 HR @ -65 ± 10° F = 1690 u G

AVERAGE BIAS AFTER 2 HR @ 235 ± 10° F = 1870 u G

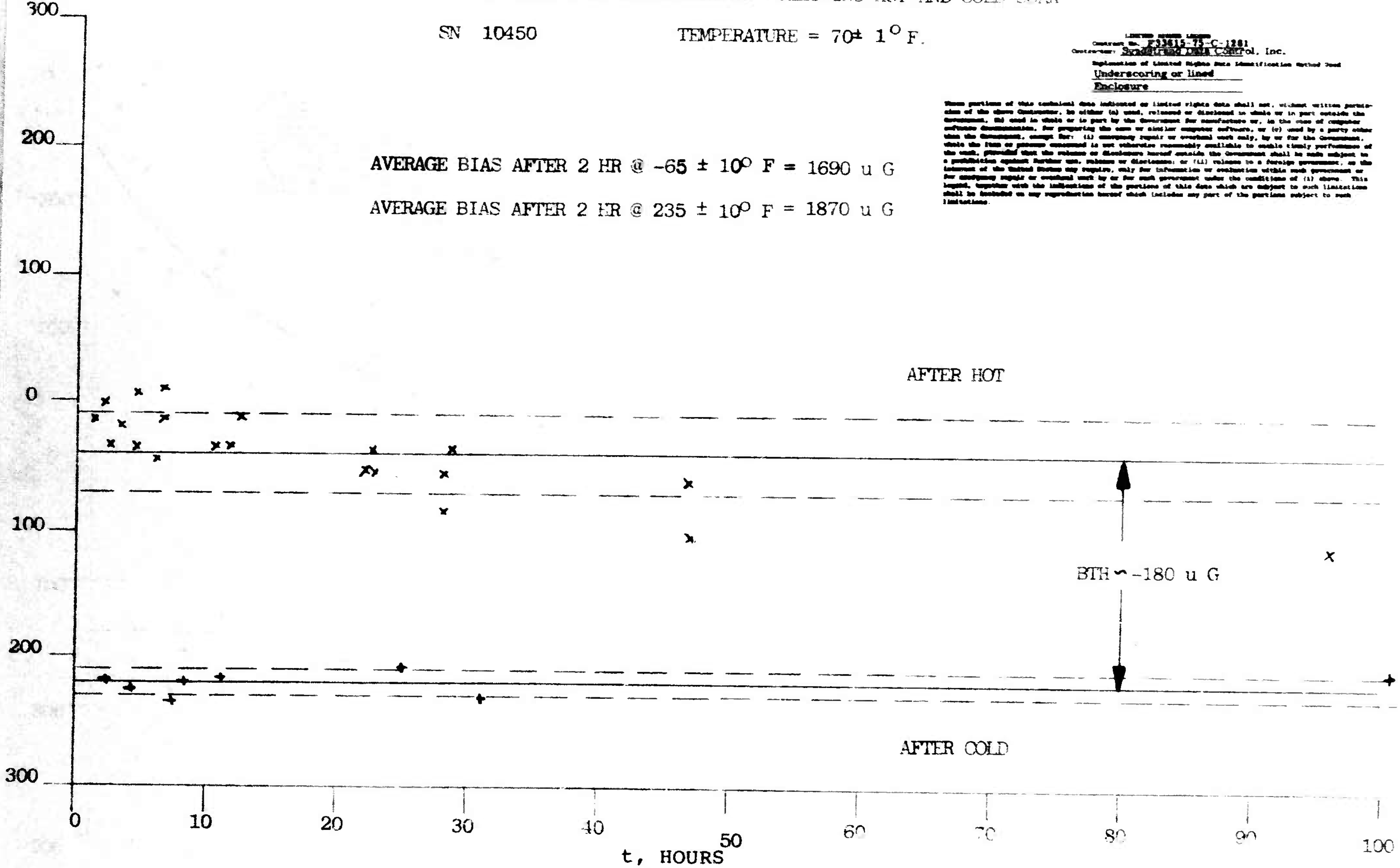

Figure 61

BIAS DURING SCALE FACTOR RELAXATION FOLLOWING HOT AND COLD SOAK

SN 20114 TEMPERATURE = 70 ± 1° F

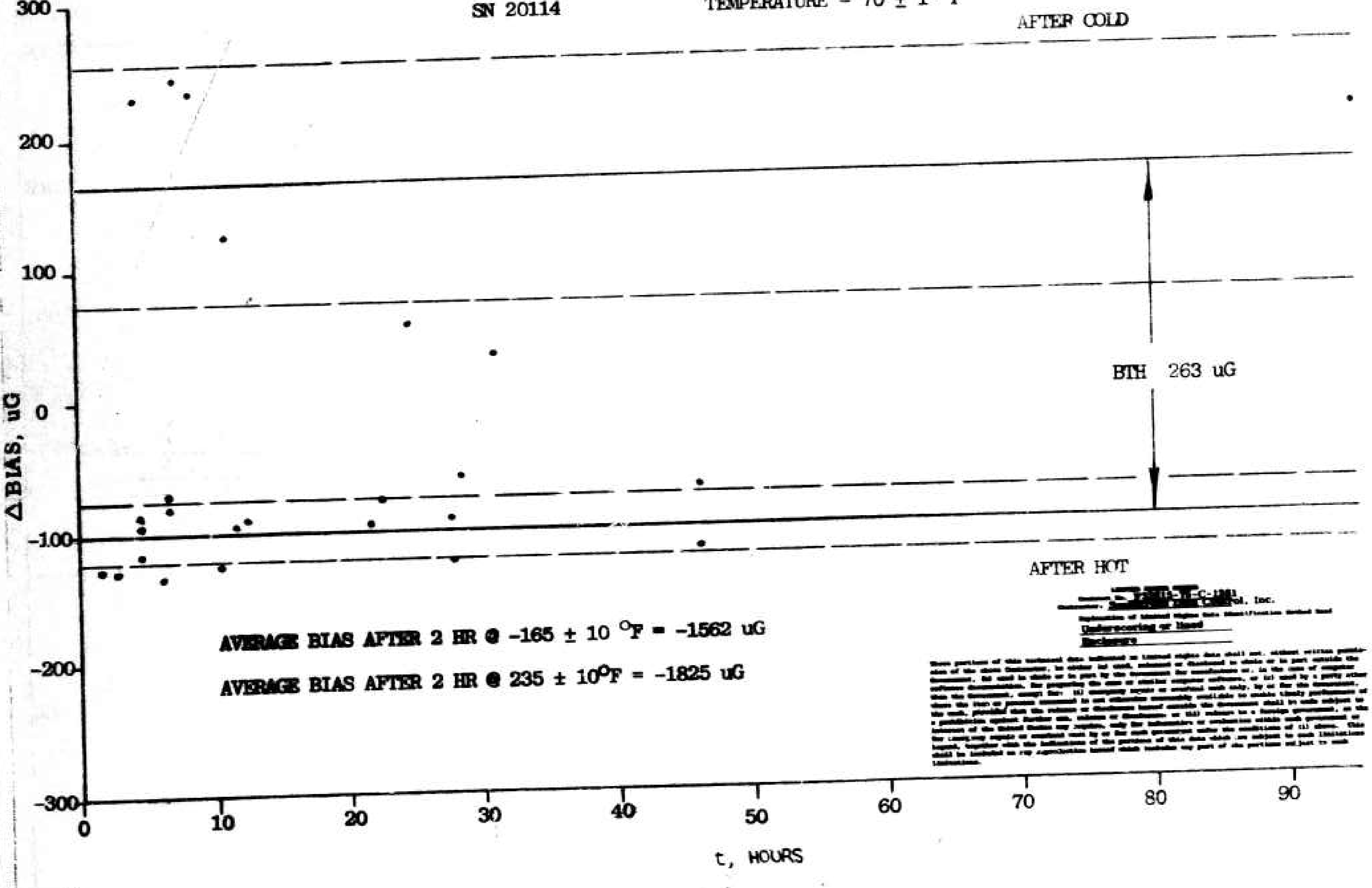

Figure 62

BIAS DURING SCALE FACTOR RELAXATION FOLLOWING HOT AND COLD

SN 20210 TEMPERATURE = 70± 1° F

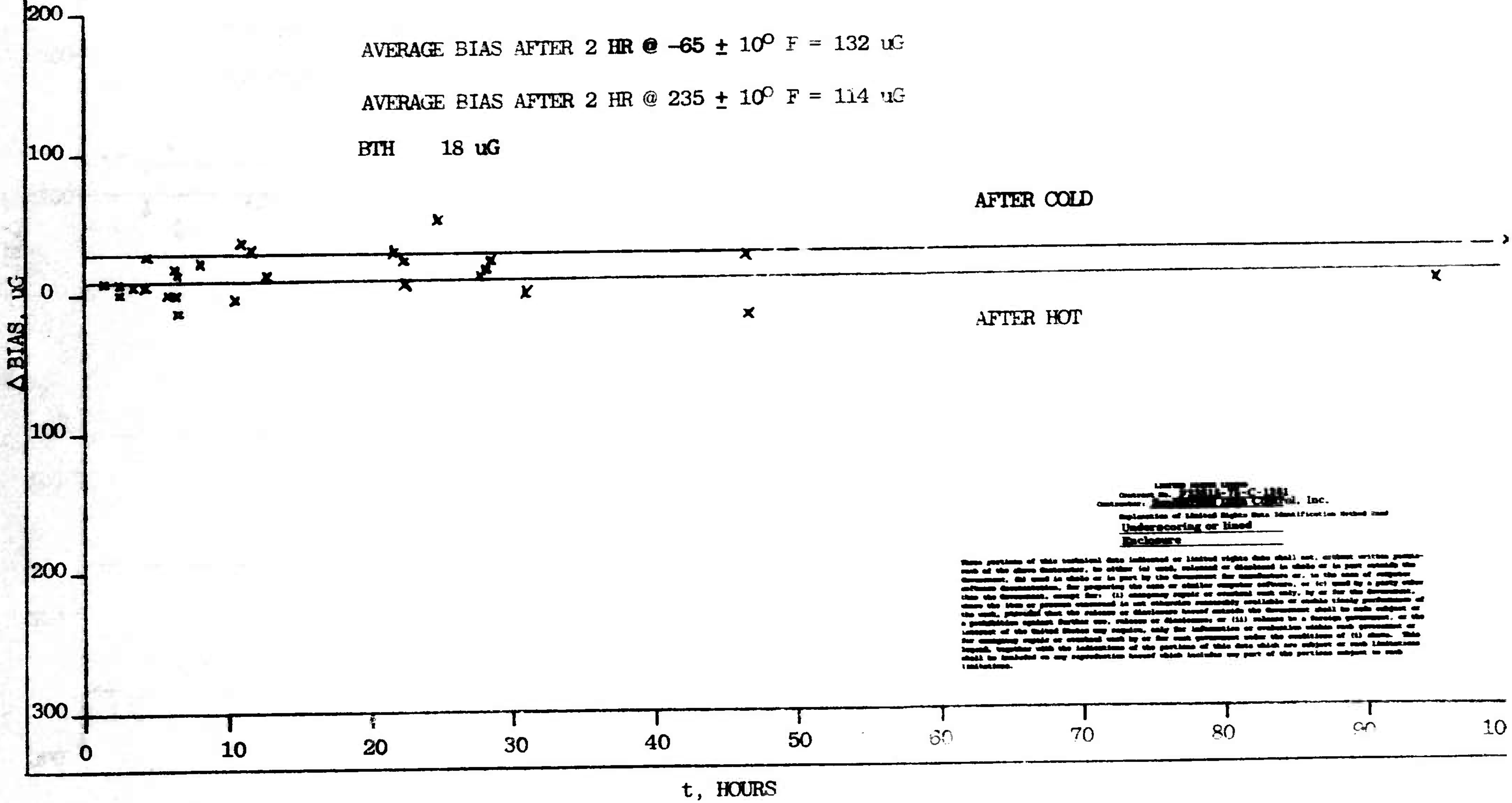

Scale Factor Theory and Design Considerations

The value of scale factor has been derived theoretically to better than 10% at room temperature. The theoretical equation for Q-Flex accelerometer scale factor is

$$K_1 = i/a = \frac{P \times 10^4}{B_g \, L_w \, r_f} = \frac{C_1}{B_g \, N}$$

where

K_1 = scale factor, mA/g

P = pendulousity, gm - cm

L_w = total coil length in flux field, cm

r_f = effective lever arm for air gap flux, cm

B_g = air gap flux density, gauss

i = force coil current, amperes

C_1 = geometry constant

N = torque coil turns

This is the expression for total scale factor. It is important to note that the scale factor is, in fact, the result of two nearly identical magnetic and mechanical structures operating in series. Therefore, the product of coil length and flux gap density in detail is:

$$B_g \, L_w = B_L \, l_L = B_u \, l_u$$

where

$B_g \, L_w$ = Coil length - gap flux density product

$B_u \, L_u$ = Coil length - gap flux denisty product for upper structure

$B_L \, l_L$ = Coil length - gap flux density product lower structure

The flux density in the air gap (B_g) or the field strength (H_g) in the air gap are given by the following basic formulae:

$$B_g = \frac{B_d A_m}{F A_g} \quad \text{and} \quad H_g = \frac{H_d L_m}{f \, L_g}$$

where:

B_g = air gap flux density, gauss

B_d = magnet induction level, gauss

A_m = magnet cross sectional area normal to flux direction, cm^2

f = reluctance factor

A_g = cross sectional area of air gap at right angles to flux, cm^2

H_g = demagnetizing force of magnet, oersteds

L_g = length of air gap parallel to flux direction, cm

F = leakage factor

L_m = magnet length parallel to flux direction, cm

The scale factor temperature coefficient is inversely proportional to the temperature sensitivity of the air gap flux density, B_g. The air gap flux density as a function of temperature can be expressed as:

$$B_g = \frac{(MMF_m)\ (1 + \alpha_m T)}{A_g\ (R_g(1 + \alpha_g T) + R_j(1 + \alpha_j T) + R_i(1 + \alpha_i T))}$$

where:

MMF_M = magnet mangetomotive force, gilberts

$R_g = \dfrac{L_g}{{}_g A_g}$ = air gap reluctance, cm^{-1}

$R_j = \dfrac{L_j}{{}_j A_j}$ = reluctances of epoxy joints, cm^{-1}

$R_i = \dfrac{L_i}{{}_i A_i}$ = reluctance of invar return path, cm^{-1}

$\alpha_m, \alpha_g, \alpha_j, \alpha_i$ = temperature sensitivity coeffcients of the magnet, air gap, epoxy gaps and invar that effect the air gap flux density, ppm/°F

T = operating temperature, °F

The temperature differential is:

$$\frac{dB_g}{dT} = \frac{(R_g + R_j + R_i)\ (MMF_m)\ \alpha_m - (MMF_m)(R_g \alpha_g + R_j \alpha_j + R_i \alpha_i)}{A_g\ (R_g + R_j + R_i)^2}$$

where the operating point flux density, B_{g_o}, is

$$B_{g_o} = \frac{MMF_m}{A_g\ (R_g + R_i + R_j)}$$

Combining Equations expressing B_{g_o} and $\frac{dB_g}{dT}$ gives:

$$\frac{1}{B_{g_o}} \frac{dB_g}{dT} = \alpha_m - \alpha_g - \frac{MMF_j}{MMF_m} \alpha_j - \frac{MMF_i}{MMF_m} \alpha_i$$

This equation describes the air gap flux density temperature sensitivity. The air gap temperature changes give rise to the accelerometer scale factor temperature coefficient.

The general equation defines the four elements that together give rise to the scale factor temperature sensitivity, the magnet temperature coefficient, the dimensional temperature change of the air gap, the dimensional temperature change of the epoxy joints, and the permeability temperature change of the invar return path. The air gap change with increasing temperature causes the field strength in the air gap to increase while the three other effects cause a decrease in scale factor.

The general equation for scale factor temperature coefficient, SFTC, is as follows:

$$SFTC = \frac{D_m}{2L_g} \left(\gamma_i \frac{\gamma_m L_m + \gamma_p L_p}{L_a} \right) + \gamma_i - \alpha_m$$

$$- \frac{1}{H_d L_m} \left(\frac{\gamma_{jL} + \gamma_{jv}}{2} \right) \left(\frac{\Sigma B_g A_g L_j}{A_j} \right) + \Sigma L \frac{dH_i}{{}_i dT}$$

where:

- D_m = magnet diameter, cm
- L_m and L_p = length portions of the magnet and pole piece
- L_a = total axial length of the gap normal to the flux, cm
- γ_i = linear coefficient of thermal expansion of Invar ppm/°F
- γ_{jL} = linear coefficient of thermal expansion of epoxy ppm/°F
- γ_{jv} = Volumetric expansion coefficient, ppm/°F
- L_j = length of epoxy gap parallel to flux, cm
- A_j = cross section area of epoxy joint normal to flux, cm^2
- H_i = field strength in invar structure, oersteds
- L_i = path length of invar parallel to flux, cm

The quantity α m or magnet temperature coefficient is a function of the magnet flux density-field strength ratio, B_d/H_d and the magnet length to diameter ration, L_m/D_m.

Analysis and empirical testing has allowed these sensitivities to be accurately estimated. For example, at 110°F, the thermal coefficients have been described and are depicted in Table 28.

Table 28

STRUCTURE TEMPERATURE SENSITIVITY COEFFICIENTS

MAGNET	INVAR	EPOXY GAPS	AIR GAP	TOTAL
+49	+35	+1	-28	+55

NOTE: Coefficients in ppm/°F

To reduce the thermal coefficient of expansion, techniques such as magnetic shunts have been employed. In addition, Sundstrand has demonstrated the capability to reduce this coefficient dramatically using its own proprietory, negative temperature coefficient thin film resistor network. The voltage scale factor temperature coefficient on these units is less than 15 ppm/°F over a 160°F temperature range . All these approaches, however, add networks which increase cost and probably reduce stability by the addition of a new material or process. Another approach is being pursued which attacks the fundamental magnet coefficient characteristics. This technique would minimize cost and enhance reliability by not having additional hardware added to the structure. This proprietary approach has just been funded under a MICOM research and development program.

Scale Factor Stability Design Considerations *

The long term stability of scale factor is determined by the two Alnico IX magnets which produce the magnetic gap flux density. The Alnico IX magnets used in the Q-Flex accelerometer are characterized by a uniaxial anisotropic structure, with rod like domains of magnetic precipitate of high saturation magnetization imbedded within a matrix of lower magnetization. These regions are aligned parallel to a magnetic field which is applied during the annealing process and are on the order of 100A in width. As a result of the small size and elongated shape of the Alnico regions, the magnet is devoid of Bloch walls and does not suffer from easy magnetization reversal due to motion of these walls. The size and shape of the precipitate regions in the Alnicos are responsible for their superior stability and why they have been chosen for the Q-Flex sensor design.

Following magnetization the precipitate regions find themselves in a self-demagnetizing field and this situation is maintained for long periods of time. The self-demagnetizing field is not constant but contains a component called the Néel Field which fluctuates with time due to external conditions such as temperature changes, stray magnetic fields, and mechanical shock. The Néel Field varies exponentially as shown in Figure 63.

The dominant process for magnetic reversal in Alnico IX is buckling of the precipitate regions following magnetization. To reduce this process and therefore improve the scale factor stability of the Q-Flex sensor, the magnets and sensors are artificially aged. By subjecting the magnets to magnetic reversal and temperature cycling immediately following assemlby, the magnets can be artificially driven down their natural stabilization curve to a region where the dB/dT slope is essentially zero. The effect of articial aging is shown in Figure 64. The subassembly processing to accomplish the articifial aging is as follows. Non-magnetized Alnico IX magnets are mounted into upper and lower stator. The magnets are individually magnetized to saturation and the sensor is assembled.

Following assembly on AC current is applied through the torque coil which reduces the scale factor 5% to 15% by knocking down the magnetization of each magnet. The knockdown effects those regions in the magnet which are unstable and would be susceptible to the Néel Field over long periods of time. Following

* Technical information and graphs have been condensed from Permanent Magnets as Precision Instrument Elements, W. L. Zingery, Autonetics, Downey, California. August, 1962.

Figure 63
UNTREATED ALNICO STABILITY

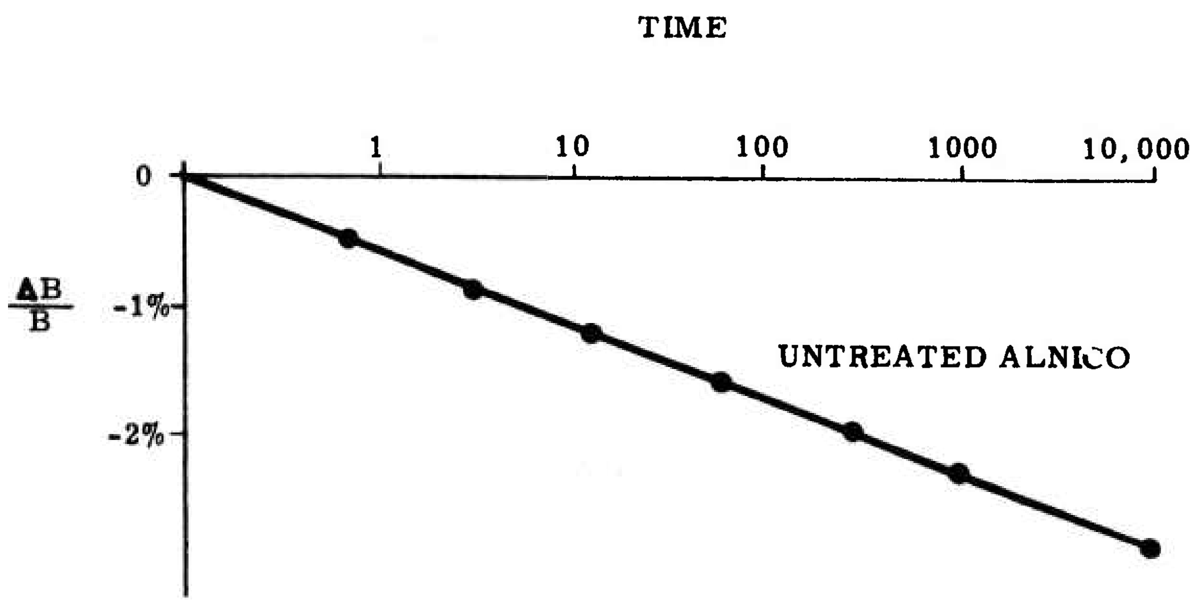

Figure 6 4
NATURAL AND ACCELERATED AGING OF ALNICO MAGNETS

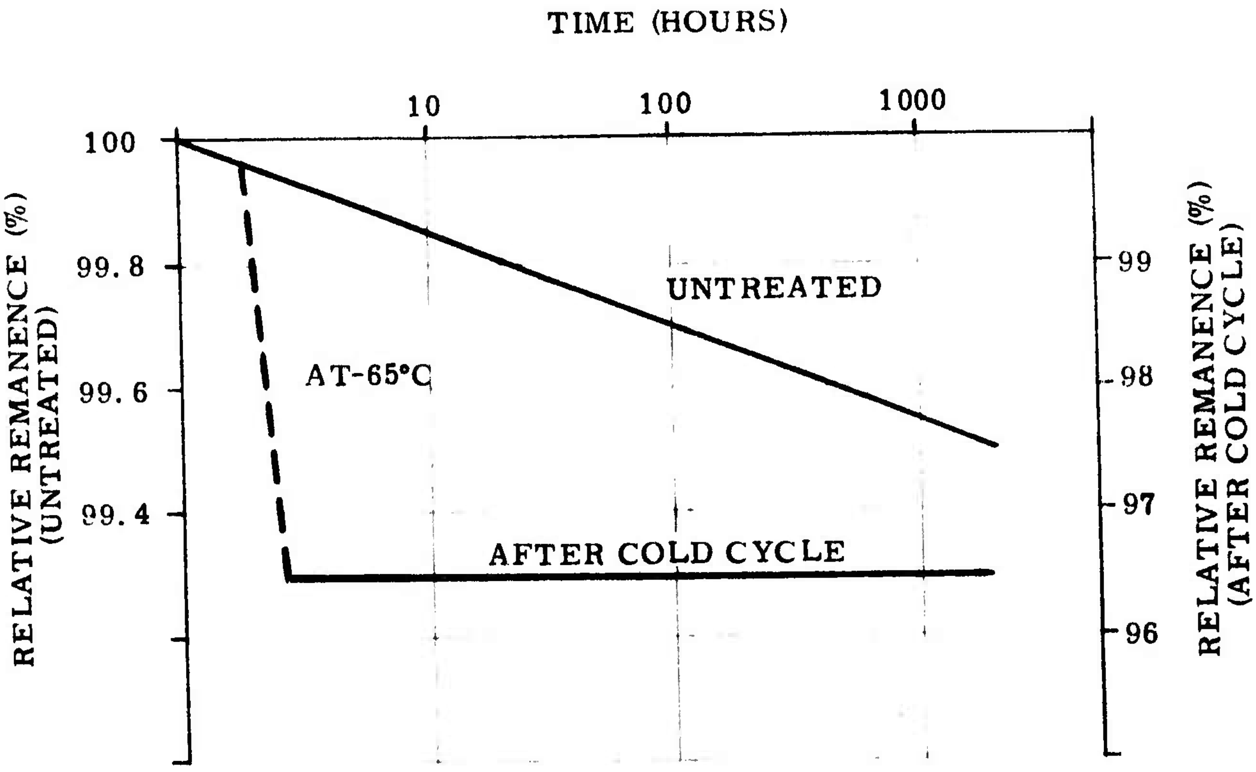

knockdown the sensors are mounted into their sensor cover assemblies and thermal cycled for 96 hours between -65°F and 255°F (approximately 24 cycles). This thermal cycling removes the remaining non-reversible magnet changes and stabilizes the magnets at their final operating points.

In addition to these sensor processing techniques, the Q-Flex scale factor stability is insured by completely surrounding the magnets in Invar which shields them from external magnetic fields. The magnets also have opposing magnetic fields so that the torque coil magnetic field alternately magnetizes and demagnetizes the magnets in plus and minus acceleration.

Design Factors Affecting Scale Factor Thermal Hysteresis

Scale factor thermal hysteresis, as now understood, consists of a fixed non-reversible change in the flux field geometry and a time dependent change which has a significantly long time constant. This newly acquired knowledge strongly suggests elastic meterial property changes, probably due to thermal stresses developed within components in the magnetic structure. To examine factors contributing to SFTH, the following possible errors souces were examined:

1) Magnet thermal hysteresis.

2) Variable, non-reversible change in the magnetic gap.

3) Variation of torque coil geometry and position.

Magnetic Thermal Hysteresis- The thermal cycling of a magnet can be viewed as operating the magnet on a minor hysteretic loop because the self-demagnetizing field seen by the magnetic domain varies with temperature. However, scale factor thermal hysteresis due to this effect is not considered likely for several reasons. First, several types of magnet materials with significantly different material properties, including rare earth magnets, have been used to fabricate Q-Flex sensors and all have shown no significant difference in SFTH. Second, other manufacturers of sensors similar to the Q-Flex and using identical stabilization processes and magnetic material do not report scale factor thermal hysteresis in their sensors. It, therefore, is concluded that the SFTH observed in the Q-Flex sensor is due to the physical processing and mechanical geometry of the mechanical structure.

Magnetic Gap Geometry- The most likely cause of scale factor thermal hysteresis is the high sensitivity to variations of the magnetic gap geometry. Figure 65 shows a conceptual view of the gap flux density. Field mapping has indicated that there is a significant gradient flux field in the upper gap of the present Q-Flex design. The magnitude and direction of flux in this portion of the gap is very sensitive to variation in the position of the pole piece and magnet with respect to the Invar return path structure.

Data to support this thesis came from a company funded activity during the 1976 time frame.

To study the sensitivity to axial positional changes in the magnet-pole piece geometry with respect to the Invar return path, the epoxy material coupling these components was changed. The existing system uses the low thermal expansion coefficient LCA4/LV epoxy. This system was chosen to minimize the thermal stresses developed between the Alnico IX magnet and the Invar structure. The glue line for this system varies between 0.001 and 0.002 inches per joint.

A sample of nine units was fabricated using an extremely thin glue line material. The epoxy gaps at the pole piece-magnet interface and magnet-Invar structure interface were less than 200 micro-inches each. If positional displacement occurred due to epoxy creep then one would expect reduced thermal hysteresis with the thin glue line material. The production temperature tumble test data from these units are presented in Table 29. The table also presents a comparison of scale factor thermal hysteresis from the current production build. The improvement observed has statistical significance at the 95% level.

Figure 65

MAGNETIC FLUX DENSITY FOR THE CURRENT Q - FLEX SENSOR

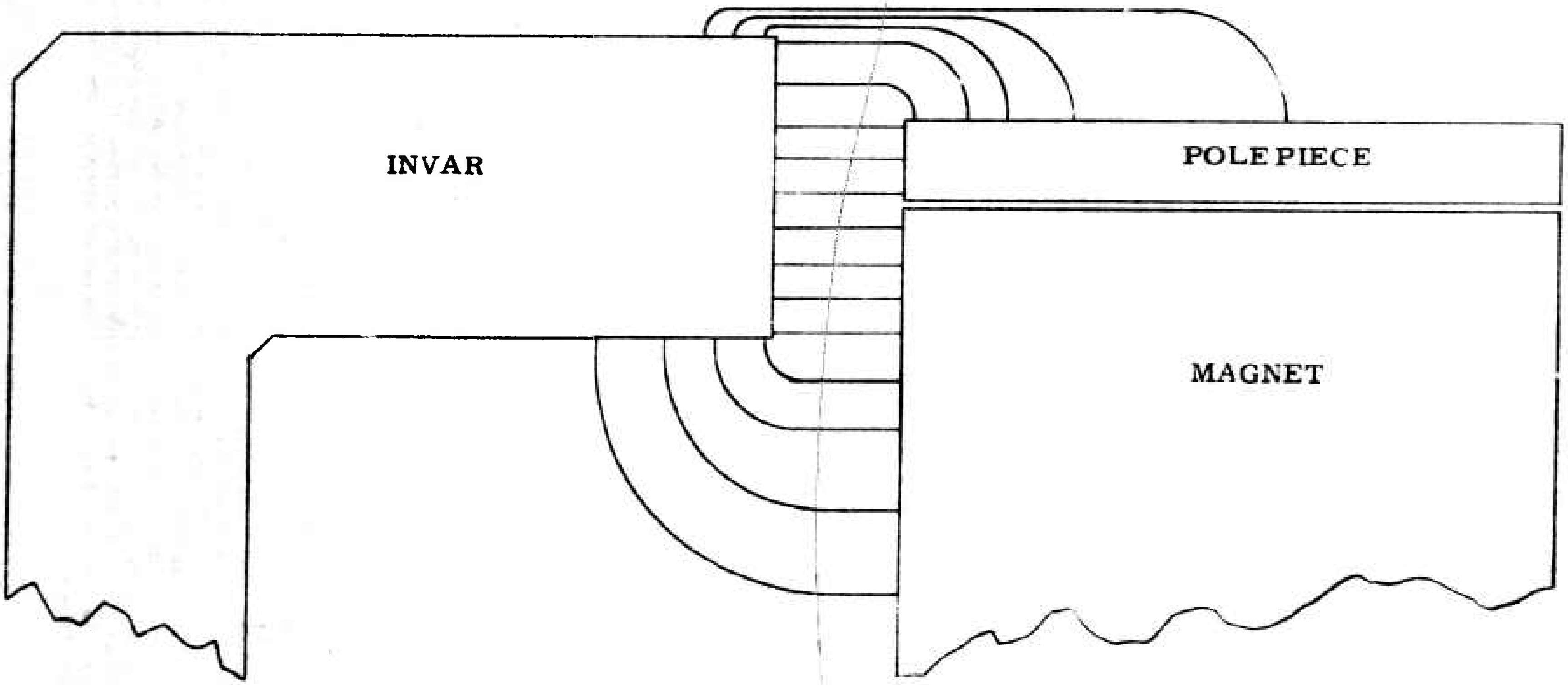

The data thus qualitatively demonstrates the following:

1) The magnetic gap geometry is extremely sensitive to relative axial displacements of the magnet and the Invar return path.
2) The existing epoxy system does exhibit a non-reversible dimensional change after thermal cycling.

To obtain better quantative data and a further understanding of the property dynamics at the structural interface, additional tests are required.

TABLE 29
SCALE FACTOR DATA
THIN GLUE LINE SENSORS

S/N	SCALE FACTOR (ma/g)	SCALE FACTOR THERMAL HYSTERESIS (ppm)
2290-1	1.148243	26
2290-4	1.182294	56
2290-5	1.125500	144
2290-7	1.205206	18
2290-8	1.145382	96
2290-9	1.211581	42
2290-10	1.87360	229
2290-11	1.174279	119
2290-12	1.120250	-20
AVERAGE AND STANDARD DEVIATION	1.166677	79
	±.033307	±77
CURRENT PRODUCTION	1.2802	189
	±.0401	±107

Variation of Torque Coil Position- If large gradient flux fields exist in the magnetic structure then axial and radial displacements of the torque coil in the gap must be another significant error contributor. As has been noted, both of the torque coils are mounted on the quartz element using a low stress elastomer to reduce bias and bias temperature coefficient. This elastic isomer may allow a non-reversible variation of the torque coil within the magnetic gap flux field. This can contribute to SFTH if the gap flux density is not symmetrical about the middle of the torque coil. As the torque coil moves through a gap field with a horizontal or vertical gradient, a net change in the flux density coil length product would occur and a resultant scale factor change would be measured. Under a parallel performance improvement program within Sundstrand, tests to evaluate radial displacements were completed in early 1976. Three sensors were tested in their "C" clamp closing tools prior to "belly banding". In this configuration controlled radial displacements of the proof mass assembly with respect to the magnetic structures could be accomplished. Tests were performed to measure proof mass radial sensitivity along the pendulous axis of the sensor. The results of this test demonstrated a significant sensitivity to radial motion which could not be explained by positional displacements of a non-gradient flux field. The radial displacement sensitivity along the pendulous axis was measured at approximately 4 ppm/ per micro-inch.

Conclusion- This data in conjunction with the thin glue line experiment results indicate a very large flux gradient field exists within the magnetic gap. The time dependent hysteretic effect can now be explained by slow relaxation or creep on either

or both the coil-quartz interface material and/or pole piece-magnet, magnet-Invar interface epoxy. The fixed hysteretic behaviour is again believed to be associated with fixed displacements within the air gap due to bonding material characteristics. To reduce the susceptability to micro-inch motion within the sensor, a structural modification as shown in Figure 66 is presented. The step in the Invar return path should concentrate and linearize the flux towards the middle of the gap. By reducing the flux gradient field of the upper gap, scale factor thermal hysteresis should be dramatically improved. The shape and geometry of this modification will result from further flux field mapping experments.

Another modification that will be examine is the change from thick glue line material to a thin glue line material in the magnetic structure. In addition to reducing the axial displacement sensitivity, the epoxy gaps acts as reluctance in the magnetic circuit. A 0.002 inch glue line in the magnetic circuit causes approximately a 6% loss in flux density in the air gap. This effect can be seen in Table 29 by comparing scale factor data from current production and the thin glue line units.

With the incorporation of a more linear flux field and a thin glue line structure the average thermal hysteresis of scale factor should be less than 25 ppm for the family of Q-Flex sensors.

Figure 66
PROPOSED DESIGN MODIFICATION FOR
REDUCING UPPER GAP FLUX DENSITY

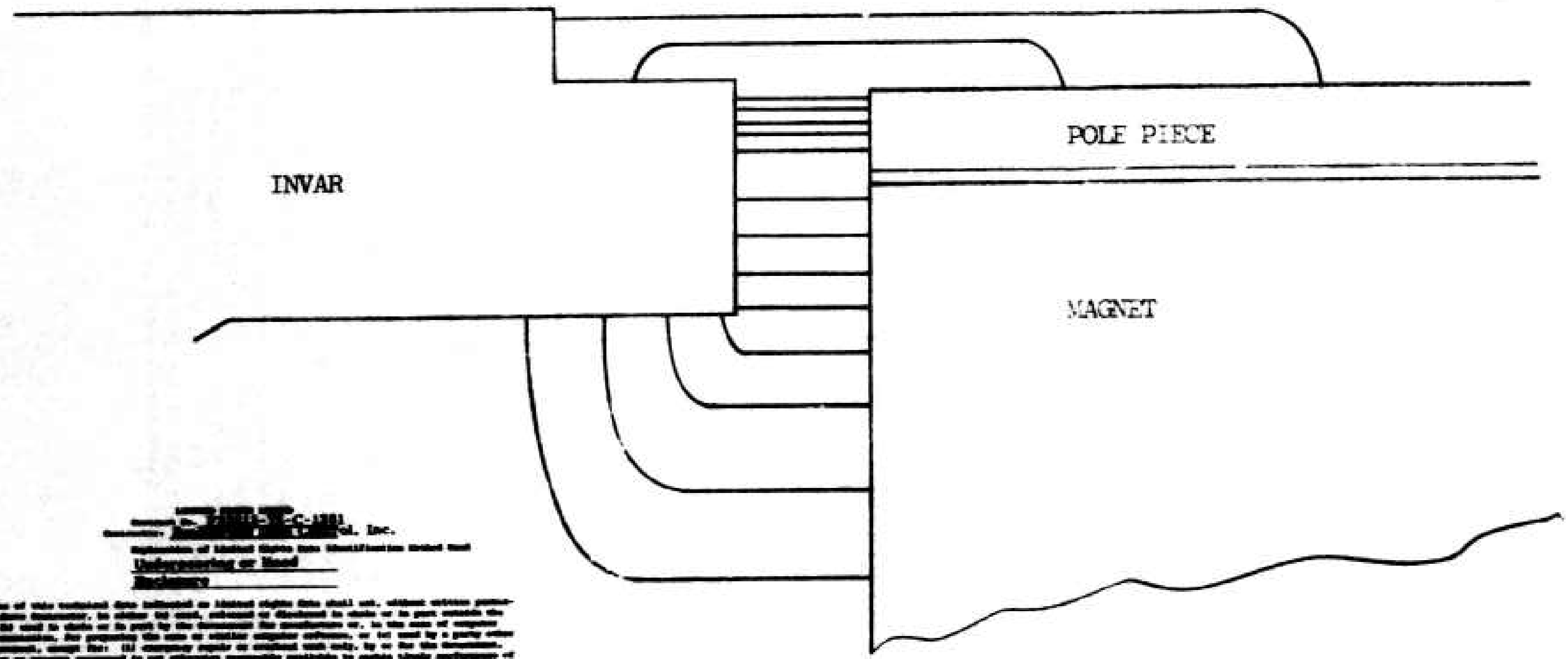

SECTION IV

RAPID WARM-UP PERFORMNCE

Goals

The general objective of the rapid warm-up tests was to obtain a description of the accelerometer output current characteristics in a rapidly changing thermal environment.

The ultimate goals were: (1) to extract the dominant driving forces for the current scale factor and bias transients from temperature measurements taken at specific test locations inside the Q-Flex sensor assembly during dynamic temperature environments, and (2) to uniquely assign each of the physical driving forces to its source of origin in the Q-Flex structure.

The immediate goal was to find the ideal location for a temperature sensor somewhere inside the Q-Flex mechanism which would exhibit a temperature characteristic that corresponded to the simultaneous output current in the most effective way.

More specifically, the ideal sensor location is defined by its unique property through which its instant temperature is related to the simultaneous output current of the unit. This instant, measurable temperature at any point in time has the same relationship to the output current during a dynamic temperature environment, as it has for the unit in a static temperature environment at the same thermal sensor temperature.

This ideal location provides valid temperature-output current data regardless of the particular arrangement of the heating system and the particular conditions of warm-up rates, and final, stationary temperature distributions across the internal structure of the Q-Flex mechanism.

In search of this ideal point, the accelerometer was tooled to accept several thermocouples that were embedded inside the sensor assembly at characteristic locations specifically selected for their projected effectiveness. In addition to the thermocouples the electrical resistance of the torque coil was utilized to provide temperature measurements at the very heart of the instrument. Any other extraneous sensor would have been hard to fit without distortion of the sensor parameters and disturbance of the thermal environment in the vicinity of the sensor.

The test findings present the dynamic temperature characteristics of the output current as they relate to the

immediate program goal of disclosing the ideal sensor location. As a by-product of the underlying tests, the temporal temperature gradients and thermal time delays between structural sections of the mechanism are made visible in the test data and graphs supporting this investigation.

RAPID WARM-UP TESTS

Test Description

The transient thermal response of the Q-Flex sensor output and temperature upon application of constant heater power was chosen as the most convenient method of measuring rapid warm-up performance. The method simulates the rapid warm up conditions encountered in temperature controlled, fast reaction guidance systems. Typically a large power input is applied to bring such a system to operating temperature followed by heater cut back to maintain that temperature.

A typical heater power program for a rapid warm up experiment or 'Heat' is shown in Figure 67. A hypothetical temperature response of the accelerometer output current is also shown and events in the experiment are identified. This particular type of warm-up program is convenient because the theoretical modeling consists of a linear system response to a temperature ramp.

During a Heat, each temperature at 5 locations within the sensor assembly were recorded at 5 second intervals. The accelerometer output current and torque coil voltage were measured at 20 second intervals. The chamber temperature was maintained at the initial temperature while the accelerometer and its mounting fixture heated up. In most of the Heats the accelerometer was tumbled tested at the initial and final stabilized temperatures.

Q-Flex Sensor Instrumentation

Five copper-constantan thermocouples were imbedded in the Q-Flex sensor/cover assembly to measure the temperature distribution and identify the heat flow paths within the structure. As shown in the cutaway drawing Figure 68, the thermocouples were located at the centers of the upper and lower excitation rings and bracketing the sensor belly band. The fifth thermocouple was located in the sensor cover flange. The thermocouple beads were less than .025 inch diameter and formed from .010 inch diameter insulated wire. The beads were potted into holes .050 inch diameter deep using thermally conductive epoxy. Heat shrink tubing and thermally insulating epoxy were used to attach and

Figure 67

A TYPICAL RAPID WARM-UP

HEAT PROGRAM

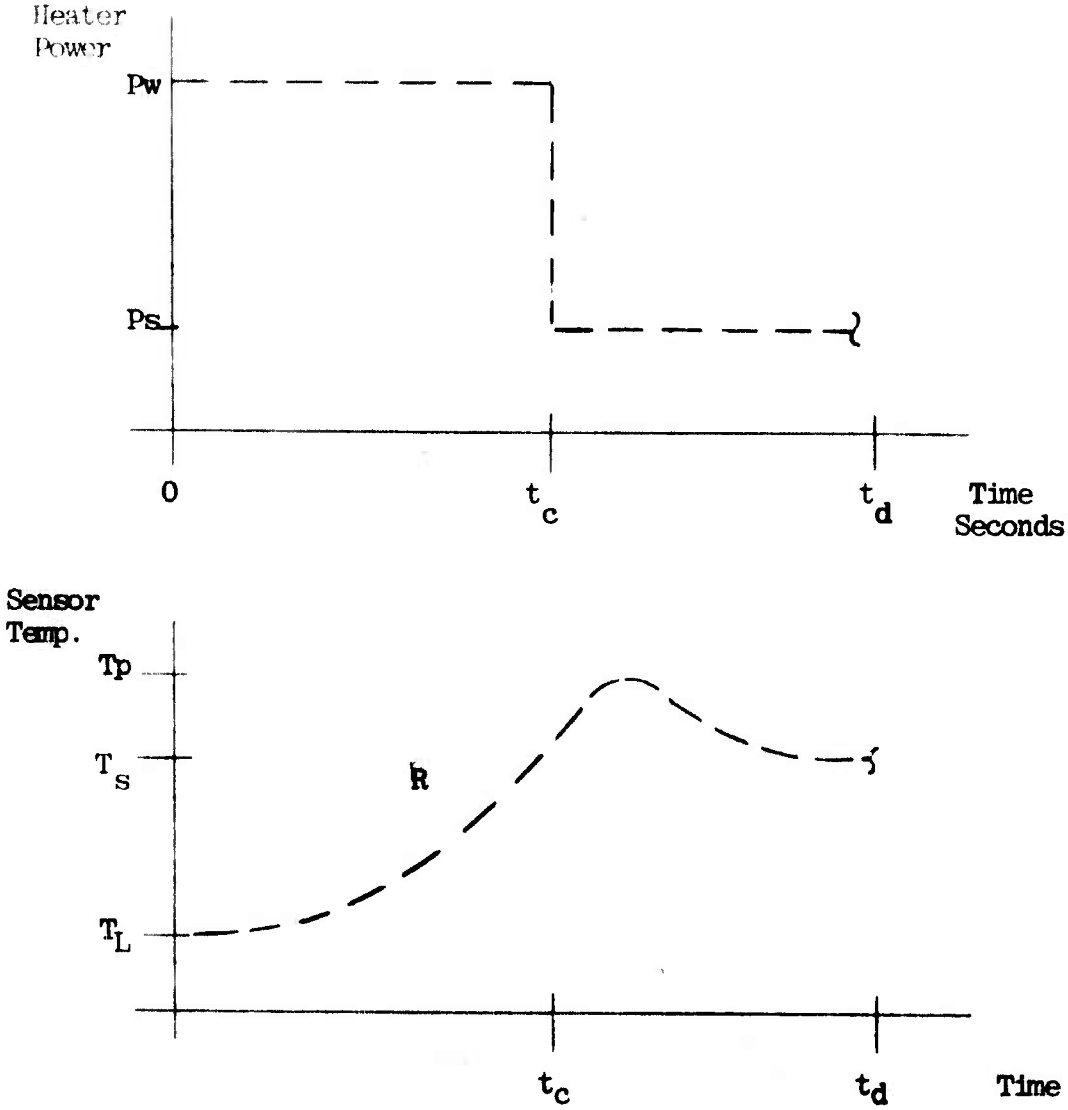

Pw - Warm Up Power
Ps - Sustaining Power
t_c - Power Cut Back Time
t_d - Heat Duration
T_L - Initial Temperature
T_p - Peak Temperature
T_s - Stabilized Temperature
R - Max. Warm Up Rate

Figure 68
Q-FLEX SENSOR INSTRUMENTATION

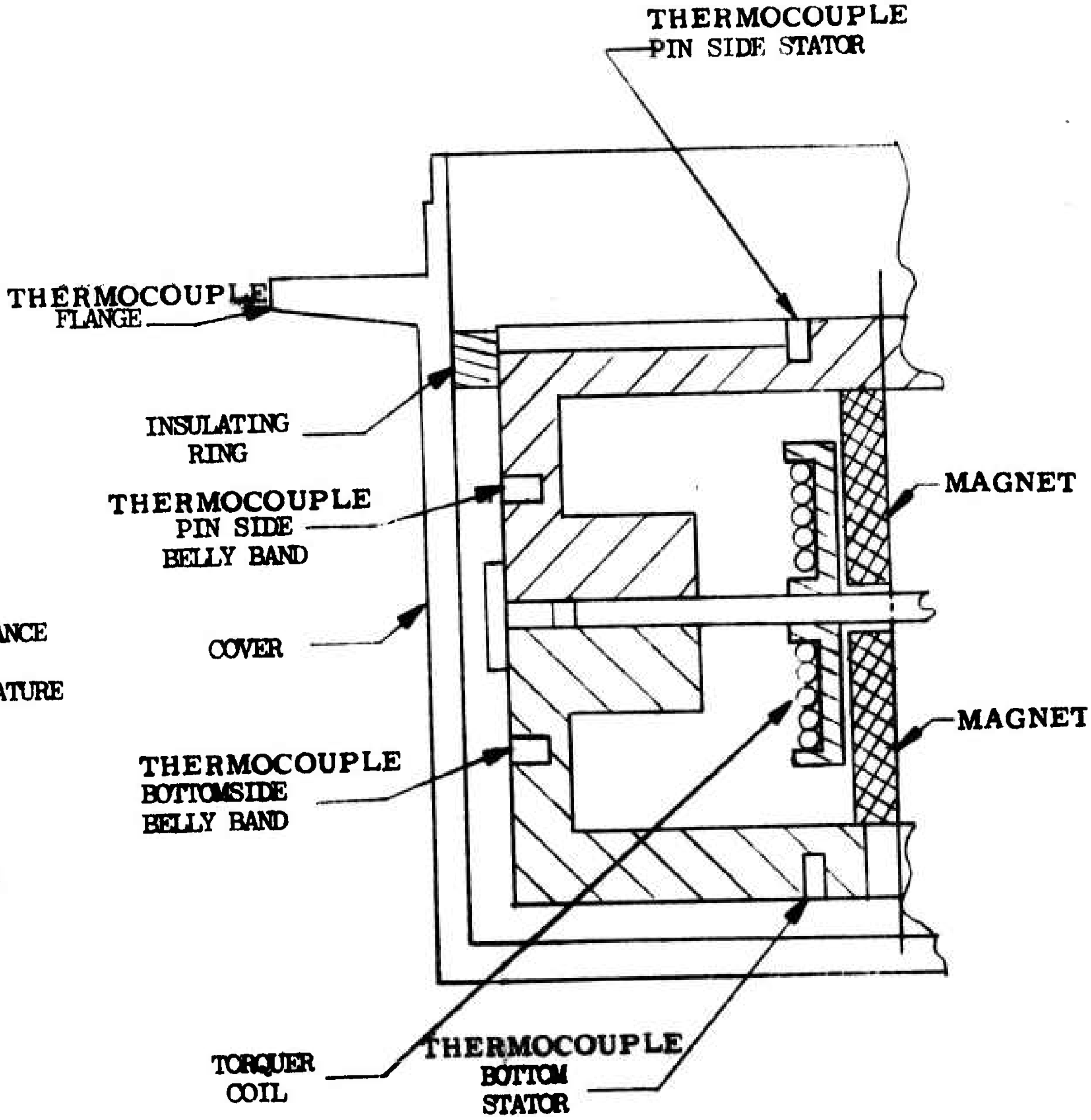

TORQUER COIL RESISTANCE

MODELED WITH TEMPERATURE

$T = SR + T_O$

S/N 10738

$S = 3.1^{O}F$ per ohm

$T_O = -409^{O}$ F

stress relieve the thermocouples. This mounting, as shown for a fully instrumented accelerometer in Figure 69, provided adequate durability and temperature measurement capability throughout the series of rapid warm-up tests. In addition to thermocouples, the torque coil voltage and current were measured and the torque coil resistance modeled versus temperature.

Inertial grade accelerometers with Harpoon transformer type servo hybrid electronics were used in the rapid warm-up tests. Performance was measured before and after instrumentation. No performance degradation occurred as a result of machining and reassembly of the sensor/cover assemblies.

Rapid Warm-Up Apparatus

The rapid warm-up fixture is pictured in Figure 70. The accelerometer was mounted on an aluminum block heated by four 40 watt strip heaters. The accelerometer and block are insulated from the chamber and from the tumble test dividing head by a phenolic plate. Flange warm-up rates to 90°F per minute starting at -65°F were achieved with this fixture. The accelerometer could be calibrated or tested in the plus or minus 1*g* position.

The five temperatures within the sensor were measured every thirty seconds on a multichannel temperature recorder. Torque coil voltage and output voltage across in external load resistor were measured with separate digital voltmeters. Chamber temperature was maintained within ±1°F of the initial temperature. Up to 160 watts were applied to the heaters to warm up the accelerometer at various rates. Since the resistance of the heaters varied less than 5% between -70°F and 250°F, nearly constant heater power input was maintained by simply setting and monitoring the heater power supply voltage during warm-up. The power versus time programs used for the high and low warm-up rate experiments are shown in Figure 71. The warm-up fixture had adequate thermal insulation and sufficiently small heat capacity so that the accelerometer flange temperature was very nearly a straight line ramp over a major portion of most warm-up profiles.

Rapid Warm-Up Data Reduction

The result of the Heat experiments was a plot of +1*g* or -1*g* output current versus temperatures at six points in the sensor as shown in solid lines in Figure 72, which is a hypothetical plot of results. The dotted line in Figure 72 is the static temperature output current obtained in normal temperature tumble testing.

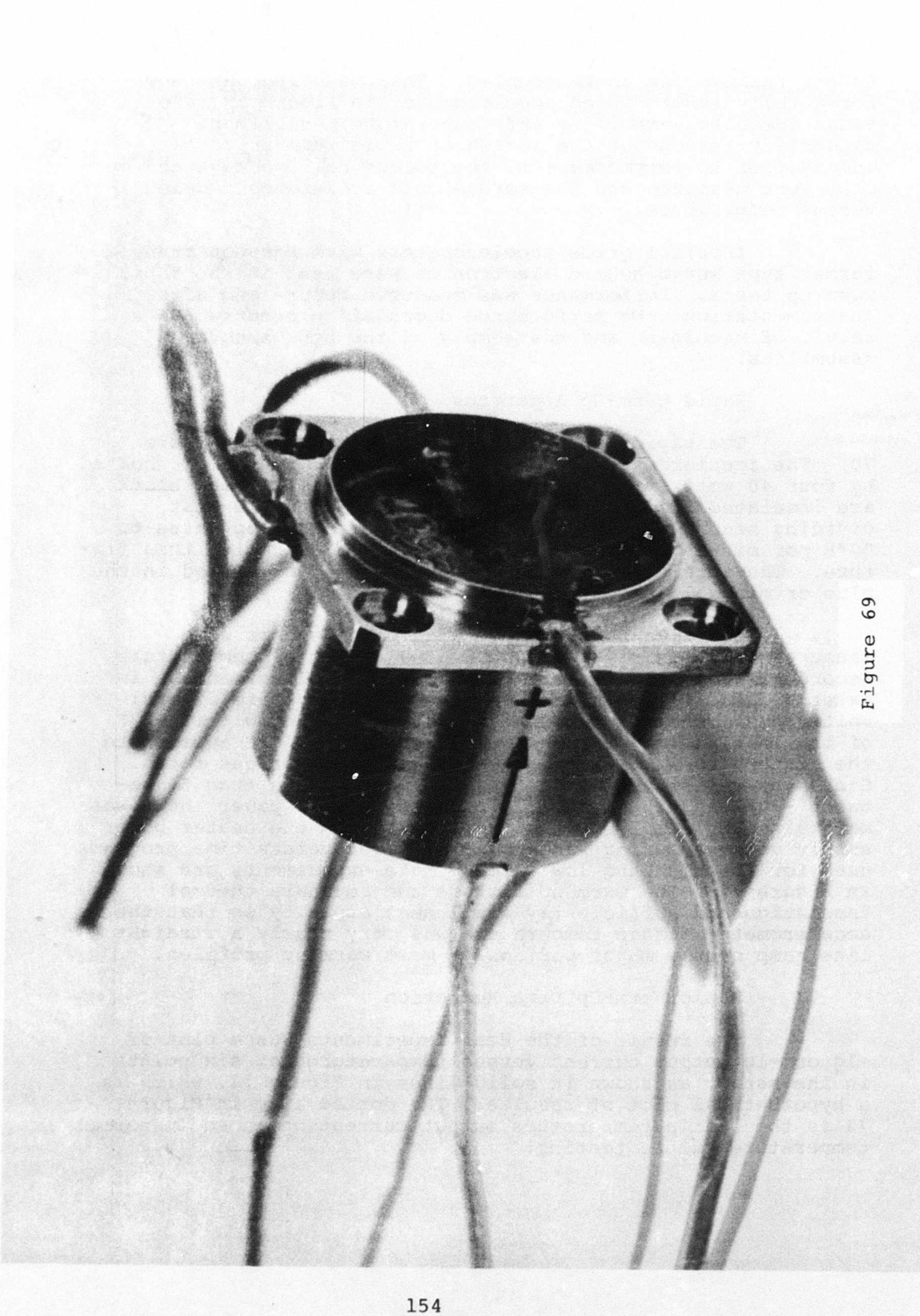

Figure 69

Figure 70

RAPID WARM UP EXPERIMENT FIXTURE

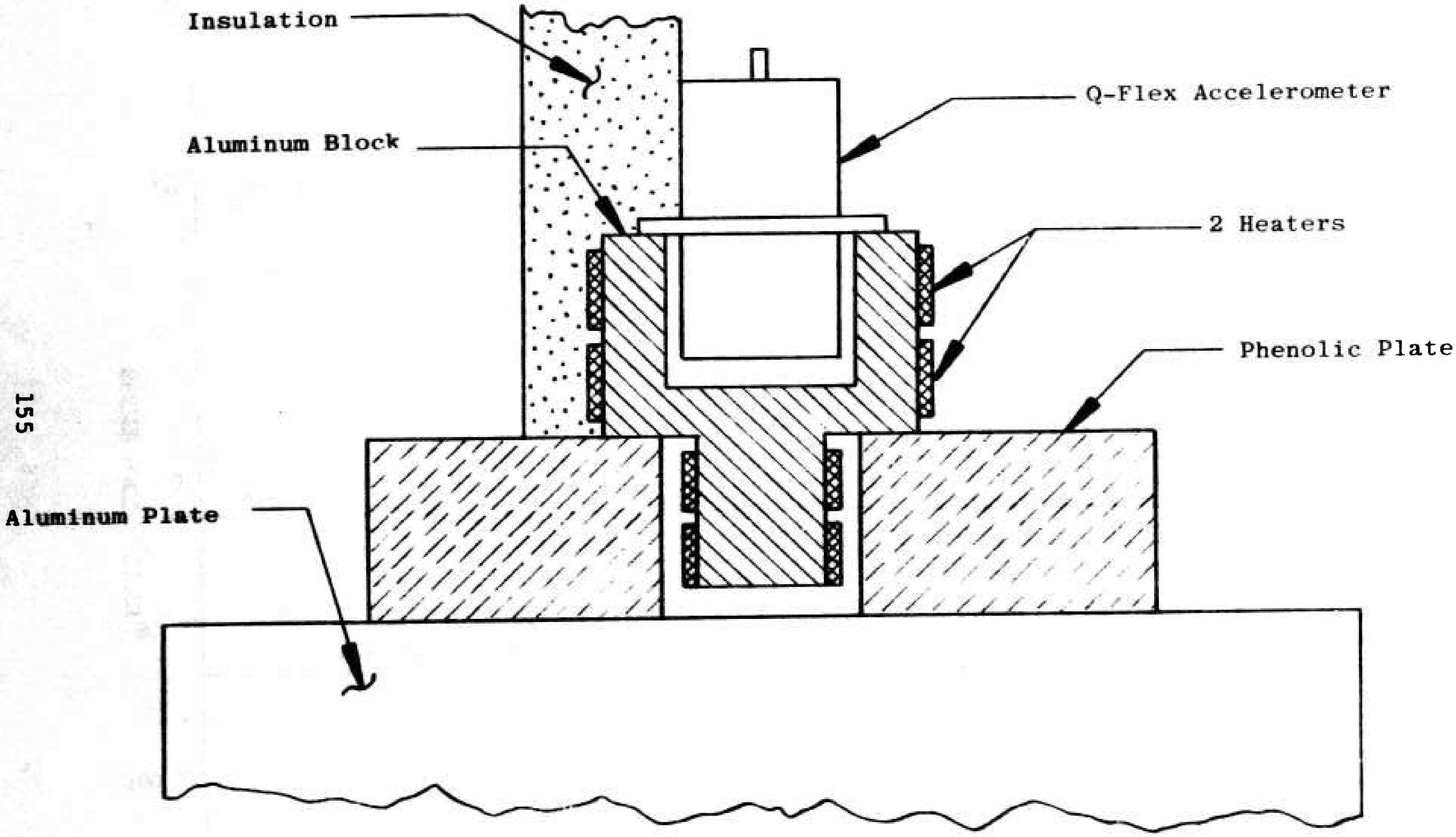

Figure 71

HEATER POWER PROFILES FOR RAPID

WARM UP EXPERIMENTS

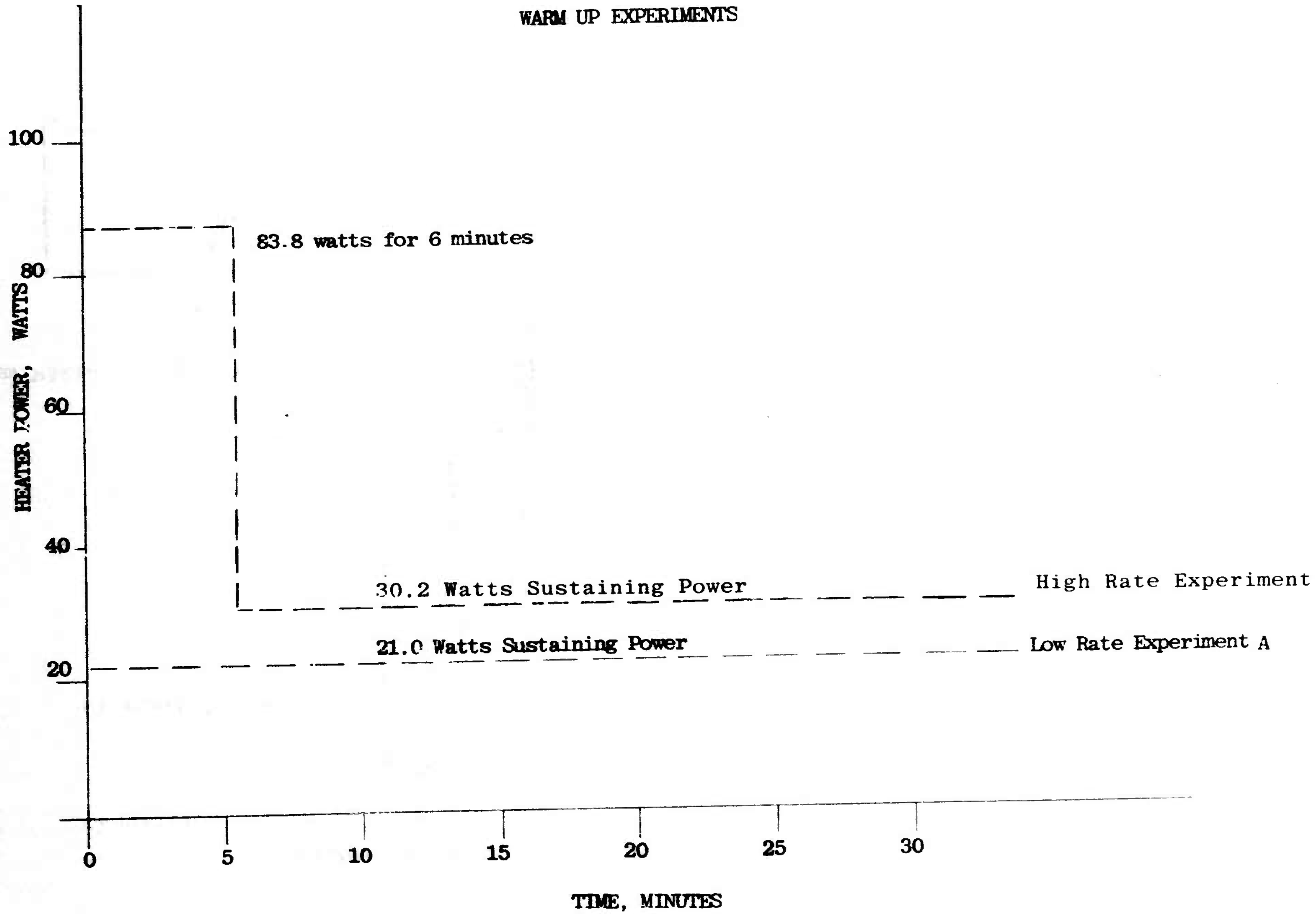

Figure 72
HYPOTHETICAL RAPID WARM UP OUTPUT VERSUS TEMPERATURE AT 6 LOCATIONS WITHIN Q-FLEX SENSOR

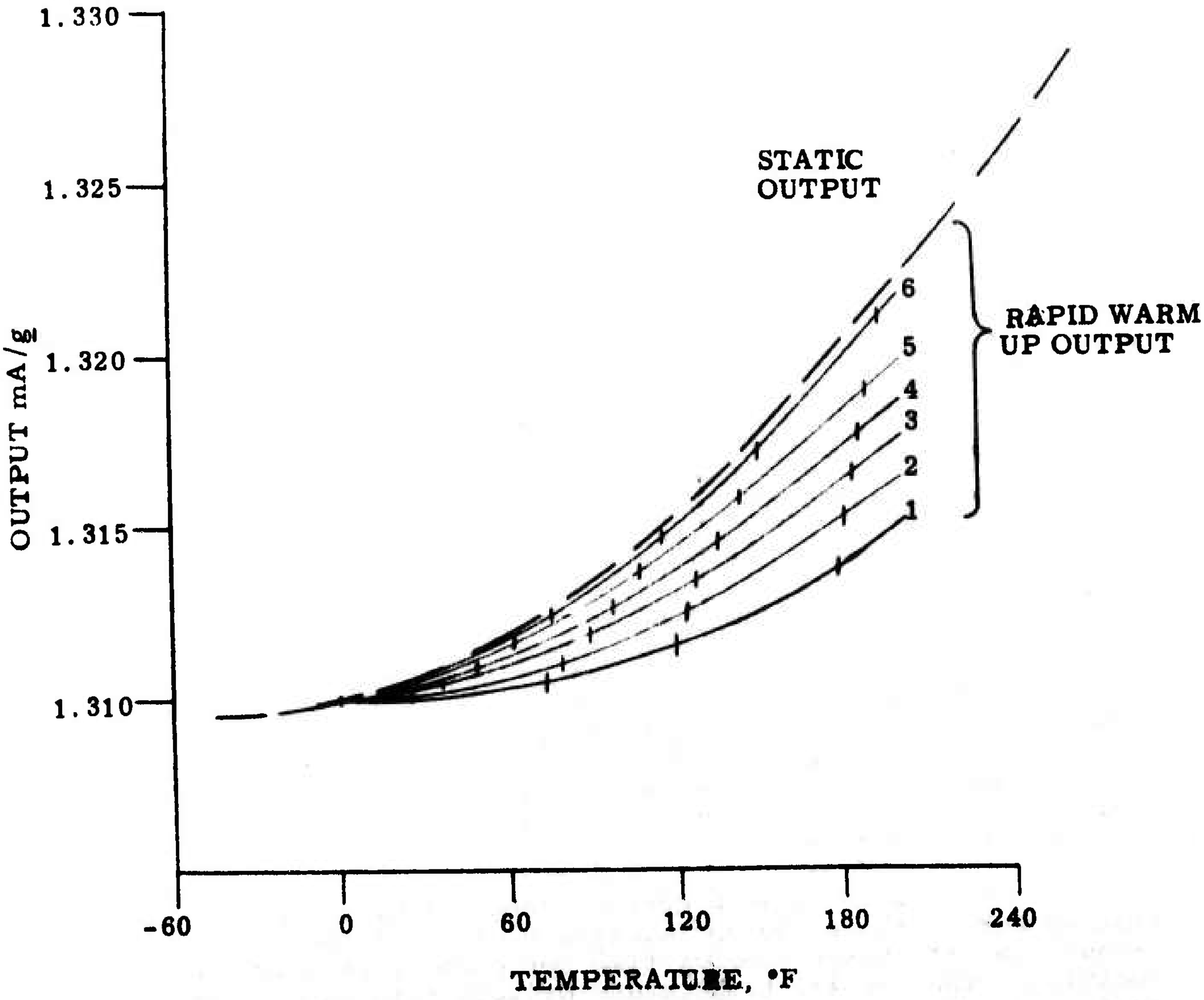

Note that because each location within the sensor has a particular time constant, the time base is slightly different for each curve as shown by the tick marks for multiples of a unit of time, t. Temperature versus time is shown in Figure 73. An ideal temperature sensor location would provide an output versus temperature plot under most rapid warm-up rates similar to the static output characteristic. This behavior is reported for the rapid warm-up experiments in plots similar to Figure 72, that is, the entire output characteristic for static as well as rapid warm-up conditions. An alternate method used to report results is called the difference function for rapid warm-up response.

The difference function is used to report empirical results and is derived theoretically. It is defined as the difference function, D(T) in PPM, between the static and rapid warm-up characteristics:

$$D(T) = \frac{I_{RW}(T) - I_S(T)}{I_O} \times 10^6$$

Where:

$D(T)$=Difference function as a function of temperature T

I_{RW}=Rapid Warm-Up output current at temperature T

$I_S(T)$=Static output current at temperature T

I_O=Reference output current

In Figure 72 the difference functions for hypothetical curves 1 through 6 are negative with curve 1 having the largest value at all temperatures. These difference functions are plotted in Figure 74. The difference function gives the error between predicted static output current and rapid warm-up output current. Since a system for temperature compensation will be based upon the accelerometer's static temperature output characteristics, sensor location having a minimum difference function is mandatory.

The rapid warm-up current versus temperature results were obtained by correlating plots of temperature versus time and output versus time for each temperature sensor location. The initial temperature or zero time output current was normalized to the static output current at that temperature. Scale factor and bias shifts between tests

Figur 73
TYPICAL TEMPERATURE VERSUS TIME PLOT FOR 6 LOCATIONS WITHIN A Q-FLEX ACCELEROMETER

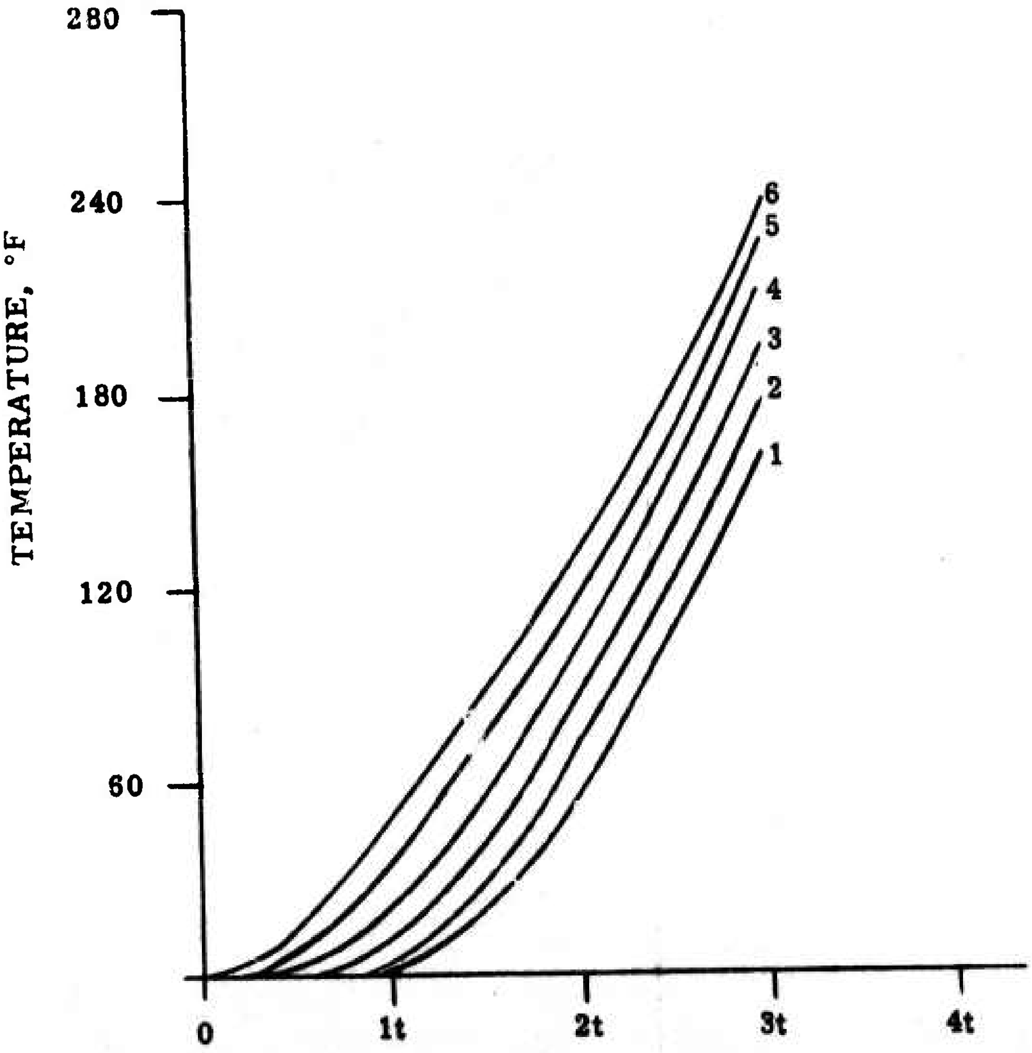

Figure 74
HYPOTHETICAL D(T) FOR 6 LOCATIONS WITHIN Q-FLEX SENSOR

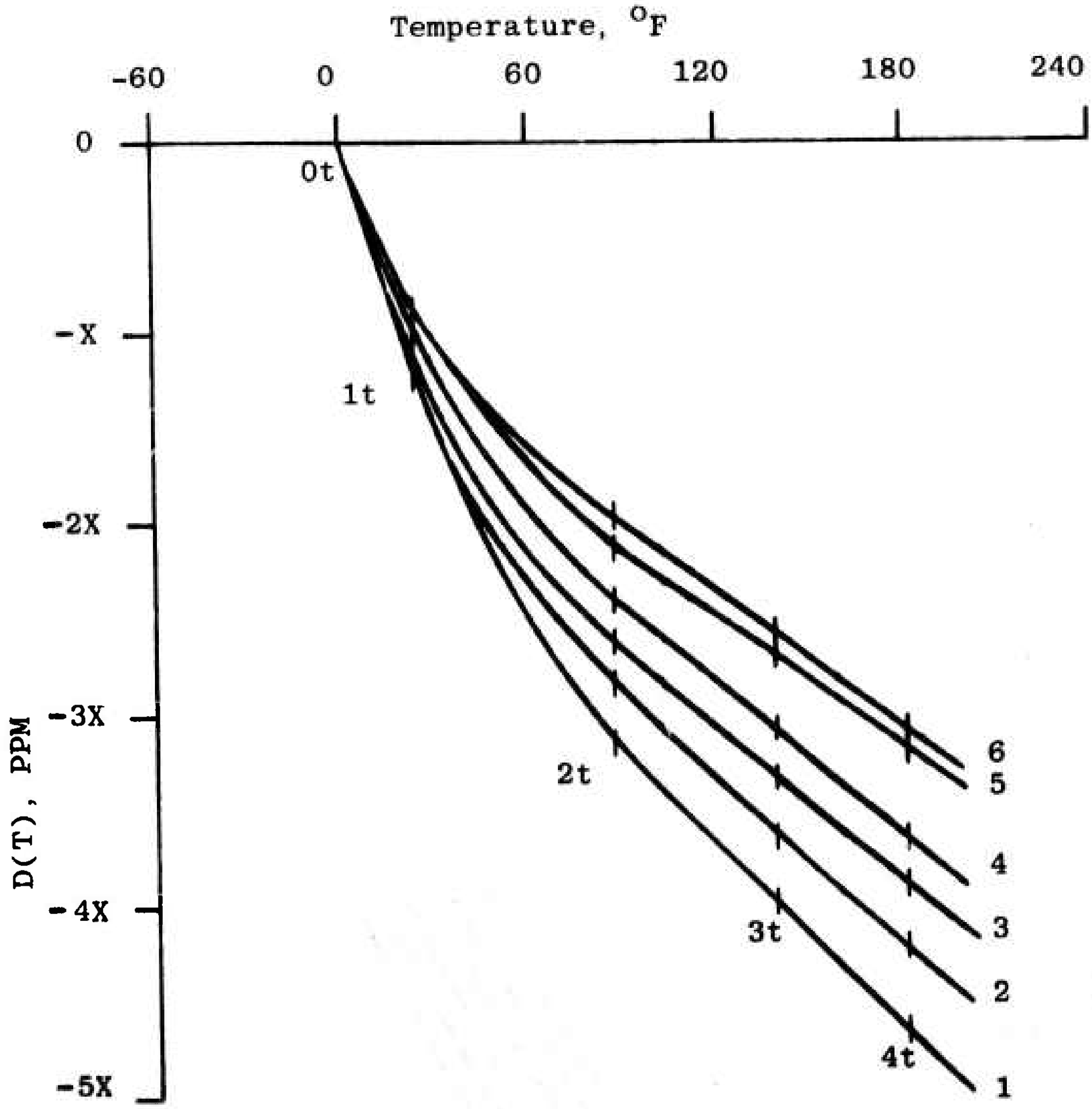

were eliminated from the data by a tumble test immediately prior to rapid warm-up. The initial temperature at all sensor locations was normalized. The temperature versus time, output versus temperature, and difference functions versus temperature are used to report results.

EXPERIMENTAL RAPID WARM-UP RESULTS

The rapid warm up experiments included high and low warm-up rate tests. Flange temperature rates ranged from 0 to 89°F per minute in these tests. Although data collection was hampered by fast changes in output current and sensor temperatures, the high rate experiments provided a worst case environment in which the driving forces behind rapid warm-up performance were accentuated. Large temperature gradients over the sensor occurred during rapid warm-up, allowing heat flow path to be identified. The high rate experiments cover the major portions of the Q-Flex temperature range. Initial ambient temperatures were 0°F and -60°F and final flange temperatures were between 200°F and 240°F. Accelerometer performance degradation and reliability were also tested under these worst case conditions. Tests at rates below 13°F per minute were also performed to demonstrate performance in conditioons similar to those encountered in uncontrolled temperature environments.

Slow Warm-Up Experiments

A Q-Flex accelerometer, +1g output current was measured under slow warm-up conditions. The initial temperature was 0°F and the initial flange temperature rates were 8.0°F per minute and 13.3°F per minute during the first 5 minutes of warm-up (experiments A and B). The final flange temperatures after 60 minutes were 83°F and 120°F at the accelerometer mounting flange and 89°F and 122°F at the torque coil. Experiment B had the higher initial warm-up rate and higher final temperature. A plot of flange temperature versus time for these experiments appears in Figure 75. Figure 76 shows the variation of output current in per cent versus flange temperature. The output current has been normalized to the 0°F output which is 1.35625 mA for the +1g position. The solid line is the static output current characteristic. The warm-up output current versus flange temperature is within +400 PPM of this static output characteristic for both slow rate experiments. The output current versus torque coil temperature tracks the static output more closely as shown in Figure 77. This data plot shows the difference between warm-up and static outputs in PPM relative to the torque coil temperature.

Figure 75

FLANGE TEMPERATURE VERSUS TIME FOR TWO SLOW RATE EXPERIMENTS

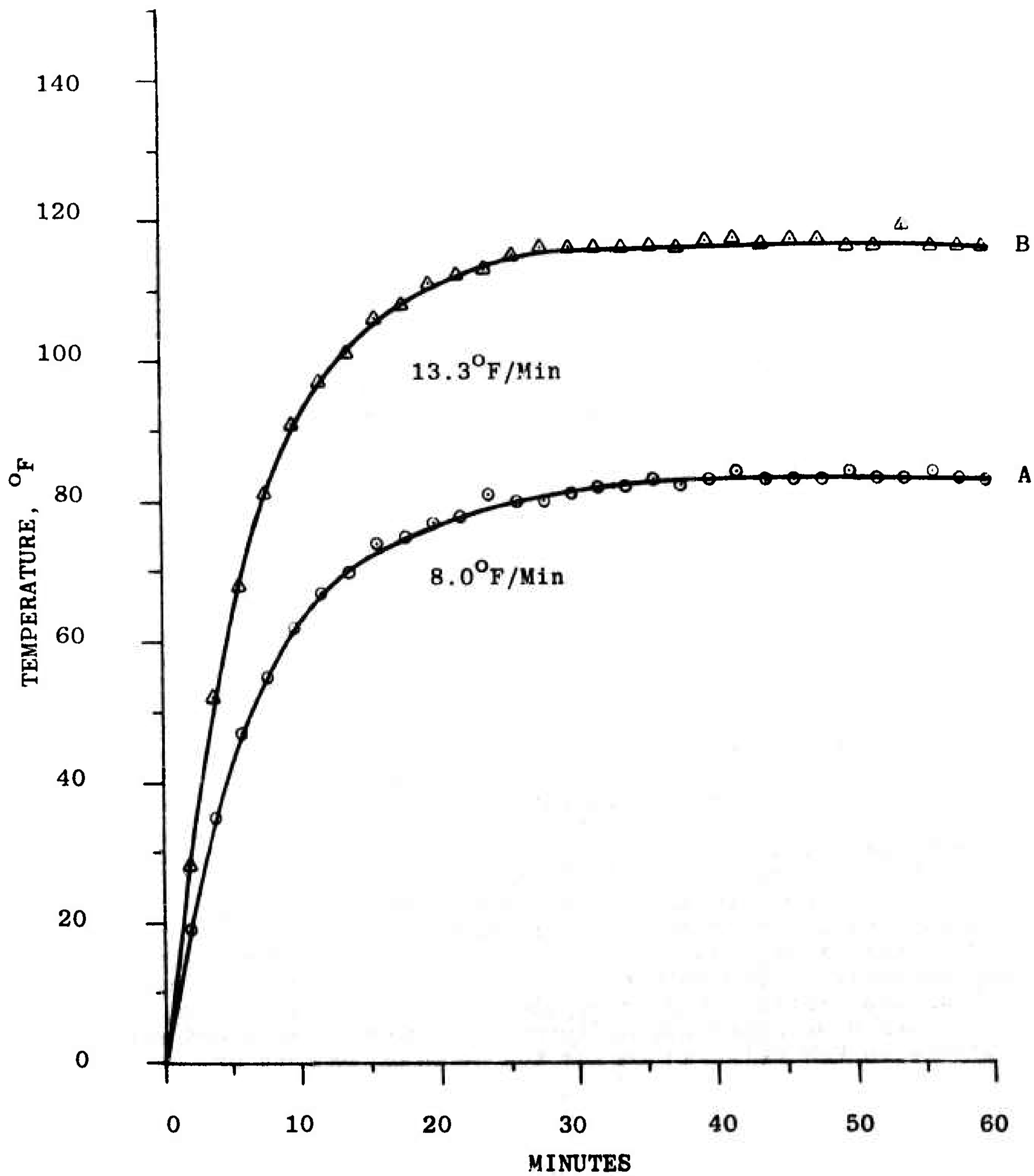

Figure 76

OUTPUT CURRENT VERSUS FLANGE

TEMPERATURE FOR SLOW RATE EXPERIMENTS

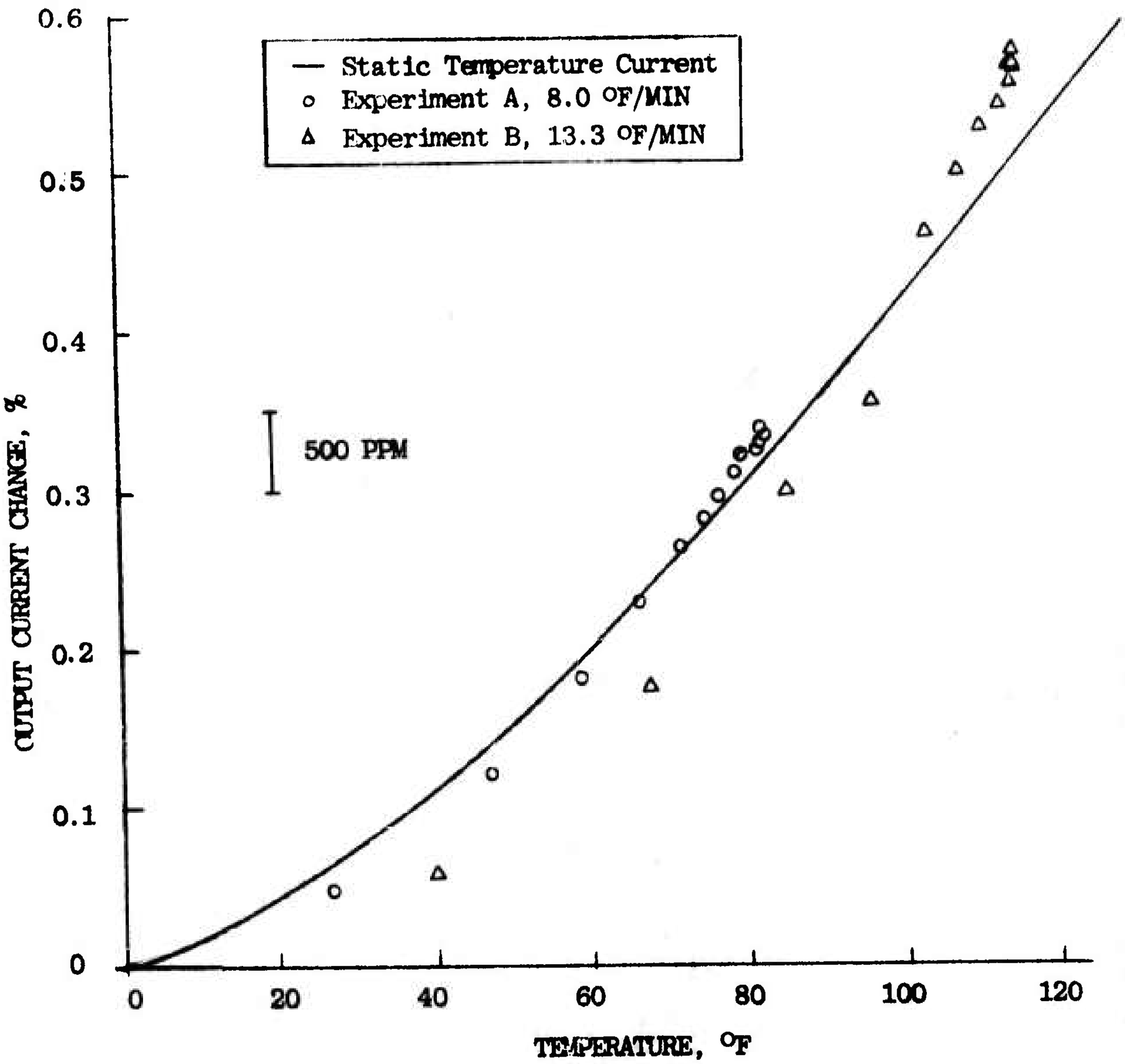

Figure 77

RAPID WARM UP CURRENT DEVIATION FROM STATIC CURRENT OUTPUT

- Slow Rate Experiments 8 & 13 ^{O}F/Min
- +1g Position, S/N 10738

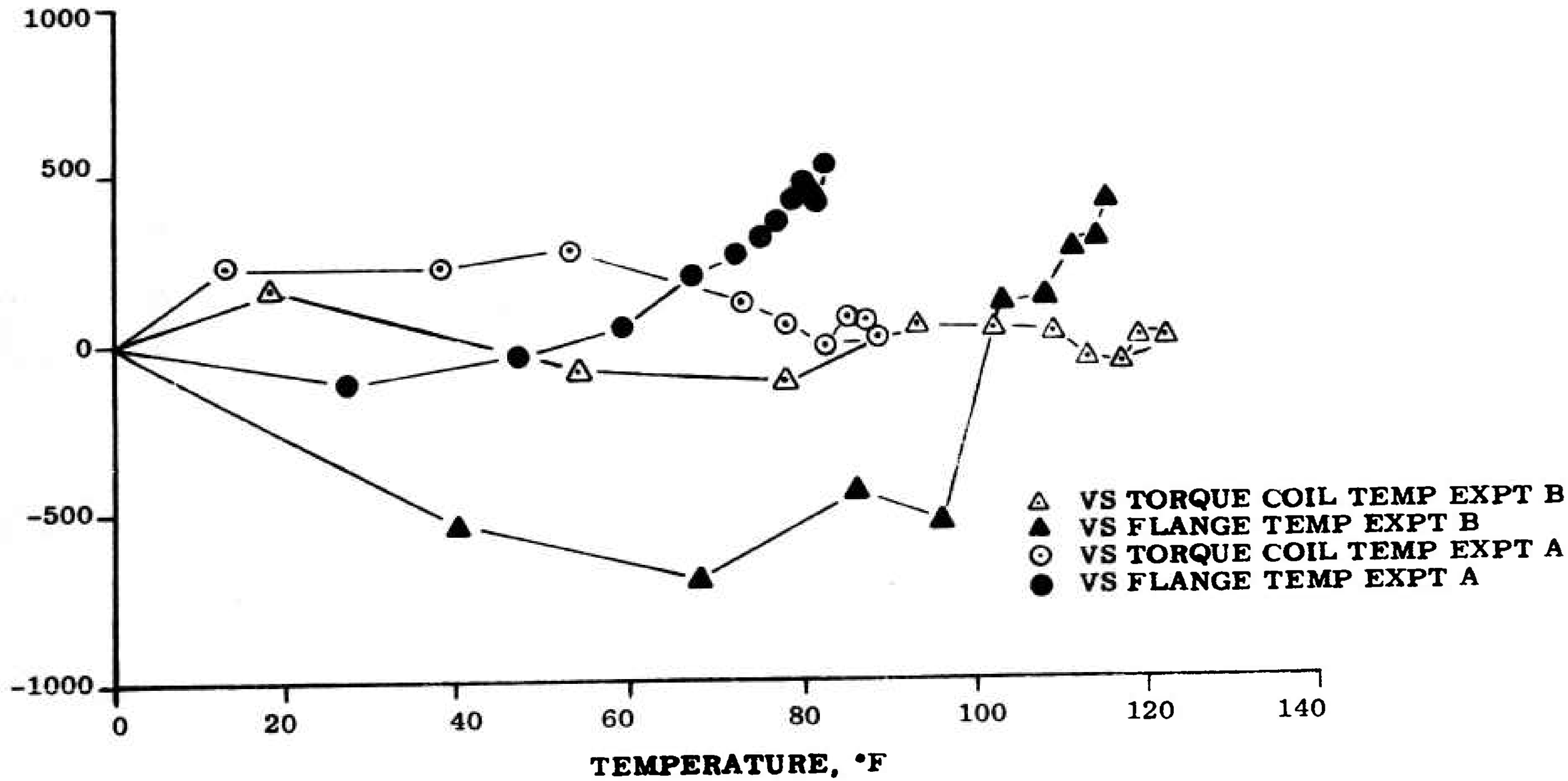

Note that the difference with respect to flange temperature has a larger final deviation than the difference versus torquer coil temperature at the final stabilized temperature. Figure 77 demonstrates that at slow warm-up rates, below 15°F/min temperature within the accelerometer sensor accurately predicts accelerometer output. The results also demonstrate that the Q-Flex accelerometer, if heated at rates below 15°F per minute can perform within 90 PPM RMS of the static temperature output current model. The RMS deviation of output versus flange temperature from the static temperature output characteristic is 208 PPM for the 8°F per minute experiment and 366 PPM for the 13.3°F per minute experiment.

High Rate Warm-Up Experiment

Figure 78 shows the temperature versus time plot for various locations within a Q-Flex accelerometer during a rapid warm-up experiment with an initial flange temperature rate of 40°F per minute. The initial temperature is 0°F, the peak temperature occurs in the lower stator at 242°F and the stabilization temperature is between 190°F and 230°F. Figure 79 shows the -1g output current versus upper and lower stator temperatures compared to the static -1g output current characteristic. The initial output was -1.370300mA. The output relative to the stator temperatures bracket the static output up to 145°F and the maximum deviation of upper stator output current is -610 PPM at 225°F.

The difference function versus torque coil temperature for the entire experiment appears in Figure 80. The total error band for the output versus torque coil temperature is ±550 PPM. The final output current is 400 to 500 PPM below the static temperature output characteristic and is due to a temperature gradient between the average stator temperature and the torque coil temperature. For an order of magnitude estimate, assume a scale factor temperature coefficient of 50 to 100 PPM per °F. If the individual magnet structures are perfectly matched and have constant, equal temperature coefficients then the output current is determined by the average temperature of the magnet structures (average stator temperatures) which is about 224°F. This is 5°F higher than final torque coil temperature and gives an output deviation of -250 to -500 PPM. Note that the magnet structure TC's are approximately the negative of the scale factor TC's because the scale factor is determined by the reciprocal of the magnet structure properties. The final output deviation is understood to be due directly to gradients between the modeling temperature, which in this case is the torque coil temperature, and the average magnetic structure temperature. Deviations due to gradients across the magnetic structure itself

Figure 78

TEMPERATURE VERSUS TIME FOR A FAST RATE

RAPID WARM-UP EXPERIMENT

40°F/MIN, - 1G Position

SN 10738

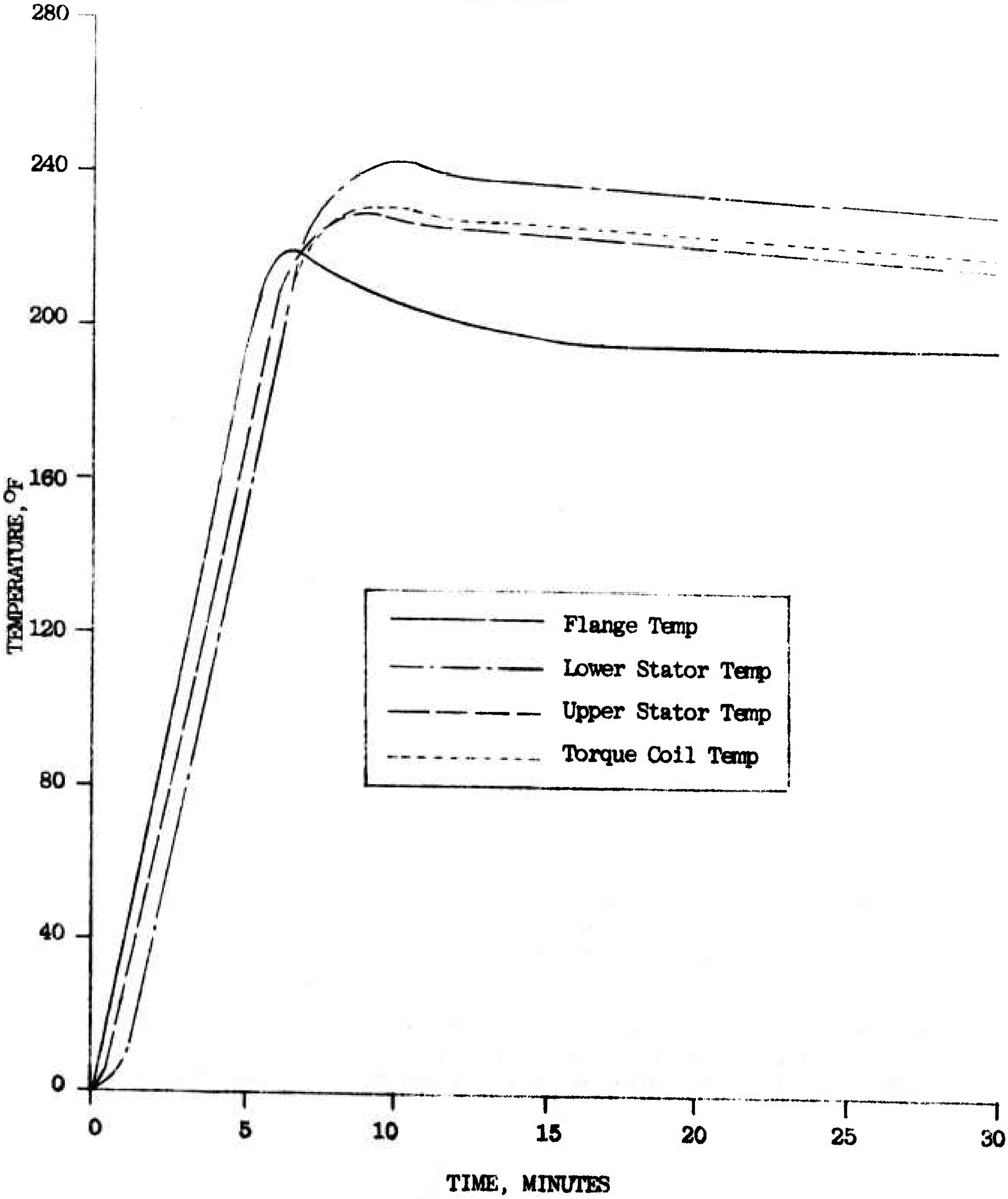

Figure 79

SENSOR OUTPUT CURRENT VARIATION VERSUS TEMPERATURE

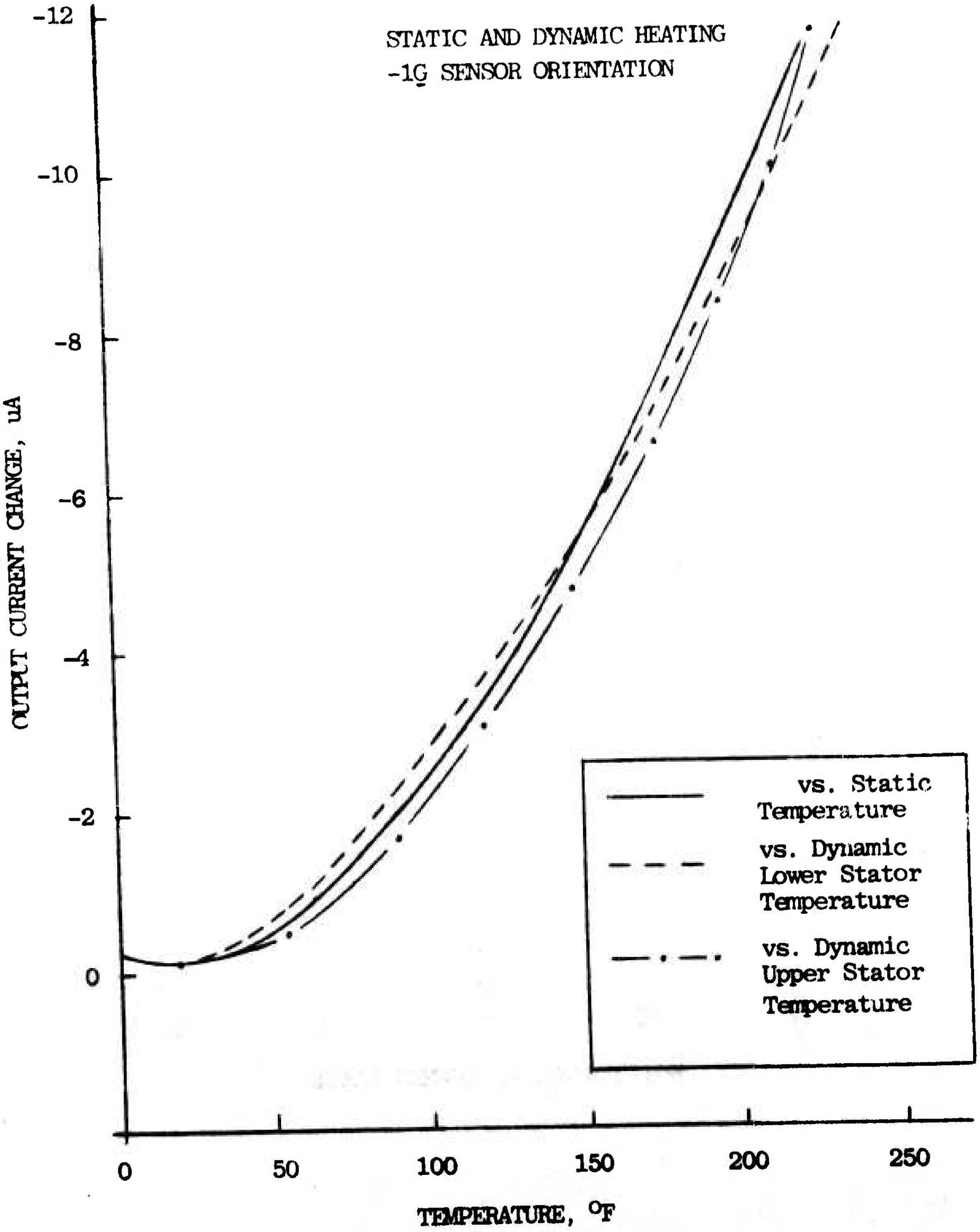

Figure 80
RAPID WARM UP OUTPUT CURRENT DEVIATION FROM STATIC CURRENT OUTPUT

Fast Rate Experiment, 40°F/MIN

-1G Position, SN 10738

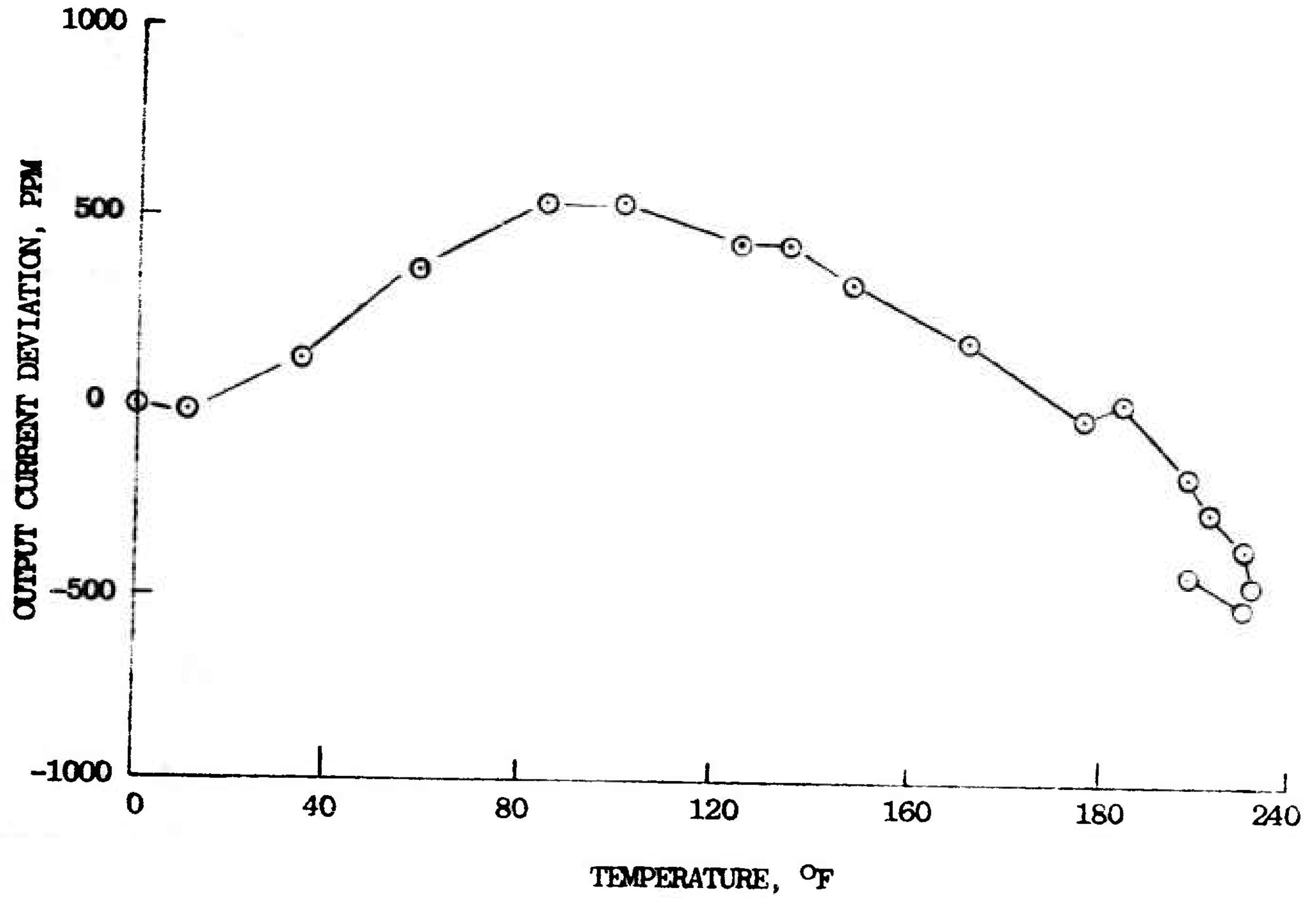

are very small due to the matching of the magnets in each Q-Flex sensor.

THEORETICAL RAPID WARM-UP PERFORMANCE MODEL

Model Derivation

A simplified thermal schematic of the accelerometer with respect to its environment is presented in Figure 81.

Let T_e be a function of time, t

$$T_e(t) = 0 \quad , t \leq 0$$

$$= Bt \quad , t > 0$$

and let the sensor be in thermal equilibrium with the environment for $t \leq 0$.

$$T_s(t) = T_e(t) = 0 \quad , t \leq 0$$

For $t>0$ the sensor temperature is derived from heat flow balance between sensor and environment.

$$\frac{d \; T_s}{d \; t} + \frac{T_s}{R \; \rho cV} = \frac{Bt}{R \; \rho cV}$$

Integrating and applying the initial conditions gives the sensor temperature with time.

$$T_s = Bt - B\tau \; (1 - \exp\,(-t/\tau\,))$$

where $\tau = R \; \rho cV$

The result is plotted in Figure 82.

Figure 81

ACCELEROMETER THERMAL SCHEMATIC

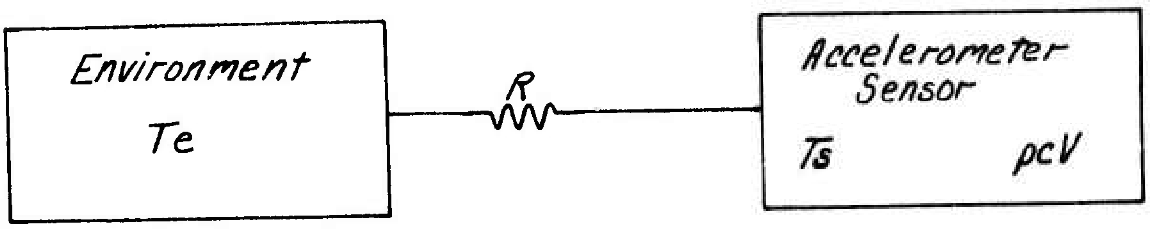

R = Total Accelerometer to Environment Thermal Resistance, Conductive and Convective

Te = Temperature of Environment

Ts = Temperature of Sensor

pcV = Accelerometer Sensor Heat Capacity

Figure 82
ENVIRONMENT AND SENSOR TEMPERATURES AS A FUNCTION OF TIME

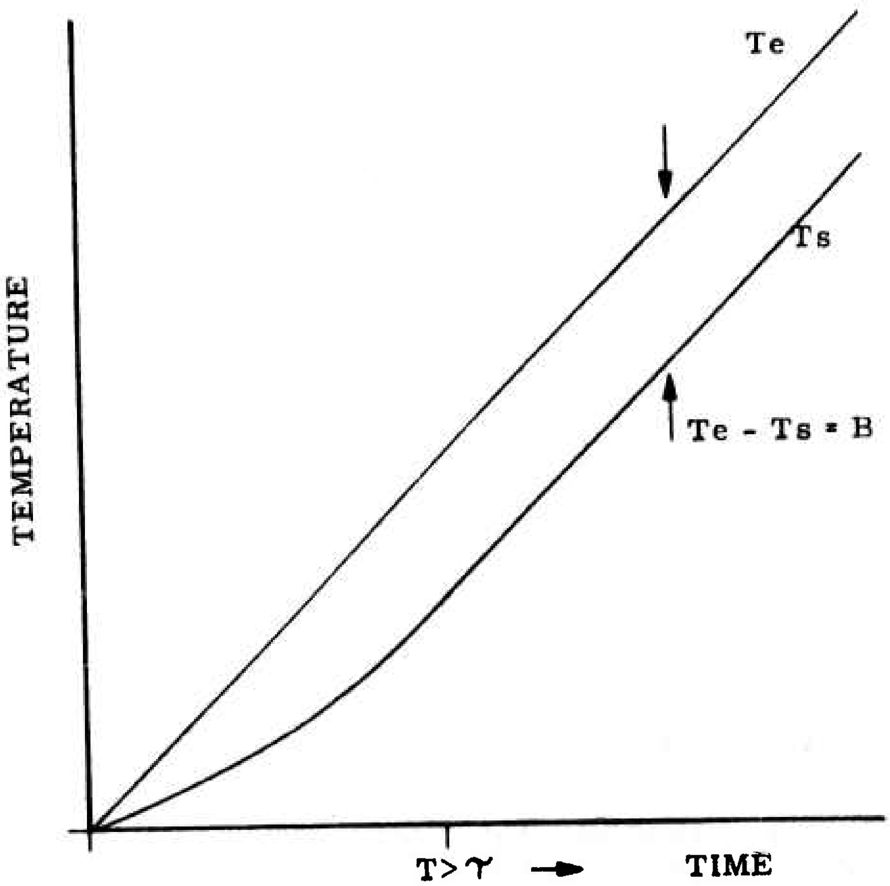

At t much larger than τ or

$$T_e \gg B\tau$$

$$T_s = Bt - B\tau$$

$$T_e - T_s = B\tau \text{ , constant}$$

The sensor has a finite, constant temperature difference with the environment and its temperature changes at the same rate.

Finally, the sensor temperature is expressed in a more useful form as a function of environment temperature.

$$T_s = Te - B\tau \quad (1 - \exp(-Te/B\tau))$$

Accelerometer Ouput Model

The +1g output current as a function of temperature is

$$I(T) = Io \quad (1 + ITC \times T \times 10^{-6} + ITC \times T^2 \times 10^{-6})$$

I(T) = Output Current, Milli-amperes

ITC = Output current temperature coefficient, PPM/^{O}F

ITCL = Output current temperature coefficient linearity, PPM/$^{O}F^2$

The output current coefficients are directly related to scale factor and bias temperature models, i.e.,

$$I(T) = K_1(T)(G + K_o(T) \times 10^{-3})$$

I(T) is a model determined at static temperatures, T, in temperature tumble tests.

Rapid Warm-Up Performance Model

The derivation of the difference between real sensor output and sensor output as predicted by the environment's temperature under conditions of rapid warm-up follows:

Define the ideal output current, $I_i(T)$, as the accelerometer output current that would be observed if $\tau = 0$. In this case $T_s = Te$ and the accelerometer would be isothermal throughout rapid warm up.

$$I_i(T) = I(T_e) = I_o \times (1 + ITC \times T_e \times 10^{-6} + ITCL \times T_e^2 \times 10^{-6})$$

Next define the real output current, $I_r(T)$, as the observed output current. This current is determined by the temperature of the sensor.

$$I_r(T) = I(T_s) = I_o (1 + ITC \times T_s \times 10^{-6} + ITCL \times T_s^2 \times 10^{-6})$$

Substituting T_s in terms of T_e, the equation becomes

$$I_r(T_e) = I_o (1 + ITC \times 10^{-6} (T_e - B\tau \exp (T-T_e/B\tau))$$
$$+ITCL \times 10^{-6} (T_e - B\tau \exp (-T_e/B\tau))^2)$$

D is defined as the difference of real and ideal output in PPM. D is expressed as

$$D = \frac{I_r (T_s) \times 10^6}{I_o} - \frac{I_i(T_e) \times 10^6}{I_o}$$

$$D = ITC \times (T_s - T_e) + ITCL \times (T_s^2 - T_e^2)$$

Substituting T_s in terms of T_e from the T_s equation gives D as a function of T_e.

$$D(T_e) = B\tau\alpha (B\tau\alpha \times ITCL - ITC)$$
$$-2B\tau \times ITCL \times T_e$$

where $\alpha = 1 - \exp (-T_e/B\tau)$

At times larger than τ or $T_e >> B\tau$

$$\alpha(T_e >> B\tau) = 1$$

and D (T_e) becomes

$$D(T_e >> B\tau) = B\tau(B\tau \times ITCL - ITC)$$
$$-2B\tau \times ITCL \times T_e$$

Figure 83 shows the behavior of $D(T_e)$ for three cases.

Figure 83
THE DIFFERENCE FUNCTION FOR RAPID WARM-UP RESPONSE

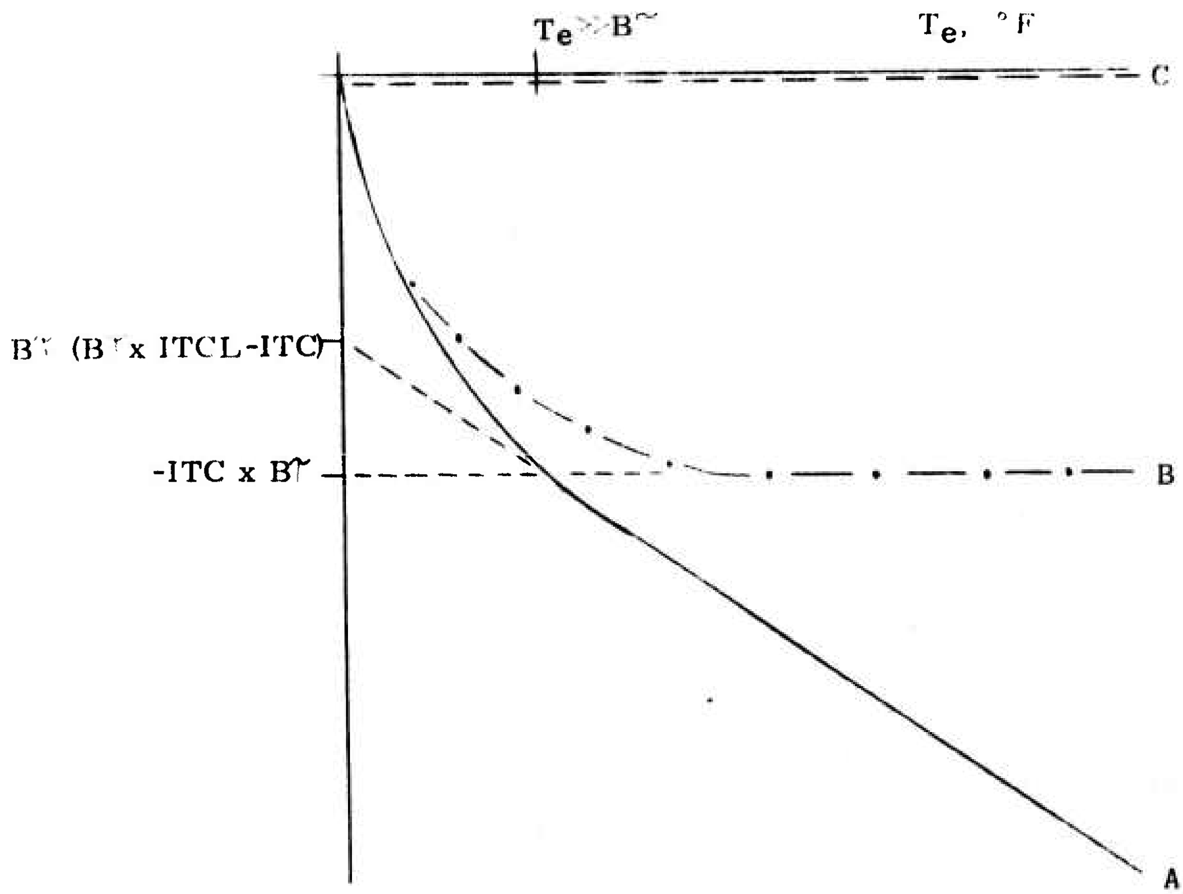

A: $\tau \neq 0$, ITC > 0, ITCL > 0, B > 0

B: $\tau \neq 0$, ITC = 0, ITCL = 0, B > 0

C: IDEAL RESPONSE = REAL RESPONSE

Experimental Verification of The Rapid Warm-Up Performance Model

The results of the high rate warm-up experiment can be used to verify the rapid warm-up performance model.

From the static temperature -1g output current characteristic for sensor S/N 10738 used in the rapid warm-up experiments, the average temperature coefficient between 0°F and 220°F was determined to be 36 PPM/°F. The average output temperature coefficient linearity was determined to range between 0 and 0.3 PPM/°F^2 for the same temperature range. From the flange, torque coil, and stator temperature versus time plots of the 40°F per minute experiment, the product $B\tau$ was found to range between 30°F and 40°F. Since the stator most nearly represents the active region determining scale factor, the lower value, $B\tau$ = 30°F was chosen for model verification. Although the torque coil resides at the geometric center of the Q-Flex sensor, the average temperature of the sensor does not occur at the torque coil for this -1g experiment, and the stator temperatures are more representative of the sensor temperature. Also the value of $B\tau$ = 48°F gives a value of τ = 1.22 minutes for B = 39.4°F per minute in this experiment. Calculations of the sensor heat capacity (C = 10 watt-sec/°F) and order of magnitude estimates of thermal impedances within the sensor (R = 6°F/watt) give an upper limit of τ = RC = 60 seconds.

To summarize, the relevant parameters for the performance model verification are as follows:

$B\tau$ = 30°F

B = 39.4°F per minute

τ = .76 minutes

ITC = 36 PPM/°F

ITCL = 0→0.3 PPM/°F^2

A sample calculation of $D(T_e)$ using ITCL = 0 follows:

$$T_e = 192.6°F$$

$$\alpha = 1 - \exp(-T_e/B\tau)$$

$$\alpha = 1 - \exp(-192.6/30)$$

$$\alpha = .998$$

$$B\tau\alpha = 29.94$$

$$D(T_e) = B\tau_d\,(B\tau_d \times ITCL - ITC) - 2B\tau \times ITCL \times T_e$$

$$D(T_e) = 29.94\,(29.94 \times 0 - 36) - 2 \times 30.00 \times 0 \times 192.6$$

$$D(T_e) = -1078 \text{ PPM}$$

A list of experimental and theoretical values of $D(T_e)$ for the high rate experiment with ITCL equal 0 and .3 PPM per °F^2 appears in Table 30 and the results are plotted in Figure 84.

Figure 84 shows that the performance model provides a worst case prediction of the difference function as compared with experiment. The experimental data however behaves qualitatively as predicted. The experimental data grows nearly linearly between 80°F. This is due to a finite value of ITCL in the lower temperature ranges and because the sensor temperature and environmental temperatures are parallel ramps in this temperature range. The deviations begin to decrease above 200°F because the output temperature coefficient becomes linear at higher temperatures. In other words, ITCL goes to 0 at higher temperatures.

The experimental data between 0°F and 80°F does not follow the predicted difference function for several reasons. First, the theoretical curves are based upon a linearly increasing environmental temperature. In fact the finite heat capacity of the warm-up fixture causes the environmental temperature to increase slower than B = 39.4°F/min. at low temperatures and thus the observed response lags behind the predicted. Secondly, large gradients across the sensor during the early portion of warm-up also contribute to the observed response lag. At low temperatures, the scale factor is highly sensitive to all geometry and material properties within the sensor and, indeed, scale factor temperature coefficient variability in the family varies three times as much as at high temperature. Thus, under high gradient conditions at low temperatures, the static output current characteristic is not as good a predictor of output current as at higher temperatures with the same gradient conditions. The derived difference function is thus less accurate at low temperatures under gradient conditions.

Table 30

EXPERIMENTAL AND THEORETICAL DIFFERENCE FUNCTION FOR A HIGH RATE RAPID WARM-UP EXPERIMENT

BT = 30°F B = 39.4°F/Min ITC = 36 PPM/°F

Time Seconds	T_e °F	$D(T_e)$ Experiment	$D_o(T_e)$ Theory ITCL=0	$D_1(T_e)$ Theory ITCL=.3
0	.6	0	-21	-21
30	9.3	40	-288	-313
60	34.3	-28	-736	-1031
90	56.6	-234	-916	-1586
120	79.6	-849	-1004	-2103
150	101.8	-1184	-1044	-2562
180	121.4	-1385	-1061	-2947
210	140.4	-1453	-1070	-3309
240	159.2	-1619	-1075	-3659
270	176.3	-1801	-1077	-3973
300	192.6	-2009	-1078	-4270
330	205.6	-1947	-1079	-4506
360	217.4	-1725	-1079	-4720

Figure 84

EXPERIMENTAL AND THEORETICAL DIFFERENCE MODEL

$D\ (T_e)$ Experiment

$D_0\ (T_e)$ Theory, ITCL = 0, ITC = 36, $B\tau$ = 30

$D_1\ (T_e)$ Theory, ITCL = .3, ITC = 36, $B\tau$ = 30

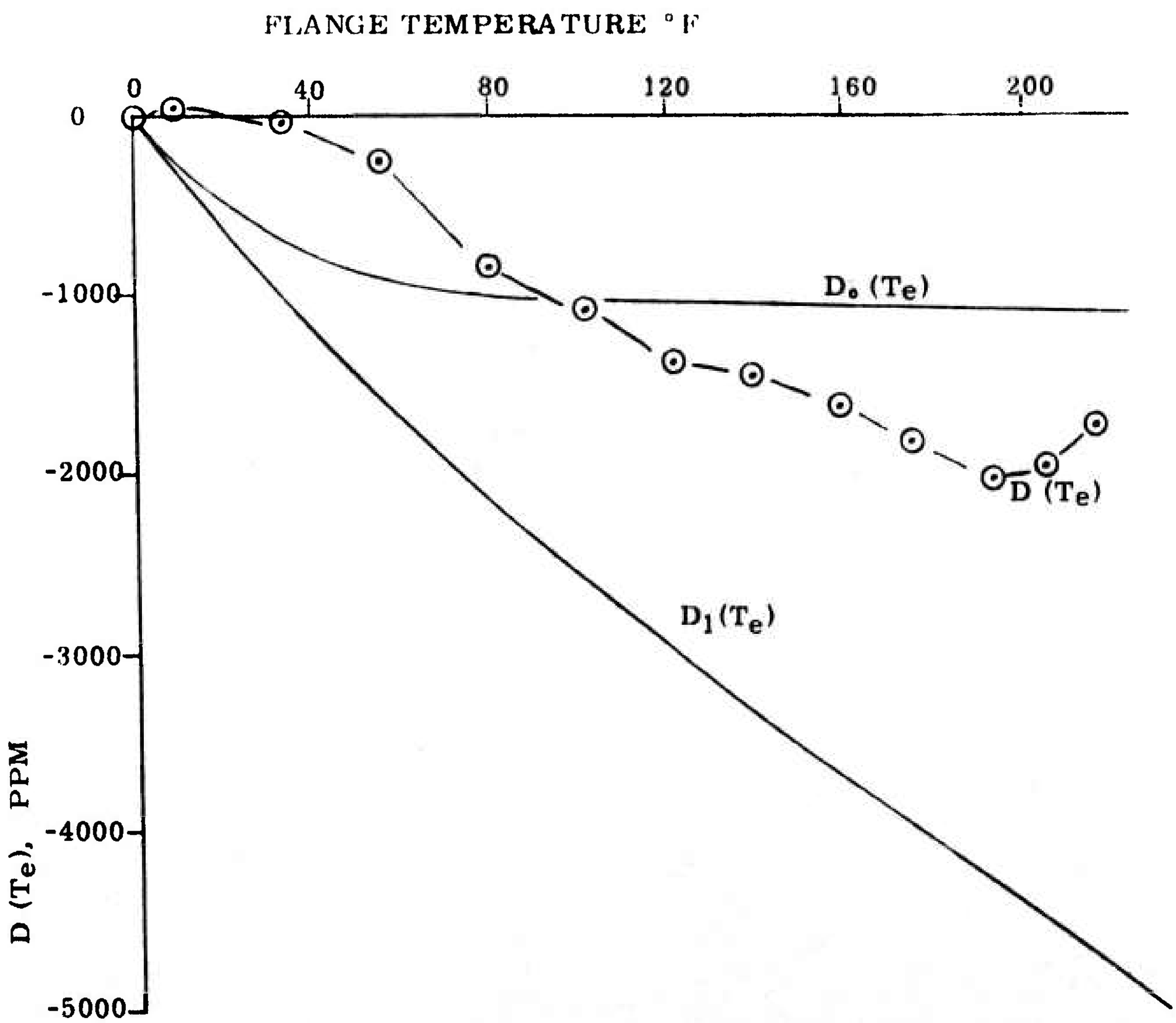

Q-Flex Output Current Compensation

The results of high rate rapid warm-up experiments indicate that the Q-Flex accelerometer current can be accurately compensated by measuring the average sensor temperature. For severe environments with warm-up rates to 40°F per minute, temperature sensitive elements would be located in the upper and lower magnetic structures of the Q-Flex sensor. For less severe environments where lower sensor gradients and rates below 15°F per minute are expected, a single temperature sensitive element at the lower stator would be adequate for temperature compensation.

Expected errors for compensated Q-Flex accelerometer output current over the operating temperature range of -65°F to 225°F can be estimated from the following:

1) Modelability of Q-Flex sensor output

2) Temperature sensor accuracy

3) Compensation network accuracy

The modelability of Q-Flex scale factor and bias are ±40 PPM and ±30μg respectively. Thermal hysteresis contributions for bias and scale factor are typically ±75μg and ±150 PPM. The total uncertainty due to modelability is approximately ±175 PPM RMS for ±1g output.

Temperature sensor accuracy, estimated to be ±1°F, couples through the output temperature coefficient to contribute an error to the compensated output. Average scale factor and bias temperature coefficients are 50 PPM/°F and 10μg/°F respectively and give a total output current coefficient of approximately 60 PPM/°F per +1g output. The resulting error due to temperature sensor is about ±60 PPM.

The total RMS error due to all sources is not less than ±185 PPM for ±1g output. The major contributor to compensation error is accelerometer modelability. These estimates ignore the compensation electronics which are external to the accelerometer. If such a network is estimated to be accurate to 1% of the total deviation of the non-compensated output between -65°F and 225°F or about 174 PPM (.01 x 290°F x 60 PPM/°F = 174 PPM) the total RMS error for the compensated output is about 250 PPM. It is the goal of future Q-Flex development to improve the modelability and lower the scale factor temperature coefficient of the Q-Flex accelerometer and thus improve both its compensated and non-compensated output characteristics.

RAPID WARM-UP CONCLUSIONS

The rapid warm-up experimental and theoretical results provided valuable information for confirming, predicting, and improving the Q-Flex accelerometer rapid warm-up response. The following conclusions are made.

1) The output current is determined by the temperatures of the two accelerometer sensor magnetic structures.

2) At slow warm-up rates, below 15°F per minute, the Q-Flex output current accurately tracks the static temperature output current if the reference temperature is measured within the accelerometer sensor.

3) At fast warm-up rates to 40°F per minute output current deviations from the static output current characteristics are caused by gradients across the accelerometer sensor. Indications are that under low gradient conditions, the rapid warm-up current would accurately track the static output current.

4) The rapid warm-up performance model gives the maximum deviation of warm-up current from the temperature.

5) The accelerometer thermal properties determining the rapid warm-up performance are the sensor to environment thermal resistances, R, and the sensor heat capacity, C. The product of C and R determines the sensor time constant.

6) Accelerometer performance properties determining rapid warm-up performance are the output current temperature coefficient, temperature coefficient linearity and higher order coefficients.

RAPID WARM-UP DESIGN RECOMMENDATIONS

Rapid warm-up conditions represent a severe operating environment for any transducer. Design principles which can improve performance under rapid warm-up conditions will, thus, have considerable value in improving performance

for more benign environments. The following design recommendations are made to improve the rapid warm-up response of the Q-Flex accelerometer.

1) Decrease the thermal time constant of the accelerometer sensor by decreasing thermal impedances within the sensor and between the cover and the sensor. This can be accomplished by using thermally conductive epoxies to assemble and mount the sensor.

2) For active or passive temperature compensation, when rates exceed 15°F/minute two thermal sensors should be mounted in each of the magnetic structures and connected in series to provide an average sensor temperature. For rates below 15°F/minute a single thermal sensor may be employed.

3) Decrease the gradient sensitivity by reducing the scale factor temperature coefficient. Sundstrand has recently tested Q-Flex accelerometers with different magnet material. These units have demonstrated thermal coefficients over the entire temperature range of less than 20 PPM/°F.

SECTION V

Q-FLEX LOW COST, MAINTAINABILITY AND RELIABILITY

LOW COST

The Q-Flex production philosophy is characterized by a vertical type manufacturing organization. The capability exists within the company to process most raw materials through all required machining, etching, plating, anodizing, passivating and lapping processes. Certain heat treatment and quartz processing operations are performed out-plant, but multiple sources have been validated through purchase and evaluation of production detail parts. The Q-Flex fabrication and assembly operations are planned and scheduled on the basis of batch processing. For example, 24 reeds are chemically etched simultaneously, 12 etched reeds are simultaneously metal vapor deposited. Actual manufacturing material, labor, and scrap rates are computer accumulated and compared to previously established standard measures. Follow-up on operational variances is an integral part of the manufacturing engineering effort.

The Q-Flex accelerometer is the evolutionary result of a purposeful, multifunction design philosophy. Sundstrand Engineering has combined the following functions within the three part proof mass assembly.

1) Seismic mass (quartz disk plus attached torquer coils)

2) Pickoff and torquer interconnect (vapor-deposited chrome/gold traces across quartz flexures)

3) Circuit isolation side-to-side (intermediate quartz)

4) Pendulum hinge suspension (chemically milled dual quartz flexures)

5) Pickoff gap spacing (lands on rim)

6) Input axis definition (location of hinge axis reference to proof mass center of gravity and rim lands plane).

In similar fashion, the Invar excitation rings serve as pickoff electrical ground, magnet flux return path, proof mass rim clamps, electrical connector retainer, and magnet/pole piece housing. The result is a dramatically small parts count (15 parts including five connector pins) and a demonstrated high reliability.

A key element in the Q-Flex accelerometer low cost concept is standardization. One standard sensor assembly and one standard servo hybrid electronics is the goal. In reality, significant configuration changes require a transition phase as the new design is phased in and the old design is phased out. One example is the conversion from servo hybrid electronics which require a pickoff transformer and, consequently, high frequency carrier signal to a "monochip" servo hybrid with no transformer, lower carrier signal frequency, improved performance, lower parts count and improved reliability. All new program applications and current program reorder updating activities receive the new servo configuration. The commercial varients of the Q-Flex accelerometer are being converted as inventory of the old design is reduced to zero.

Standardization and batch processing also apply to burn-in and functional test of major subassemblies. Batches of 24 sensor/cover assemblies proceed through standard 96 hour, -75°F to +250°F temperature cycles to non-operative shock exposure (250g, 1/2 sine, 6 m-sec) and then to mechanized temperature-tumble functional test. Sensors are sorted into primary performance categories based on measured values of scale factor, bias, scale factor and bias temperature coefficient, scale factor and bias thermal hysteresis at 75°F, and bias temperature coefficient linearity. Non-standard special screen tests and additional burn-in tests are performed as required to support special program applications.

Even the specific program calibration and acceptance test operations are performed on standardized test consoles and automatic sweep vibration equipment and simultaneous readout of frequency response and rectification error. Standard format procedures with variable conditions, test fixtures, and acceptance limits are used extensively.

The net result of this commitment to one standard Q-Flex sensor, one standard Q-Flex servo hybrid, and batch processing using standardized procedures with mechanized, multichannel test equipment is production efficiency. Economies of large scale raw material purchase and detail part fabrication possible from common usage throughout multiple programs, and the avoidance of subcontractor add-on profit margins by doing most operations in-plant contribute to the favorable Q-Flex accelerometer low cost position.

MAINTAINABILITY

The maintainability of the Q-Flex accelerometer is well served by the constant striving for low cost and standardization. Simply breaking the electronics cover epoxy seal permits discrete component exchange for factor or field depot recalibration. Neither the sensor nor the servo hybrid electronics have any known wear-out modes, but if out-of-specification or damaged, either one can be easily replaced with an interchangeable assembly. Standardization of subassemblies supports quick turn around from existing inventory.

The exterior surfaces of the Q-Flex accelerometer are entirely stainless steel, except for the solder-plated pins and glass of the unit header. There are no maintenance schedules for preservation, lubrication, or periodic operation required for long term storage.

RELIABILITY

Sundstrand Data Control, Inc. recognizes the need for reliable operation of the Q-Flex accelerometer in user systems.

The sincere commitment to standardization forces reliability consideration to the lowest levels of the entire fabrication, assembly, and test sequences of the Q-Flex accelerometer. Not knowing beforehand which accelerometers will be selected for high reliability programs requires that all fabrication, cleaning, lapping, metal vapor despotiion, and assembly procedures meet rigid quality and reliability standards. Sensor final cleaning and closing operations are performed in clean room areas. Prior to epoxy cure, each sensor is subjected to an automatic pendulum freedom test. Daily samples of thermocompression bonds are subjected to pull tests. This adherance to rigid quality and reliability standards for all aspects of Q-Flex production has proven effective in meeting or exceeding all user system reliability requirements.

SECTION VI

THERMAL STUDY CONCLUSIONS

A review of the entire Thermal Study Program leads to the following conclusions:

BIAS CONCLUSIONS

1) Individual bias polynomial models based upon least squares curve fitting have unique coefficients from unit to unit.

2) The short term bias modelability, as measured by the RMS residuals, was consistent from unit to unit and had an overall RMS residual of 24μg.

3) No indication of long term bias magnitude or shape instability is apparent from the magnitude of RMS residuals from any single test when least squares fit to the bias polynomial model.

4) Q-Flex accelerometer, S/N 10450, was less stable than any of the other three accelerometers tested.

This accelerometer had old configuration, rigid coil attachment epoxy and a deliberately excessive quantity of rigid conductive epoxy at the coil center-tap connection.

Direct correlation from multiple sources, and confirmed in this thermal study, exists between proof mass strain, induced

by material thermal coefficient differences and resultant large bias thermal hysteresis (BTH) and degraded bias temperature coefficient linearity (BTCL).

5) Bias stability on one of the current configuration Q-Flex accelerometers, S/N 20196, was clearly inferior when compared to the stable bias accelerometers, S/N's 20204 and 20210.

This variation between accelerometers of the current production design indicates that driving functions for bias parameter shifts are still present on the proof mass, though clearly much reduced from the old configuration.

Both bias and bias temperature coefficient shifts are significant error sources for the long term bias model when wide temperature range operation is assumed.

6) Q-Flex accelerometers, S/N's 20204 and 20210, demonstrated extremely stable bias performance.

For these units, the RMS bias residuals from the initial calibration curves were approximately 60μg.

In addition, the bias thermal hysteresis was less than 30μg when tested over a 220°F temperature span (± 110°F about midpoint).

Four and one-half months of extensive thermal testing verified the excellent long term bias stability of these Q-Flex accelerometers.

7) The maximum BTH error occurs near the temperature range midpoint.

For temperature excursions less than full range, the resulting minor loop BTH error stays within the extended temperature range BTH error envelope.

The contribution of BTH error to bias model uncertainty can be reduced by one-half by averaging the increasing and decreasing temperature bias models.

BTH was demonstrated to be very repeatable.

8) It is evident that bias model stability is dependent upon more than one source of proof mass strain. Available evidence points towards conductive epoxy stress on the proof mass and coil attachment temperature dependent stress as the prime driving functions causing bias thermal instabilities.

SCALE FACTOR CONCLUSIONS

1) Individual scale factor polynomial models based upon least squares curve fitting have unique coefficients from unit to unit.

The coefficient differences were much smaller than bias model coefficient differences and indicate that for some applications a 'family' scale factor model would be sufficiently accurate.

Short term modelability of the Q-Flex accelerometer, as evidenced by the RMS residuals, was consistent from unit to unit and had an overall residual of 37 ppm.

2) The Q-Flex scale factor temperature coefficient (SFTC) is stable to better than 0.7ppm/°F over 135 days.

SFTC is significantly influenced by the inherent modelability of scale factor.

SFTC does not appear to have major impact upon rapid reaction performance.

3) Long term scale factor stability was bounded below 0.5 ppm per day over 135 days by the study data.

Error analysis of scale factor measurement and steady state temperature measurement accuracies indicate a measurement uncertainty of actual scale factor of approximately 50 ppm, RMS, (50 ppm/°F x 0.5°F, RMS + 25 ppm, RMS, alternate load resistor calibration uncertainty).

4) All Q-Flex accelerometers exhibit positive scale factor hysteresis (SFTH) that is, the scale factor following hot soak is smaller than that before hot soak at all temperatures within the operating range.

The maximum SFTH error occurs near the temperature range midpoint.

For temperature excursions less than full range, the resulting minor loop SFTH error stays within the extended temperature range SFTH error envelope.

The contribution of SFTH error to scale factor model uncertainty can be reduced by one half by averaging the increasing and decreasing temperature scale factor models.

SFTH was demonstrated to be very repeatable.

5) Scale factor relaxation effects after hot soak were observed.

Scale factor was stable after cold soak and bias was stable after both hot and cold soaks.

The time constant for scale factor relaxation is less than 40 hours.

Scale factor relaxation contributes up to 63% of the observed SFTH.

6) All scale factor data indicate the existence of a very large flux density gradient near the proof mass interface. It is concluded that time dependent hysteretic scale factor effects are the result of epoxy creep causing relative motion between the proof mass coils and the magnet circuit geometry.

RAPID WARM-UP CONCLUSIONS

1) Accelerometer performance properties determining rapid warm-up performance are the output current temperature coeffient, temperature coefficient linearity and higher order coefficients. These coefficients are directly related to the scale factor/bias thermal models.

The output current is determined by the temperatures of the two accelerometer sensor magnetic structures.

At slow warm-up rates, below 15°F per minute, the Q-Flex output current accurately tracks the static temperature output current if the reference temperature is measured within the accelerometer sensor.

At fast warm-up rates to 40°F per minute output current deviations from the static output current characteristics are caused by gradients across the accelerometer sensor.

2) The rapid warm-up performance model gives the maximum deviation of warm-up current from the static current referenced to the flange temperature.

3) The accelerometer thermal properties determining the rapid warm-up performance are the sensor to environment thermal resistances, R, and the sensor heat capacity, C. The product of C and R determines the sensor time constant.

SECTION VII

RECOMMENDATIONS

To maintain the low cost posture, keep and preserve the simplification concept of maintainability, and to retain the high reliability standard established for Q-Flex production, the design modifications recommended were closely analyzed to insure these concepts were not violated. The conclusions reached about present instrument performance and the proposed modifications recommended to enhance performance do indeed satisfy the existing tenets established for the Q-Flex accelerometer.

The accelerometer modifications recommended to improve performance are:

BIAS IMPROVEMENTS

1) Eliminate all usage of conductive epoxy from the proof mass assembly.

Develop welding techniques to connect the torque coil wires directly to the proof mass thin-film metal circuits.

2) Modify the proof mass conductor circuits to accomplish torque coil center-tap connection via a thin-film 'wrap-around' trace.

3) Optimize the torque coil bobbin material and attachment means to minimize thermal expansion coefficient difference effects at the bobbin/proof mass interface. Materials such as quartz or ceramic should be evaluated for the coil bobbin material.

SCALE FACTOR IMPROVEMENTS

1) Redesign the magnet circuit geometry to reduce flux field gradients.

2) Incorporate adhesive materials that reduce bond-line thicknesses at the excitation ring/magnet/pole piece interfaces.

RAPID WARM-UP IMPROVEMENTS

1) Improve the heat flow path from external housing flange to internal magnets by means of thermally conductive epoxy substitution for present adhesives.

2) Evaluate rare earth magnet materials and sources.

3) Modify torque coil bobbin design to reposition coil turns within the linear portion of the magnet circuit flux field.

4) Provide optional means for the installation of one or two temperature sensors in intimate contact at the magnet-Invar interface.

THIS REPORT HAS BEEN DELIMITED
AND CLEARED FOR PUBLIC RELEASE
UNDER DOD DIRECTIVE 5200.20 AND
NO RESTRICTIONS ARE IMPOSED UPON
ITS USE AND DISCLOSURE.

DISTRIBUTION STATEMENT A

APPROVED FOR PUBLIC RELEASE;
DISTRIBUTION UNLIMITED.